



## APPROVAL SHEET

Title of Thesis: Investigating septic system impacts on a rural subwatershed using fluorescent dissolved organic matter and contaminants of emerging concern

Name of Candidate: Anna McClain  
Master of Science, 2023

Thesis and Abstract Approved: Lee Blaney  
Lee Blaney, PhD  
Professor  
Chemical, Biochemical and Environmental  
Engineering

Date Approved: April 27, 2023

## CURRICULUM VITAE

Name: Anna McClain

Degree and date to be conferred: M.S., 2023

Secondary education: August 2008 – June 2012  
Carolina Friends School, Durham, NC

Collegiate institutions attended: August 2012 – May 2016  
St. Mary's College of Maryland  
Bachelor of Arts (Chemistry)

August 2021 – May 2023  
University of Maryland, Baltimore County  
Master of Science (Environmental Engineering)

Major: Environmental Engineering

Presentations: **McClain, A.**, Batista-Andrade, J. A., Siao, M., Ellington, M., Blaney, L. *New fluorescence- and chemical-based strategies to identify the impacts of septic systems on water quality in a suburban subwatershed.* American Chemical Society (ACS) Spring 2023 National Meeting (Indianapolis, IN), Oral presentation, March 26, 2023.

Batista-Andrade, J. A., Iglesias Vega, D., **McClain, A.**, Blaney, L. *Predicting wastewater loads in urban streams using fluorescence spectroscopy and multiple linear regression.* American Chemical Society (ACS) Spring 2023 National Meeting (Indianapolis, IN), Oral presentation, March 26, 2023.

Batista-Andrade, J. A., Iglesias Vega, D., **McClain, A.**, Rose, M., Blaney, L. *Contaminants of emerging concern and fluorescent dissolved organic matter as wastewater indicators in urban watersheds that do not receive wastewater effluent.* Association of Environmental Engineering and Science Professors (AEESP) Research and Education Conference (St. Louis, MO), Oral presentation, June 30, 2022.

**McClain, A.**, Cornwell, J., Owens, M., Kellogg, L. *Carbonate chemistry in experiment incubations of*

*restored Chesapeake Bay oyster communities.*  
Coastal Estuarine Research Federation (CERF)  
Biennial Meeting (Portland, OR), Poster  
presentation, 2015.

Professional positions held:

Graduate Research Assistant  
(August 2021 – May 2023)  
University of Maryland, Baltimore County

DOE Science Undergraduate Laboratory Intern  
(January 2017 – April 2017)  
Oak Ridge National Laboratory Biosciences  
Division

DOE Science Undergraduate Laboratory Intern  
(August 2016 – December 2016)  
Oak Ridge National Laboratory Electrical and  
Electronic Systems Research Division

Maryland Sea Grant REU Summer Intern  
(May 2015 – August 2015)  
Horn Point Laboratory, University of Maryland

Summer-Student Organic Chemistry Researcher  
(May 2014 – August 2014)  
St. Mary's College of Maryland, Department of  
Chemistry and Biochemistry



## ABSTRACT

Title of Document: INVESTIGATING SEPTIC SYSTEM IMPACTS IN A RURAL SUBWATERSHED USING FLUORESCENT DISSOLVED ORGANIC MATTER AND CONTAMINANTS OF EMERGING CONCERN

Anna McClain  
Master of Science, 2023

Directed By: Dr. Lee Blaney, Professor  
Department of Chemical, Biochemical and Environmental Engineering

Septic systems introduce partially treated wastewater, which contains contaminants of emerging concern (CECs) like pharmaceuticals, antibiotics, UV filters, and hormones, into nearby surface water via groundwater transport. In addition to CECs, septic effluent contains wastewater-derived fluorescent dissolved organic matter (FDOM), which we hypothesized could be employed to quickly and economically identify sections of streams impacted by septic effluent. We used fluorescence excitation-emission matrix (EEM) spectroscopy and parallel factor analysis (PARAFAC) in conjunction with CEC measurements to characterize septic wastewater and identify potential EEM and EEM-PARAFAC based indicators of septic effluent. The potential indicators were applied to spatially resolved samples from a rural subwatershed with variable septic density and no municipal wastewater infrastructure. We proposed three ratiometric FDOM parameters as effective indicators of septic effluent: the area-normalized ratio of tryptophan-like to humic acid-like fluorescence ( $R2/R5$ ); the ratio of wastewater EEM-PARAFAC components with tryptophan-like and humic-like fluorescence ( $W2/W1$ ); and the ratio of North Branch EEM-PARAFAC components with microbially derived protein-like and

humic-like fluorescence (C4/C1). All three ratiometric indicators were considered conservative and well correlated with concentrations of the artificial sweetener sucralose in areas with medium (41 – 80 tanks/km<sup>2</sup>) and high (>80 tanks/km<sup>2</sup>) septic density. In medium septic density areas, C4/C1 and W2/W1 were also well correlated with the pharmaceutical carbamazepine. The absence of correlations between FDOM parameters and CEC concentrations in areas with low septic density suggests that 40 tanks/km<sup>2</sup> serves as a threshold for measurable impacts of septic systems on nearby surface waters. For areas above this septic density threshold, the identified ratiometric FDOM indicators can provide an economical method for evaluating the impacts of septic systems on water quality. The indicators were employed to evaluate the complex pathways involved with septic effluent transport to streams via preferential groundwater seeps during baseflow and subsurface mobilization during a storm event. Overall, these findings confirmed the potential for using FDOM-based parameters to identify and assess the impacts of septic effluent on nearby surface water quality.

INVESTIGATING SEPTIC SYSTEM IMPACTS IN A RURAL SUBWATERSHED  
USING FLUORESCENT DISSOLVED ORGANIC MATTER AND  
CONTAMINANTS OF EMERGING CONCERN

By

Anna Grace King McClain

Thesis submitted to the Faculty of the Graduate School of the  
University of Maryland, Baltimore County in partial fulfillment  
of the requirements for the degree of  
Master of Science  
2023

© Copyright by  
Anna Grace King McClain  
2023



## **Dedication**

To my family, who support and believe in me no matter what. I love y'all!

## **Acknowledgments**

I would like to thank my advisor and mentor, Dr. Lee Blaney. His thoughtful way of challenging me pushed me to become a better researcher while making me feel seen and appreciated for more than just my work in the lab.

I could not have completed this work without the guidance and friendship of Jahir Batista-Andrade. He took me under his wing and made me feel safe and welcome in the lab. Not to mention he taught me all the technical skills I needed for this project.

Emily Majcher at USGS provided expertise that elevated the outcomes of this project. She generously took the time to mentor me and patiently answer my questions and offer valuable advice.

Barbara Johnson at Blue Water Baltimore provided key insights on how to share this research with a broader audience and initiated important conversations about the broader impacts of the research.

Dr. Andy Miller from the UMBC GES department gave me helpful feedback during the proposal process and provided equipment that I used for my storm sampling campaign.

My ICARE cohort and the ICARE program provided invaluable support. The lessons I learned with you about DEJI and community engagement in environmental research will be an important part of whatever work I pursue in the future.

The Peacemaker fellows program provided space to engage in conversations and learning beyond what is possible in a classroom, and helped me remember what really matters.

I would like to thank all the members of the Blaney lab. Their encouragement and camaraderie got me through many long days and nights in the lab. I would also like to acknowledge Andrea Miller and Victor Fulda, who make sure everything in the department run smoothly.



## Table of Contents

Dedication .....	ii
Acknowledgments.....	iii
List of Tables .....	vii
List of Figures .....	ix
Chapter 1: Introduction .....	1
1.1 Motivation .....	1
1.2 Research objectives .....	3
1.3 Structure of this thesis .....	4
Chapter 2: Literature review .....	5
2.1 Septic systems are an important source of conventional contaminants to the Chesapeake Bay watershed .....	5
2.2 Wastewater treatment and drainage in septic systems .....	6
2.3 Septic system impacts .....	7
2.4 Indicators of septic wastewater .....	8
2.5 FDOM and EEMs in septic wastewater .....	9
2.6 Storm event mobilization of septic wastewater.....	12
2.7 Previous studies of wastewater impacts in the Jones Falls watershed and preliminary data from the Upper Jones Falls watershed .....	13
Chapter 3: Materials and methods .....	16
3.1 Chemicals .....	16
3.2 Wastewater sampling .....	22
3.2.1 Municipal wastewater sampling.....	22
3.2.2 Septic wastewater sampling.....	22
3.3 Stream sampling .....	23
3.3.1 North Branch walkup sampling.....	23
3.3.2 TIR survey and groundwater seep sampling .....	26
3.3.3 Wet weather sampling .....	28
3.4 EEM analysis.....	30
3.5 EEM-PARAFAC modeling .....	34
3.6 Dissolved organic carbon and total nitrogen analysis.....	35
3.7 CEC analysis .....	36
3.7.1 Water samples.....	36
3.7.2 Solid samples .....	37
3.7.3 LC-MS/MS methods.....	38

Chapter 4: Septic wastewater characterization .....	46
4.1 Contaminants of emerging concern (CECs) in septic wastewater .....	46
4.2 Fluorescent dissolved organic matter (FDOM) in conventional septic tanks .....	50
4.3 FDOM and CECs in advanced septic system .....	56
4.4 Wastewater EEM-PARAFAC modeling.....	58
4.5 Septic wastewater characterization conclusion .....	72
Chapter 5: Septic wastewater indicator profiles in the North Branch .....	74
5.1. EEM-PARAFAC model for the North Branch .....	74
5.2 CECs in the North Branch.....	82
5.3 EEM and EEM-PARAFAC parameters in the North Branch .....	87
5.4 Correlation analysis of wastewater indicators in the North Branch.....	91
5.5 Conclusions related to septic wastewater indicators in the North Branch .....	103
Chapter 6: Septic wastewater transport pathways to surface water .....	106
6.1 Thermal infrared (TIR) survey of preferential groundwater flows.....	106
6.1.1 CEC concentrations measured in areas of preferential groundwater discharge .....	107
6.1.2 FDOM composition in samples from the TIR survey .....	112
6.2 Case study: storm mobilization of CECs and septic wastewater-derived FDOM into streams.....	116
6.2.1 CEC concentrations during the storm event.....	116
6.2.1 Composition of storm-mobilized FDOM .....	120
Chapter 7: Conclusion.....	124
7.1 Summary .....	124
7.2 Future opportunities .....	126
Appendix A.....	128
Appendix B .....	132
Appendix C .....	152
References.....	157

## List of Tables

Table 3.1. Composition of the four spiking solutions used for standard additions analysis. ....	18
Table 3.2. Internal standard solutions used to account for matrix effects during LC-MS/MS analysis. ....	20
Table 3.3. Measured absorbance and fluorescence parameters with descriptions. ....	33
Table 3.4. LC-MS/MS parameters for the wastewater indicators, antibiotics, and UV filters and hormones methods. ....	40
Table 4.1. Core consistency, explained variance, sum of squared errors (SSE), and validation status for preliminary EEM-PARAFAC models of FDOM in septic wastewater. ....	59
Table 4.2. Percent fluorescence in each region for the FDOM components in the septic wastewater EEM-PARAFAC model. ....	60
Table 4.3. Top OpenFluor matches for the spectra of each component in the septic wastewater EEM-PARAFAC model. Unless indicated, the top 10 significant matches are shown for Tucker’s correlation coefficient greater than 0.95. Data were collected in February 2023. ....	62
Table 4.4. Core consistency, explained variance, SSE, and validation status for preliminary EEM-PARAFAC models of FDOM in septic and municipal wastewater. ....	65
Table 4.5. Percent fluorescence in each region for the FDOM components in the global wastewater EEM-PARAFAC model. ....	67
Table 4.6. Top OpenFluor matches for the spectra of each component in the global wastewater EEM-PARAFAC model. Unless indicated, the top 10 significant matches are shown for Tucker’s correlation coefficient greater than 0.95. Data were collected in February 2023. ....	68
Table 5.1. Core consistency, explained variance, sum of squared errors (SSE), and validation status for preliminary EEM-PARAFAC models of FDOM in the North Branch. ....	75
Table 5.2. Percent fluorescence in each region for the FDOM components in the North Branch EEM-PARAFAC model. ....	76
Table 5.3. Top OpenFluor matches for the spectra of each component in the North Branch EEM-PARAFAC model. Unless indicated, the top 10 significant matches are shown for Tucker’s correlation coefficient greater than 0.95. Data were collected in February 2023. ....	78
Table A.1. North Branch walkup site names and coordinates. ....	128
Table A.2. TIR groundwater seep survey site names, coordinates, and temperature differences between the seeps and the surface water. ....	131
Table B.1. CEC concentrations (ng/L) in samples collected from conventional Septic B. Concentrations are reported as mean ± standard deviation. ....	132
Table B.2. CEC concentrations (ng/L) in samples collected from conventional Septic C. Concentrations are reported as mean ± standard deviation. ....	133

Table B.3. CEC concentrations (ng/L) in samples collected from conventional Septic D. Concentrations are reported as mean $\pm$ standard deviation. ....	134
Table B.4. CEC concentrations (ng/L) in municipal wastewater samples. Concentrations are reported as mean $\pm$ standard deviation.....	135
Table B.5. CEC concentrations in the liquid (ng/L) and solid (ng/g) phases of septic sludge. Concentrations are reported as mean $\pm$ standard deviation. ....	137
Table B.6. Dates, times, and air temperature for collection of samples from the conventional septic systems.....	139
Table B.7. CEC concentrations (ng/L) at the inlet and outlet of the advanced septic system. Concentrations are reported as mean $\pm$ standard deviation. ....	140

## List of Figures

Figure 2.1. Septic wastewater transport pathways. Adapted from Tamang <i>et al.</i> (2022) <sup>22</sup> . .....	7
Figure 2.2. Representative EEMs for Suwannee River natural organic matter (SRNOM) and municipal wastewater. The five major fluorescence regions established by Chen <i>et al.</i> (2003) <sup>48</sup> are outlined and labeled in the figure. ....	10
Figure 2.3. Septic system density, preliminary sampling locations, and relative sucralose concentrations and R4/R5 values in the Upper Jones Falls. Samples were collected in March 2022 and included three sites from previous sampling campaigns (JON) and nine new sites along the Deep Run (DR), Dipping Pond Run (DP), and North Branch (NB) tributaries. Sucralose concentrations and R4/R5 values are plotted as a percentage of the total (sum across all sites) so both parameters can be visualized on the same scale. Map created by Jahir Batista-Andrade. ....	15
Figure 3.1. The sampling sections and sites in the North Branch of the Jones Falls.....	25
Figure 3.2. Groundwater seep sampling sites selected based on the TIR survey. ....	27
Figure 3.3. Discharge measurements in the North Branch and from the USGS gauge for the Jones Falls at Sorrento, MD (latitude 39.23447, longitude -76.39464) normalized to the drainage area with precipitation data for November 11, 2022.....	29
Figure 3.4. The streambed profile and water level were used to measure the cross-sectional area and calculate discharge. ....	30
Figure 3.5. Mobile phase gradient for the (a) wastewater indicators, (b) antibiotics, and (c) UV filter and hormones methods. ....	45
Figure 4.1. Measured CEC (a) detection frequencies in conventional septic tanks and (b) concentration distributions in septic and municipal wastewater. The filled box represents the interquartile range (IQR). The bottom of the filled box represents the 25 <sup>th</sup> percentile value (Q1), the horizontal line dividing the box represents the 50 <sup>th</sup> percentile or median value, the top of the filled box is the 75 <sup>th</sup> percentile value (Q3), and the open square is the mean. The bottom and top whiskers represent the minimum value above $Q1 - 1.5(IQR)$ and the maximum value below $Q3 + 1.5(IQR)$ , respectively. Values outside of the whiskers are outliers. ....	47
Figure 4.2. Representative excitation-emission matrices (EEMs) for septic wastewater, municipal wastewater, stream water from the North Branch, and reconstituted SRNOM. The dissolved organic carbon (DOC) content for each sample is overlaid on the EEM. .	51
Figure 4.3. EEMs measured for samples collected from three conventional septic tanks. Septic C was pumped out at the beginning of September, as indicated by the pumping truck label in the July EEM. ....	52
Figure 4.4. FDOM in Septic B and municipal wastewater expressed as (a) differential EEMs and (b) box plots. In (a), the fluorescence in the "Delta" plots indicate regions with higher fluorescence in Septic B wastewater compared to municipal wastewater. ....	54
Figure 4.5. Distribution of ratiometric FDOM parameters for Septic B and municipal wastewater.....	55

Figure 4.6. FDOM in the inlet and outlet of Septic A expressed as (a) differential EEMs and (b) box plots. In (a), the fluorescence in the "Removal" plots indicates regions with high FDOM removal. ....	56
Figure 4.7. The distribution of (a) CEC concentrations and (b) ratiometric FDOM parameters in the inlet and outlet samples collected from the advanced septic system. ..	58
Figure 4.8. The fluorescence spectra of the four components in the EEM-PARAFAC model for FDOM in septic wastewater. ....	59
Figure 4.9. The fluorescence spectra of the five components in the global EEM-PARAFAC model for FDOM in septic and municipal wastewater. ....	66
Figure 4.10. (a) The distribution of EEM-PARAFAC components and (b) correlations between ratiometric FDOM parameters and caffeine concentrations in samples collected from the inlet and outlet of the advanced septic system. ....	72
Figure 5.1. The fluorescence spectra of the four components in the EEM-PARAFAC model for FDOM in the North Branch. ....	75
Figure 5.2. The distribution of (a) components and (b) ratiometric parameters from the North Branch EEM-PARAFAC model in the inlet and outlet samples collected from the advanced septic system. ....	82
Figure 5.3. Concentrations of (a) sucralose, (b) carbamazepine and sulfamethoxazole, and (c) atrazine and mecoprop in the North Branch. The x-axis increases with downstream distance. The filled circles connected by lines represent CEC concentrations in samples collected from the main stem, and open symbols indicate CEC concentrations in samples collected from tributaries. Concentrations below LOQ are plotted as "x" symbols. Error bars show standard deviation. The grayscale bar at the top of the figure shows the septic system density along the stream. ....	86
Figure 5.4. The profiles of ratiometric parameters related to wastewater FDOM in the North Branch. Correlated parameters were plotted together. The x-axis increases with downstream distance. The filled circles connected by lines represent ratiometric parameters measured in samples collected from the main stem, and open symbols indicate ratiometric parameters measured in samples collected from tributaries. The grayscale bar at the top of the figure shows the septic density along the stream. ....	90
Figure 5.5. Spearman correlations between CEC concentrations, dissolved organic carbon (DOC) contents, total nitrogen (TN) levels, and the magnitude of ratiometric fluorescence parameters for all North Branch samples. The CECs included are sucralose (SUC), carbamazepine (CBZ), atrazine (ATZ), mecoprop (MEC), and sulfamethoxazole (SMX). ....	93
Figure 5.6. Spearman correlations between CEC concentrations, DOC contents, TN levels, and ratiometric fluorescence parameters for North Branch samples from the (a) main stem and (b) tributaries. The CECs were sucralose (SUC), carbamazepine (CBZ), atrazine (ATZ), mecoprop (MEC), and sulfamethoxazole (SMX). ....	93
Figure 5.7. Spearman correlations between CEC concentrations, DOC contents, TN levels, and ratiometric fluorescence parameters for North Branch samples in areas with (a) low (10-40 systems/km <sup>2</sup> ), (b) medium (41-80 systems/km <sup>2</sup> ), and (c) high (81-173 systems/km <sup>2</sup> ) septic density. The CECs were sucralose (SUC), carbamazepine (CBZ), atrazine (ATZ), mecoprop (MEC), and sulfamethoxazole (SMX). ....	101

Figure 5.8. Correlations between sucralose concentration and the W2/W1, R2/R5, R4/R5, and C4/C1 fluorescence indicators for samples collected from areas with low, medium, and high septic density.....	101
Figure 5.9. Pearson correlations between (a) sulfamethoxazole and C4/C2, W2/W5, and W4/W5 in areas with high septic density and (b) carbamazepine and R1/R5, C4/C1, W2/W1, and W4/W1 in areas with medium septic density.....	102
Figure 5.10. Distribution of z-scores for the ratiometric fluorescence indicators (top to bottom: R1/R5, R2/R5, R4/R5, C4/C1, C4/C2, C4/C3, W2/W1, W2/W5, W4/W1, and W4/W5) at each site from the headwaters to the confluence with the Jones Falls (left to right). The grayscale bar at the top of the figure shows the septic density along the stream. The stream runs dry between NB-85 and NB-84, so the sites downstream of NB-85 are not connected to the upstream sites.....	102
Figure 5.11. Summary of the potential CEC and FDOM indicators and recommendations from each analysis step.....	105
Figure 6.1. Box plots comparing (a) sucralose and (b) carbamazepine concentrations in seeps from low/medium and high septic density areas.....	110
Figure 6.2. Concentrations of (a) sucralose, (b) carbamazepine, and (c) atrazine in groundwater seep samples collected in September plotted with concentrations measured in the main stem and tributaries during the North Branch sampling campaign in June – July. The x-axis increases with downstream distance. Concentrations below LOQ are plotted as "×" symbols. Error bars show standard deviation. The grayscale bar at the top of the figure shows the septic density along the stream.....	111
Figure 6.3. Comparison of TIR images, EEMs, and CEC concentrations for (a) GW-17 and GW-18, (b) GW-19 and GW-20, and (c) GW-23 and GW-26. Concentrations below LOQ are plotted as "*" symbols.....	115
Figure 6.4. Concentration profiles of (a) sucralose, (b) caffeine and paraxanthine, (c) carbamazepine, (d) sulfamethoxazole and azithromycin, and (e) atrazine during a single storm event. Error bars are standard deviation (n = 3).....	119
Figure 6.5. Profiles of (a) EEM regional volumes, (b) $F_{max}$ values for North Branch EEM-PARAFAC components, and (c) $F_{max}$ values for global wastewater EEM-PARAFAC components during the November 11, 2022 storm event. Error bars are standard deviation with n = 3.....	122
Figure 6.6. The profiles of the ratiometric FDOM parameters identified as indicators of septic wastewater during the November 11, 2022 storm event. Error bars are standard deviation with n = 3.....	123
Figure 6.7. EEMs from samples collected before, during, and after the discharge began to increase at 10:55 am.....	123
Figure B.1. EEMs from three unique septic sludge samples collected directly from a septic pumping truck.....	141
Figure B.2. FDOM in Septic C and municipal wastewater expressed as (a) differential EEMs and (b) box plots. In (a), the fluorescence in the "Delta" plots indicate regions with higher fluorescence in Septic C wastewater compared to municipal wastewater.....	142

Figure B.3. FDOM in Septic D and municipal wastewater expressed as (a) differential EEMs and (b) box plots. In (a), the fluorescence in the "Delta" plots indicate regions with higher fluorescence in Septic D wastewater compared to municipal wastewater. ....	143
Figure B.4. Spectral loadings for preliminary EEM-PARAFAC models with 2–8 components for FDOM in septic wastewater. The dashed curves are excitation loadings, and the solid curves are emission loadings. Only models with 2, 3, and 4 components were validated by split-half analysis. ....	144
Figure B.5. Spectral loadings for the validated four-component EEM-PARAFAC model for FDOM in septic wastewater. ....	145
Figure B.6. Correlations between the component scores for the four-component EEM-PARAFAC model for septic wastewater before data normalization. The strongest correlation was observed between C4 and C2. ....	146
Figure B.7. Correlations between the component scores for the four-component EEM-PARAFAC model for septic wastewater after data normalization. No strong correlations were observed. ....	147
Figure B.8. Spectral loadings for preliminary EEM-PARAFAC models with 2–8 components for FDOM in septic and municipal wastewater. The dashed curves are excitation loadings, and the solid curves are emission loadings. Only models with 2, 5, 6, and 7 components were validated by split-half analysis. ....	148
Figure B.9. Spectral loadings for the validated five-component EEM-PARAFAC model for FDOM in septic and municipal wastewater. ....	149
Figure B.10. Correlations between the component scores for the five-component EEM-PARAFAC global wastewater model before data normalization. No strong correlations were observed. ....	150
Figure B.11. Correlations between the component scores for the five-component EEM-PARAFAC global wastewater model after data normalization. No strong correlations were observed. ....	151



## Chapter 1: Introduction

### 1.1 Motivation

Septic systems have the potential to negatively impact nearby surface water quality, but the extent of those impacts is not well understood. Most studies, especially in the Chesapeake Bay watershed, have concentrated on nutrient loading from septic systems<sup>1,2</sup>. Legislation aimed at limiting environmental impacts from non-sewered sanitation systems and innovative technologies developed to upgrade septic system performance also focus on nutrient removal. These strategies will help to reduce nutrient loading, but they may not address other pollutants, including contaminants of emerging concern (CECs). CECs raise risks for public health (*e.g.*, antimicrobial resistance) and ecological systems (*e.g.*, endocrine disruption) at low, environmentally relevant concentrations<sup>3</sup>. CECs have been reported at high levels in septic systems. For example, the sulfamethoxazole antibiotic was present at concentrations up to 29,000 ng L<sup>-1</sup> in septic wastewater, with nearby groundwater having concentrations of 450 ng L<sup>-1</sup><sup>4</sup>. Oxybenzone, a UV filter found in sunscreens and other personal care products, and estrone, a steroid hormone, were measured at concentrations up to 16,100 ng L<sup>-1</sup> and 74 ng L<sup>-1</sup> in septic tanks, respectively<sup>5,6</sup>. Due to the high concentrations, a small fraction of septic effluent could considerably impact CEC levels in adjacent groundwater and surface water sources.

CECs have been ubiquitously reported throughout the Chesapeake Bay watershed<sup>7-9</sup>. Previous studies have linked these contaminants to municipal wastewater effluent, sanitary sewer leaks, and agricultural runoff. Yet, the impact of non-sewered sanitation systems has not been fully considered, and no previous studies in Baltimore or Maryland

have confirmed that septic systems introduce CECs into the watershed. To address this knowledge gap, we used multiple assessment techniques. In addition to CECs, septic systems contain wastewater-derived dissolved organic matter (DOM). Fluorescent DOM (FDOM), which is typically measured as excitation-emission matrices (EEMs), can be used to identify wastewater inputs because the fluorescence fingerprints from wastewater-derived DOM are significantly different from those of natural DOM<sup>10-12</sup>. For this study, we employed CEC concentrations and detections to validate EEM-based parameters that were proposed as rapid and inexpensive indicators of septic wastewater in streams.

This study will inform the scientific community's understanding of the impact of septic systems on low-order streams by (1) measuring contaminant concentrations in septic and municipal wastewater, (2) developing new fluorescence parameters to quickly and easily identify impacted streams, and (3) generating EEM and CEC datasets to understand storm-driven mobilization of septic wastewater. These outcomes will not only provide important and actionable information for homeowners, community members, and local government agencies, but also inform water quality in other watersheds. The Upper Jones Falls Small Watershed Action Plan includes "informing homeowners about septic system maintenance" as a principal management strategy for restoring and protecting the watershed<sup>13</sup>. This research can be adapted by the Baltimore County government for septic system education campaigns. The County can also use the data to determine the best strategies to protect the watershed and mitigate septic system impacts on water quality. We are working with Blue Water Baltimore to communicate our findings to community members, community organizations, and government agencies in a clear,

targeted, and relatable manner that conveys the essential points without inciting fear or blame about the presence of CECs in water bodies.

## 1.2 Research objectives

The **objective** of this project was to employ EEM parameters and CEC concentrations to identify, confirm, and assess the impacts of non-sewered sanitation systems in the rural Upper Jones Falls subwatershed. We investigated these parameters in an area with variable septic system density and no municipal sewer infrastructure. We **hypothesized** that (1) CECs and other contaminants were introduced to the stream from septic systems, (2) differences in FDOM signatures from natural sources and septic systems could be used to identify septic inputs, and (3) storm events increased septic wastewater transport to streams. The **specific aims** were to:

Aim 1: Characterize and compare FDOM and CECs in septic tanks and municipal wastewater.

Aim 2: Measure EEMs and CECs along a tributary to the Upper Jones Falls and develop EEMs as a screening tool for septic system inputs.

Aim 3: Employ thermal infrared (TIR) imaging to identify groundwater inputs at the impacted locations identified in Aim 2 and confirm septic wastewater mobilization during storm events via time-resolved EEM and CEC measurements.

### 1.3 Structure of this thesis

Chapter 1 describes the motivation and research objectives for this project. Chapter 2 provides a literature review of septic system impacts on the environment, potential indicators of septic wastewater, and previous water quality campaigns in the Jones Falls Watershed. Chapter 3 details the experimental materials and methods used to complete this project. Chapter 4 reports and discusses EEM and CEC data collected from septic and municipal wastewater (specific aim 1). Chapter 5 evaluates potential septic effluent FDOM indicators via a spatially resolved sampling campaign (specific aim 2). Chapter 6 details two case studies investigating septic effluent transport to surface water (specific aim 3). Chapter 7 summarizes the main conclusions from this thesis.

## Chapter 2: Literature review

### 2.1 Septic systems are an important source of conventional contaminants to the Chesapeake Bay watershed

The water quality impacts of excess nutrients from non-sewered sanitation systems are a concern in Maryland and throughout the Chesapeake Bay watershed<sup>1,2,14</sup>. Nutrients contributed by septic systems need to be quantified and taken into consideration for the Watershed Implementation Plans that are being used to meet the Chesapeake Bay Total Maximum Daily Load agreement<sup>15</sup>. Harrison *et al.* (2012) estimated that septic systems in Maryland contribute 7% of nitrogen pollution to the Chesapeake Bay<sup>1</sup>. In fact, approximately 420,000 septic systems in Maryland contribute around 3.6 million pounds of nitrogen to the Bay every year. Baltimore County accounts for about 13% (56,200) of the septic systems in the state<sup>1</sup>. Shields *et al.* (2008) investigated nitrogen exports from septic systems in the Gwynns Falls watershed. They found that septic systems are a major contributor to downstream nitrogen loading and proposed disrupting the connection between septic systems and streams to significantly reduce nitrogen export<sup>2</sup>. Maryland has already taken several steps to address septic system impacts, including through Bay Restoration Fund legislation that provides funds for upgrading septic tanks for nitrogen removal. In 2009, Maryland passed the Chesapeake Bay Nitrogen Reduction Act, which requires all new septic systems to include additional nitrogen-reducing units<sup>1</sup>. While these steps could improve nutrient loading from septic systems, other steps may need to be taken to address other contaminants.

## 2.2 Wastewater treatment and drainage in septic systems

Over 20% of US households use non-sewered sanitation systems to treat their wastewater<sup>16</sup>. These systems are generally located in areas that do not have access to centralized municipal wastewater infrastructure. Conventional septic systems consist of one or two anaerobic chambers for solids decomposition and a drainfield for additional treatment via filtration, adsorption, nitrification, and denitrification. While septic tanks remove solids and some organic matter, percolation through the drainage field is mostly responsible for treatment of nutrients, pathogens, and chemical contaminants<sup>17</sup>. The rate of contaminant removal depends on soil properties and effluent composition<sup>18-20</sup>. Effluent constituents that are not attenuated are eventually dispersed into shallow groundwater (Figure 2.1) and may reach nearby surface waters. Even properly functioning septic systems will not fully remove nutrients or CECs leading to a persistent source regardless of the age or condition of the septic tank<sup>21</sup>.

Groundwater transport is the most common pathway for septic wastewater to reach streams, but other pathways are important to consider (Figure 2.1)<sup>22</sup>. For example, wet weather events may cause contaminants from septic tank overflows or clogged drain fields to be rapidly transported to surface water via overland runoff or preferential subsurface flow<sup>17,20</sup>. In addition, high water tables during storm events can connect septic fields with drainage ditches and lead to faster transport<sup>18,20,23</sup>. Some septic systems are also illegally connected to drainage ditches or primary streams, resulting in consistent inputs of partially treated wastewater<sup>17</sup>. The contributions of these transport phenomena vary depending on site characteristics like soil type, topography, and the age and

condition of the nearby septic systems. No studies have investigated these transport phenomena in Baltimore County.

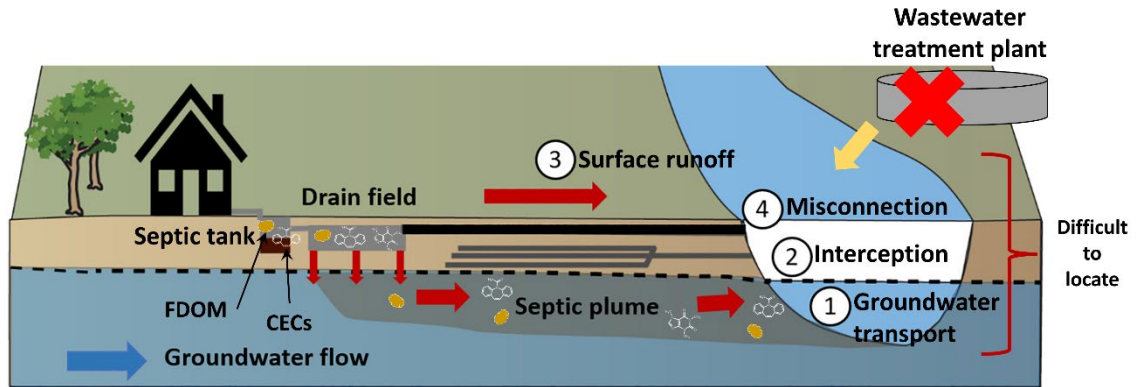


Figure 2.1. Septic wastewater transport pathways. Adapted from Tamang *et al.* (2022) <sup>22</sup>.

### 2.3 Septic system impacts

Non-sewered sanitation systems can be a major and potentially underestimated source of contaminants to the environment. Even when functioning properly, septic tank effluent contributes nutrients and other contaminants to shallow groundwater, enabling transport to streams and downstream locations <sup>18,24–27</sup>. High septic density has been linked to higher nutrient export, greater fecal pollution, and increased artificial sweetener concentrations <sup>22,28,29</sup>. Oldfield *et al.* (2020) used artificial sweeteners to estimate that 2 – 33% of septic effluent reaches adjacent streams <sup>30</sup>, and Spoelstra *et al.* (2020) reported that septic system effluent constitutes up to 0.5% of streamflow based on measured artificial sweetener concentrations <sup>31</sup>.

Septic systems are a known source of primary pollutants (*i.e.*, carbon, nitrogen, phosphorus) in nearby surface water <sup>18,24–27</sup>. Nutrient inputs from septic systems contribute to eutrophication in rural headwaters and cause ecosystem-level problems,

including algal blooms, anoxic conditions, and disruptions to in-stream nutrient cycling<sup>18,26,32,33</sup>. Septic systems often fail to remove CECs and are, therefore, sources of personal care products, pharmaceuticals, per- and polyfluoroalkyl substances, and artificial sweeteners in rural streams<sup>6,21,31,34–36</sup>. Importantly, CECs from septic systems have been confirmed to cause antibiotic resistance in streams<sup>37</sup> and have other ecotoxicological outcomes, but the relationship between CEC loads, the risks associated with those loads, and septic system density has not been assessed.

#### 2.4 Indicators of septic wastewater

Many indicators have been suggested to track septic system inputs. Some studies suggest using ions or ratiometric parameters involving ions, total nitrogen, and bacteria levels (*e.g.*, Na<sup>+</sup>, Cl<sup>-</sup>/Br<sup>-</sup>, NO<sub>3</sub><sup>-</sup>/NO<sub>2</sub><sup>-</sup>, Cl<sup>-</sup>/total nitrogen (TN), Cl<sup>-</sup>/total coliforms)<sup>25,27,38,39</sup>, but these indicators are not source specific and are more suitable as initial screening tools. One study that employed ultrahigh-resolution mass spectrometry suggested that nitrogen-containing features in the lipid- and protein-like areas of van Krevelen space could be used as indicators of septic system impacts<sup>25</sup>, but this analytical method is complex, expensive, and not quantitative. Previous reports have also used CECs, including artificial sweeteners, pharmaceuticals, and personal care products, as indicators of wastewater from septic tanks<sup>25,31,34,38–44</sup>. Artificial sweeteners are useful indicators because they are widely consumed, present at high concentrations, exclusively derived from human consumption, mobile, and persistent in the environment<sup>22,31,38,41,42,44</sup>. These features enable monitoring and source-tracking campaigns even in areas where other CECs have not been detected<sup>31,42,44</sup>.



Given the variable fate and transport of individual CECs, the composition of CECs in streams can indicate the extent of CEC attenuation in septic systems, inform how recently the wastewater entered the stream, and imply how far the CECs were transported from the source. Higher concentrations or detection frequencies for more degradable CECs (e.g., caffeine, ibuprofen) could indicate shorter or more direct transport pathways from the septic tank to the stream <sup>31,34,45</sup>. Under long-distance transport scenarios, some wastewater constituents, including pathogens, nutrients, and pharmaceuticals, may be effectively removed; however, artificial sweeteners may still be detectable due to their conservative nature and high mobility. Therefore, artificial sweeteners may not necessarily indicate the presence of other wastewater contaminants or ecological health concerns, but these indicators do provide insight for more persistent CECs <sup>31</sup>. CECs can be useful indicators but they involve expensive, resource-intensive analytical tools <sup>40,46</sup>. In this project, we employed CECs to confirm the feasibility of FDOM-based indicators, which are cheaper and easier to measure in water samples. Chapter 5 describes this analysis.

## 2.5 FDOM and EEMs in septic wastewater

Along with nutrients and CECs, septic systems introduce effluent-derived DOM (EfOM) into shallow groundwater and streams. The DOM in aquatic systems is derived from allochthonous (derived from degraded terrestrial material <sup>47</sup>), autochthonous (derived from aquatic organisms and sediments <sup>47</sup>), and anthropogenic (originating from human activities) sources. Because fluorescence signatures provide more information on DOM composition than conventional absorbance measurements, FDOM is being increasingly

used to identify the source and fate of DOM in water systems <sup>10</sup>. The fluorescence fingerprints of EfOM are significantly different than those of natural organic matter (NOM), enabling the use of EEMs to determine the presence of wastewater in stream samples <sup>11,12</sup>. EEM spectra are typically presented as contour plots with excitation wavelength on the x-axis, emission wavelength on the y-axis, and fluorescence intensity on the z-axis (Figure 2.2). Chen *et al.* (2003) delineated the fluorophores in EEMs into five major regions: (1) tyrosine-like, (2) tryptophan-like, (3) fulvic acid-like, (4) soluble microbial product-like, and (5) humic acid-like <sup>48</sup>.

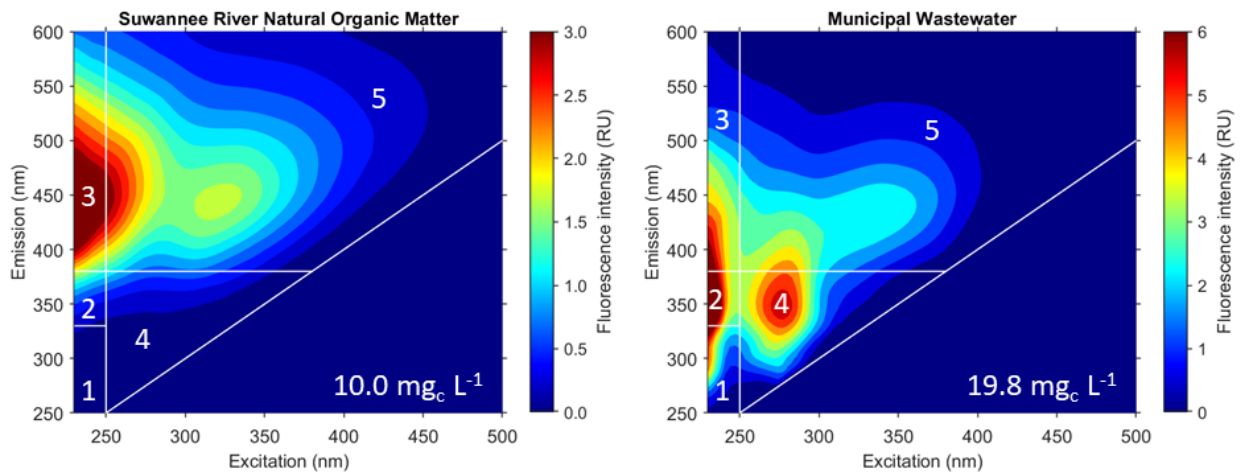


**Figure 2.2. Representative EEMs for Suwannee River natural organic matter (SRNOM) and municipal wastewater.** The five major fluorescence regions established by Chen *et al.* (2003) <sup>48</sup> are outlined and labeled in the figure.

For quantitative analysis of FDOM, the volume under each region in an EEM can be computed and normalized to the excitation-emission area of that region <sup>48</sup>. This approach allows for the comparison of spatially and temporally unique samples <sup>11</sup>. EEM regions help to characterize FDOM, but the boundaries are arbitrarily defined, and real fluorescence peaks can and often do span the regional boundaries. Parallel factor analysis (PARAFAC) can be used to establish more specific wastewater indicators for a particular

aquatic system by deconvoluting EEMs into a small number of representative components<sup>49</sup>. EEM spectroscopy and PARAFAC modeling have been used to describe FDOM in surface water, groundwater, marine water, and wastewater<sup>50–56</sup>. For example, Dubber *et al.* (2021) characterized FDOM in septic systems and drainage fields using EEMs and EEM-PARAFAC models. Their results indicated that FDOM in septic system wastewater was dominated by protein-like compounds and whitening compounds, such as the optical brighteners used in laundry detergents. As septic effluent moved through the drainfield, the fluorescence from protein-like compounds and whitening compounds decreased. Humic acid-like fluorescence increased because of contributions from terrestrially derived soil organic matter<sup>57</sup>. Richards *et al.* observed tryptophan-like fluorescence in septic tank effluent and downstream water samples<sup>39,58</sup>. This fluorescence signature was not present in upstream samples, suggesting the potential use of tryptophan-like fluorescence as an indicator of septic systems.

Other studies have identified protein-like, soluble microbial product-like, and humic acid-like fluorescence as indicators of raw and treated municipal wastewater<sup>12,55,59</sup>. CEC concentrations from wastewater inputs were positively correlated to protein-like and soluble microbial product-like fluorescence<sup>60</sup>. Tyrosine-like fluorescence was correlated to indicators of untreated wastewater (*e.g.*, caffeine, ibuprofen), while humic acid-like fluorescence was associated with more recalcitrant CECs (*e.g.*, sucralose, carbamazepine)<sup>61</sup>. Tryptophan-like fluorescence was connected to water quality parameters, including fecal coliforms and nutrients derived from wastewater inputs<sup>39,62–64</sup>. The ratio of tryptophan-like to fulvic acid-like fluorescence peaks (Peak T/Peak C) was used to identify the influence of wastewater effluent, wastewater exfiltration, and sanitary sewer

overflows in streams <sup>59,65</sup>. Given the strong soluble microbial product-like fluorescence (Region 4) in wastewater compared to SRNOM (Figure 2.2), recent work has proposed the use of a ratiometric parameter, defined as the area normalized volume of Region 4 divided by that of Region 5 (*i.e.*, R4/R5), as an indicator of wastewater; furthermore, the R2/R5 parameter was proposed for similar reasons. These ratios represent the relative concentration of EfOM to NOM <sup>7</sup>. These parameters were developed based on sampling of municipal wastewater-impacted surface water, but no studies have attempted to apply similar fluorescence indicators in subwatersheds solely impacted by septic systems. Chapter 5 describes our efforts to address this knowledge gap.

## 2.6 Storm event mobilization of septic wastewater

Several studies have investigated how discharge and wet weather events change the impacts of non-sewered sanitation systems on water quality, but those reports reached different conclusions. One study found that the highest nutrient concentrations were recorded under low discharge conditions due to the low infiltration capacity of clay soils in the drainfield, which led to rapid transport of septic wastewater to surface waters and dilution of septic inputs during storm events <sup>32</sup>. In contrast, studies with well-drained soils reported greater impacts of septic systems during high discharge because the groundwater table rose, intercepted the drainfield, and facilitated wastewater transport <sup>66,22,30,67</sup>. For example, fecal coliform counts increased up to four times during rain events compared to dry weather <sup>67</sup>, and artificial sweetener concentrations were positively correlated with stream discharge <sup>22,30</sup>. Recent work showed that fluorescence measurements can also be used to track contaminant inputs from municipal wastewater

during storm events, with the ratio of tryptophan-like to humic acid-like fluorescence increasing with the rising limb of the hydrograph and tracking with *Escherichia coli* and caffeine loads <sup>65</sup>. These findings suggest the presence of complex and site-specific transport pathways between septic tanks and streams during wet and dry weather conditions. Higher contaminant concentrations during storm events could indicate failing septic systems and the dominance of rapid surface or subsurface transport through the aforementioned mechanisms <sup>22,30,66</sup>. Lower contaminant levels during storm events suggest dilution from surface or subsurface runoff, particularly if those additional flows are not transporting septic effluent <sup>22</sup>.

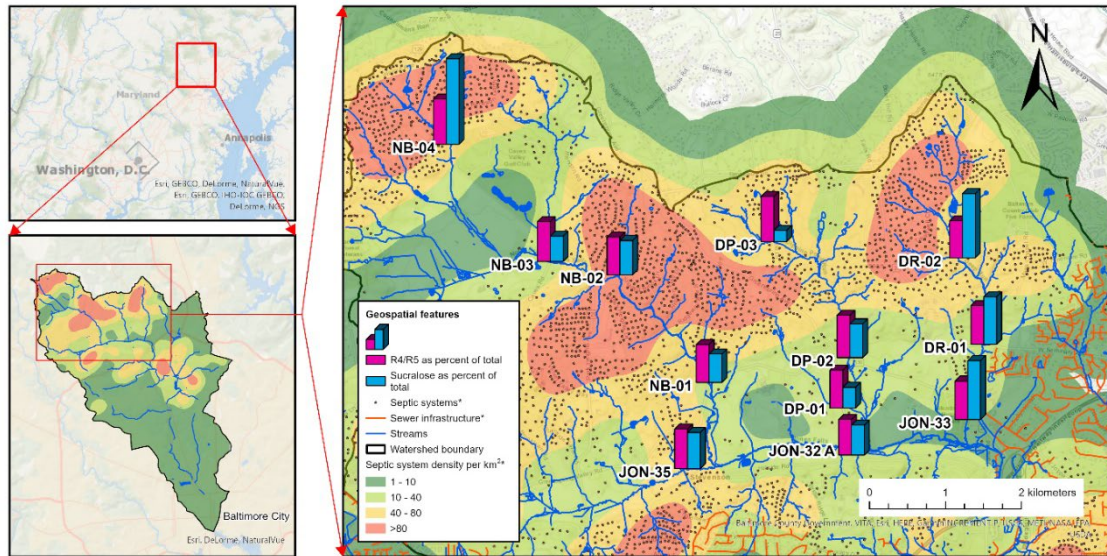
Previous sampling in the Upper Jones Falls watershed showed that the majority of wastewater-impacted samples were collected in the spring and early summer (*i.e.*, April, May, June, July) <sup>7</sup>. This could suggest a positive relationship between precipitation and the extent of septic system impacts, but that study was not designed to test this relationship. Chapter 6 seeks to address this knowledge gap.

### 2.7 Previous studies of wastewater impacts in the Jones Falls watershed and preliminary data from the Upper Jones Falls watershed

Over the past few years, our group has measured EEMs and CEC concentrations at 13 sites in the Jones Falls watershed, which contains 3,244 septic systems <sup>7</sup>. The data suggested a higher prevalence of wastewater indicators in rural/suburban areas of the Upper Jones Falls, which has 1,061 septic systems <sup>13</sup>, including high levels of FDOM-based wastewater indicators ( $R4/R5 > 0.85$ ) in 25% of samples and 100% detection

frequency for sucralose (artificial sweetener) with concentrations up to 276 ng L<sup>-1</sup> <sup>7</sup>. These outcomes were surprising because the upstream sites have lower population density, less development, and no municipal wastewater infrastructure. Instead, this area is primarily serviced by septic systems, suggesting that these non-sewered sanitation systems influence stream water quality. Previous work on the regional water balance and groundwater flow in this area highlights the importance of both natural factors (*i.e.*, soil hydraulic conductivity, porosity, geology, topography) and anthropogenic impacts (*i.e.*, residential well water demands, storm water infrastructure, urban development) <sup>68-70</sup>. For example, a portion of the Upper Jones Falls watershed is underlain by Cockeysville Marble which likely creates different groundwater dynamics than areas with schist bedrock. Local soil properties and geology are important for groundwater flow and impact how shallow groundwater moves from septic systems to nearby surface water, but a full investigation of such aspects was outside the scope of this study.

Our previous research only had three sampling sites in the Upper Jones Falls area and did not include key tributaries with higher septic density, namely Deep Run, Dipping Pond Run, and the North Branch (Figure 2.3). According to the Upper Jones Falls Small Watershed Action Plan, 99, 166, and 342 septic systems or 17.4, 22.9, and 18.6 septic systems/km<sup>2</sup> are present in Deep Run, Dipping Pond Run, and the North Branch subwatersheds, respectively <sup>13</sup>. To preliminarily evaluate the influence of septic systems on stream water quality, we collected 12 samples from sites along the major tributaries of the Upper Jones Falls watershed (Figure 2.3).



\*Data obtained from the Baltimore County Department of Environmental Protection and Sustainability, 2022

**Figure 2.3. Septic system density, preliminary sampling locations, and relative sucralose concentrations and R4/R5 values in the Upper Jones Falls.** Samples were collected in March 2022 and included three sites from previous sampling campaigns (JON) and nine new sites along the Deep Run (DR), Dipping Pond Run (DP), and North Branch (NB) tributaries. Sucralose concentrations and R4/R5 values are plotted as a percentage of the total (sum across all sites) so both parameters can be visualized on the same scale. Map created by Jahir Batista-Andrade.

In our March 2022 preliminary sampling campaign, sucralose was detected at every site at levels of 54 – 412 ng L<sup>-1</sup> (Figure 2.3). The anticonvulsant drug, carbamazepine, was also detected at every site, but the concentrations were lower than 14.6 ng L<sup>-1</sup>. Caffeine was not detected, which may indicate effective removal in septic systems or attenuation in drainage fields. The EEMs from these samples showed only minor variations, but all EEMs exhibited fluorescence in Regions 2 and 4, suggesting the possible presence of wastewater signatures. The combined CEC and EEM data suggested that all three tributaries of the Jones Falls were impacted by septic systems, but more samples needed to be collected and analyzed to verify the feasibility of using fluorescence to detect septic system impacts. The proposed fluorescence indicators could then be used to investigate the impacts of wet weather, discharge, and transport pathways on septic effluent inputs.

## Chapter 3: Materials and methods

### 3.1 Chemicals

Unless stated otherwise, all chemicals were purchased from Fisher Scientific (Hampton, USA). SRNOM (International Humic Substances Society; Denver, USA), which is a common natural organic matter reference material, was prepared following protocols from Janssen *et al.*<sup>71</sup>. The freeze-dried isolate was reconstituted to prepare a 400 mg<sub>c</sub> L<sup>-1</sup> stock solution. Most CEC standards were purchased from Sigma-Aldrich (St. Louis, USA) or Fisher Scientific. Erythromycin-d<sub>6</sub>, mecoprop-d<sub>3</sub>, sucralose-d<sub>6</sub>, and chlortetracycline-<sup>13</sup>C-d<sub>3</sub> were purchased from Toronto Research Chemicals (Toronto, Canada). Diclofenac-d<sub>4</sub> and ibuprofen-d<sub>3</sub> were obtained from Cayman Chemical (Ann Arbor, USA). Tetracycline-d<sub>6</sub> and azithromycin-d<sub>3</sub> were purchased from Santa Cruz Biotechnology (Dallas, USA), and 17 $\alpha$ -ethinylestradiol-2,4,16,16-d<sub>4</sub>, and 3-(4-methylbenzylidene-d<sub>4</sub>) camphor were acquired from CDN Isotopes (Pointe-Claire, Canada). The purity of all chemical standards was at least 95%.

All stock and working solutions were prepared in liquid chromatography-mass spectrometry (LC-MS)-grade methanol. Four spiking solutions were generated for standard additions analysis. Standard additions analysis was used to calculate analyte concentrations and absolute recovery. The four spiking solutions grouped similar analytes and corresponded to the three different methods used for liquid chromatography with tandem mass spectrometry (LC-MS/MS) analysis (Section 3.7.3): wastewater indicator spiking solution (4 analytes), herbicide spiking solution (4 analytes), antibiotics spiking solution (41 analytes), and UV filter/hormone spiking solution (21 analytes). New analytical methods were developed for the compounds in the herbicide spiking solution



for this project as runoff indicators. Atrazine (agricultural herbicide) and mecoprop (residential herbicide) were associated with non-septic sources (runoff)<sup>40,72</sup>. Paraxanthine (caffeine degradation product) enabled the evaluation of caffeine degradation in wastewater and environmental samples<sup>6</sup>. Ibuprofen (pharmaceutical) is a commonly used wastewater indicator<sup>73</sup>, but the high limit of quantitation led to few detections in environmental samples. Table 3.1 identifies the analytes included in the four spiking solutions; note, the spiked concentration was designed to be in the middle of the calibration range for environmental samples. Five internal standard solutions were also generated to correct for matrix effects that occur during electrospray ionization. Details of the five internal standard solutions are available in Table 3.2: wastewater indicators (4 internal standards), herbicides (3 internal standards), antibiotics (10 internal standards), UV filter/hormones (10 internal standards), and the mecoprop internal standard. All working solutions were stored at -20 °C.

**Table 3.1. Composition of the four spiking solutions used for standard additions analysis.**

Standard	Acronym	Molecular formula	CAS Number	Conc. (µg/L)
<i>Wastewater indicator spiking solution</i>				
Caffeine	CAF	C <sub>8</sub> H <sub>10</sub> N <sub>4</sub> O <sub>2</sub>	58-08-2	500
Carbamazepine	CBZ	C <sub>15</sub> H <sub>12</sub> N <sub>2</sub> O	298-46-4	500
Diclofenac	DIC	C <sub>14</sub> H <sub>11</sub> Cl <sub>2</sub> NO <sub>2</sub>	15307-86-5	500
Sucralose	SUC	C <sub>12</sub> H <sub>19</sub> Cl <sub>3</sub> O <sub>8</sub>	56038-13-2	1000
<i>Herbicide spiking solution</i>				
Atrazine	ATZ	C <sub>8</sub> H <sub>14</sub> ClN <sub>5</sub>	1912-24-9	500
Ibuprofen	IBU	C <sub>13</sub> H <sub>18</sub> O <sub>2</sub>	15687-27-1	500
Mecoprop	MEC	C <sub>10</sub> H <sub>11</sub> ClO <sub>3</sub>	93-65-2	1000
Paraxanthine	PAR	C <sub>7</sub> H <sub>8</sub> N <sub>4</sub> O <sub>2</sub>	611-59-6	500
<i>Antibiotics spiking solution</i>				
Azithromycin	AZI	C <sub>38</sub> H <sub>72</sub> N <sub>2</sub> O <sub>12</sub>	83905-01-5	1000
Chlortetracycline	CTC	C <sub>22</sub> H <sub>23</sub> ClN <sub>2</sub> O <sub>8</sub>	57-62-5	1000
Ciprofloxacin	CIP	C <sub>17</sub> H <sub>18</sub> FN <sub>3</sub> O <sub>3</sub>	85721-33-1	1000
Clarithromycin	CLA	C <sub>38</sub> H <sub>69</sub> NO <sub>13</sub>	81103-11-9	1000
Demeclocycline	DMC	C <sub>21</sub> H <sub>21</sub> ClN <sub>2</sub> O <sub>8</sub>	127-33-3	1000
Difloxacin	DIF	C <sub>21</sub> H <sub>19</sub> F <sub>2</sub> N <sub>3</sub> O <sub>3</sub>	91296-86-5	1000
Doxycycline	DC	C <sub>22</sub> H <sub>24</sub> N <sub>2</sub> O <sub>8</sub>	24390-14-5	1000
Enrofloxacin	ENR	C <sub>19</sub> H <sub>22</sub> FN <sub>3</sub> O <sub>3</sub>	93106-60-6	1000
Erythromycin	ERY	C <sub>37</sub> H <sub>67</sub> NO <sub>13</sub>	114-07-8	1000
Fleroxacin	FLE	C <sub>17</sub> H <sub>18</sub> F <sub>3</sub> N <sub>3</sub> O <sub>3</sub>	79660-72-3	1000
Gatifloxacin	GAT	C <sub>19</sub> H <sub>22</sub> FN <sub>3</sub> O <sub>4</sub>	112811-59-3	1000
Lomefloxacin	LOM	C <sub>17</sub> H <sub>19</sub> F <sub>2</sub> N <sub>3</sub> O <sub>3</sub>	98079-51-7	1000
Marbofloxacin	MAR	C <sub>17</sub> H <sub>19</sub> FN <sub>4</sub> O <sub>4</sub>	115550-35-1	1000
Meclocycline	MC	C <sub>22</sub> H <sub>21</sub> ClN <sub>2</sub> O <sub>8</sub>	2013-58-3	1000
Methacycline	MTC	C <sub>22</sub> H <sub>22</sub> N <sub>2</sub> O <sub>8</sub>	914-00-1	1000
Moxifloxacin	MOX	C <sub>21</sub> H <sub>24</sub> FN <sub>3</sub> O <sub>4</sub>	186826-86-8	1000
Nadifloxacin	NAD	C <sub>19</sub> H <sub>21</sub> FN <sub>2</sub> O <sub>4</sub>	124858-35-1	1000
Norfloxacin	NOR	C <sub>16</sub> H <sub>18</sub> FN <sub>3</sub> O <sub>3</sub>	70458-96-7	1000
Ofloxacin	OFL	C <sub>18</sub> H <sub>20</sub> FN <sub>3</sub> O <sub>4</sub>	82419-36-1	1000
Orbifloxacin	ORB	C <sub>19</sub> H <sub>20</sub> F <sub>3</sub> N <sub>3</sub> O <sub>3</sub>	113617-63-3	1000
Oxytetracycline	OTC	C <sub>22</sub> H <sub>24</sub> N <sub>2</sub> O <sub>9</sub>	79-57-2	1000
Pefloxacin	PEF	C <sub>17</sub> H <sub>20</sub> FN <sub>3</sub> O <sub>3</sub>	70458-92-3	1000
Roxithromycin	ROX	C <sub>41</sub> H <sub>76</sub> N <sub>2</sub> O <sub>15</sub>	80214-83-1	1000
Sarafloxacin	SAR	C <sub>20</sub> H <sub>17</sub> F <sub>2</sub> N <sub>3</sub> O <sub>3</sub>	98105-99-8	1000
Sparfloxacin	SPA	C <sub>19</sub> H <sub>22</sub> F <sub>2</sub> N <sub>4</sub> O <sub>3</sub>	110871-86-8	1000
Sulfacetamide	SCM	C <sub>8</sub> H <sub>10</sub> N <sub>2</sub> O <sub>3</sub> S	144-80-9	1000
Sulfadiazine	SDZ	C <sub>10</sub> H <sub>10</sub> N <sub>4</sub> O <sub>2</sub> S	68-35-9	1000
Sulfadimethoxine	SDM	C <sub>12</sub> H <sub>14</sub> N <sub>4</sub> O <sub>4</sub> S	122-11-2	1000
Sulfadoxine	SDX	C <sub>12</sub> H <sub>14</sub> N <sub>4</sub> O <sub>4</sub> S	2447-57-6	1000
Sulfamerazine	SMR	C <sub>11</sub> H <sub>12</sub> N <sub>4</sub> O <sub>2</sub> S	127-79-7	1000
Sulfamethazine	SDD	C <sub>12</sub> H <sub>14</sub> N <sub>4</sub> O <sub>2</sub> S	57-68-1	1000

<b>Standard</b>	<b>Acronym</b>	<b>Molecular formula</b>	<b>CAS Number</b>	<b>Conc. (µg/L)</b>
Sulfamethizole	SMZ	C <sub>9</sub> H <sub>10</sub> N <sub>4</sub> O <sub>2</sub> S <sub>2</sub>	144-82-1	1000
Sulfamethoxazole	SMX	C <sub>10</sub> H <sub>11</sub> N <sub>3</sub> O <sub>3</sub> S	723-46-6	1000
Sulfaphenazole	SPZ	C <sub>15</sub> H <sub>14</sub> N <sub>4</sub> O <sub>2</sub> S	526-08-9	1000
Sulfapyridine	SPD	C <sub>11</sub> H <sub>11</sub> N <sub>3</sub> O <sub>2</sub> S	144-83-2	1000
Sulfaquinolaxaline	SQX	C <sub>14</sub> H <sub>12</sub> N <sub>4</sub> O <sub>2</sub> S	59-40-5	1000
Sulfathiazole	STZ	C <sub>9</sub> H <sub>9</sub> N <sub>3</sub> O <sub>2</sub> S <sub>2</sub>	72-14-0	1000
Sulfisomidine	SSD	C <sub>12</sub> H <sub>14</sub> N <sub>4</sub> O <sub>2</sub> S	515-64-0	1000
Tetracycline	TC	C <sub>22</sub> H <sub>24</sub> N <sub>2</sub> O <sub>8</sub>	60-54-8	1000
Tosufloxacin	TOS	C <sub>19</sub> H <sub>15</sub> F <sub>3</sub> N <sub>4</sub> O <sub>3</sub>	100490-36-6	1000
Tylosin	TYL	C <sub>46</sub> H <sub>77</sub> NO <sub>17</sub>	1401-69-0	1000
<b><i>UV filters/hormones spiking solution</i></b>				
17α-ethinylestradiol	EE2	C <sub>20</sub> H <sub>24</sub> O <sub>2</sub>	57-63-6	500
17β-estradiol	E2	C <sub>18</sub> H <sub>24</sub> O <sub>2</sub>	50-28-2	500
2-ethylhexyl 4-methoxycinnamate	EHMC	C <sub>18</sub> H <sub>26</sub> O <sub>3</sub>	5466-77-3	500
3-(4-methylbenzylidene) camphor	4-MBC	C <sub>18</sub> H <sub>22</sub> O	36861-47-9	500
Androsterone	AN	C <sub>19</sub> H <sub>30</sub> O <sub>2</sub>	53-41-8	5000
Avobenzone	BMDBM	C <sub>20</sub> H <sub>22</sub> O <sub>3</sub>	70356-09-1	500
Cinoxate	CX	C <sub>14</sub> H <sub>18</sub> O <sub>4</sub>	104-28-9	500
Dioxybenzone	BP-8	C <sub>14</sub> H <sub>12</sub> O <sub>4</sub>	131-53-3	500
Ensulizole	ESZ	C <sub>13</sub> H <sub>10</sub> N <sub>2</sub> O <sub>3</sub> S	27503-81-7	1000
Equilin	EN	C <sub>18</sub> H <sub>20</sub> O <sub>2</sub>	474-86-2	500
Estetrol	E4	C <sub>18</sub> H <sub>24</sub> O <sub>4</sub>	15183-37-6	1000
Estriol	E3	C <sub>18</sub> H <sub>24</sub> O <sub>3</sub>	50-27-1	1000
Estrone	E1	C <sub>18</sub> H <sub>22</sub> O <sub>2</sub>	53-16-7	500
Homosalate	HMS	C <sub>16</sub> H <sub>22</sub> O <sub>3</sub>	118-56-9	500
Octisalate	OS	C <sub>15</sub> H <sub>22</sub> O <sub>3</sub>	118-60-5	500
Octocrylene	OC	C <sub>24</sub> H <sub>27</sub> NO <sub>2</sub>	6197-30-4	500
Oxybenzone	BP-3	C <sub>14</sub> H <sub>12</sub> O <sub>3</sub>	131-57-7	500
Padimate O	ODPABA	C <sub>17</sub> H <sub>27</sub> NO <sub>2</sub>	21245-02-3	10
Progesterone	P4	C <sub>21</sub> H <sub>30</sub> O <sub>2</sub>	57-83-0	500
Sulisobenzene	SSB	C <sub>14</sub> H <sub>12</sub> O <sub>6</sub> S	4065-45-6	100
Trolamine salicylate	TEAS	C <sub>13</sub> H <sub>21</sub> NO <sub>6</sub>	2174-16-5	50

**Table 3.2. Internal standard solutions used to account for matrix effects during LC-MS/MS analysis.**

Internal standard	Acronym	Molecular formula	CAS Number	Conc. (µg/L)	Corresponding analytes
<i>Wastewater indicators</i>					
Caffeine-d <sub>9</sub>	CAF-d <sub>9</sub>	C <sub>8</sub> D <sub>9</sub> HN <sub>4</sub> O <sub>2</sub>	72238-85-8	500	CAF
Carbamazepine-d <sub>10</sub>	CBZ-d <sub>10</sub>	C <sub>15</sub> H <sub>2</sub> D <sub>10</sub> N <sub>2</sub> O	132183-78-9	500	CARB
Diclofenac-d <sub>4</sub>	DIC-d <sub>4</sub>	C <sub>14</sub> H <sub>7</sub> D <sub>4</sub> Cl <sub>2</sub> NO <sub>2</sub>	153466-65-0	500	DIC
Sucralose-d <sub>6</sub>	SUC-d <sub>6</sub>	C <sub>12</sub> H <sub>13</sub> D <sub>6</sub> Cl <sub>3</sub> O <sub>8</sub>	1459161-55-7	1000	SUC
<i>Herbicides</i>					
Atrazine-d <sub>5</sub>	ATZ-d <sub>5</sub>	C <sub>8</sub> H <sub>9</sub> D <sub>5</sub> ClN <sub>5</sub>	163165-75-1	500	ATZ
Ibuprofen-d <sub>3</sub>	IBU-d <sub>3</sub>	C <sub>13</sub> D <sub>3</sub> H <sub>15</sub> O <sub>2</sub>	121662-14-4	500	IBU
Paraxanthine-d <sub>6</sub>	PAR-d <sub>6</sub>	C <sub>7</sub> H <sub>2</sub> D <sub>6</sub> N <sub>4</sub> O <sub>2</sub>	117490-41-2	500	PAR
<i>Antibiotics</i>					
Azithromycin-d <sub>3</sub>	AZI-d <sub>3</sub>	C <sub>38</sub> H <sub>69</sub> D <sub>3</sub> N <sub>2</sub> O <sub>12</sub>	163921-65-1	100	AZI, CLA
Chlorotetracycline- <sup>13</sup> C-d <sub>3</sub>	CTC- <sup>13</sup> C-d <sub>3</sub>	C <sub>21</sub> <sup>13</sup> CH <sub>21</sub> D <sub>3</sub> Cl <sub>2</sub> N <sub>2</sub> O <sub>8</sub>	57-62-5 <sup>a</sup>	100	CTC, DMC, DC, MC, MTC
Ciprofloxacin-d <sub>8</sub>	CIP-d <sub>8</sub>	C <sub>17</sub> H <sub>10</sub> D <sub>8</sub> FN <sub>3</sub> O <sub>3</sub>	1130050-35-9	100	CIP, ENR, LOM
Difloxacin-d <sub>3</sub>	DIF-d <sub>3</sub>	C <sub>21</sub> H <sub>16</sub> D <sub>3</sub> F <sub>2</sub> N <sub>3</sub> O <sub>3</sub>	1173147-93-7	100	DIF, GAT, MOX, NAD, ORB, SAR, SPA, TOS
Erythromycin-d <sub>6</sub>	ERY-d <sub>6</sub>	C <sub>37</sub> H <sub>61</sub> D <sub>6</sub> NO <sub>13</sub>	959119-25-6	100	ERY, ROX, TYL
Ofloxacin-d <sub>3</sub>	OFL-d <sub>3</sub>	C <sub>18</sub> D <sub>3</sub> H <sub>17</sub> FN <sub>3</sub> O <sub>4</sub>	1173147-91-5	100	FLE, MAR, NOR, OFL, PEF
Sulfamethizole- <sup>13</sup> C <sub>6</sub>	SMZ- <sup>13</sup> C <sub>6</sub>	<sup>13</sup> C <sub>6</sub> C <sub>3</sub> H <sub>10</sub> N <sub>4</sub> O <sub>2</sub> S <sub>2</sub>	1334378-92-5	100	SCM, SDZ, SMR, SDD, SMZ, SPD, STZ, SSD
Sulfamethoxazole- <sup>13</sup> C <sub>6</sub>	SMX- <sup>13</sup> C <sub>6</sub>	<sup>13</sup> C <sub>6</sub> C <sub>4</sub> H <sub>11</sub> N <sub>3</sub> O <sub>3</sub> S	1196157-90-0	100	SMX, SPZ
Sulfaquinolaxaline- <sup>13</sup> C <sub>6</sub>	SQX- <sup>13</sup> C <sub>6</sub>	C <sub>8</sub> <sup>13</sup> C <sub>6</sub> H <sub>12</sub> N <sub>4</sub> O <sub>2</sub> S	1202864-52-5	100	SDM, SDX, SQX
Tetracycline-d <sub>6</sub>	TC-d <sub>6</sub>	C <sub>22</sub> H <sub>18</sub> D <sub>6</sub> N <sub>2</sub> O <sub>8</sub>	60-54-8 <sup>a</sup>	100	OTC, TC
<i>UV filters and hormones</i>					
2-ethyl-d <sub>5</sub> -hexyl-2,3,3,4,4,5,5,6,6,6-d <sub>10</sub> 4-methoxycinnamate	EHMC-d <sub>15</sub>	C <sub>18</sub> D <sub>15</sub> H <sub>11</sub> O <sub>3</sub>	1793071-38-1	100	EHMC
3-(4-methylbenzylidene-d <sub>4</sub> ) camphor	4-MBC-d <sub>4</sub>	C <sub>18</sub> H <sub>18</sub> D <sub>4</sub> O	1219806-41-3	100	4-MBC
17α-ethinylestradiol-2,4,16,16-d <sub>4</sub>	EE2-d <sub>4</sub>	C <sub>20</sub> H <sub>20</sub> D <sub>4</sub> O <sub>2</sub>	350820-06-3	100	EE2
17β-estradiol-16,16,17-d <sub>3</sub>	E2-d <sub>3</sub>	C <sub>18</sub> D <sub>3</sub> H <sub>21</sub> O <sub>2</sub>	79037-37-9	1000	E2, EN, E4, E3, E1

<b>Internal standard</b>	<b>Acronym</b>	<b>Molecular formula</b>	<b>CAS Number</b>	<b>Conc. (µg/L)</b>	<b>Corresponding analytes</b>
Benzoic acid-d <sub>5</sub>	BA-d <sub>5</sub>	C <sub>7</sub> HD <sub>5</sub> O <sub>2</sub>	1079-02-3	500	ESZ, SSB, TEAS
Benzophenone-d <sub>10</sub>	BP-d <sub>10</sub>	(C <sub>6</sub> D <sub>5</sub> ) <sub>2</sub> CO	22583-75-1	1000	CX, BP-8
Homosalate-(benzoic ring-d <sub>4</sub> )	HMS-d <sub>4</sub>	C <sub>16</sub> D <sub>4</sub> H <sub>18</sub> O <sub>3</sub>	118-56-9 <sup>a</sup>	1000	HMS, OS
Octocrylene-(2-ethyl-d <sub>5</sub> -hexyl-2,3,3,4,4,5,5,6,6,6-d <sub>10</sub> )	OC-d <sub>15</sub>	C <sub>24</sub> D <sub>15</sub> H <sub>12</sub> NO <sub>2</sub>	6197-30-4 <sup>a</sup>	100	BMDBM, OC, ODPABA
Oxybenzone-(phenyl-d <sub>5</sub> )	BP-3-d <sub>5</sub>	C <sub>14</sub> D <sub>5</sub> H <sub>7</sub> O <sub>3</sub>	1219798-54-5	100	BP-3
Progesterone-d <sub>9</sub>	P4-d <sub>9</sub>	C <sub>21</sub> H <sub>21</sub> D <sub>9</sub> O <sub>2</sub>	15775-74-3	100	AN, P4
<b><i>Mecoprop</i></b>					
Mecoprop-d <sub>3</sub>	MEC-d <sub>3</sub>	C <sub>10</sub> H <sub>8</sub> D <sub>3</sub> ClO <sub>3</sub>	352431-15-3	500	MEC

a: CAS numbers were not available for these compounds, the listed CAS number are for the analogous compounds without mass labels

## 3.2 Wastewater sampling

### *3.2.1 Municipal wastewater sampling*

Municipal wastewater samples were collected from the Jones Falls Pumping Station (Baltimore, MD) in June, July, October, and December 2022. The pumping station is located 11 miles downstream of the confluence of the Jones Falls and the North Branch. Grab samples were manually collected from the inflow to the pumping station. The 1-L amber glass sample bottles were rinsed once with wastewater before the sample was collected with no headspace.

### *3.2.2 Septic wastewater sampling*

Septic wastewater samples were collected from three conventional septic tanks, which are representative of non-sewered sanitation systems in this region, and one newer system designed for advanced nutrient removal. The septic samples were collected within a week of the municipal wastewater samples. In the three conventional tanks, samples were collected from the cleanout pipe located near the inlet of the tank using a customized sampling device. The advanced septic system included an inlet pretreatment holding tank, an extended aeration chamber, and a final clarification and effluent pumping unit that leads to the drainfield. The system had large access covers, which allowed us to easily collect samples from the inlet and outlet tanks. All sampling bottles were rinsed once with septic wastewater before the sample was collected. All sites were sampled in June, July, October, and December 2022. One of the conventional septic tanks (labeled Septic

C, below) was pumped out in September 2022, which provided more information about how sludge removal impacted the CEC levels and FDOM signatures in the tank.

Three septic sludge samples were collected from septic pumping trucks in July, October, and December 2022. Sludge samples were separated into liquid and solid contents. To achieve this separation, 50-mL aliquots were transferred to centrifuge tubes and centrifuged at 6000g for 10 min. The supernatant was analyzed for both EEMs and CECs, and the solids were combined and stored at -20 °C until further processing and analysis for CECs.

### 3.3 Stream sampling

#### *3.3.1 North Branch walkup sampling*

After seven days without rain, 103 100-mL and 45 1-L samples were collected from different locations of the North Branch of the Jones Falls for analysis of EEMs and CECs, respectively. This campaign occurred over two consecutive dry days (June 30 – July 1, 2022). Samples were collected in amber-glass bottles at low flow. The filled bottles were carried in cooler backpacks with ice and transferred to an ice-filled cooler after each section. The stream was divided into five sections to facilitate sample drop-offs (Figure 3.1). Water was flowing through the Sections 1-3, which were sampled on the first day. The last sample from June 30 and the first sample from July 1 were collected from the same location to assess the consistency of water quality parameters across the 2-d campaign. Sections 4-5 were completed on the second day. Because the streambed dried out, we only collected samples from a 0.6-km stretch of section 4. Three samples

were collected from standing water in the dry streambed of this section; however, those samples (*i.e.*, NB-82, NB-83, NB-84) were hydrologically disconnected from the others (Figure 3.1). Water was flowing for 0.9 km in section 5 before the stream dried out again. The coordinates of each sampling location were recorded using the Gaia GPS app (Table A.1). To prevent contamination, all members of the sampling team avoided the consumption of pharmaceuticals, caffeine, and sucralose for 24 h before the campaign. For similar reasons, team members did not wear sunscreen. A field blank of deionized water was carried during the campaign to identify any potential contamination that could occur in the field. Samples were transported to the lab and processed at the end of each day.



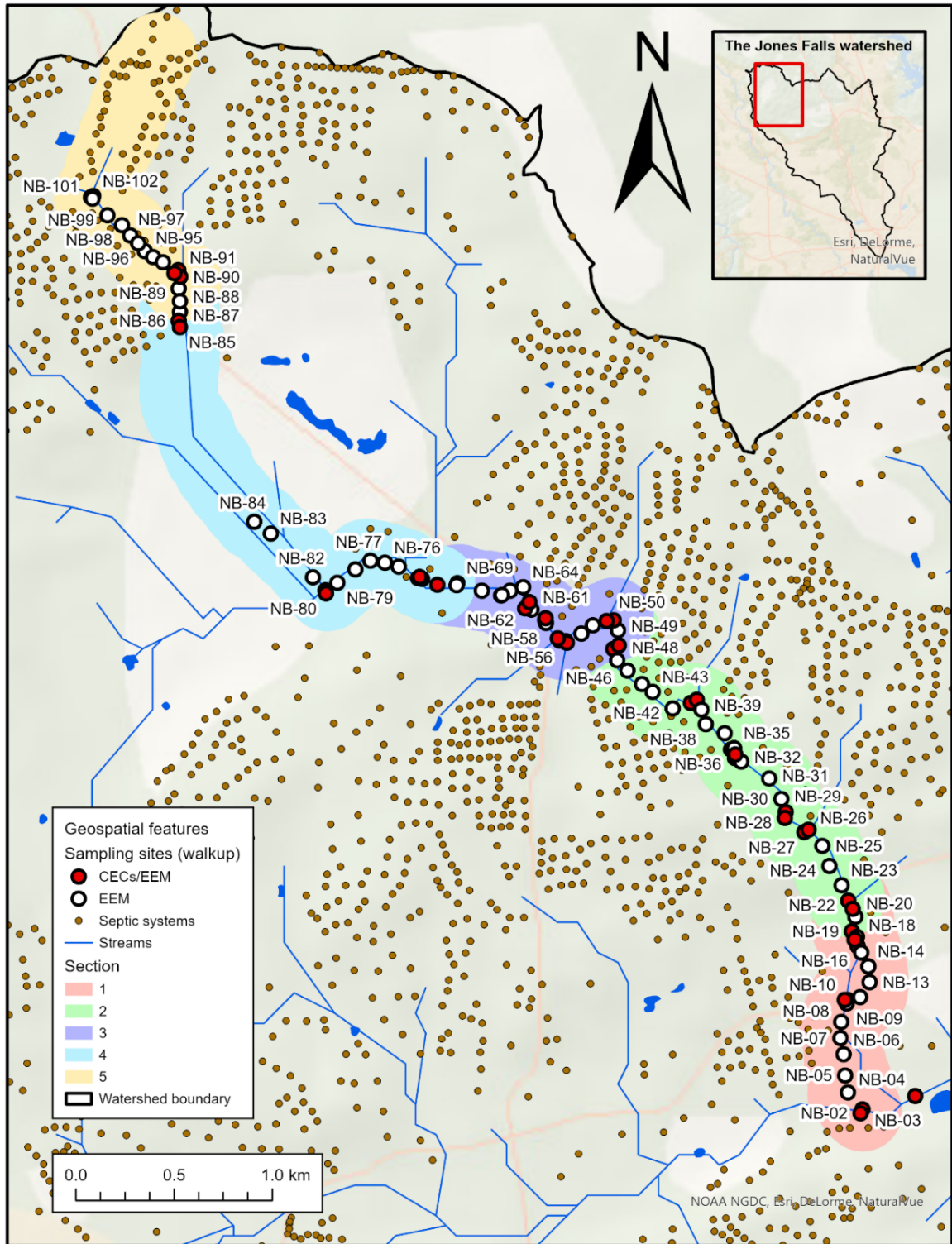


Figure 3.1. The sampling sections and sites in the North Branch of the Jones Falls.

### *3.3.2 TIR survey and groundwater seep sampling*

In September 2022, we borrowed a FLIR thermal infrared camera (Wilsonville, OR) from the United States Geological Survey Maryland-Delaware-D.C. Water Science Center (Catonsville, MD). On September 8-10, 20-21, and 23-24, the TIR camera was used to survey sections of the North Branch. In particular, the TIR camera was employed to scan both banks of the stream for areas where the surface temperature was significantly colder than the rest of the surface water. Such observations indicate areas with preferential groundwater discharges. The TIR camera only measured the temperature at the water surface and was not able to directly identify discharges in the streambed. We recorded the locations using the Gaia GPS app and marked them using flags (Table A.2). We took photographs of each location using the TIR camera and my phone.

The TIR measurements were initiated in section 5, where the highest CEC concentrations were measured, but no obvious groundwater inputs were discovered. Based on the TIR data from sections 1, 2, and 3, we selected 2, 13, and 11 sites, respectively, for further analysis (Figure 3.2). Six sites (GW-03 to GW-08) in section 2 were included, but preferential groundwater pathways were not confirmed by TIR due to the negligible temperature gradients caused by the cool surface water on September 24. After five days without rain, samples were collected from the 26 sites (September 27-28) for analysis of EEMs and CECs. Where possible, samples were collected directly from the groundwater seep. The other samples were collected from the surface water adjacent to the seep. Samples were carried in a cooler backpack with ice before being transferred to coolers and transported to the laboratory. A field blank of deionized water was carried during the sampling campaign for quality assurance and quality control purposes.

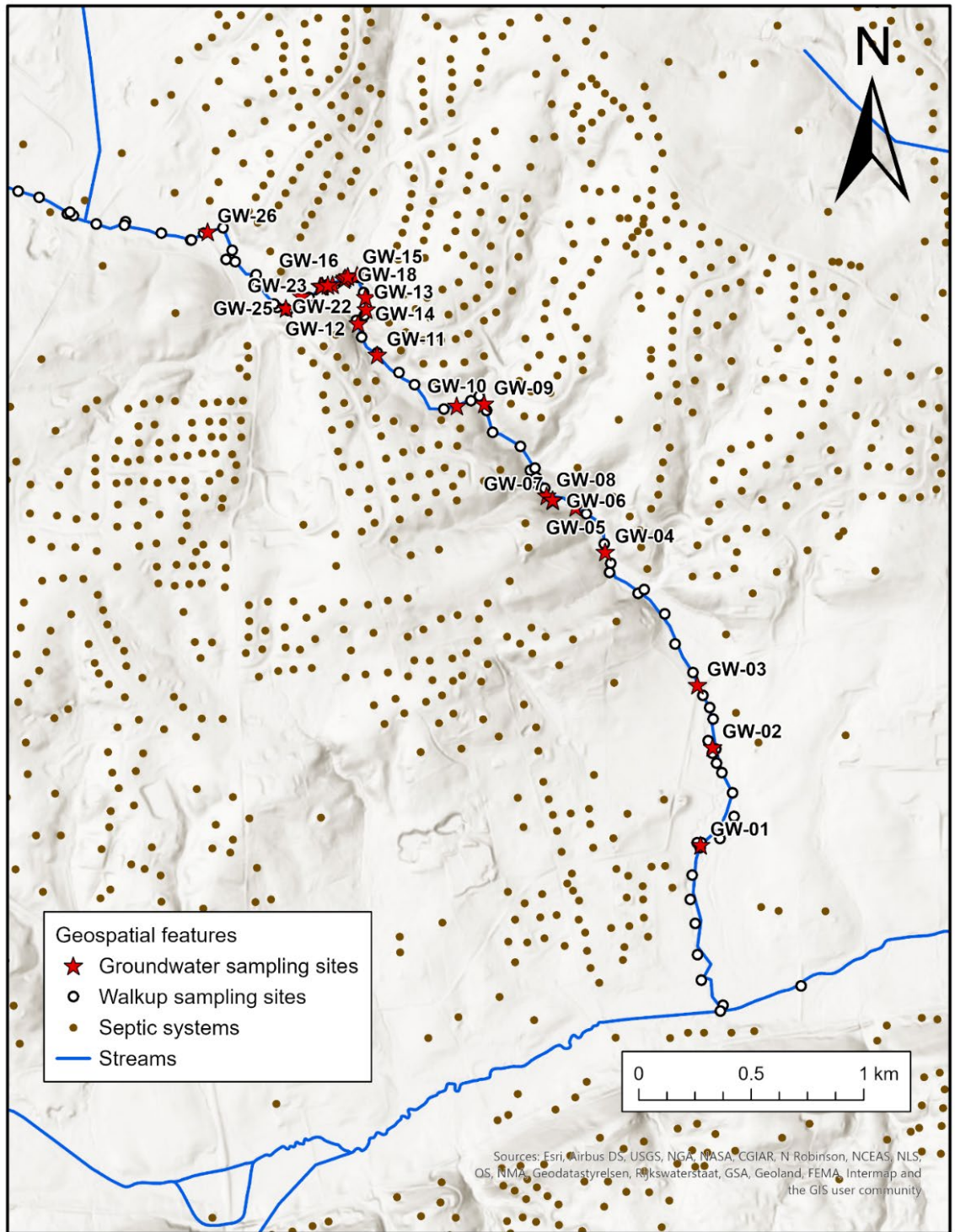
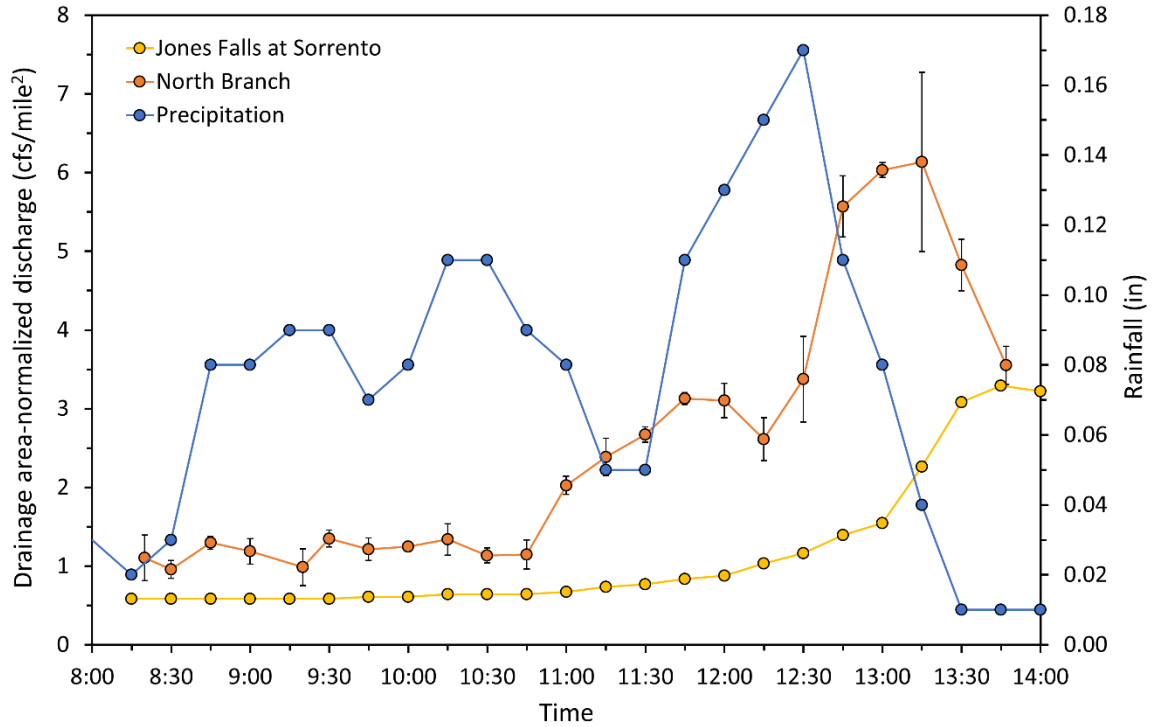


Figure 3.2. Groundwater seep sampling sites selected based on the TIR survey.

### 3.3.3 *Wet weather sampling*

Samples were collected from NB-89 in section 5 (Figure 3.1) during a storm event on November 11, 2022. No rain occurred for five days before this date. The site was selected based on easy access to the stream (for safety reasons) and previous data, which indicated high CEC concentrations. Weather predictions indicated that most rainfall would occur at 9:00 – 10:00 am. Based on that estimate, sampling was initiated at 8:15 am. The rainfall peaked at 12:30 pm, and we captured the rising limb of the hydrograph before concluding the campaign at 1:35 pm (Figure 3.3). Rainfall data was downloaded from Weather Underground Station KMDOWING43 located near the NB-89 sampling site. Two 130-mL samples were collected in amber-glass bottles every 5 min and stored in a cooler until being transported to the lab. A field blank of deionized water was stored with the samples. After returning to the lab, five 160-mL aliquots from each time point were composited to create an 800-mL sample for CEC analysis for each 20-min period; one exception was the 8:15 – 8:40 am period, for which six samples were combined. The remaining 100-mL samples were frozen at -20 °C for EEM analysis at the 5-min interval level.



**Figure 3.3. Discharge measurements in the North Branch and from the USGS gauge for the Jones Falls at Sorrento, MD (latitude 39.23447, longitude -76.39464) normalized to the drainage area with precipitation data for November 11, 2022.**

To measure stream discharge, we staked a level string several feet above the water surface at the midpoint of a straight 25-ft section of the stream and determined the streambed profile by measuring the distance to the string in 6-in increments. The water depth was measured every 15 min at a marked location in the middle of the stream (Figure 3.4). The streambed profile and water depth were used to calculate the cross-sectional area, which was multiplied by the stream velocity to determine discharge. Stream velocity (average  $\pm$  standard deviation) was calculated using the time it took for three tennis balls to travel down the 25-ft reach. Figure 3.3 shows the measured discharge in the North Branch compared to the discharge recorded by the USGS gauge located 14 km downstream. Both discharges were normalized to their drainage area to compare the

shape of the hydrographs, which exhibited a similar profile (Spearman correlation  $\rho = 0.896, p < 0.01$ ). The North Branch drainage area was 0.69 square miles and the USGS gage at Sorrento has a drainage area of 25.2 square miles. The North Branch peak discharge of  $4.23 \text{ ft}^3 \text{ s}^{-1}$  (cfs) was offset 30 min from the peak precipitation. The initial discharge before 11:00 am (*i.e.*, 0.66 – 0.93 cfs) was similar to the low flow discharge (*i.e.*, 0.75 cfs) measured 24 days later for comparative purposes. The USGS gage recorded a peak discharge of 83.0 cfs, which placed this storm in the 30 biggest storms of 2022.

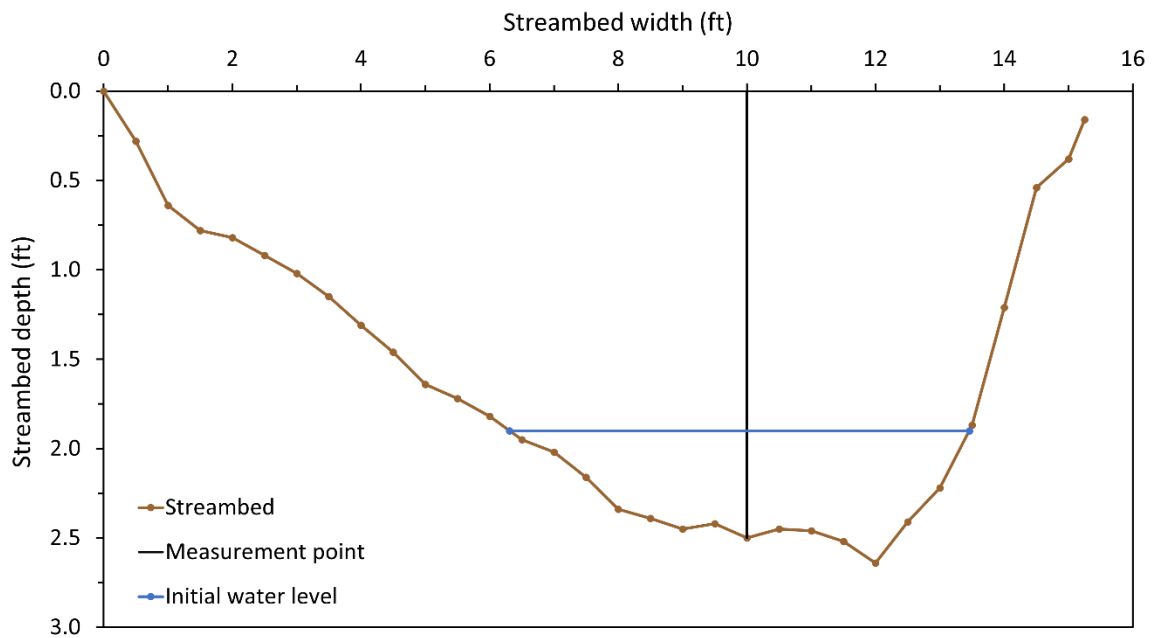


**Figure 3.4.** The streambed profile and water level were used to measure the cross-sectional area and calculate discharge.

### 3.4 EEM analysis

The 100-mL stream samples gathered for EEM analysis were collected in amber-glass bottles, stored on ice in a cooler, transported to the lab, and kept at  $-20 \text{ }^\circ\text{C}$ . Wastewater samples were passed through a  $1.2\text{-}\mu\text{m}$ , glass-fiber filter and then stored at  $-20 \text{ }^\circ\text{C}$ . Before

analysis, samples were thawed to room temperature and passed through a 0.45- $\mu\text{m}$  hydrophilic polyvinylidene fluoride syringe filter, which was pre-rinsed with 60 mL of deionized water and conditioned with 10 mL of sample. For stream samples, the next 4 mL of the filtrate were added to a quartz cuvette with a 1-cm optical pathlength for EEM analysis. Wastewater samples were measured after 2, 4, and 8 $\times$  dilution with deionized water to reduce inner filter effects. EEMs were measured by an Aqualog (Horiba Scientific; Edison, USA) fluorescence spectrometer at excitation wavelengths of 230 – 500 nm and emission wavelengths of 250 – 600 nm. The analysis used an integration time of 2 s and step sizes of 3 nm and 3.2 nm for the excitation and emission wavelengths, respectively.

The EEMs were blank-corrected using deionized water and converted to Raman Units (RU) using a sealed Raman water fluorescence standard (Agilent Technologies; Santa Clara, USA). The Aqualog recorded both fluorescence and absorbance data, allowing for direct correction of inner filter effects. Rayleigh and Raman scattering were removed from the raw data using the Horiba masking tool. Residual scattering was removed using Matlab R2021b (Mathworks; Natick, USA). A 10 mg<sub>c</sub> L<sup>-1</sup> SRNOM solution was run every ten samples for quality control purposes. EEMs were plotted in Matlab as contour plots with excitation wavelength on the x-axis, emission wavelength on the y-axis, and fluorescence intensity on the z-axis; dilution factors were accounted for when plotting the EEMs. A Matlab program adapted from Gonsior *et al.*<sup>74</sup> was used to calculate regional volumes ( $\Phi_i$ ) (Eq. 1) and the other spectral parameters noted in Table 3.3. For quantitative analysis, the volume under each region was normalized to the excitation-



emission area within that region ( $\Phi_{area-norm,i}$ ) using Eq. 2<sup>48</sup>. The fractional area-normalized volumes ( $\Phi_{frac,area-norm,i}$ ) of each region were calculated with Eq. 3.

$$\Phi_i = \sum_{ex(i)} \sum_{em(i)} I_{FL}(\lambda_{ex}, \lambda_{em}) \Delta\lambda_{ex} \Delta\lambda_{em} \quad (\text{Eq. 1})$$

$$\Phi_{area-norm,i} = \frac{\Phi_i}{\Delta\lambda_{ex(i)} \Delta\lambda_{em(i)}} \quad (\text{Eq. 2})$$

$$\Phi_{frac,area-norm,i} = \frac{\Phi_{area-norm,i}}{\sum_i \Phi_{area-norm,i}} \quad (\text{Eq. 3})$$

In Eq. 1-3,  $I_{FL}(\lambda_{ex}, \lambda_{em})$  is the fluorescence intensity at specified excitation ( $\lambda_{ex}$ ) and emission ( $\lambda_{em}$ ) wavelengths, the fluorescence intensities were summed over the boundaries of Region  $i$ , and the total fluorescence was normalized ( $\Phi_{area-norm,i}$ ) to the calculated areas ( $\Delta\lambda_{ex(i)} \Delta\lambda_{em(i)}$ ) of each region: 1600 nm<sup>2</sup> (Region 1); 1000 nm<sup>2</sup> (Region 2); 4400 nm<sup>2</sup> (Region 3); 8450 nm<sup>2</sup> (Region 4); and 47,800 nm<sup>2</sup> (Region 5). The area-normalized regional volume of Region  $i$  was then divided by the sum of all five area-normalized regional volumes to get the fractional area-normalized regional volumes. Building on recently proposed ratiometric wastewater indicators from Batista-Andrade *et al.*<sup>7</sup>, specific regional ratios were calculated for R1/R5 (Eq. 4), R2/R5 (Eq. 5), and R4/R5 (Eq. 6) using area-normalized regional volumes.

$$\frac{R1}{R5} = \frac{\Phi_{area-norm,1}}{\Phi_{area-norm,5}} \quad (\text{Eq. 4})$$

$$\frac{R2}{R5} = \frac{\Phi_{area-norm,2}}{\Phi_{area-norm,5}} \quad (\text{Eq. 5})$$

$$\frac{R4}{R5} = \frac{\Phi_{area-norm,4}}{\Phi_{area-norm,5}} \quad (\text{Eq. 6})$$



**Table 3.3. Measured absorbance and fluorescence parameters with descriptions.**

<b>Parameter</b>	<b>Description</b>	<b>Calculation</b>	<b>Reference</b>
<b>Absorbance</b>			
UV <sub>254</sub>	Measure of DOM aromaticity	$A_{254}$	Derrien et al. (2017) <sup>75</sup>
E2:E3	Inversely proportional to humic substance aromaticity and molecular weight	$\frac{A_{254}}{A_{365}}$	Derrien et al. (2017) <sup>75</sup>
<b>Fluorescence</b>			
Region 1	Tyrosine-like fluorophores	$\lambda_{ex}$ : 200–250 $\lambda_{em}$ : 280–330	Chen <i>et al.</i> (2003) <sup>48</sup>
Region 2	Tryptophan-like fluorophores	$\lambda_{ex}$ : 200–250 $\lambda_{em}$ : 330–380	Chen <i>et al.</i> (2003) <sup>48</sup>
Region 3	Fulvic acid-like fluorophores	$\lambda_{ex}$ : 200–250 $\lambda_{em}$ : 380–600	Chen <i>et al.</i> (2003) <sup>48</sup>
Region 4	Soluble microbial product-like fluorophores	$\lambda_{ex}$ : 250–340 $\lambda_{em}$ : 280–380	Chen <i>et al.</i> (2003) <sup>48</sup>
Region 5	Humic acid-like fluorophores	$\lambda_{ex}$ : 250–500 $\lambda_{em}$ : 380–600	Chen <i>et al.</i> (2003) <sup>48</sup>
Peak A	Humic-like fluorophores (UVC)	$\lambda_{ex}$ : 250–260 $\lambda_{em}$ : 400–460	Coble (2007) <sup>76</sup>
Peak C	Humic-like fluorophores (UVA)	$\lambda_{ex}$ : 320–360 $\lambda_{em}$ : 420–460	Coble (2007) <sup>76</sup>
Peak B	Tyrosine-like fluorophores	$\lambda_{ex}$ : 270–280 $\lambda_{em}$ : 300–320	Coble (2007) <sup>76</sup>
Peak T	Tryptophan-like fluorophores	$\lambda_{ex}$ : 270–280 $\lambda_{em}$ : 320–350	Coble (2007) <sup>76</sup>
Fluorescence Index (FI)	Indicates if DOM source is microbial (>1.9), terrestrial (<1.4), or blended (1.4-1.9)	$\frac{I_{Em450,Ex370}}{I_{Em500,Ex370}}$	Lu <i>et al.</i> (2022) <sup>77</sup>
Biological Index (BIX)	Proportion of recently produced DOM: low autochthonous origin (0.6-0.8), moderate autochthonous origin (0.8-1.0), or recent biological origin (>1.0)	$\frac{I_{Em380,Ex310}}{I_{Em430,Ex310}}$	Lu <i>et al.</i> (2022) <sup>77</sup>
Humification Index (HIX)	Indicates degree of humification: autochthonous biological derived DOM (<4.0) or strong humified terrestrial derived DOM (>10)	$\frac{\sum I_{Em335-480,Ex254}}{\sum I_{Em300-345,Ex254}}$	Rodriguez-Vidal <i>et al.</i> (2020) <sup>78</sup>

### 3.5 EEM-PARAFAC modeling

A comprehensive EEM-PARAFAC model was developed using all the stream samples collected during the North Branch walkup, TIR survey, and wet weather campaign. Two EEM-PARAFAC models were built for wastewater: one for septic wastewater samples; and one for the combined septic and municipal wastewater samples. EEM-PARAFAC models were developed and validated using protocols from Murphy *et al.*<sup>49</sup>. The models were built using the drEEM (version 0.6.4) and N-way (version 1.8.0) toolboxes in Matlab (R2021b). In the literature, low excitation wavelengths are sometimes removed due to high noise but, in this case, fluorescence at lower excitation wavelengths were included due to their potential use as wastewater indicators. Before running preliminary models, each EEM was normalized to its total signal to increase leverage for samples with both low and high fluorescence<sup>49</sup>. Four samples from the TIR survey (*i.e.*, GW-17, GW-19, GW-23, GW-26) were excluded from the dataset used to build the stream EEM-PARAFAC model because the fluorescence (580–1800 RU) was much lower than the average signal (24,500 RU) and negatively affected the model. Preliminary EEM-PARAFAC models with 2–8 components were generated from the normalized data sets using the nonnegativity constraint with 10 iterations and a convergence criterion of  $10^{-8}$ . The preliminary models were assessed using split validation. In particular, the EEMs were split into four groups and paired with each of the other splits, yielding six new datasets that contained half of the samples. Split validation compared the excitation and emission spectra for EEM-PARAFAC models built from the six datasets. The model was validated if the components were congruent for all splits using a Tucker's correlation coefficient greater than 0.95<sup>49</sup>. The appropriate number of EEM-PARAFAC components

was selected based on the shape of the spectral loads, residual analysis, core consistency, explained variance, and split validation tests. After selecting an appropriate number of components for each model, a new EEM-PARAFAC model was built using 50 iterations and a convergence criterion of  $10^{-10}$ . Then, the data was reverse-normalized and re-validated by split validation <sup>49</sup>. The EEM-PARAFAC components for each finalized model were characterized and externally validated by comparing them to previously published models in the OpenFluor database <sup>79</sup> using a Tucker's correlation coefficient greater than 0.95. The maximum intensity ( $F_{\max}$ ) for each EEM-PARAFAC component and calculated ratios of components were employed for spatiotemporal analyses and to investigate correlations with CEC concentrations.

### 3.6 Dissolved organic carbon and total nitrogen analysis

Samples were analyzed for the dissolved organic carbon (DOC) and total nitrogen (TN) contents using high-temperature combustion and chemiluminescence detection, respectively, with a Shimadzu TOC-L Analyzer with a TNM-L attachment (Kyoto, Japan). The instrument was run for non-purgeable organic carbon (NPOC) measurements. Inorganic carbon and purgeable organic carbon are sparged from the acidified samples, leaving just the NPOC in the sample. Calibration curves for both TOC and TN analysis were made from standards from Fisher Scientific. For stream samples, both calibration curves ranged from 0.25 to 50 mg L<sup>-1</sup> but the upper end was increased to 100 mg L<sup>-1</sup> for wastewater samples. Calibration curves had to have  $R^2 > 0.95$ . After passing 4 mL of filtrate into the cuvette for EEM analysis, an additional 20 mL was collected into a 40 mL glass vial. Wastewater samples were diluted 2 and 4× before DOC

and TN analysis. Samples were analyzed in triplicate, and a deionized water blank was run every five samples. The DOC concentration was used to calculate  $SUVA_{254}$  by dividing the absorbance at 254 nm by the DOC concentration (Table 3.3).

### 3.7 CEC analysis

#### *3.7.1 Water samples*

Within 12 h of collection, the 1-L samples were passed through a 1.2- $\mu$ m glass-fiber filter and acidified to  $pH < 3$  with 0.1% (v/v) 3 M HCl. The acidified filtrates were stored at 4 °C until they were processed by solid-phase extraction (SPE) to remove interfering substances and concentrate the analytes<sup>8</sup>. Within 4 d, SPE was performed according to protocols developed by He *et al.*<sup>8</sup>. In particular, each sample was divided into six subsamples in amber glass bottles. Stream subsamples were 100 mL, and wastewater subsamples were 10 or 25 mL. Three of the subsamples were not modified, but the other three were spiked with known concentrations of the analytes to determine recovery efficiency during extraction. Samples were spiked with 100  $\mu$ L of the wastewater indicator, herbicide, and UV filters and hormones spiking solutions and 50  $\mu$ L of the antibiotics spiking solution (Table 3.1).

SPE was performed with hydrophobic-lipophilic balanced (HLB) cartridges (150 mg, 6  $cm^3$ ; Waters Corporation; Milford, MA) that were conditioned with 5 mL methanol (MeOH) and 5 mL deionized water acidified to  $pH < 3$  with 0.1% (v/v) 3 M HCl.

Samples were introduced to the HLB cartridges at a flow rate of 4–8  $mL\ min^{-1}$ . Once the sample was loaded, each cartridge was washed with 5 mL of deionized water. The

analytes were eluted from the cartridge by gravity with 7 mL acetonitrile (ACN). The extracts were evaporated in the dark under nitrogen gas. The dried extracts were then reconstituted with 100  $\mu$ L of each of the internal standard solutions noted in Table 3.2. After adding 500  $\mu$ L LC-MS-grade MeOH with 29 isotopically-labeled internal standards, each vial was vortexed. Then, 500  $\mu$ L of LC-MS-grade water was added, and each 1-mL sample was vortexed again. The reconstituted extracts were transferred to amber vials and stored at -20 °C until analysis by LC-MS/MS.

### 3.7.2 Solid samples

Sludge samples were lyophilized and stored at -20 °C until extraction following the protocols of He *et al.*<sup>8</sup>. Each sample was divided into six subsamples of 0.25 or 0.50 g and transferred to 15-mL centrifuge tubes. Three subsamples were not modified. The other subsamples were spiked with either 150 or 200  $\mu$ L of the wastewater indicator, herbicide, and UV filters and hormones spiking solutions and 75 or 100  $\mu$ L of the antibiotics spiking solution (Table 3.1) for standard additions analysis. The subsamples were vortexed for 30 s and equilibrated at 4 °C overnight. Samples were extracted using a previously reported modified QuEChERS method followed by reverse-SPE clean-up<sup>80</sup>. After equilibrating overnight, 5 mL deionized water was added to the solids and then the tubes were vortexed for 30 s, 5 mL ACN was added, and the tubes were vortexed for another 30 s. Next, 2.5 g MgSO<sub>4</sub> and 1.0 g NaCl were added to each centrifuge tube, followed by 30 s vortexing, and 10 min centrifugation at 6000g. At this stage, the analytes partitioned into the upper ACN layer, from which 2 mL was removed and cleaned using reverse-SPE with HLB cartridges (60 mg, 3 cm<sup>3</sup>; Waters Corp.). The ACN

extracts were transferred to new centrifuge tubes, and 20 mg activated carbon was added to each tube for dispersive SPE cleanup of interfering substances. The samples were vortexed and centrifuged at 6000g for 10 min. Then, the supernatant was transferred to test tubes and evaporated under nitrogen in the dark. The extracts were reconstituted following the same protocol described for the water samples. When LC-MS-grade water was added to the reconstituted extracts, the samples were turbid; therefore, an additional 10 mg of activated carbon was used for cleanup. After an additional centrifugation step, the samples were clear, and the supernatant was removed and stored at -20°C until analysis by LC-MS/MS.

### *3.7.3 LC-MS/MS methods*

CECs were measured using an Agilent 6400 Series triple quadrupole LC-MS/MS (Agilent Technologies; Santa Clara, USA). Three separate methods were employed based on previous protocols designed to enable the separation of analytes based on their physicochemical properties<sup>8,81</sup>. The methods were categorized as follows: (1) wastewater indicators; (2) antibiotics; and (3) UV filters and hormones. For all three methods, the gas temperature and flow rate were 300 °C and 5 L min<sup>-1</sup>, respectively. The nozzle and capillary voltage were held at 500 V and 3500 V, respectively. The sheath gas flow was 11 L min<sup>-1</sup>, and the sheath gas temperature was 250 °C for the analysis of wastewater indicators and antibiotics but increased to 350 °C for the UV filters and hormones method. The column compartment was always maintained at 40 °C. The optimization software was used to determine the fragmentor voltage, collision energy, cell accelerator voltage, mass-to-charge ratio of the precursor ion, and mass-to-charge ratios of two

product ions for each analyte. The most abundant product ion was used for quantitation, and the other product ion was used for confirmation.

The wastewater indicator method included an artificial sweetener, herbicides, pharmaceuticals, and stimulants. The antibiotics method measured 16 fluoroquinolones, 5 macrolides, 13 sulfonamides, and 7 tetracyclines. The UV filters and hormones method incorporated 13 UV filters, 8 hormones, mecoprop (herbicide), and ibuprofen (pharmaceutical), all of which require negative electrospray ionization (ESI). The analytes and parameters for each method are reported in Table 3.4; note, the UV filter dioxybenzone is listed twice because it was analyzed in both positive and negative ESI mode. The sample injection volume was 20  $\mu\text{L}$  for all methods. Analytes in the wastewater indicator and UV filter and hormones methods were separated along an Xbridge C18 column (3.0 $\times$ 150 mm, 2.5  $\mu\text{m}$ ) with a C18 guard column (2.1 $\times$ 5 mm, 3.0  $\mu\text{m}$ ). A Waters Symmetry C18 column (3.0 $\times$ 150 mm, 3.5  $\mu\text{m}$ ) with a C18 guard column (3.0 $\times$ 10 mm, 3.0  $\mu\text{m}$ ) was employed for the antibiotics method. All three LC-MS/MS methods ran for 12 min, but the mobile phases and elution gradients varied. The wastewater indicator method employed 0.1% formic acid in LC-MS-grade water and LC-MS-grade MeOH at a flow rate of 0.3  $\text{mL min}^{-1}$  (Figure 3.5a). The antibiotics method also used a 0.3  $\text{mL min}^{-1}$  flow rate, but the mobile phases were 0.5% formic acid in LC-MS-grade water and 0.5% formic acid in LC-MS-grade MeOH (Figure 3.5b). Finally, the UV filters and hormones method separated analytes using 0.1%  $\text{NH}_4\text{OH}$  in LC-MS-grade water and 0.1%  $\text{NH}_4\text{OH}$  in LC-MS-grade MeOH at 0.2  $\text{mL min}^{-1}$  (Figure 3.5c).

**Table 3.4. LC-MS/MS parameters for the wastewater indicators, antibiotics, and UV filters and hormones methods.**

Chemical	Acronym	Class	MW <sup>a</sup>	Mode	Precursor	MS-1 <sup>b</sup>	CE-1 (V) <sup>c</sup>	MS-2 <sup>b</sup>	CE-2 (V) <sup>c</sup>	RT (min) <sup>d</sup>	IS <sup>e</sup>
<i>Wastewater indicators</i>											
Atrazine	ATZ	Herbicide	215.7	+	216.1	174.0	16	96.0	28	7.19	ATZ-d <sub>5</sub>
Atrazine-d <sub>5</sub>	ATZ-d <sub>5</sub>	-	220.7	+	221.1	179.1	20	101.1	28	7.12	-
Caffeine	CAF	Stimulant	194.2	+	195.1	137.8	20	109.8	24	2.96	CAF-d <sub>9</sub>
Caffeine-d <sub>9</sub>	CAF-d <sub>9</sub>	-	203.3	+	204.2	143.9	20	115.9	28	2.94	-
Carbamazepine	CBZ	Pharmaceutical	236.3	+	237.1	193.8	20	178.9	56	5.52	CBZ-d <sub>10</sub>
Carbamazepine-d <sub>10</sub>	CBZ-d <sub>10</sub>	-	246.3	+	247.2	203.9	24	172.5	68	5.36	-
Diclofenac	DIC	Pharmaceutical	296.1	+	296.0	213.8	40	150.8	80	9.67	DIC-d <sub>4</sub>
Diclofenac-d <sub>4</sub>	DIC-d <sub>4</sub>	-	300.2	+	300.1	218.0	40	181.7	76	9.63	-
Paraxanthine	PAR	Stimulant	180.2	+	181.1	124.1	20	42.2	40	2.81	PAR-d <sub>6</sub>
Paraxanthine-d <sub>6</sub>	PAR-d <sub>6</sub>	-	186.2	+	187.1	127.1	24	45.2	40	2.81	-
Sucralose	SUC	Artificial Sweetener	397.6	+	419.0	239.0	15	221.1	15	2.99	SUC-d <sub>6</sub>
Sucralose-d <sub>6</sub>	SUC-d <sub>6</sub>	-	403.7	+	425.0	243.0	30	223.0	30	2.99	-
<i>Antibiotics</i>											
Azithromycin	AZI	Macrolide	749.0	+	749.5	591.4	32	158.0	40	7.09	AZI-d <sub>3</sub>
Azithromycin-d <sub>3</sub>	AZI-d <sub>3</sub>	-	752.0	+	752.5	594.4	32	158.0	40	7.08	-
Chlorotetracycline- <sup>13</sup> C-d <sub>3</sub>	CTC- <sup>13</sup> C-d <sub>3</sub>	-	482.9	+	483.0	448.0	20	466.1	16	7.02	-
Chlortetracycline <sup>f</sup>	CTC	Tetracycline	478.9	+	479.1	444.0	20	154.0	28	7.03	CTC- <sup>13</sup> C-d <sub>3</sub>
Ciprofloxacin	CIP	Fluoroquinolone	331.4	+	332.1	231.0	44	288.0	16	4.39	CIP-d <sub>8</sub>
Ciprofloxacin-d <sub>8</sub>	CIP-d <sub>8</sub>	-	339.4	+	340.2	322.1	20	235.0	44	4.33	-
Clarithromycin	CLA	Macrolide	748.0	+	748.5	158.0	28	590.3	16	8.58	AZI-d <sub>3</sub>
Demeclocycline	DMC	Tetracycline	464.3	+	465.1	448.0	16	430.0	24	6.24	CTC- <sup>13</sup> C-d <sub>3</sub>
Difloxacin <sup>f</sup>	DIF	Fluoroquinolone	399.4	+	400.2	356.1	20	299.1	32	5.90	DIF-d <sub>3</sub>
Difloxacin-d <sub>3</sub>	DIF-d <sub>3</sub>	-	402.4	+	403.2	385.1	24	359.1	20	5.85	-



Chemical	Acronym	Class	MW <sup>a</sup>	Mode	Precursor	MS-1 <sup>b</sup>	CE-1 (V) <sup>c</sup>	MS-2 <sup>b</sup>	CE-2 (V) <sup>c</sup>	RT (min) <sup>d</sup>	IS <sup>e</sup>
Doxycycline <sup>f</sup>	DC	Tetracycline	444.4	+	445.2	428.1	16	321.0	32	7.53	CTC- <sup>13</sup> C-d <sub>3</sub>
Enrofloxacin <sup>f</sup>	ENR	Fluoroquinolone	359.4	+	360.2	316.1	20	245.0	28	4.78	CIP-d <sub>8</sub>
Erythromycin	ERY	Macrolide	733.9	+	716.3	158.1	30	558.2	10	7.90	ERY-d <sub>6</sub>
Erythromycin-d <sub>6</sub>	ERY-d <sub>6</sub>	-	740.0	+	722.4	163.9	30	564.3	40	7.90	-
Fleroxacin	FLE	Fluoroquinolone	369.3	+	370.1	326.1	20	269.0	28	2.90	OFL-d <sub>3</sub>
Gatifloxacin	GAT	Fluoroquinolone	375.4	+	376.2	261.0	36	332.2	16	6.66	DIF-d <sub>3</sub>
Lomefloxacin	LOM	Fluoroquinolone	351.4	+	352.2	265.1	24	308.2	16	5.25	CIP-d <sub>8</sub>
Marbofloxacin <sup>f</sup>	MAR	Fluoroquinolone	362.4	+	363.2	320.2	12	205.1	36	2.65	OFL-d <sub>3</sub>
Meclocycline	MC	Tetracycline	476.9	+	477.1	460.0	20	234.9	40	7.88	CTC- <sup>13</sup> C-d <sub>3</sub>
Methacycline	MTC	Tetracycline	442.4	+	443.2	426.1	16	201.0	40	7.33	CTC- <sup>13</sup> C-d <sub>3</sub>
Moxifloxacin	MOX	Fluoroquinolone	401.4	+	402.2	364.1	28	220.2	40	6.98	DIF-d <sub>3</sub>
Nadifloxacin	NAD	Fluoroquinolone	360.4	+	361.2	283.2	44	257.2	45	9.43	DIF-d <sub>3</sub>
Norfloxacin	NOR	Fluoroquinolone	319.3	+	320.1	231.1	44	276.2	16	3.91	OFL-d <sub>3</sub>
Ofloxacin	OFL	Fluoroquinolone	361.4	+	362.2	318.1	20	261.0	28	3.35	OFL-d <sub>3</sub>
Ofloxacin-d <sub>3</sub>	OFL-d <sub>3</sub>	-	364.4	+	365.2	321.1	20	261.0	32	3.34	-
Orbifloxacin <sup>f</sup>	ORB	Fluoroquinolone	395.4	+	396.2	352.1	20	295.0	24	5.81	DIF-d <sub>3</sub>
Oxytetracycline <sup>f</sup>	OTC	Tetracycline	460.4	+	461.2	426.1	20	443.1	12	4.14	TC-d <sub>6</sub>
Pefloxacin	PEF	Fluoroquinolone	333.4	+	334.2	290.1	20	233.0	28	3.45	OFL-d <sub>3</sub>
Roxithromycin	ROX	Macrolide	836.5	+	837.5	679.4	20	158.0	36	8.66	ERY-d <sub>6</sub>
Sarafloxacin <sup>f</sup>	SAR	Fluoroquinolone	385.4	+	386.1	342.2	20	299.1	32	6.41	DIF-d <sub>3</sub>
Sparfloxacin	SPA	Fluoroquinolone	392.4	+	393.2	349.1	20	292.1	28	6.83	DIF-d <sub>3</sub>
Sulfacetamide	SCM	Sulfonamide	214.2	+	215.0	156.0	8	92.0	24	2.26	SMZ- <sup>13</sup> C <sub>6</sub>
Sulfadiazine	SDZ	Sulfonamide	250.3	+	251.1	156.0	16	92.0	28	2.45	SMZ- <sup>13</sup> C <sub>6</sub>
Sulfadimethoxine <sup>f</sup>	SDM	Sulfonamide	310.3	+	311.1	156.0	20	92.1	36	6.95	SQX- <sup>13</sup> C <sub>6</sub>

Chemical	Acronym	Class	MW <sup>a</sup>	Mode	Precursor	MS-1 <sup>b</sup>	CE-1 (V) <sup>c</sup>	MS-2 <sup>b</sup>	CE-2 (V) <sup>c</sup>	RT (min) <sup>d</sup>	IS <sup>e</sup>
Sulfadoxine	SDX	Sulfonamide	310.3	+	311.1	108.0	28	140.0	28	6.95	SQX- <sup>13</sup> C <sub>6</sub>
Sulfamerazine <sup>f</sup>	SMR	Sulfonamide	264.3	+	265.1	92.0	32	156.0	16	3.22	SMZ- <sup>13</sup> C <sub>6</sub>
Sulfamethazine <sup>f</sup>	SDD	Sulfonamide	278.3	+	279.1	186.0	16	92.0	32	4.31	SMZ- <sup>13</sup> C <sub>6</sub>
Sulfamethizole	SMZ	Sulfonamide	270.3	+	271.0	155.9	12	92.0	28	4.67	SMZ- <sup>13</sup> C <sub>6</sub>
Sulfamethizole- <sup>13</sup> C <sub>6</sub>	SMZ- <sup>13</sup> C <sub>6</sub>	-	276.3	+	277.0	162.0	12	98.1	28	4.65	-
Sulfamethoxazole	SMX	Sulfonamide	253.3	+	254.1	92.0	28	155.9	16	6.79	SMX- <sup>13</sup> C <sub>6</sub>
Sulfamethoxazole- <sup>13</sup> C <sub>6</sub>	SMX- <sup>13</sup> C <sub>6</sub>	-	259.2	+	260.0	98.1	28	162.0	16	6.80	-
Sulfaphenazole	SPZ	Sulfonamide	314.4	+	315.1	158.0	32	92.1	40	7.50	SMX- <sup>13</sup> C <sub>6</sub>
Sulfapyridine	SPD	Sulfonamide	249.3	+	250.1	156.0	16	92.1	32	2.82	SMZ- <sup>13</sup> C <sub>6</sub>
Sulfaquinoxaline <sup>f</sup>	SQX	Sulfonamide	300.4	+	301.1	156.0	16	92.1	36	7.81	SQX- <sup>13</sup> C <sub>6</sub>
Sulfaquinoxaline- <sup>13</sup> C <sub>6</sub>	SQX- <sup>13</sup> C <sub>6</sub>	-	306.3	+	307.1	162.0	16	98.1	32	7.80	-
Sulfathiazole <sup>f</sup>	STZ	Sulfonamide	255.3	+	256.0	156.0	12	92.0	28	2.60	SMZ- <sup>13</sup> C <sub>6</sub>
Sulfisomidine	SSD	Sulfonamide	278.3	+	279.1	124.1	24	186.0	16	1.99	SMZ- <sup>13</sup> C <sub>6</sub>
Tetracycline <sup>f</sup>	TC	Tetracycline	444.4	+	445.2	410.1	20	154.0	28	3.74	TC-d <sub>6</sub>
Tetracycline-d <sub>6</sub>	TC-d <sub>6</sub>	-	450.5	+	451.2	416.1	20	160.0	28	3.69	-
Tosufloxacin	TOS	Fluoroquinolone	404.4	+	405.1	263.0	52	314.0	44	7.07	DIF-d <sub>3</sub>
Tylosin <sup>f</sup>	TYL	Macrolide	916.1	+	916.5	174.0	40	772.4	32	7.87	ERY-d <sub>6</sub>
<b><i>UV filters and hormones</i></b>											
2-ethyl-d <sub>5</sub> -hexyl-2,3,3,4,4,5,5,6,6,6-	EHMC-d <sub>15</sub>	-	305.5	+	306.3	180	4	161.4	20	8.51	-

Chemical	Acronym	Class	MW <sup>a</sup>	Mode	Precursor	MS-1 <sup>b</sup>	CE-1 (V) <sup>c</sup>	MS-2 <sup>b</sup>	CE-2 (V) <sup>c</sup>	RT (min) <sup>d</sup>	IS <sup>e</sup>
d <sub>10</sub> 4-methoxycinnamate											
2-ethylhexyl 4-methoxycinnamate	EHMC	UV filter	290.4	+	291.2	179	4	161.0	20	8.51	EHMC-d <sub>15</sub>
3-(4-methylbenzylidene) camphor	4-MBC	UV filter	254.2	+	255.2	104.9	36	170.8	20	8.00	4-MBC-d <sub>4</sub>
3-(4-methylbenzylidene-d <sub>4</sub> ) camphor	4-MBC-d <sub>4</sub>	-	258.0	+	259.2	216.1	20	108.1	32	7.98	-
17 $\alpha$ -ethinylestradiol	EE2	Hormone	296.4	-	295.0	145	40	183.0	40	4.18	EE2-d <sub>4</sub>
17 $\alpha$ -ethinylestradiol-2,4,16,16-d <sub>4</sub>	EE2-d <sub>4</sub>	-	300.4	-	299.0	147	40	161.0	40	4.03	-
17 $\beta$ -estradiol	E2	Hormone	272.4	-	271.0	183.1	45	145.1	45	4.15	E2-d <sub>3</sub>
17 $\beta$ -estradiol-16,16,17-d <sub>3</sub>	E2-d <sub>3</sub>	-	275.2	-	274.1	185	50	145.1	45	4.11	-
Androsterone	AN	Hormone	290.4	+	291.2	273.3	10	199.1	20	7.31	P4-d <sub>9</sub>
Benzoic acid-d <sub>5</sub>	BA-d <sub>5</sub>	-	127.2	-	126.0	82.1	10	- <sup>g</sup>	- <sup>g</sup>	1.74	-
Benzophenone-d <sub>10</sub>	BP-d <sub>10</sub>	-	192.2	+	193.1	109.9	16	82.0	40	4.74	-
Cinoxate	CX	UV filter	250.3	+	251.1	160.7	4	132.8	28	4.71	BP-d <sub>10</sub>
Dioxybenzone	BP-8	UV filter	244.3	-	243.1	123	20	93.1	40	4.24	BP-d <sub>10</sub>
Dioxybenzone	BP-8	UV filter	244.3	+	245.1	120.8	16	250.8	20	4.22	BP-d <sub>10</sub>
Ensulizole	ESZ	UV filter	274.3	-	273.0	193.1	30	117.2	70	1.74	BA-d <sub>5</sub>
Equilin	EN	Hormone	268.4	-	267.0	223	40	142.7	40	4.17	E2-d <sub>3</sub>
Estetrol	E4	Hormone	304.4	-	303.1	240.9	15	273.0	15	2.35	E2-d <sub>3</sub>
Estriol	E3	Hormone	288.4	-	287.0	171	40	145.1	40	2.45	E2-d <sub>3</sub>
Estrone	E1	Hormone	270.1	-	269.0	145	40	182.9	50	4.37	E2-d <sub>3</sub>
Homosalate	HMS	UV filter	262.3	-	261.3	137	20	93.0	30	8.83	HMS-d <sub>4</sub>
Homosalate-(benzoic ring-d <sub>4</sub> )	HMS-d <sub>4</sub>	-	266.4	-	265.2	141	20	139.1	30	8.67	-

Chemical	Acronym	Class	MW <sup>a</sup>	Mode	Precursor	MS-1 <sup>b</sup>	CE-1 (V) <sup>c</sup>	MS-2 <sup>b</sup>	CE-2 (V) <sup>c</sup>	RT (min) <sup>d</sup>	IS <sup>e</sup>
Ibuprofen	IBU	Pharmaceutical	206.3	-	205.0	160.9	5	-	-	2.06	IBU-d <sub>3</sub>
Ibuprofen-d <sub>3</sub>	IBU-d <sub>3</sub>	-	209.3	-	208.1	164	5	-	-	2.06	-
Mecoprop	MEC	Herbicide	214.7	-	213.0	141.1	9	71.0	9	2.28	MEC-d <sub>3</sub>
Mecoprop-d <sub>3</sub>	MEC-d <sub>3</sub>	-	217.7	-	216.0	143.8	10	70.9	10	2.26	-
Octisalate	OS	UV filter	250.3	-	249.1	136.9	20	92.9	25	8.72	HMS-d <sub>4</sub>
Octocrylene	OC	UV filter	361.5	+	362.2	249.6	4	231.6	20	8.13	OC-d <sub>15</sub>
Octocrylene-(2-ethyl-d <sub>5</sub> -hexyl-2,3,3,4,4,5,5,6,6,6-d <sub>10</sub> )	OC-d <sub>15</sub>	-	376.6	+	377.3	233.3	20	250.6	8	8.11	-
Oxybenzone	BP-3	UV filter	228.2	+	229.1	150.8	20	104.9	20	6.73	BP3-d <sub>5</sub>
Oxybenzone-(phenyl-d <sub>5</sub> )	BP-3-d <sub>5</sub>	-	233.3	+	234.1	151	20	110.0	20	6.63	-
Padimate O	ODPABA	UV filter	277.4	+	278.0	166	20	150.9	40	8.46	OC-d <sub>15</sub>
Progesterone	P4	Hormone	314.5	+	315.2	97	25	109.0	25	7.17	P4-d <sub>9</sub>
Progesterone-d <sub>9</sub>	P4-d <sub>9</sub>	-	323.5	+	324.3	113.1	20	288.2	20	7.13	-
Sulisobenzone	SSB	UV filter	308.3	-	307.0	210.9	40	227.0	30	1.78	BA-d <sub>5</sub>
Trolamine salicylate	TEAS	UV filter	287.3	+	150.1	132.1	10	88.1	20	2.12	BA-d <sub>5</sub>

a: MW, molecular weight (g/mol)

b: MS-1 was used for quantitation, and MS-2 was used for confirmation

c: CE, collision energy

d: RT, retention time

e: IS, internal standard used for quantitation of the listed chemicals

f: animal-labeled antibiotics

g: only one product ion

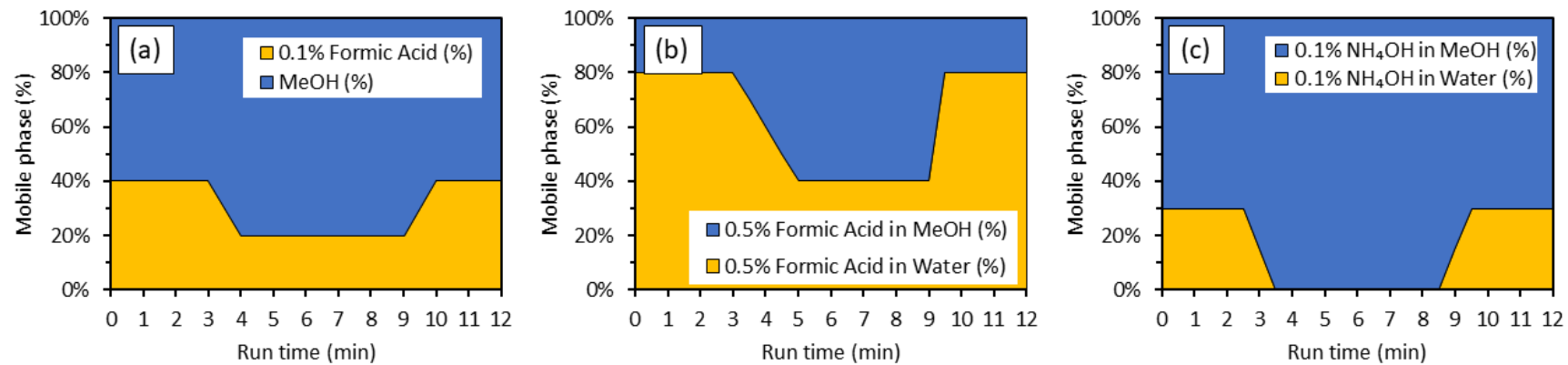
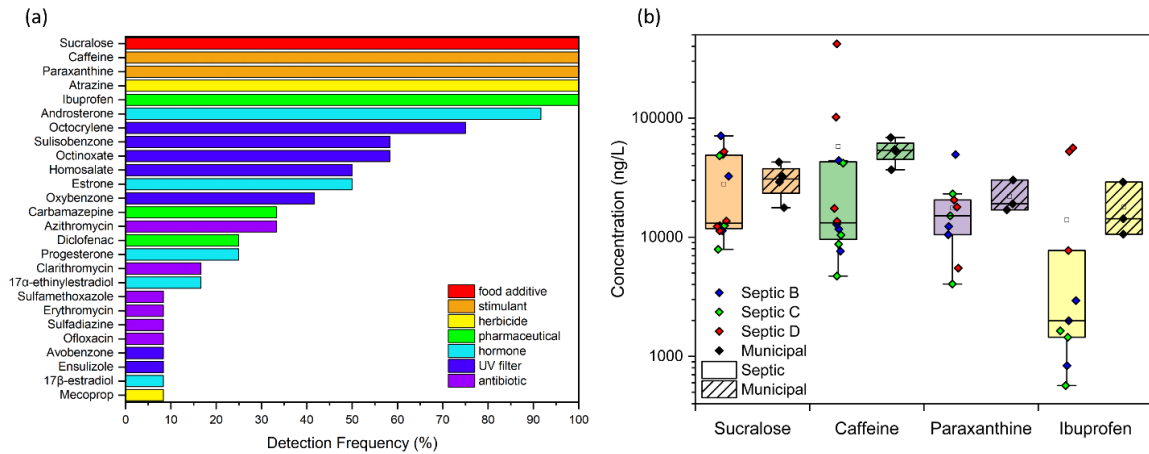


Figure 3.5. Mobile phase gradient for the (a) wastewater indicators, (b) antibiotics, and (c) UV filter and hormones methods.

## Chapter 4: Septic wastewater characterization

### 4.1 Contaminants of emerging concern (CECs) in septic wastewater

In previous studies, CECs were measured at high concentrations in septic wastewater and proposed as wastewater indicators in nearby surface water<sup>35,40,46</sup>. In this project, four samples were collected between June and December 2022 from three conventional septic tanks built in 1976. A group of 26 CECs, including a food additive, two stimulants, three pharmaceuticals, two herbicides, six antibiotics, seven UV filters, and five hormones, were detected at least once in septic wastewater (Figure 4.1a). The full set of CEC data for the three conventional septic tanks can be found in Tables B.1, B.2, and B.3 in Appendix B. Sucralose and caffeine exhibited 100% detection frequency in the conventional septic systems, and the corresponding concentrations were 7,900-71,000 ng/L and 4,700-420,000 ng/L, respectively (Figure 4.1b). The range of sucralose concentrations was similar to prior reports for septic effluent<sup>36,82,83</sup>, but the maximum caffeine concentration was higher than previously reported levels (*i.e.* up to 130,000 ng/L)<sup>6,35,84</sup>. Ibuprofen and paraxanthine were not measured in June (due to ongoing method development) but were detected at concentrations of 570-5,600 ng/L and 4,000-49,000 ng/L, respectively, in samples from the other three months. Previous studies found caffeine makes up a low percentage (0.5–10%) of the sum of paraxanthine and caffeine in urine<sup>85</sup>. However, this ratio is susceptible to differences in household practices related to the consumption and disposal of caffeinated products<sup>6</sup>. For example, if a single 12-ounce cup of coffee is poured down the sink, then the caffeine concentration in a 1000-gallon septic tank would increase by 50,000 ng/L<sup>84</sup>. The concentrations of other CECs were not outside of expected ranges for wastewater.



**Figure 4.1. Measured CEC (a) detection frequencies in conventional septic tanks and (b) concentration distributions in septic and municipal wastewater.** The filled box represents the interquartile range (IQR). The bottom of the filled box represents the 25<sup>th</sup> percentile value (Q1), the horizontal line dividing the box represents the 50<sup>th</sup> percentile or median value, the top of the filled box is the 75<sup>th</sup> percentile value (Q3), and the open square is the mean. The bottom and top whiskers represent the minimum value above  $Q1 - 1.5(IQR)$  and the maximum value below  $Q3 + 1.5(IQR)$ , respectively. Values outside of the whiskers are outliers.

Municipal wastewater contained a similar number of detected CECs ( $n = 28$ ), but some unique antibiotics and UV filters were present compared to the conventional septic wastewater. All CEC data for the municipal wastewater samples are available in Table B.4. Figure 4.1b compares the concentrations of the four most commonly detected CECs in municipal ( $n = 4$ ) and conventional septic ( $n = 12$ ) wastewater. No significant differences were observed between the CEC concentrations in the two wastewater types. The CEC profiles did vary between specific septic systems, presumably due to differences in household consumption before sample collection. For example, ibuprofen levels were lower in Septics B and C compared to Septic D (Figure 4.1b); other differences can be observed for antibiotics, UV filters, and hormones in Tables B.1, B.2, and B.3. Previous studies supported the greater variability in CEC levels in single-source septic systems compared to centralized municipal wastewater collection systems<sup>86</sup>. In

septic systems, Teerlink *et al.* measured CEC concentrations that varied by up to four orders of magnitude in a 24-h period <sup>86</sup>. Municipal wastewater contained more antibiotics, but the highest antibiotic concentration was 2,600 ng/L azithromycin in Septic D. The androsterone hormone was present in all municipal wastewater samples and 91.7% of septic wastewater samples; furthermore, the highest concentration was 8,500 ng/L, which was measured in Septic C and 3.7× the average concentration in municipal wastewater. Other hormones, including estrone, 17β-estradiol, 17α-ethinylestradiol, and progesterone, also exhibited higher concentrations in septic wastewater. These results supported the potential importance of septic systems as a source of CECs in adjacent groundwater and surface water systems.

Atrazine is an agricultural herbicide that is also applied as a weed killer on residential lawns. This CEC was detected in both municipal (up to 117 ng/L) and septic (up to 156 ng/L) wastewater. This result was somewhat surprising because the source of herbicides in wastewater was not immediately obvious. Nevertheless, atrazine was previously reported in municipal wastewater <sup>87,88</sup> and drinking water sources, leading EPA to regulate atrazine under the Safe Drinking Water Act <sup>89</sup>. Due to its use as an herbicide, atrazine is commonly found in groundwater in agricultural regions <sup>90</sup>. The neighborhood where the three conventional septic tanks were located was converted into a residential area from previous use as farmland. Well water samples were collected from two of the households. For Household B, atrazine was detected at 11.7 ng/L, over 7× the average concentration in Septic B wastewater (1.6 ng/L). Similar results were attained for Household C, wherein the well water contained 129 ng/L of atrazine and the septic



wastewater had 65.2 ng/L. These findings suggested that well water was a primary source of atrazine in septic wastewater.

Some CECs were not expected to be detected at high concentrations in septic wastewater due to physicochemical properties that favor partitioning into septic sludge. The CEC concentrations measured in the liquid and solid phases of septic sludge (Table B.5) confirmed that hydrophobic CECs were more present in the sludge and hydrophilic CECs remained in the liquid effluent. The hydrophobicity of CECs was defined using the octanol-water distribution coefficient ( $\log D$ ). Unlike  $\log K_{ow}$ ,  $\log D$  accounts for partitioning of the neutral and ionic forms of the chemical at each pH value; generally, chemicals with  $\log D > 2$  are considered hydrophobic. The average pH for the three septic sludge samples was 7.3, and this condition was used to standardize and compare  $\log D$  values, which were estimated by Marvin version 22.3.0 (ChemAxon). CECs with low  $\log D$  values, such as caffeine ( $\log D = -0.55$ ) and sulfamethoxazole ( $\log D = 0.03$ ), were almost exclusively present in the water phase. The clarithromycin ( $\log D = 1.53$ ) and erythromycin ( $\log D = 0.89$ ) macrolide antibiotics exhibited slightly higher  $\log D$  values and were, therefore, present in both phases. The data in Table B.5 confirm high concentrations of octinoxate ( $\log D = 5.38$ ), octocrylene ( $\log D = 6.78$ ), oxybenzone ( $\log D = 3.20$ ), and progesterone ( $\log D = 4.15$ ) in septic solids. Prior work indicated that 90-100% of octinoxate and 84-100% of octocrylene distributed into sludge<sup>91,92</sup>. The partitioning of these hydrophobic compounds into sludge reduced CEC loads entering the environment; however, the sludge served as a continuous source of CECs to the drainfield, resulting in more consistent CEC levels in the water phase over time.

Previous studies indicated that CECs undergo adsorption and/or biotransformation reactions as septic effluent percolates through the drainfield <sup>93</sup>. The hydraulic loading rate to the drainfield is typically 1–5 cm/d <sup>94</sup>. The flow rate can rapidly increase during times of intensive household inputs, leading to greater hydraulic loading and reduced attenuation efficiency <sup>95</sup>. Caffeine and ibuprofen were measured at high concentrations in septic tanks, but previous studies have shown both CECs were readily attenuated (*i.e.*, > 99% and 65–99% removal, respectively) in the drainfield <sup>4,5,82,96,97</sup>. These two CECs are considered labile and, therefore, recommended as indicators of partially treated wastewater that recently entered downgradient water sources. In contrast, Teerlink *et al.* found that 56% of sulfamethoxazole, one of the most widely prescribed antibiotics in the US <sup>98</sup>, in septic tanks reached shallow groundwater <sup>95</sup>. Carbamazepine <sup>99</sup> and sucralose <sup>100</sup> are recalcitrant and exhibited low removal efficiencies in drainfields (5% <sup>95</sup>) and biological treatment processes (< 2% <sup>101</sup>). Based on the data in Figure 4.1 and Tables B.1, B.2, and B.3 and prior findings from literature, sucralose, carbamazepine, and sulfamethoxazole were elevated as conservative indicators of septic wastewater in nearby surface water. However, analysis of these CECs is expensive and time-consuming and alternative indicators may be needed for more extensive monitoring campaigns.

#### 4.2 Fluorescent dissolved organic matter (FDOM) in conventional septic tanks

Both septic and municipal wastewater-derived FDOM were enriched with aromatic protein (Regions 1-2) and soluble microbial product (Region 4)-like fluorophores, whereas Suwannee River natural organic matter (SRNOM) mostly contained fulvic (Region 3) and humic (Region 5) acid-like fluorophores (Figure 4.2). The FDOM

contents in stream water samples were much lower than the levels observed in wastewater. The majority of FDOM in the stream samples occurred in Regions 3 and 5, similar to that of SRNOM (Figure 4.2); however, fluorescence signatures were also observed in Regions 1, 2, and 4, suggesting the potential presence of wastewater-derived FDOM.

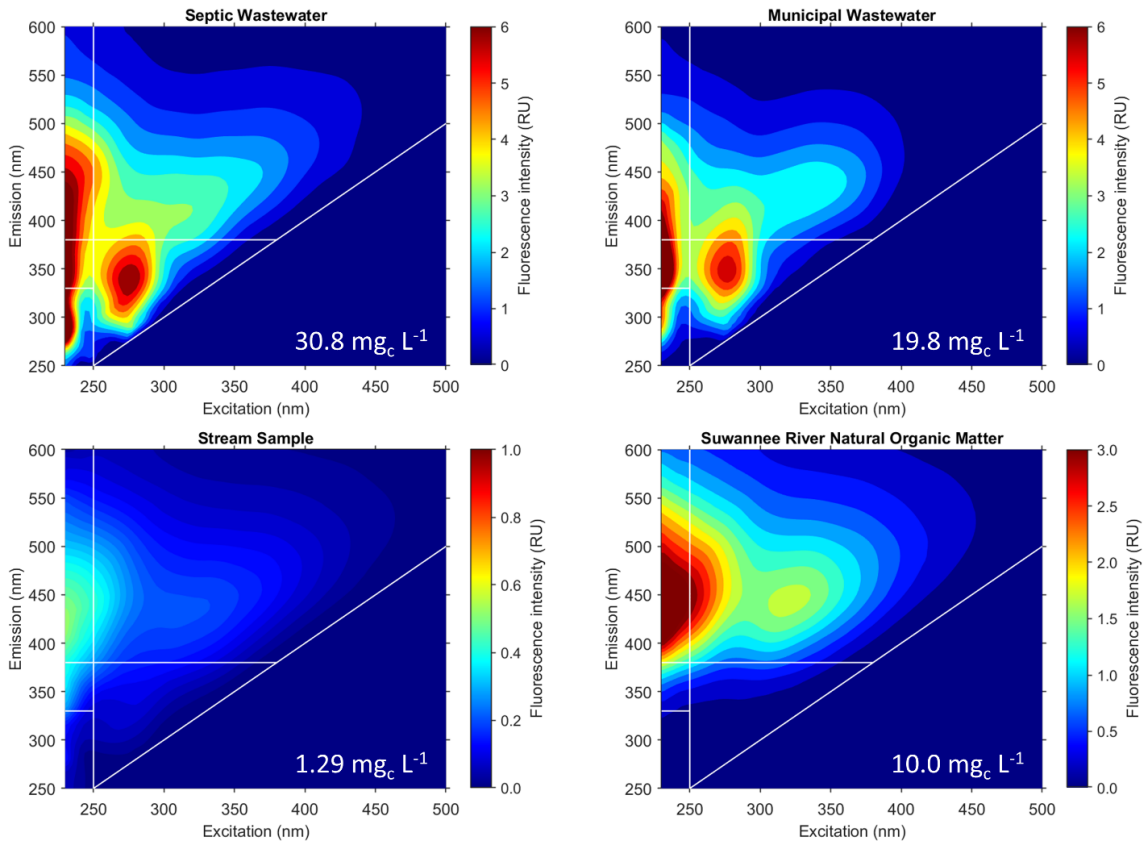


**Figure 4.2. Representative excitation-emission matrices (EEMs) for septic wastewater, municipal wastewater, stream water from the North Branch, and reconstituted SRNOM. The dissolved organic carbon (DOC) content for each sample is overlaid on the EEM.**

Figure 4.3 shows the EEMs generated from the samples collected from the three conventional septic tanks and four sampling periods. The fluorescence fingerprint of each septic tank remained consistent across all four sampling dates, but the fluorescence

intensity varied between samples. The composition of EEMs from Septics B and C was similar, with well-defined peaks in Regions 1, 2, 3, and 4. Septic D exhibited an additional peak centered at an excitation wavelength ( $\lambda_{ex}$ ) of 320 nm and emission wavelength ( $\lambda_{em}$ ) of 420 nm (Region 5). This peak may have been related to whitening compounds, which are used in laundry detergents, and known to fluoresce at similar wavelengths<sup>57</sup>.

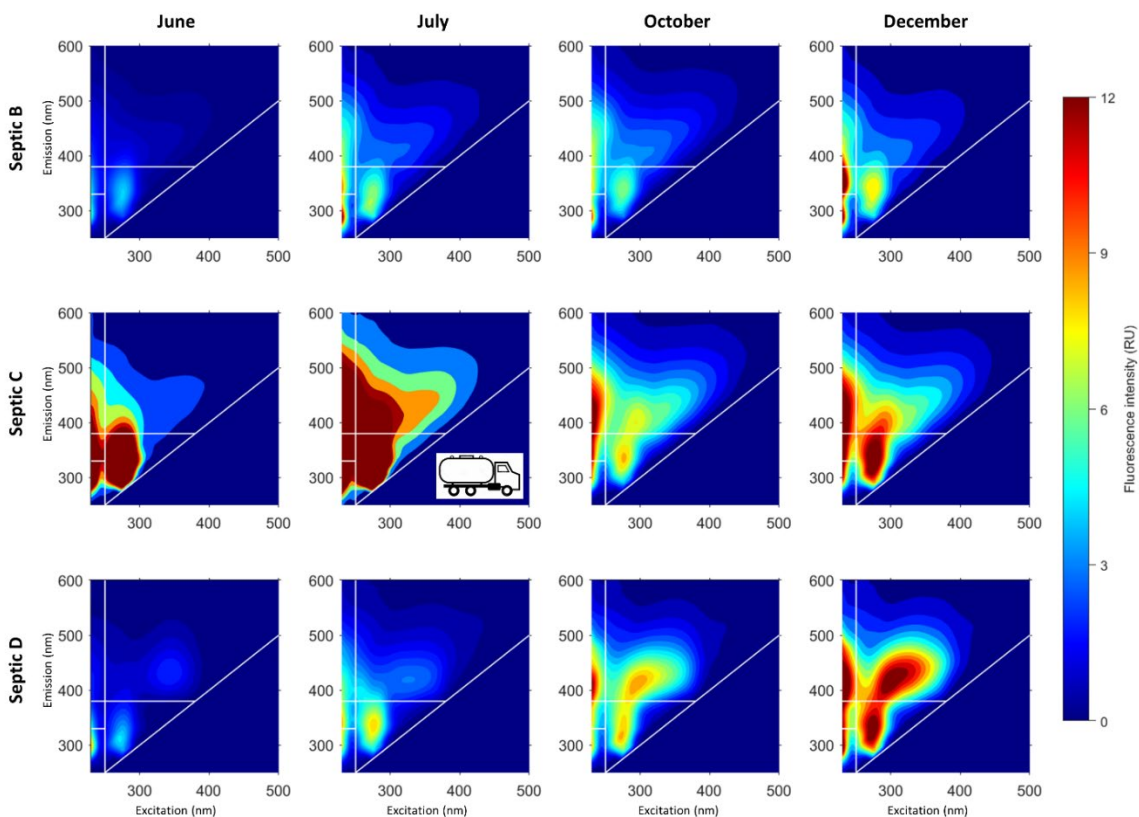


**Figure 4.3. EEMs measured for samples collected from three conventional septic tanks.** Septic C was pumped out at the beginning of September, as indicated by the pumping truck label in the July EEM.

The fluorescence intensity of wastewater from Septics B and D increased from June to December 2022. Septic C did not follow the same pattern, possibly because the tank was

pumped out in September. Before the pump out of Septic C, the fluorescence intensity was similar to that observed in the water component of samples collected from septic pumping trucks (Figure B.1 in Appendix B). After being emptied, the fluorescence magnitude of wastewater in Septic C was similar to the other tanks. The temporal variation in fluorescence intensity was attributed to multiple factors. Septic tanks only contain wastewater from one residence, and the fluorescence signature can vary between septic systems and over time depending on the activities of the household. Patterson reported that septic tank pH, conductivity, temperature, redox potential, and flow rate can significantly vary throughout the day and across the week <sup>102</sup>. The composition of septic effluent also changes by season, because microbial degradation is slower at lower temperatures <sup>103,104</sup>. The consistent increase in FDOM intensity in Septics B and D from June to December generally agreed with expectations from the monthly temperature profiles. While July was the warmest sampling month, those samples were collected on a weekend, leading to more recent inputs and shorter residence times that resulted in less biodegradation and higher FDOM levels (Table B.6).

The fluorescence peaks in Regions 1, 2, and 4 were observed in all septic systems and sampling months, reinforcing the potential use of these regions as wastewater indicators in nearby surface waters. The levels of septic FDOM in these three regions were generally amplified in comparison to municipal wastewater. Figure 4.4a shows differential EEMs for Septic B and municipal wastewater, wherein the "Delta" EEM indicates fluorescence regions that were enriched in Septic B. The magnitude of the R1 and R4 parameters was higher in Septic B wastewater for all four months, but the differences were not significant ( $p > 0.05$ ) (Figure 4.4b). The difference in R1

fluorescence was lowest in June (+32%) and highest in December (+63%). Similar patterns were noted for R4. Septic B wastewater was deficient with respect to R2 fluorescence in June (−77%) and October (−24%) but enriched with R2 in December (+47%). Septics C and D followed similar patterns with respect to R1 and R4 fluorescence compared to municipal wastewater (Figures B.2 and B.3). These compositional differences were primarily driven by the high variability in septic wastewater FDOM (Figure 4.4b), which is vulnerable to household activities, compared to municipal wastewater, which has more consistent FDOM signatures due to the low leverage of any one household.

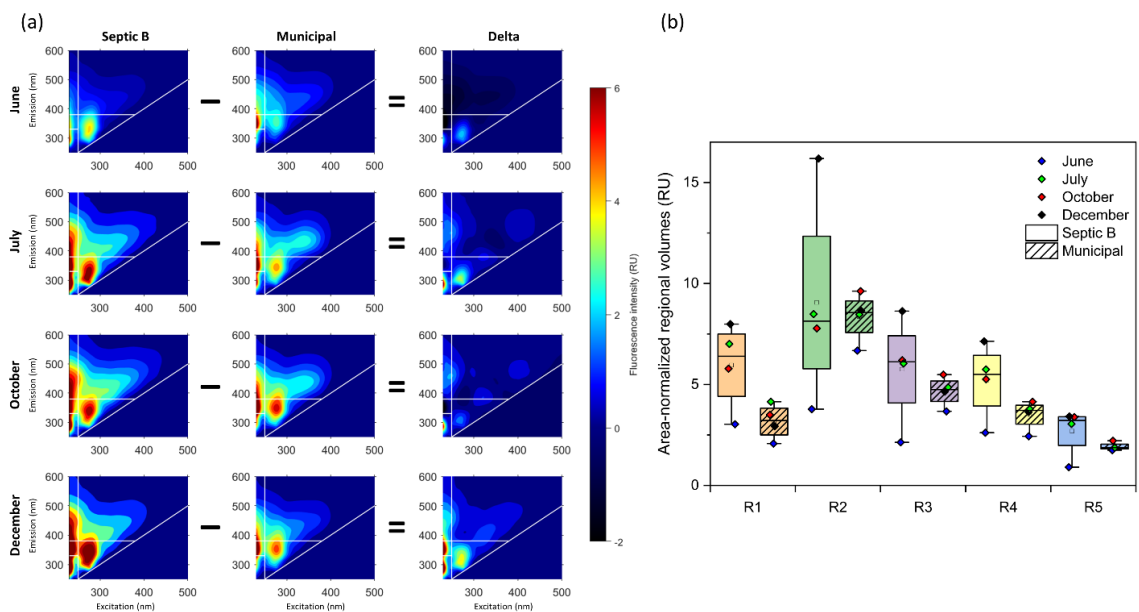


**Figure 4.4. FDOM in Septic B and municipal wastewater expressed as (a) differential EEMs and (b) box plots.** In (a), the fluorescence in the "Delta" plots indicate regions with higher fluorescence in Septic B wastewater compared to municipal wastewater.

The above analyses indicated that septic tanks contained FDOM signals that could potentially serve as wastewater indicators in nearby surface water, but the high variability

in fluorescence intensity between septic systems suggested that normalization strategies were needed to ensure proper source attribution in streams that also contain natural FDOM. Ratiometric parameters provide a robust strategy for differentiating the fluorescence composition of natural and wastewater-derived FDOM <sup>7</sup>. The ratiometric parameters of interest were more variable for septic wastewater than municipal wastewater (Figure 4.5). The R2/R5 ratios were generally higher for municipal wastewater, indicating that R2/R5 may be less suitable as a septic indicator. The median R4/R5 ratios were similar for septic and municipal wastewater, suggesting that R4/R5 could be a robust indicator for either type of wastewater <sup>7</sup>. The R1/R5 parameter tended to be higher for septic wastewater, potentially due to the biological processes occurring in the septic tank. For Septic B, the R1/R5 and R4/R5 ratiometric parameters were highest in June, despite June producing the lowest overall fluorescence intensity. This outcome highlights the critical insights from FDOM compositional analysis compared to the more typical regional integration techniques.

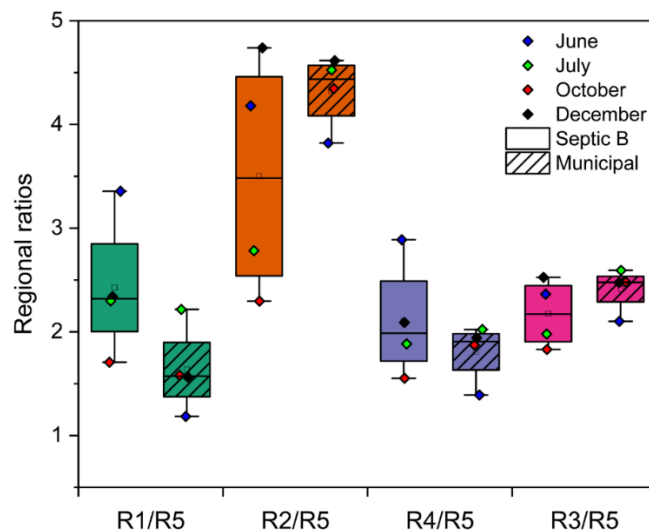


**Figure 4.5. Distribution of ratiometric FDOM parameters for Septic B and municipal wastewater.**

### 4.3 FDOM and CECs in advanced septic system

In addition to the three conventional septic tanks discussed above, samples were also collected from the inlet and outlet of an advanced septic system equipped with an aeration unit (*i.e.*, Septic A). The FDOM signature of the wastewater dramatically changed due to aerobic biodegradation processes (Figure 4.6a). The fluorescence in all regions experienced significant decreases: 61% for R1 ( $p = 0.01$ ); 34% for R2 ( $p = 0.01$ ); 31% for R3 ( $p = 0.01$ ); 57% for R4 ( $p < 0.01$ ); and 23% for R5 ( $p = 0.02$ ) (Figure 4.6b). R1 and R4 degraded the most, which may suggest that the R1/R5 and R4/R5 ratiometric parameters are more appropriate as indicators of wastewater from conventional septic tanks but not advanced septic systems or as partially treated wastewater indicators.

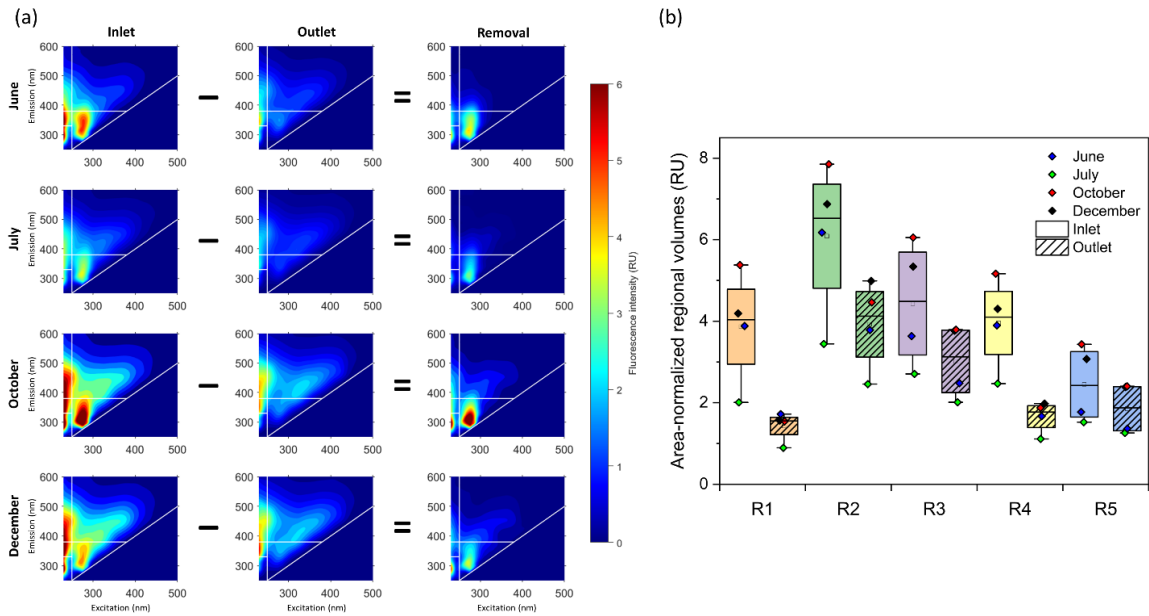


**Figure 4.6. FDOM in the inlet and outlet of Septic A expressed as (a) differential EEMs and (b) box plots. In (a), the fluorescence in the "Removal" plots indicates regions with high FDOM removal.**



Major changes were also observed between the inlet and outlet of Septic A for concentrations of labile CECs; note, all CEC concentrations for Septic A are available in Table B.7 of Appendix B. Caffeine and paraxanthine exhibited significant degradation efficiencies of 92% ( $p = 0.01$ ) and 95% ( $p < 0.01$ ), respectively (Figure 4.7a). The aeration process also caused the concentrations of octinoxate, homosalate, octocrylene, and androsterone to decrease below the corresponding detection limits. The concentrations of more stable CECs, such as sucralose, did not exhibit major changes in the advanced septic system.

Caffeine concentrations were well correlated to the R1/R5 ( $R^2 = 0.89$ ,  $p < 0.01$ ) and R4/R5 ( $R^2 = 0.90$ ,  $p < 0.01$ ) ratiometric parameters. This outcome aligned with findings from previous reports, in which caffeine degradation was correlated to the removal of R1 fluorescence in municipal wastewater treatment plants<sup>105</sup> and wastewater-impacted rivers<sup>61</sup>. The significant correlations between caffeine, R1/R5, and R4/R5 suggested that the ratiometric parameters serve as indicators of more labile CECs. In contrast, R2/R5 was significantly (but not as well) correlated to caffeine concentrations ( $R^2 = 0.56$ ,  $p = 0.03$ ). The data in Figure 4.7b indicated that the R2/R5 parameter was more stable than R1/R5 and R4/R5 in the advanced septic system, potentially enabling R2/R5 to serve as an indicator for more conservative CECs.

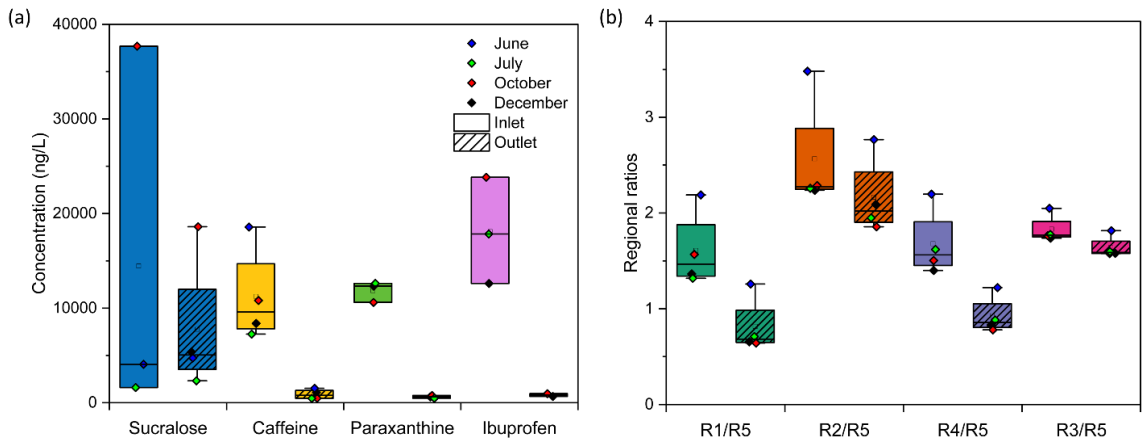


**Figure 4.7. The distribution of (a) CEC concentrations and (b) ratiometric FDOM parameters in the inlet and outlet samples collected from the advanced septic system.**

#### 4.4 Wastewater EEM-PARAFAC modeling

To improve the specificity of the EEM analysis, an EEM-PARAFAC model was developed from the septic wastewater samples. The fluorescence spectra of septic samples were analyzed three times with different dilution factors, and a total of 72 EEMs were generated from 24 unique samples. Three EEMs were excluded due to detector saturation, so the EEM-PARAFAC model was generated from 69 EEMs. Preliminary EEM-PARAFAC models were validated with 2–4 components but not 5–8 components. The 2, 3, and 4-component models had high core consistency and explained variance (Table 4.1), and the sum of squared errors decreased by 34% when the number of components was changed from 3 to 4. All three models had reasonable spectral features (Figure B.4 in Appendix B), but Component 3 of the four-component model exhibited a shoulder in its emission spectrum that was comprised of two overlapping peaks in Regions 1 and 2. A five-component model was considered to separate the noted emission peaks, but that model was not validated by split-half analysis. Previous studies have reported EEM-PARAFAC components with shoulders in the emission spectra<sup>106–108</sup>;

therefore, the four-component EEM-PARAFAC model was used to describe FDOM in septic wastewater (Figure 4.8). Spectral loadings for the model are shown in Figure B.5. The component scores for the model were not correlated before (Figure B.6) or after (Figure B.7) normalization, confirming that the components were independent.

**Table 4.1. Core consistency, explained variance, sum of squared errors (SSE), and validation status for preliminary EEM-PARAFAC models of FDOM in septic wastewater.**

Components	Core consistency (%)	Explained variance (%)	SSE	Validated
2	99.4	95.3	30,900	Yes
3	79.5	96.9	20,700	Yes
4	65.9	97.9	13,700	Yes
5	28.0	98.7	8,390	No
6	6.2	99.1	6,000	No
7	3.3	99.3	4,900	No
8	5.1	99.4	3,990	No

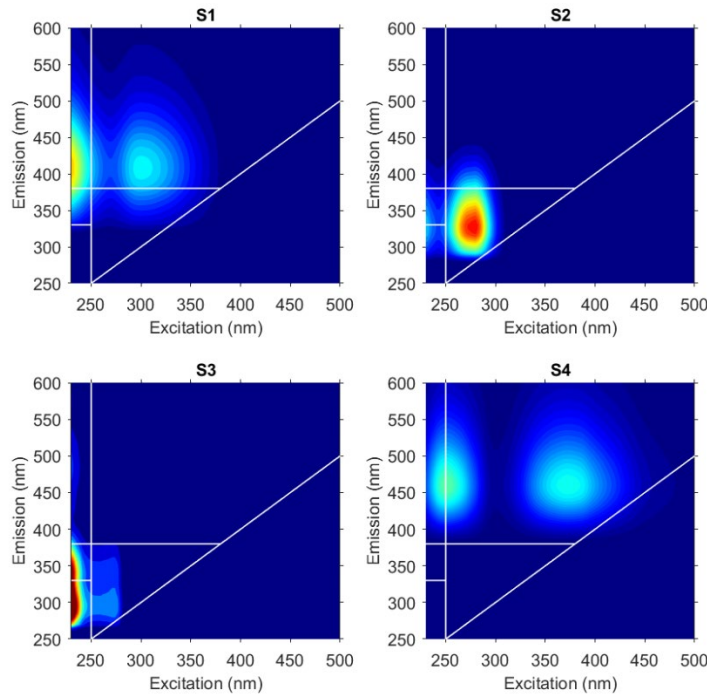


**Figure 4.8. The fluorescence spectra of the four components in the EEM-PARAFAC model for FDOM in septic wastewater.**

Septic wastewater Component 1 (S1) had excitation peaks at 230 and 300 nm and an emission peak at 405 nm. In contrast, Component 2 (S2) only contained one fluorescence peak centered at  $\lambda_{\text{ex}} = 280$  nm and  $\lambda_{\text{em}} = 330$  nm. Component 3 (S3) exhibited an excitation peak at 230 nm with a primary emission peak at 295 nm and a secondary emission shoulder at 340 nm. Similar to S1, Component 4 (S4) displayed two fluorescence peaks at  $\lambda_{\text{ex}} = 250$  and 373 nm and  $\lambda_{\text{em}} = 460$  nm. All four components spanned multiple regions (Table 4.2), but the two humic-like components (*i.e.*, S1, S4) were primarily contained in Region 5. While most of the volume under S1 was in Region 5 (72.4%), S4 almost exclusively fluoresced in Region 5 (95.8%). In contrast, the two protein-like components (*i.e.*, S2, S3) exhibited fluorescence in all five regions. The majority of S2 fluorescence occurred in Region 4 (57.7%), but the volumes in Regions 1 and 2 were much higher than those for S1 and S4. Similarly, S3 exhibited the highest combined fluorescence in the three regions related to wastewater FDOM: 18.9% in Region 1; 10.2% in Region 2; and 38.0% in Region 4. Because all four components spanned the conventional regions used to describe EEMs, the EEM-PARAFAC model improved the specificity of FDOM analysis and characterization for septic wastewater.

**Table 4.2. Percent fluorescence in each region for the FDOM components in the septic wastewater EEM-PARAFAC model.**

Component	Region 1	Region 2	Region 3	Region 4	Region 5
S1	0.2%	2.8%	14.7%	9.9%	72.4%
S2	4.8%	5.4%	7.8%	57.7%	24.2%
S3	18.9%	10.2%	16.9%	38.0%	16.0%
S4	< 0.1%	< 0.1%	4.0%	0.2%	95.8%

The fluorescence spectra for the four-component EEM-PARAFAC model for septic wastewater were uploaded to the OpenFluor database <sup>79</sup>. For a Tucker's correlation

coefficient greater than 0.95, S1, S2, and S4 generated significant matches with 41, 43, and 7 previously reported models, respectively. Wavelengths below 250 nm are often excluded from EEM-PARAFAC models due to noisy fluorescence signals. With a peak at  $\lambda_{\text{ex}} = 230$  nm, S3 did not generate any matches at the 0.95 level, but six significant matches were obtained for a Tucker's correlation coefficient greater than 0.90. The top matches for each component are described in Table 4.3. Based on prior reports, S1 was representative of marine humic-like fluorophores and related to Peak M, S2 was a tryptophan-like fluorophore associated with Peak T, S3 was related to tyrosine-like fluorophores and similar to Peak B, and S4 was a terrestrial humic-like fluorophore related to Peaks A and C.

**Table 4.3. Top OpenFluor matches for the spectra of each component in the septic wastewater EEM-PARAFAC model.** Unless indicated, the top 10 significant matches are shown for Tucker’s correlation coefficient greater than 0.95. Data were collected in February 2023.

Reference	Component assignment and description <sup>a</sup>	Location	Sample type	Excitation/emission similarity score
<b>Septic Wastewater Component 1 (S1)</b>				
Gao and Gueguen (2017) <sup>109</sup>	C1: marine humic-like	Beaufort Sea, Canada Basin	Seawater	0.9971 / 0.9892
Gao and Gueguen (2018) <sup>110</sup>	C2: combination of ultraviolet (UV) humic-like and marine humic-like	Canada Basin and Canadian Arctic Archipelago	Seawater	0.9947 / 0.9913
Chen <i>et al.</i> (2016) <sup>111</sup>	C2: marine / microbial humic-like	Chukchi-East Siberian Seas, Arctic Ocean	Sediment pore waters	0.9877 / 0.9942
Sheng <i>et al.</i> (2021) <sup>112</sup>	C2: terrestrially-derived, humic-like	Nanchang City, China	Settled dust	0.9866 / 0.9930
Pitta and Zeri (2021) <sup>113</sup>	ALL2: marine humic-like, Peak M	Eastern Mediterranean Sea	Sea, river, and lagoon	0.9783 / 0.9987
Schafer <i>et al.</i> (2021) <sup>114</sup>	C2: UV-A humic-like, Peak A	St. Augustine, Florida, USA	Photodegraded <i>Taxodium distichum</i> leachate in deionized water	0.9888 / 0.9866
Chen <i>et al.</i> (2018) <sup>115</sup>	C <sub>&lt;260(305)/404</sub> : humic-like	Chukchi Sea, Arctic Ocean	Seawater	0.9877 / 0.9859
Dainard and Gueguen (2013) <sup>116</sup>	C2: UV humic-like	Bering, Chukchi and Beaufort Seas and North Pacific Ocean	Seawater	0.9897 / 0.9829
Wunsch <i>et al.</i> (2018) <sup>117</sup>	C <sub>410</sub> : humic-like	Arctic Fjords, Greenland and Iceland	Seawater	0.9915 / 0.9786
Vines and Terry (2020) <sup>118</sup>	C2: microbial humic-like	Tuscaloosa, AL, USA	Wastewater treatment plant effluent	0.9770/ 0.9923
<b>Septic Wastewater Component 2 (S2)</b>				
Yamashita <i>et al.</i> (2010) <sup>119</sup>	C7: protein-like	Everglades, Florida, USA	Surface water	0.9957 / 0.9947
Graeber <i>et al.</i> (2021) <sup>120</sup>	C <sub>T</sub> : tryptophan / protein-like, microbially produced, bioavailable	Bode River, Germany	Freshwater	0.9957 / 0.9929
Ryan <i>et al.</i> (2022) <sup>121</sup>	C3: tryptophan-like	Salmon aquaculture facilities, Chile	Upstream and effluent from aquaculture facilities	0.9965 / 0.9916
Harjung <i>et al.</i> (2018) <sup>122</sup>	C3: amino acids, free or bound in proteins, may indicate intact proteins, Peak T	Austria	Constructed streamside flumes	0.9902 / 0.9921

Reference	Component assignment and description <sup>a</sup>	Location	Sample type	Excitation/emission similarity score
Wunsch <i>et al.</i> (2018) <sup>117</sup>	C <sub>330</sub> : protein-like	Arctic Fjords, Greenland and Iceland	Seawater	0.9986 / 0.9834
Gueguen <i>et al.</i> (2014) <sup>123</sup>	C4: protein-like	Canadian Arctic Archipelago	Seawater	0.9952 / 0.9858
Cohen <i>et al.</i> (2014) <sup>124</sup>	C1: protein-like, tryptophan-like	Israel	Municipal wastewater from treatment plants	0.9985 / 0.9825
Stedmon and Markager (2005) <sup>125</sup>	C4: protein-like, tryptophan-like, tyrosine-like, Peak T	Bergen, Norway	Fjord water	0.9887 / 0.9914
Wang <i>et al.</i> (2020) <sup>126</sup>	C4: protein-like, tyrosine-like, tryptophan-like	Minjiang River, China	Freshwater	0.9985 / 0.9784
Yamashita <i>et al.</i> (2010) <sup>127</sup>	C4: tyrosine-like	Okhotsk Sea and North Pacific Ocean	Seawater	0.9865 / 0.9898
<b>Septic Wastewater Component 3 (S3) <sup>b</sup></b>				
Dall'Osto <i>et al.</i> (2022) <sup>128</sup>	P2: protein-like, Peak B	Bransfield Strait, Weddell Sea	Sea ice and seawater	0.9709 / 0.9460
Schafer <i>et al.</i> (2021) <sup>114</sup>	C1: amino acid-like	St. Augustine, Florida, USA	Estuarine and freshwater	0.9376 / 0.9662
Brogi <i>et al.</i> (2022) <sup>129</sup>	C6: polycyclic aromatic hydrocarbon-like	Arno River, Italy	Surface water	0.9804 / 0.9226
D'Andrilli and McConnell (2021) <sup>130</sup>	GISP2 C1: monolignol-like, tyrosine-like, tannin-like, simple phenol/amino acid-like	Greenland Ice Sheet, Greenland	Ice cores	0.9466 / 0.9546
D'Andrilli and McConnell (2021) <sup>130</sup>	Agassiz C1: monolignol-like, tyrosine-like, tannin-like, simple phenol/amino acid-like	Agassiz Ice Cap, Canada	Ice cores	0.9472 / 0.9527
Kida <i>et al.</i> (2019) <sup>131</sup>	C <sub>300</sub> : protein-like, tyrosine-like	Lutzow-Holm Bay and Amundsen Bay, Antarctica	Lake water	0.9556 / 0.9440
<b>Septic Wastewater Component 4 (S4) <sup>c</sup></b>				
Gao and Gueguen (2017) <sup>109</sup>	C3: terrestrial humic-like	Beaufort Sea, Canada Basin	Seawater	0.9801 / 0.9965
Lozada <i>et al.</i> (2021) <sup>132</sup>	C2: humic-like, Peaks A and C	Punta Este, Chubut, Argentina	Seawater	0.9830 / 0.9854
Shakil <i>et al.</i> (2020) <sup>133</sup>	C4: terrestrial humic-/fulvic-like	Peel Plateau, Northwest Territories, Canada	Surface water	0.9733 / 0.9843
Sheng <i>et al.</i> (2021) <sup>112</sup>	C3: microbial humic-like	Nanchang City, China	Settled dust	0.9739 / 0.9818
Vines and Terry (2020) <sup>118</sup>	B2: microbially-derived, humic-like from terrestrial aquatic environment	Tuscaloosa, AL, USA	River surface water	0.9680 / 0.9853

<b>Reference</b>	<b>Component assignment and description <sup>a</sup></b>	<b>Location</b>	<b>Sample type</b>	<b>Excitation/emission similarity score</b>
Bernal <i>et al.</i> (2018) <sup>134</sup>	C3: humic-like	Font del Regas catchment, Montseny Natural Park, Spain	Surface water and groundwater	0.9592 / 0.9930
Murphy <i>et al.</i> (2011) <sup>135</sup>	G1: terrestrial humic-like fluorescence in high nutrient and wastewater-impacted environments	Australia	Recycled water from treatment plants	0.9549 / 0.9973

a: component labels stem from the original references

b: no significant matches were obtained for Tucker's correlation coefficient > 0.95, the reported matches are for Tucker's correlation coefficient > 0.90

c: only seven significant matches were obtained for Tucker's correlation coefficient > 0.95



A more robust EEM-PARAFAC model was generated for wastewater FDOM using the 69 EEMs from septic wastewater and 12 additional EEMs from four unique municipal wastewater samples. Preliminary models were developed with 2–8 components, but only the 2, 5, 6, and 7-component models were validated by split-half analysis. Spectral loadings for the preliminary models are available in Figure B.8. The SSE decreased by more than 70% when the number of components was increased from 2 to 5 (Table 4.4). When the number of components was changed from 5 to 6, the core consistency decreased from 31.6% to 3.4%. Therefore, a five-component EEM-PARAFAC model was developed and validated as a global representation of wastewater FDOM in the study area (Figure 4.9). The spectral loadings for each component were reasonable (Figure B.9), and component scores were not correlated before (Figure B.10) or after (Figure B.11) normalization, confirming their independent nature.

**Table 4.4. Core consistency, explained variance, SSE, and validation status for preliminary EEM-PARAFAC models of FDOM in septic and municipal wastewater.**

<b>Components</b>	<b>Core consistency (%)</b>	<b>Explained variance (%)</b>	<b>SSE</b>	<b>Validated</b>
2	99.3	95.2	36,500	Yes
3	70.5	96.7	25,000	No
4	52.5	97.7	17,500	No
5	31.6	98.7	10,100	Yes
6	3.4	99.0	7,430	Yes
7	3.8	99.2	5,890	Yes
8	5.6	99.4	4,810	No

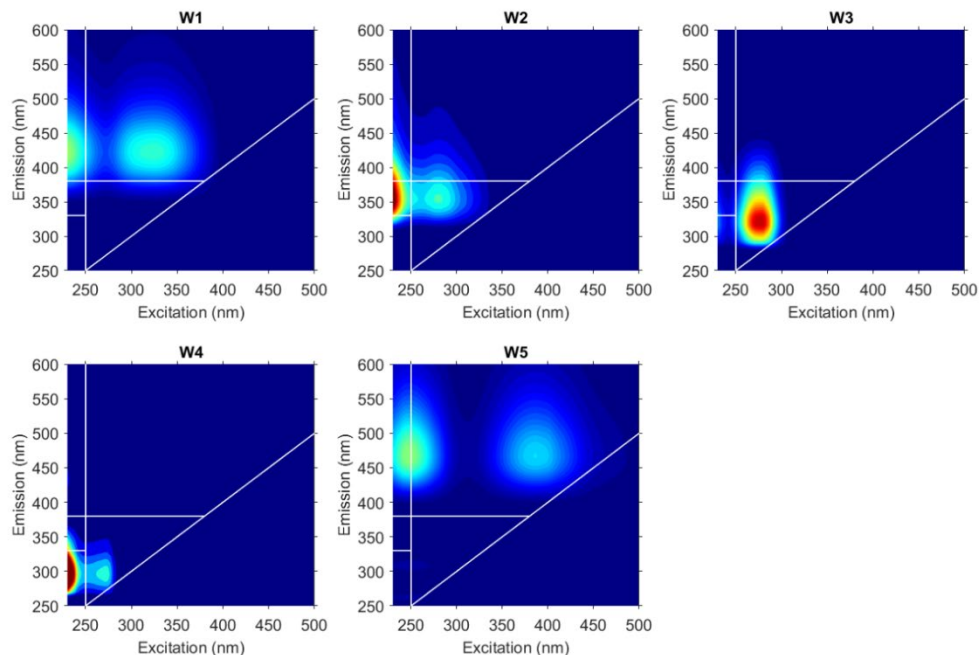


**Figure 4.9. The fluorescence spectra of the five components in the global EEM-PARAFAC model for FDOM in septic and municipal wastewater.**

By including the municipal wastewater samples in the fluorescence model, a more robust EEM-PARAFAC model was generated with three wastewater-like components.

Components 3 (W3) and 5 (W5) of the global wastewater EEM-PARAFAC model were similar to S2 and S4 in the septic wastewater model. The fluorescence associated with S1 and S3 was split into W1, W2, and W4. W1 was similar to S1 but with minor hypsochromic shifts in the secondary excitation peak (325 nm) and emission peak (420 nm). W2 comprised aspects of S1 and S3, namely peaks at  $\lambda_{ex} = 230$  and 280 nm and  $\lambda_{em} = 355$  nm. W4 also exhibited similar fluorescence characteristics as S1 and S3, with two fluorescence peaks centered at excitation wavelengths of 230 and 271 nm and emission at 295 nm. All five components spanned multiple regions (Table 4.5). W1 and W5 were primarily located in Region 5 but with secondary fluorescence in Region 3, suggesting

that these components were less useful as wastewater indicators. In contrast, W3 primarily fluoresced in Region 4 (61.2%), W4 exhibited fluorescence in both Region 1 (30.1%) and Region 4 (46.3%), and W2 showed notable fluorescence in Region 2 (9.4%), Region 3 (18.7%), Region 4 (27.3%), and Region 5 (43.3%). As with the septic wastewater model, the wide coverage of global wastewater EEM-PARAFAC components across regions added specificity to potential indicators derived from FDOM signatures.

**Table 4.5. Percent fluorescence in each region for the FDOM components in the global wastewater EEM-PARAFAC model.**

Component	Region 1	Region 2	Region 3	Region 4	Region 5
<b>W1</b>	< 0.1%	0.8%	11.4%	3.3%	84.6%
<b>W2</b>	1.4%	9.4%	18.7%	27.3%	43.3%
<b>W3</b>	4.7%	4.4%	6.3%	61.2%	23.4%
<b>W4</b>	30.1%	5.1%	9.1%	46.3%	9.4%
<b>W5</b>	0.1%	< 0.1%	5.9%	0.9%	93.1%

The excitation and emission spectra for the five-component global wastewater EEM-PARAFAC model were uploaded to the OpenFluor database. For Tucker’s correlation coefficient greater than 0.95, W1, W2, W3, W4, and W5 generated significant matches with 8, 17, 38, 3, and 5 previously reported components, respectively. The top matches for each component are reported in Table 4.6. Based on the OpenFluor data, W1 and W5 were associated with ubiquitous humic-like fluorophores and terrestrially-derived, microbial humic-like fluorophores, respectively. W2 was primarily composed of tryptophan-like fluorophores (Region 2), and W4 aligned with tyrosine-like fluorophores (Region 1). W3 showed similar fluorescence as protein-like fluorophores that were recently produced by bacteria. These associations confirmed the potential relationship between W2, W3, and W4 and wastewater.

**Table 4.6. Top OpenFluor matches for the spectra of each component in the global wastewater EEM-PARAFAC model.** Unless indicated, the top 10 significant matches are shown for Tucker’s correlation coefficient greater than 0.95. Data were collected in February 2023.

Reference	Component assignment and description <sup>a</sup>	Location	Sample type	Excitation/emission similarity score
<b>Global Wastewater Component 1 (W1)<sup>b</sup></b>				
Dainard and Gueguen (2013) <sup>116</sup>	C2: UV humic-like, Peak A	Bering, Chukchi and Beaufort Seas and North Pacific Ocean	Seawater	0.9974 / 0.9835
Bittar <i>et al.</i> (2016) <sup>136</sup>	C1: humic-like, terrigenous material, with potential agricultural influence	Skidaway River, Savannah, GA, USA	Estuary water	0.9856 / 0.9843
Ren <i>et al.</i> (2021) <sup>137</sup>	C1: humic-like, Peak C	Xiandao, Baoan, Daye, and Qingshan lakes, Hubei Province, China	Freshwater	0.9665 / 0.9934
Kida <i>et al.</i> (2019) <sup>131</sup>	C <sub>415</sub> : humic-like, ubiquitous	Lutzow-Holm Bay and Amundsen Bay, Antarctica	Lake water	0.9704 / 0.9865
Garcia <i>et al.</i> (2015) <sup>138</sup>	C1: humic-like, terrestrially derived, Peaks A and M	Glacial Lake District, Southern Andes, Nahuel Huapi National Park, Patagonia, Argentina	Stream samples	0.9658 / 0.9902
Yamashita <i>et al.</i> (2011) <sup>139</sup>	C1: humic-like, fulvic acid-like, Peak C	Nantahala Mountains, western NC, USA	Freshwater	0.9554 / 0.9994
Walker <i>et al.</i> (2013) <sup>140</sup>	C1: humic-like, terrestrially-like, Peaks A and C	Mackenzie, Lena, Kolyma, Ob, and Yenisei Arctic Rivers	Freshwater	0.9576 / 0.9950
Zhuang <i>et al.</i> (2022) <sup>141</sup>	C3: humic-like	Fuzhou City and Minjiang River, China	Plant and leaf litter leachates, wastewater influent and effluent, river surface water	0.9696 / 0.9823
<b>Global Wastewater Component 2 (W2)</b>				
Wunsch <i>et al.</i> (2017) <sup>142</sup>	C <sub>350</sub> : protein-like	Lake Lillsjon and Svartan River, Sweden; Rio Negro and Rio Tapajos, Brazil	Freshwater	0.9953 / 0.9917
Weigelhofer <i>et al.</i> (2020) <sup>143</sup>	C2: tryptophan-like, microbial-delivered autochthonous	Light versus dark lab flume experiments	Leaf and cow dung leachates	0.9981 / 0.9873

Reference	Component assignment and description <sup>a</sup>	Location	Sample type	Excitation/emission similarity score
Stedmon <i>et al.</i> (2011) <sup>144</sup>	C4: tryptophan-like, indicator of waste contamination	Farum, Denmark	Drinking water from a treatment plant	0.9939 / 0.9832
Heibati <i>et al.</i> (2018) <sup>122</sup>	F4: protein-like, tryptophan-like	Central Eastern Sweden	Municipal drinking water from a distribution network	0.9901 / 0.9829
Borisover <i>et al.</i> (2011) <sup>145</sup>	C2: tryptophan-like, labile organic matter related to phytoplankton productivity	Kishon River, Israel	Surface water	0.9888 / 0.9841
Bittar <i>et al.</i> (2016) <sup>136</sup>	C3: protein-like, microbial/ autochthonous origin	Skidaway River, Savannah, GA, USA	Estuary water	0.9935 / 0.9755
Yamashita <i>et al.</i> (2011) <sup>139</sup>	C5: protein-like, tryptophan-like	Nantahala Mountains, NC, USA	Freshwater	0.9947 / 0.9735
Queimalinos <i>et al.</i> (2019) <sup>146</sup>	C3: non-humic and aliphatic compounds, Peak T	Nahuel Huapi National Park, Patagonia, Argentina	Lake water	0.9870 / 0.9765
Kida <i>et al.</i> (2019) <sup>131</sup>	C <sub>360</sub> : non-humic, Peak N	Lutzow-Holm Bay and Amundsen Bay, Antarctica	Lake water	0.9760 / 0.9873
Graeber <i>et al.</i> (2012) <sup>147</sup>	C5: protein- and tryptophan-like, microbially produced	Brandenburg, Germany	Freshwater	0.9862 / 0.9759
<b>Global Wastewater Component 3 (W3)</b>				
Yamashita <i>et al.</i> (2010) <sup>119</sup>	C7: protein-like	Everglades, Florida, USA	Surface water	0.9709 / 0.9460
Wunsch <i>et al.</i> (2018) <sup>117</sup>	C <sub>330</sub> : protein-like	Arctic Fjords, Greenland and Iceland	Seawater	0.9376 / 0.9662
Ryan <i>et al.</i> (2022) <sup>121</sup>	C3: tryptophan-like	Salmon aquaculture facilities, Chile	Upstream and effluent from aquaculture facilities	0.9804 / 0.9226
Gueguen <i>et al.</i> (2014) <sup>123</sup>	C4: protein-like	Canadian Arctic Archipelago	Seawater	0.9466 / 0.9546
Graeber <i>et al.</i> (2021) <sup>120</sup>	C <sub>7</sub> : tryptophan/ protein-like, microbially produced, bioavailable	Bode River, Germany	Freshwater	0.9472 / 0.9527
Dainard <i>et al.</i> (2019) <sup>148</sup>	C3: protein-like	Canada Basin, Beaufort Sea	Seawater	0.9556 / 0.9440
Cory and McKnight (2005) <sup>149</sup>	C8: tryptophan-like	Lake Fryxell, Antarctica Nymph Lake, Colorado Toolik Lake, Alaska	Freshwater	0.9268 / 0.9678

Reference	Component assignment and description <sup>a</sup>	Location	Sample type	Excitation/emission similarity score
Dainard <i>et al.</i> (2015) <sup>150</sup>	C4: protein-like, recent biological production	Beaufort Sea and North Atlantic Subtropical Gyre	Seawater	0.9359 / 0.9557
Harjung <i>et al.</i> (2018) <sup>122</sup>	C3: amino acids, free or bound in proteins, may indicate intact proteins, Peak T	Austria	Constructed streamside flumes	0.9134 / 0.9750
Goncalves-Araujo (2015) <sup>151</sup>	C6: protein-like	Lena River Delta region, Laptev Sea, Siberia	Seawater	0.9746 / 0.9121
<b>Global Wastewater Component 4 (W4)<sup>c</sup></b>				
Chen <i>et al.</i> (2018) <sup>115</sup>	C-<270/302: tyrosine-like	Chukchi Sea, Arctic Ocean	Seawater	0.9931 / 0.9773
D'Andrilli and McConnell (2021) <sup>130</sup>	ACT-10 C3: tyrosine-like	Greenland Ice Sheet, Greenland	Ice cores	0.9809 / 0.9894
Dall'Osto <i>et al.</i> (2022) <sup>128</sup>	P2: protein-like, Peak B	Bransfield Strait, Weddell Sea	Sea ice and seawater	0.9819 / 0.9801
<b>Global Wastewater Component 5 (W5)<sup>d</sup></b>				
Sheng <i>et al.</i> (2021) <sup>112</sup>	C3: microbial humic-like	Nanchang City, China	Settled dust	0.9862 / 0.9986
Jutaporn <i>et al.</i> (2020) <sup>152</sup>	C3: UV-A and UV-C humic-like, terrestrially derived, Peak C	Chapel Hill and Carrboro, NC, USA	Surface water and wastewater effluent	0.9822 / 0.9983
Vines and Terry (2020) <sup>118</sup>	B2: microbially derived humic-like from terrestrial aquatic environment	Tuscaloosa, AL, USA	River surface water	0.9690 / 0.9954
Cohen <i>et al.</i> (2014) <sup>124</sup>	C4: humic-like	Israel	Municipal wastewater from treatment plants	0.9757 / 0.9852
Weigelhofer <i>et al.</i> (2020) <sup>143</sup>	C3: humic-like, terrestrial delivered, Peaks A and C, high molecular weight	Light versus dark lab flume experiments	Leaf and cow dung leachates	0.9644 / 0.9911

a: component labels stem from the original references

b: only eight significant matches were obtained for Tucker's correlation coefficient > 0.95

c: only three significant matches were obtained for Tucker's correlation coefficient > 0.95

d: only five significant matches were obtained for Tucker's correlation coefficient > 0.95

Given its better specificity, the global wastewater EEM-PARAFAC model was used to track the change in maximum fluorescence intensity ( $F_{\max}$ ) values for each component in the advanced septic system. Two of the protein-like components, W3 and W4, experienced 89.9% and 63.2% degradation, respectively, in the aerobic treatment process (Figure 4.10a). The other protein-like component, W2, and the two humic-like components, W1 and W5, were not significantly degraded. To better account for FDOM composition, ratiometric parameters were calculated from the  $F_{\max}$  values for the EEM-PARAFAC components. As discussed in Section 4.3, correlations between fluorescence ratios and CEC concentrations can highlight contaminant degradation in septic systems or attenuation in drainfields and, thereby, inform the selection of fluorescence indicators for partially and fully treated septic wastewater. Partially treated septic wastewater was defined by the presence of labile CECs, which were not present in fully treated septic wastewater. As shown in Figure 4.10b, caffeine levels were well correlated with the W3/W1 ( $R^2 = 0.91$ ,  $p < 0.01$ ), W3/W5 ( $R^2 = 0.80$ ,  $p < 0.01$ ), W4/W1 ( $R^2 = 0.84$ ,  $p < 0.01$ ), and W4/W5 ( $R^2 = 0.92$ ,  $p < 0.01$ ) ratiometric parameters; while  $R^2$  was lower (0.57), caffeine concentrations were also correlated to W2/W5 values ( $p = 0.03$ ). In contrast, W2/W1 was not correlated with caffeine concentration ( $R^2 = 0.26$ ,  $p = 0.20$ ). Taken together, these results suggest that the W3/W1, W3/W5, W4/W1, and W4/W5 ratiometric parameters should be explored as indicators of partially treated wastewater, and the W2 ratios should be considered as indicators of fully treated septic effluent.

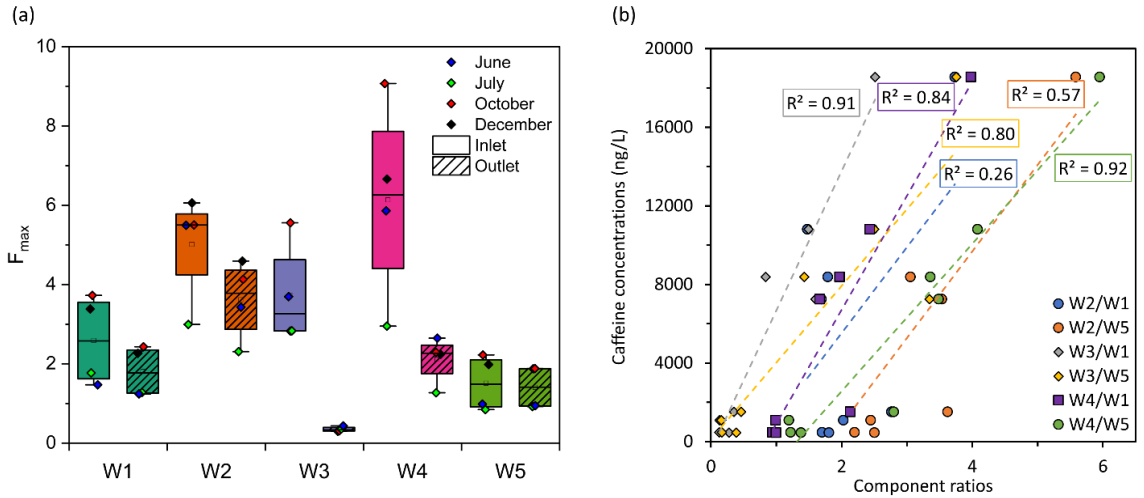


**Figure 4.10. (a) The distribution of EEM-PARAFAC components and (b) correlations between ratiometric FDOM parameters and caffeine concentrations in samples collected from the inlet and outlet of the advanced septic system.**

#### 4.5 Septic wastewater characterization conclusion

More CECs were detected in municipal wastewater, but higher CEC concentrations were measured in septic tanks, suggesting the potential for ecotoxicity concerns in areas with high septic system density. Future risk assessment based on CEC levels in septic wastewater and downgradient stream water samples is recommended to further evaluate that potential. Furthermore, these findings support the potential use of CECs as septic wastewater indicators in nearby surface water. Based on prior studies, detection frequency, and CEC levels, caffeine and ibuprofen were proposed as indicators of partially treated wastewater, while sucralose, carbamazepine, and sulfamethoxazole were suggested as conservative indicators of septic effluent. CEC analysis is expensive and time-consuming, leading to opportunities for development of alternative indicators. Septic tanks contained FDOM signals, including consistent fluorescence peaks in Regions 1, 2, and 4, that can potentially serve as wastewater indicators in nearby surface



water. Temporal variations in the fluorescence intensity of septic FDOM mandated the need for ratiometric parameters that provide insight into FDOM composition. Based on correlations with caffeine concentrations in an advanced septic system, the R1/R5 and R4/R5 parameters may effectively function as indicators of partially treated septic effluent. In contrast, the R2/R5 values were more stable, suggesting the potential use of this ratiometric parameter as an indicator of more conservative CECs. The EEM-PARAFAC models improved the specificity of FDOM parameters from EEM analysis and enabled new opportunities to monitor wastewater inputs in nearby surface water. Based on correlations between EEM-PARAFAC components and CEC levels, four ratiometric parameters (*i.e.*, W3/W1, W3/W5, W4/W1, W4/W5) were identified as potential indicators of partially treated septic wastewater; furthermore, two other component ratios (*i.e.*, W2/W1, W2/W5) were recommended as indicators of treated septic effluent. In Chapter 5, these novel parameters were applied to describe the FDOM measured in stream samples to investigate performance in real settings.

## **Chapter 5: Septic wastewater indicator profiles in the North Branch**

### 5.1. EEM-PARAFAC model for the North Branch

The EEMs from all stream samples collected during the North Branch spatially resolved sampling campaign (Section 3.3.1), thermal infrared (TIR) survey (Section 3.3.2), and wet weather sampling event (Section 3.3.3) were used to build an EEM-PARAFAC model for the North Branch. The model was constructed from 193 samples; note, four samples with low fluorescence intensity were excluded. Preliminary EEM-PARAFAC models were generated with 2 – 8 components, but the models with 6 – 8 components were not validated. The core consistency was high for models with 2, 3, and 4 components but decreased to 30.7% for the 5-component model (Table 5.1). The explained variance increased and the sum of the squared errors (SSE) decreased when the number of components was increased from two to four. The four-component model included a protein-like component (Figure C.1 in Appendix C) that was not present in models with fewer components. This component was also present in the five-component model, which was less preferred due to the low core consistency. Therefore, a four-component EEM-PARAFAC model was used to describe FDOM in the North Branch (Figure 5.1). The spectral loadings for the four components are available in Figure C.2. The component scores were not correlated before (Figure C.3) or after (Figure C.4) data normalization, confirming that the components were independent.

**Table 5.1. Core consistency, explained variance, sum of squared errors (SSE), and validation status for preliminary EEM-PARAFAC models of FDOM in the North Branch.**

Components	Core consistency (%)	Explained variance (%)	SSE	Validated
2	97.6	98.2	36,100	Yes
3	81.6	99.0	19,200	Yes
4	74.7	99.3	13,000	Yes
5	30.7	99.5	9,280	Yes
6	4.4	99.6	7,350	No
7	1.5	99.7	5,690	No
8	0.7	99.8	4,320	No

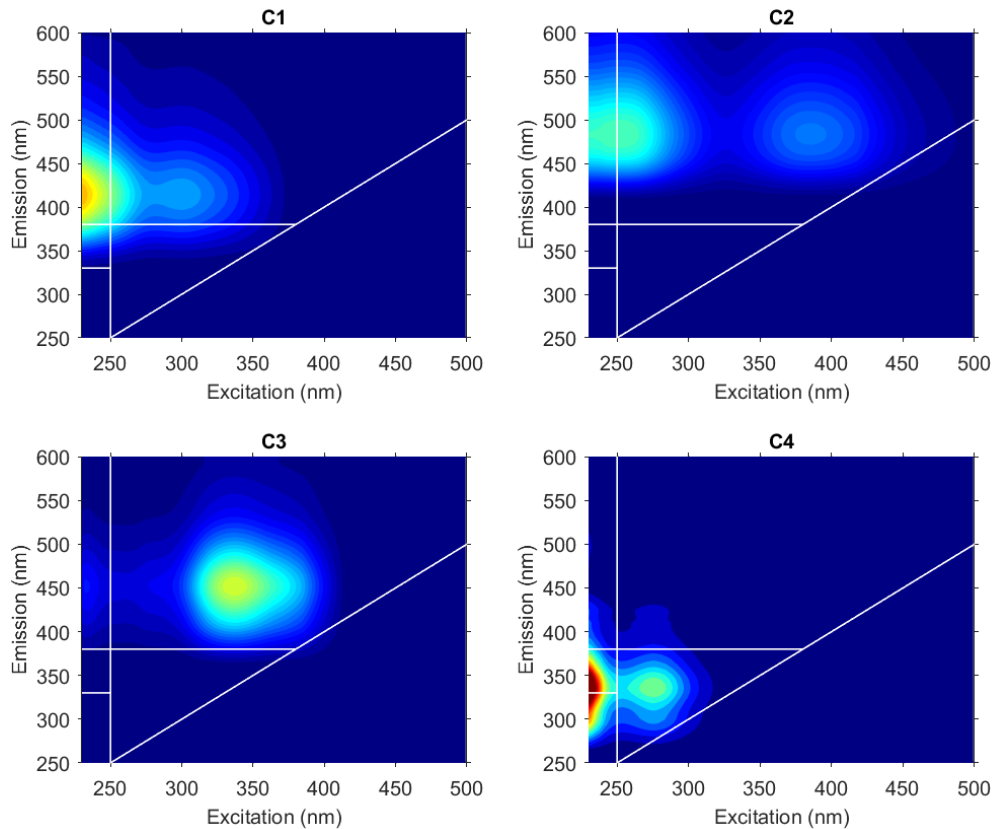


**Figure 5.1. The fluorescence spectra of the four components in the EEM-PARAFAC model for FDOM in the North Branch.**

North Branch Components 1 (C1), 2 (C2), and 3 (C3) predominantly fluoresced in Region 5 (Table 5.2). C1 was similar to S1 (septic wastewater), with primary and secondary excitation peaks at 230 and 300 nm and emission at 415 nm. With two peaks at

$\lambda_{\text{ex}} = 250$  and  $385$  nm, C2 was similar to S4 and W5 but with a hypsochromic shift in emission to  $\lambda_{\text{em}} = 485$  nm. The fluorescence peak of C3, centered at  $\lambda_{\text{ex}} = 335$  nm and  $\lambda_{\text{em}} = 450$  nm, did not appear in the wastewater models, suggesting that this fluorophore stems from natural processes. The fluorescence of C4 spanned all five regions, with 43.5% of the volume in Region 4 and 21.3% volume in Regions 1 and 2 (Table 5.2). The fluorescence peaks of C4 were located at  $\lambda_{\text{ex}} = 230$  and  $275$  nm and  $\lambda_{\text{em}} = 335$  nm. The fluorescence signature of C4 did not directly match any of the wastewater components but could be estimated using linear regressions of either S2 and S3 or W2, W3, and W4 (Figure C.5). This outcome suggests that C4 originated from septic wastewater as a mixture of the protein-like components from the wastewater models. As these protein-like components were transported into nearby surface waters, they coalesced into a single component, C4, which was then measurable throughout the North Branch.

**Table 5.2. Percent fluorescence in each region for the FDOM components in the North Branch EEM-PARAFAC model.**

Component	Region 1	Region 2	Region 3	Region 4	Region 5
C1	< 0.1%	1.4%	10.5%	7.0%	81.0%
C2	0.1%	< 0.1%	7.5%	0.5%	92.0%
C3	< 0.1%	0.2%	11.5%	0.9%	87.4%
C4	10.1%	11.2%	16.2%	43.5%	19.0%

The fluorescence spectra for the four-component North Branch EEM-PARAFAC model were uploaded to the OpenFluor database <sup>79</sup>. C1, C2, C3, and C4 generated significant matches with 83, 58, 8, and 61 previously reported components, respectively, when the Tucker's correlation coefficient was greater than 0.95. The top matches for each component are reported in Table 5.3. Based on the similarity scores, C1 was related to

marine or terrestrial humic-like fluorophores with biological or microbial origin. Both C2 and C3 exhibited terrestrial humic-like fluorescence and were closely related to Peaks A and C. Finally, C4 was associated with Peak T and contained microbially-derived, protein- or tryptophan-like fluorophores.

**Table 5.3. Top OpenFluor matches for the spectra of each component in the North Branch EEM-PARAFAC model.** Unless indicated, the top 10 significant matches are shown for Tucker’s correlation coefficient greater than 0.95. Data were collected in February 2023.

Reference	Component assignment and description <sup>a</sup>	Location	Sample type	Excitation/emission similarity score
<b>North Branch Component 1 (C1)</b>				
Romero <i>et al.</i> (2017) <sup>153</sup>	C1: terrestrial humic-like, mid-size	Bozeman, Montana, USA	Soil extracts from wheat-based cropping systems	0.9975 / 0.9951
Osburn <i>et al.</i> (2012) <sup>154</sup>	C2: humic-like, possible photodegradation product	Neuse River Basin, North Carolina, USA	Surface water	0.9971 / 0.9945
Yamashita <i>et al.</i> (2013) <sup>155</sup>	C1: marine humic-like, Peak M, microbial humic-like	Florida Keys, Florida, USA	Surface water	0.9965 / 0.9948
Gao and Gueguen (2017) <sup>109</sup>	C1: marine humic-like, Peak M, biological or microbial origin	Beaufort Sea, Canada Basin	Seawater	0.9956 / 0.9955
Cawley <i>et al.</i> (2012) <sup>156</sup>	C1: humic-like	Shark Bay, Australia	Surface water	0.9919 / 0.9981
Yamashita <i>et al.</i> (2021) <sup>157</sup>	C1: humic-like	Dorokawa, Butokamabetsu, and Akaishi Rivers, northern Hokkaido, Japan	Stream water	0.9946 / 0.9945
Shakil <i>et al.</i> (2020) <sup>133</sup>	C1: terrestrial humic-/fulvic-like	Peel Plateau, Northwest Territories, Canada	Stream water	0.9933 / 0.9950
Chen <i>et al.</i> (2018) <sup>115</sup>	C <sub>&lt;260(305)/404</sub> : Marine humic-like	Chukchi Sea, Arctic Ocean	Seawater	0.9903 / 0.9976
Shutova <i>et al.</i> (2014) <sup>158</sup>	C2: humic-like, terrestrial delivered, Peaks A and C	Yarra Glen water treatment plant, Victoria, Australia	Water samples from each treatment stage	0.9983 / 0.9895
Peleato <i>et al.</i> (2016) <sup>159</sup>	C3: processed or degraded humic-like	Pilot-scale laboratory biofiltration study with Otonabee River water, Peterborough, Ontario	River water through biofiltration treatment	0.9918 / 0.9955
<b>North Branch Component 2 (C2)</b>				
Zhuang <i>et al.</i> (2021) <sup>160</sup>	C2: terrestrial humic-like	Minjiang Watershed, China	Rainwater, fresh plant, leaf litter, wastewater, and river samples	0.9941 / 0.9911
Smith <i>et al.</i> (2021) <sup>161</sup>	C3: humic-like, autochthonous production and/or influence from anthropogenic sources	Wagner Creek, Coral Gables, and Little River, Miami, Florida, USA	Surface water	0.9881 / 0.9969

Reference	Component assignment and description <sup>a</sup>	Location	Sample type	Excitation/emission similarity score
Murphy <i>et al.</i> (2006) <sup>162</sup>	C3: humic-like	North Pacific and Atlantic oceans	Seawater	0.9913 / 0.9943
Shutova <i>et al.</i> (2014) <sup>158</sup>	C1: humic-like, terrestrial delivered, Peaks A and C	Yarra Glen water treatment plant, Victoria, Australia	Water samples from each treatment stage	0.9861 / 0.9963
Peleato <i>et al.</i> (2016) <sup>159</sup>	C2: terrestrial humic-like	Pilot-scale laboratory biofiltration study with Otonabee River water, Peterborough, Ontario	River water through biofiltration treatment	0.9892 / 0.9931
Murphy <i>et al.</i> (2008) <sup>52</sup>	C3: humic-like	North Pacific and Atlantic oceans	Seawater	0.9946 / 0.9867
Dall'Osto <i>et al.</i> (2022) <sup>128</sup>	H2: humic-like, Peak C	Bransfield Strait, Weddell Sea	Sea ice and seawater	0.9857 / 0.9941
Pitta and Zeri (2021) <sup>113</sup>	SWRV2: humic-like, Peaks A and C	Eastern Mediterranean Sea	Seawater and river water	0.9886 / 0.9910
Dainard and Gueguen (2013) <sup>116</sup>	C1: terrestrial humic-like	Bering, Chukchi, and Beaufort Seas and North Pacific Ocean	Seawater	0.9802 / 0.9993
Pitta and Zeri (2021) <sup>113</sup>	RV2: humic-like, Peaks A and C	Eastern Mediterranean Sea	River water	0.9844 / 0.9950
<b>North Branch Component 3 (C3)<sup>b</sup></b>				
Chen <i>et al.</i> (2018) <sup>163</sup>	C1: humic-like, Peak C, high molecular weight and aromatic, terrestrial	Lake Taihu and Lake Hongze, China	Surface water	0.9827 / 0.9955
Lambert <i>et al.</i> (2016) <sup>164</sup>	C3: terrestrial humic-like, Peak C, high aromaticity, high molecular weight, photosensitive	Congo River Basin, Central Africa	Surface water	0.9778 / 0.9889
Shutova <i>et al.</i> (2014) <sup>158</sup>	C5: humic-like, terrestrially-derived, Peaks A and C	Yarra Glen water treatment plant, Victoria, Australia	Water samples from each treatment stage	0.9606 / 0.9953
Wang <i>et al.</i> (2022) <sup>165</sup>	C3: humic-like	Urban and peri-urban areas of Kampala, Uganda	Surface water, groundwater, and wastewater	0.9694 / 0.9842
Murphy <i>et al.</i> (2011) <sup>135</sup>	G3: humic- and fulvic-like, wastewater/nutrient enrichment tracer	Australia	Recycled water from treatment plants	0.9633 / 0.9884
Lapierre and del Giorgio (2014) <sup>166</sup>	C4: humic- and fulvic-like	Seven boreal regions, Quebec, Canada	Lake, stream, river, and wetland samples	0.9725 / 0.9788

Reference	Component assignment and description <sup>a</sup>	Location	Sample type	Excitation/emission similarity score
Hong <i>et al.</i> (2021) <sup>167</sup>	C1: terrestrial humic-like, photochemically produced	Rudong, Jiangsu Province, China	Extracted sediment samples	0.9808 / 0.9697
Sondergaard <i>et al.</i> (2003) <sup>168</sup>	C3: humic-like, Peak C	Laboratory experiment testing changes in salinity impacts on DOC with water from Danish streams	Surface water with salinity varied	0.9942 / 0.9542
<b>North Branch Component 4 (C4)</b>				
Wunsch and Murphy (2021) <sup>169</sup>	C <sub>280/330</sub> : protein-like	Drinking water treatment plant river intake, southern Sweden	River water	0.9954 / 0.9904
Yamashita <i>et al.</i> (2010) <sup>170</sup>	C5: protein-like, freshly produced tryptophan-like	Tropical rivers in southeast Venezuela	Surface water	0.9960 / 0.9861
Kothawala <i>et al.</i> (2013) <sup>171</sup>	C6: protein-like, tryptophan-like, microbially-derived	560 lakes in Sweden	Lake water	0.9953 / 0.9853
Zhou <i>et al.</i> (2019) <sup>172</sup>	C5: protein-like, Peaks B and T	Rivers, estuaries, and coastal waters in Sarawak, Borneo, Malaysia	Surface water	0.9987 / 0.9824
Graeber <i>et al.</i> (2021) <sup>120</sup>	C <sub>T</sub> : tryptophan-/ protein-like, microbially produced, bioavailable	Bode River, Germany	Freshwater	0.9949 / 0.9852
Yamashita <i>et al.</i> (2021) <sup>157</sup>	C4: protein-like	Dorokawa, Butokamabetsu, and Akaishi Rivers, northern Hokkaido, Japan	Stream water	0.9956 / 0.9845
Gao and Gueguen (2017) <sup>109</sup>	C2: protein-like, Peak T, tryptophan-like	Beaufort Sea, Canada Basin	Seawater	0.9978 / 0.9823
Kida <i>et al.</i> (2021) <sup>173</sup>	C <sub>330</sub> : mangrove-derived aromatic compound	Secondary mangrove forest, Trat, Thailand	Extracted soil samples	0.9988 / 0.9810
Kim <i>et al.</i> (2020) <sup>174</sup>	C3: protein-like, amino acid-like, biologically produced, freshly produced	Western Indian Ocean	Seawater	0.9936 / 0.9851
Cawley <i>et al.</i> (2012) <sup>156</sup>	C4: protein-like, tryptophan-like and tyrosine-like	Shark Bay, Australia	Surface water	0.9842 / 0.9929

a: component labels stem from the original references

b: only eight significant matches were obtained for Tucker's correlation coefficient > 0.95



The North Branch EEM-PARAFAC model was applied to wastewater samples from the advanced septic system to assess component stability and degradation (Figure 5.2a). The  $F_{\max}$  parameter for the protein-like component, C4, significantly decreased by 59.5% between the inlet and outlet ( $p < 0.01$ ), similar to W4 (Figure 4.10a). C1 also exhibited a significant decrease in the advanced septic system ( $p < 0.01$ ), but  $F_{\max}$  only changed by 29.9%. In contrast, the C2 and C3 components were relatively stable during treatment. The three humic-like components, C1, C2, and C3, were linearly correlated with sucralose concentrations, and the coefficients of determination ( $R^2$ ) were 0.79 ( $p < 0.01$ ), 0.62 ( $p = 0.04$ ), and 0.82 ( $p < 0.01$ ), respectively. The  $F_{\max}$  values for C4 were associated with caffeine levels ( $R^2 = 0.68$ ,  $p = 0.01$ ), which suggests biodegradation of C4 during septic treatment processes (Figure 4.7a). The three ratiometric parameters directly related to C4 were also significantly ( $p < 0.01$ ) correlated to caffeine levels: C4/C1 ( $R^2 = 0.89$ ); C4/C2 ( $R^2 = 0.84$ ); and C4/C3 ( $R^2 = 0.83$ ). The magnitude of these three ratiometric parameters significantly ( $p < 0.05$ ) decreased by 42 – 62% during treatment (Figure 5.2b). This degradation resembled the change in W4/W1 and W4/W5 in the advanced septic system. In particular, the removal of C4/C2 (62.7%) agreed with that of W4/W5 (62.0%), and the change in C4/C3 (48.9%) was effectively the same as that for W4/W1 (49.5%). The decrease in C4/C1 (42.1%) was lower than the other ratiometric parameters. EEM-PARAFAC components are representative fluorophores that account for a group of individual compounds that fluoresce at certain wavelengths. During treatment of septic wastewater and transport of septic effluent, some fluorescent compounds are more susceptible to adsorption and degradation reactions. C4 was hypothesized to be comprised of the most mobile and persistent compounds captured by the three protein-

like W components. The C4/C1, C4/C2, and C4/C3 ratiometric parameters may, therefore, be effective indicators of septic wastewater in streams.

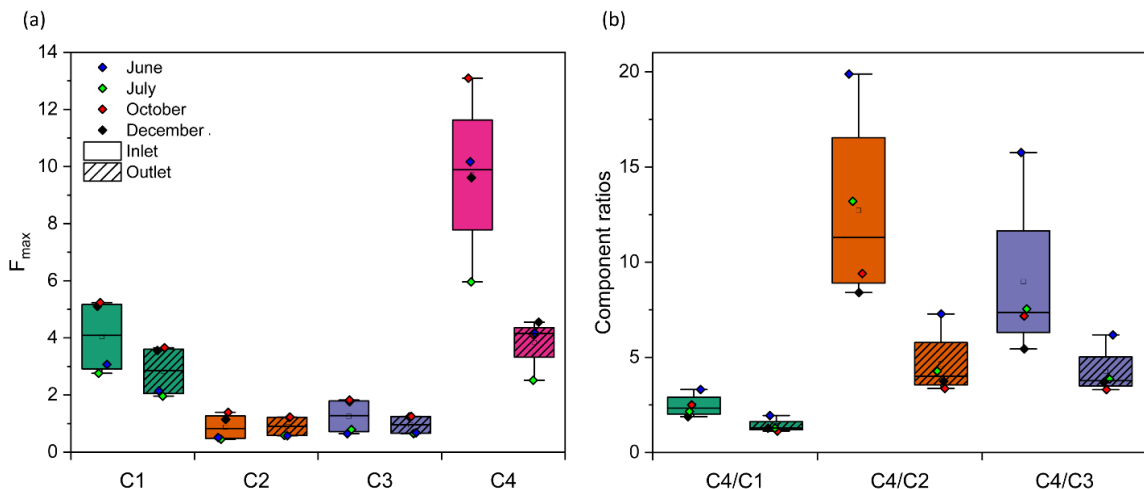


**Figure 5.2. The distribution of (a) components and (b) ratiometric parameters from the North Branch EEM-PARAFAC model in the inlet and outlet samples collected from the advanced septic system.**

### 5.2 CECs in the North Branch

Twelve CECs were detected at least once in the 45 samples collected during the North Branch sampling campaign. The highest detection frequencies were for atrazine (100%), sucralose (93%), carbamazepine (89%), and sulfamethoxazole (69%). Azithromycin (51%), mecoprop (51%), and clarithromycin (38%) were also regularly detected, but the majority of azithromycin and clarithromycin concentrations were below the corresponding limits of quantification (LOQs). The other five CECs, namely caffeine, paraxanthine, oxybenzone, octocrylene, and avobenzone, were detected in less than 20% of samples.

Figure 5.3 reports CEC concentrations and septic system density from the headwaters of the North Branch to its confluence with the Jones Falls. Note, the distances mentioned below correspond to the distance downstream of the headwaters. Sucralose concentrations were similar to previously reported values in the Upper Jones Falls watershed<sup>7</sup> (up to 290 ng L<sup>-1</sup>) and septic-impacted streams (up to 291 ng L<sup>-1</sup>)<sup>31</sup>. The highest sucralose concentrations were measured in the main stem at 0–1000 m downstream, where the septic density was 40 – 173 tanks per km<sup>2</sup>, and around 4500 m downstream in tributaries located in areas with high septic system density (*i.e.*, 81 – 173 tanks per km<sup>2</sup>). For reference, Figure 3.1 shows the sampling locations along the North Branch. The stream discharge was not measured but was notably lower near the headwaters, potentially leading to less dilution of CECs derived from septic wastewater. The lowest sucralose concentration in the main stem occurred around 2600 m (46.0 ng/L), where the septic system density was also lowest. Moving downstream, septic density increased (2600 – 5600 m) and then decreased (5600 – 8000 m), and the sucralose levels increased from approximately 150 ng/L to 200 ng/L and then remained steady, respectively. Sucralose levels in the tributaries were more variable due to differences in discharge and septic density. For example, the tributary site NB-50 (4500 m) contained 607 ng/L sucralose from an area with high septic density. This tributary apparently caused sucralose concentrations at the downstream NB-48 main stem site (167 ng/L) to increase relative to the upstream NB-51 site (135 ng/L).

Trends in the carbamazepine and sulfamethoxazole concentration profiles were similar to those of sucralose (Figure 5.3b), suggesting a common source. In fact, sucralose levels

were significantly correlated to carbamazepine (Spearman's  $\rho = 0.69$ ,  $p < 0.01$ ) and sulfamethoxazole (Spearman's  $\rho = 0.68$ ,  $p < 0.01$ ) concentrations in the main stem. However, carbamazepine and sulfamethoxazole demonstrated different patterns as septic density decreased at 5600 – 8000 m. The step-like increase in carbamazepine concentrations at 6000 m in the main stem was likely caused by inputs from the NB-28 tributary, which contained 880 ng/L carbamazepine, more than 5× higher than the maximum concentration measured in the three conventional septic systems. Similar carbamazepine concentrations (up to 1,100 ng/L) were detected in German rivers that received wastewater effluent<sup>175</sup>. In contrast, the sulfamethoxazole levels peaked around 6900 m. Unlike sucralose and carbamazepine, sulfonamide antibiotics are less persistent and undergo degradation processes<sup>95,176</sup>. The noted trends suggest natural attenuation of sulfamethoxazole in the 6900 – 8000 m reach.

Atrazine and mecoprop are both herbicides. While atrazine is applied to crops and lawns in agricultural and residential areas, mecoprop is only used in residential settings. These CECs were, therefore, expected to stem from stormwater runoff and not septic effluent. Atrazine may have been present in the groundwater from historic usage similar to what was observed in the drinking water wells in Section 4.1. Indeed, the concentration profiles of atrazine and mecoprop (Figure 5.3c) followed significantly different trends than sucralose in the main stem: atrazine (Spearman's  $\rho = -0.64$ ,  $p < 0.01$ ); and mecoprop (Spearman's  $\rho = -0.62$ ,  $p < 0.01$ ). The concentrations of the two herbicides were significantly correlated with each other (Spearman's  $\rho = 0.80$ ,  $p < 0.01$ ), suggesting a common source. Areas with high levels of herbicides coincided with lower

concentrations of sucralose and other wastewater-derived CECs, reinforcing the independence of the corresponding sources (*e.g.*, stormwater runoff, septic effluent). The noticeable spike in atrazine concentration at 6610 m may have stemmed from an adjacent application in that area perhaps from a nearby horse farm. Otherwise, atrazine levels steadily decreased from 3200 m to 8000 m. Unlike atrazine, mecoprop concentrations dropped to below the limit of quantitation (LOQ) around 6000 m. The difference between atrazine and mecoprop profiles in this section of the stream may have stemmed from the higher LOQ of mecoprop (10.7 ng/L) compared to atrazine (1.76 ng/L).

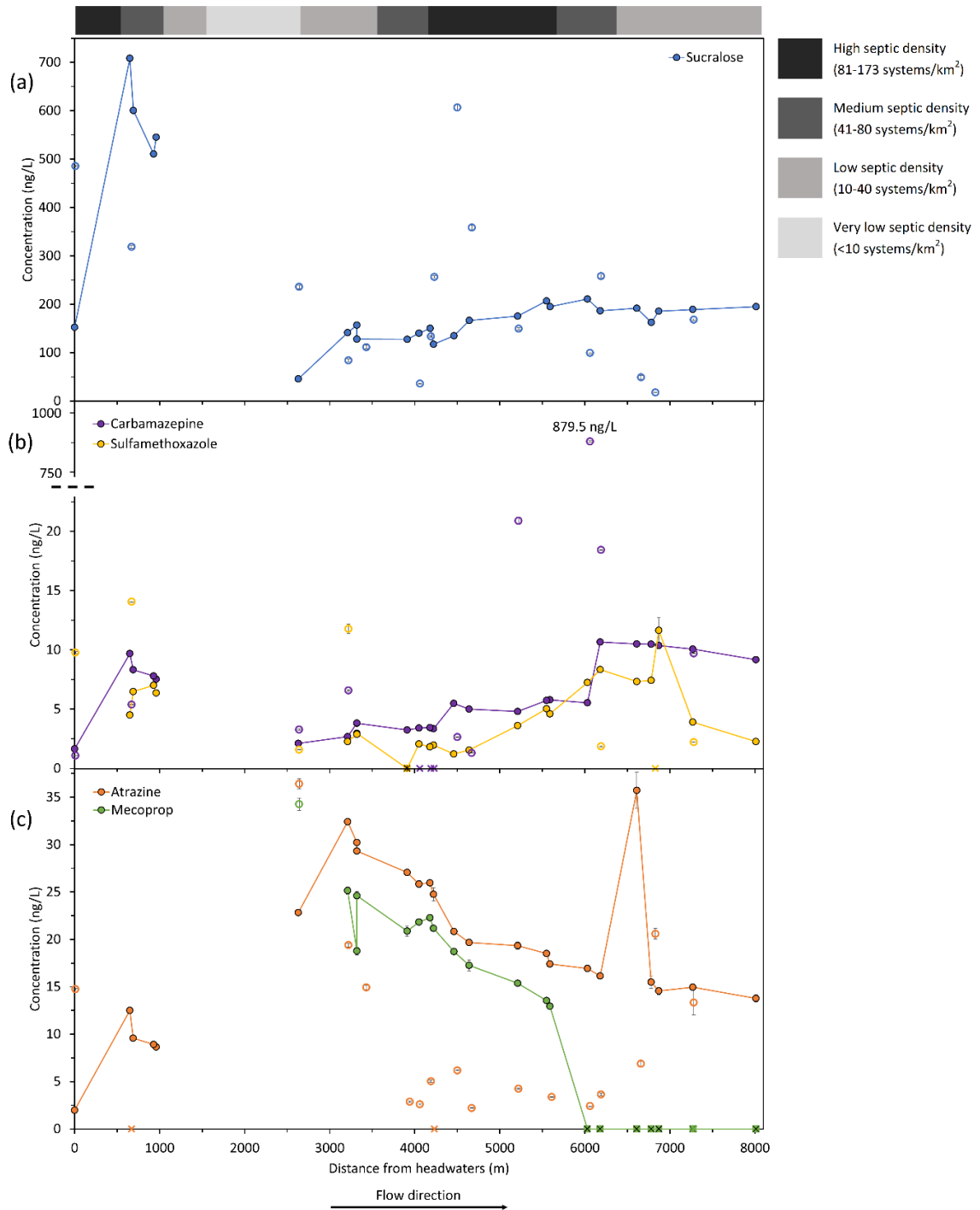


**Figure 5.3. Concentrations of (a) sucralose, (b) carbamazepine and sulfamethoxazole, and (c) atrazine and mecoprop in the North Branch.** The x-axis increases with downstream distance. The filled circles connected by lines represent CEC concentrations in samples collected from the main stem, and open symbols indicate CEC concentrations in samples collected from tributaries. Concentrations below LOQ are plotted as "x" symbols. Error bars show standard deviation. The grayscale bar at the top of the figure shows the septic system density along the stream.

### 5.3 EEM and EEM-PARAFAC parameters in the North Branch

The ratiometric parameters calculated from regional EEM volumes and EEM-PARAFAC components varied along the North Branch (Figure 5.4). Of the three regional volume ratios identified as potential septic wastewater indicators, R2/R5 demonstrated the greatest magnitude and variability with a mean and standard deviation of  $1.11 \pm 0.19$ , suggesting increased sensitivity compared to R1/R5 ( $0.36 \pm 0.11$ ) and R4/R5 ( $0.60 \pm 0.08$ ). A previous report of FDOM indicators in the Jones Falls and Gwynns Falls watersheds suggested using the top 20<sup>th</sup> percentile of R4/R5 (0.85) and R2/R5 (1.85) values as thresholds for identifying sites with potential wastewater inputs <sup>7</sup>. None of the North Branch samples exceeded the thresholds established by Batista-Andrade *et al.*; for reference, the top 20<sup>th</sup> percentiles for the North Branch samples were R4/R5 > 0.68 and R2/R5 > 1.24. The lower magnitude of the R4/R5 and R2/R5 parameters in the North Branch was reasonable because Batista-Andrade *et al.* collected samples from downstream areas adjacent to denser populations and impacted by wastewater exfiltration and sanitary sewer overflows.

Figure 5.4a shows that the R2/R5 profile in the North Branch was similar to that of W2/W1 ( $R^2 = 0.90, p < 0.01$ ), but the W2/W1 values were slightly greater than R2/R5. Similar results were observed for R4/R5 and C4/C1 ( $R^2 = 0.86, p < 0.01$ ), but C4/C1 (24.1%) displayed a larger relative standard deviation than R4/R5 (13.3%), indicating improved spatial resolution of changes in FDOM composition. The R1/R5 parameter was well correlated to W4/W1 ( $R^2 = 0.96, p < 0.01$ ) and W4/W5 ( $R^2 = 0.86, p < 0.01$ ), as suggested by the profiles in Figure 5.4b. W4/W1 ( $0.55 \pm 0.21$ ) and W4/W5 ( $0.80 \pm 0.34$ )

exhibited higher magnitude and greater variability than R1/R5 ( $0.36 \pm 0.11$ ), suggesting that the EEM-PARAFAC parameters exhibited better sensitivity to wastewater-derived FDOM.

In Section 4.4, W2/W5 was identified as a potential indicator of treated septic effluent. The profiles in Figure 5.4c highlight the correlation of W2/W5 with C4/C3 ( $R^2 = 0.88$ ,  $p < 0.01$ ) and C4/C2 ( $R^2 = 0.85$ ,  $p < 0.01$ ). Of the three parameters, C4/C3 ( $3.39 \pm 1.41$ ) displayed greater magnitude and variability compared to C4/C2 ( $1.73 \pm 0.65$ ) and W2/W5 ( $1.86 \pm 0.52$ ). High values of these three ratiometric parameters were measured in several tributaries. Two of those tributaries, NB-47 (4700 m) and NB-26 (6200 m), also exhibited sucralose concentrations that were 120% and 40% higher than the main stem, reinforcing the potential of the C4/C3 and W2/W5 indicators. However, these trends were not universal. The maximum C4/C3 and W2/W5 values were measured at NB-59 (4000 m), but the concentrations of sucralose (36.1 ng/L) and carbamazepine (< LOQ) were low. Nevertheless, the C4/C3 and W2/W5 ratiometric parameters were considered promising indicators of wastewater in the North Branch, although further analyses may be required.

The profiles of W3/W1 and W3/W5 in the North Branch are reported in Figure 5.4d. In the advanced septic system, the removal efficiencies of W3/W1 and W3/W5 were 86% and 89%, respectively. Due to their high removal efficiencies and correlations to caffeine concentrations, these ratiometric parameters were proposed as indicators of untreated septic wastewater. Unsurprisingly given their high removal efficiencies, the levels of W3/W1 and W3/W5 were quite low in the North Branch. This finding reinforced the



effective retention or degradation of W3 in the drainfield and confirmed the inefficacy of these parameters as septic indicators.

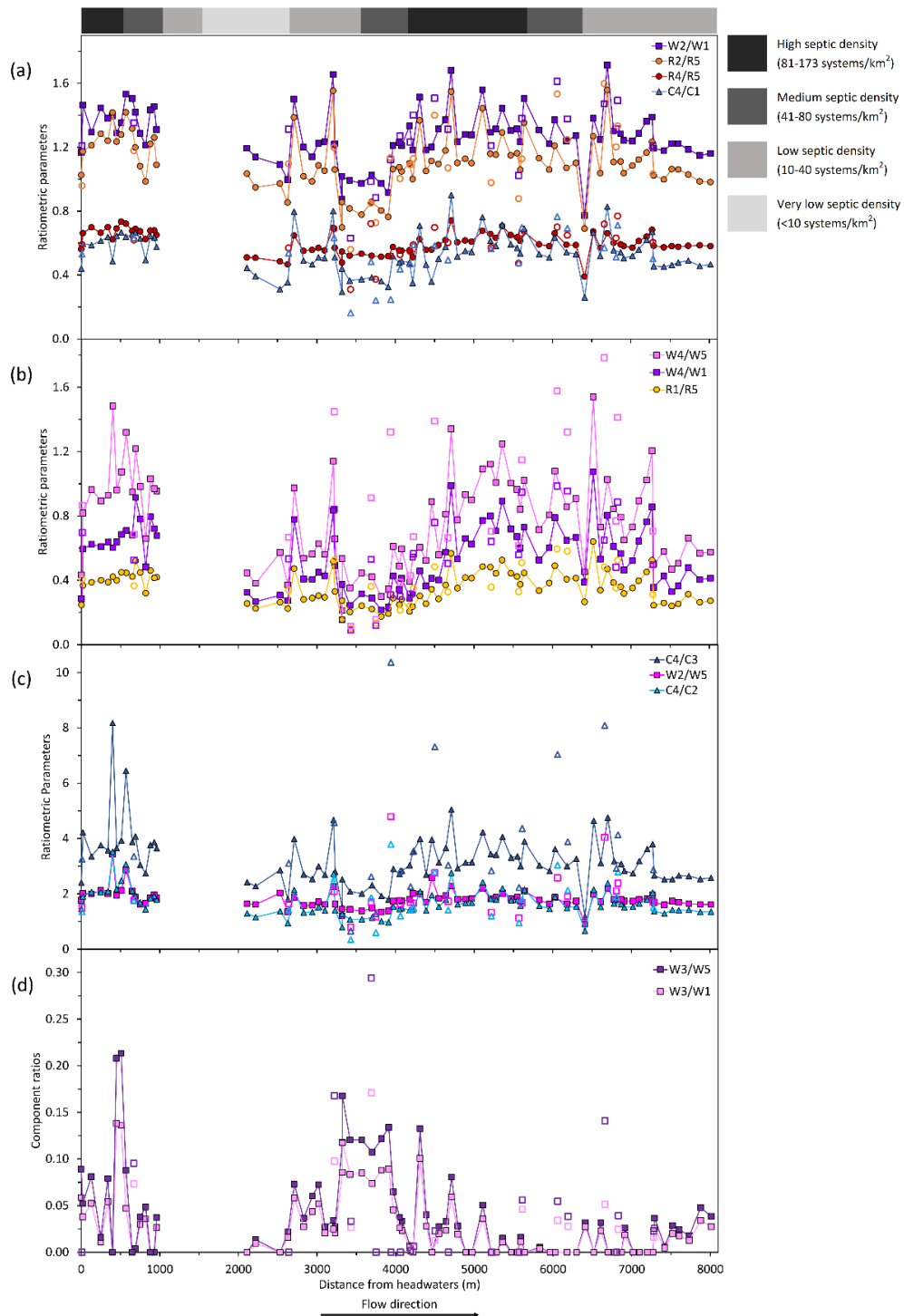


**Figure 5.4.** The profiles of ratiometric parameters related to wastewater DOM in the North Branch. Correlated parameters were plotted together. The x-axis increases with downstream distance. The filled circles connected by lines represent ratiometric parameters measured in samples collected from the main stem, and open symbols indicate ratiometric parameters measured in samples collected from tributaries. The grayscale bar at the top of the figure shows the septic density along the stream.

#### 5.4 Correlation analysis of wastewater indicators in the North Branch

A comprehensive correlation analysis was conducted to assess trends in CEC concentrations, regional EEM ratios, and ratiometric EEM-PARAFAC parameters to confirm the utility of using FDOM signatures as indicators of septic wastewater. Sucralose, carbamazepine, and sulfamethoxazole are currently employed as wastewater indicators, but these compounds undergo different fate and transport in subsurface environments. Sucralose and carbamazepine exhibit low biodegradability, but sulfamethoxazole is moderately biodegradable. Carbamazepine is more hydrophobic and adsorbs to soil, unlike sucralose and sulfamethoxazole<sup>61</sup>. A previous study of two wastewater-impacted rivers in Italy indicated that sucralose, sulfamethoxazole, and carbamazepine were well correlated with a humic-like EEM-PARAFAC component and a fluorescence index situated in Region 5<sup>61</sup>. Sulfamethoxazole levels were also correlated to the total EEM volume and sum of R1, R2, and R4 fluorescence in Chinese rivers that receive municipal wastewater<sup>60</sup>. Similarly, carbamazepine concentrations were correlated to regional EEM volumes and total fluorescence in four wastewater-impacted Portuguese rivers<sup>11</sup>. The current study was the first attempt to correlate ratiometric EEM and EEM-PARAFAC parameters to CEC concentrations in surface waters that are only impacted by septic wastewater.

For statistical comparisons, CEC concentrations that were below the LOQ were set to the limit of detection (LOD), and concentrations below the LOD were set to 0. This is a relatively conservative method for handling low concentrations and other studies have utilized different approaches<sup>177-180</sup>. Two criteria were employed to select CECs for

inclusion in the correlation analysis: (i) the detection frequency was  $\geq 33\%$ ; and (ii)  $\geq 50\%$  of detections were above the LOQ. CECs and FDOM may originate from a common source, but if they undergo different fate and transport in the environment, then non-linear relationships would be expected. Therefore, Spearman correlations, which assess the significance of rank-based relationships, were employed in this analysis. Several significant correlations were observed between sucralose concentrations and fluorescence parameters for the full dataset, but none of the relationships were very strong (Figure 5.5). The data were split into subsets corresponding to samples from the main stem and tributaries. Few correlations were observed for the tributary subgroup, which is reasonable since the composition of septic wastewater varies by system. For the tributary category, sucralose levels were only slightly positively correlated with the proposed FDOM indicators, but the correlation with W2/W1 was the only significant relationship (Figure 5.6b).

More significant and strong correlations were identified for samples in the main stem due to the common transport pathway along the North Branch (Figure 5.6a). Significant positive correlations were recorded between sucralose levels and most of the ratiometric FDOM parameters, except for W2/W5, W3/W1, and W3/W5. As noted above, W3/W1 and W3/W5 exhibited low magnitude in the stream samples. Sucralose levels were also positively correlated to carbamazepine and sulfamethoxazole concentrations, and those CECs were associated with R1/R5 and R4/R5, in alignment with previous findings from Yang *et al.*<sup>60</sup> and Barbosa *et al.*<sup>11</sup>. The carbamazepine and sulfamethoxazole concentrations were also well correlated to the C4/C1, W4/W1, and W4/W5 values,

reinforcing the potential for those ratiometric parameters to serve as indicators or septic wastewater. Atrazine and mecoprop were negatively correlated with most of the fluorescence ratios, in agreement with findings from Section 5.2, due to the different sources.

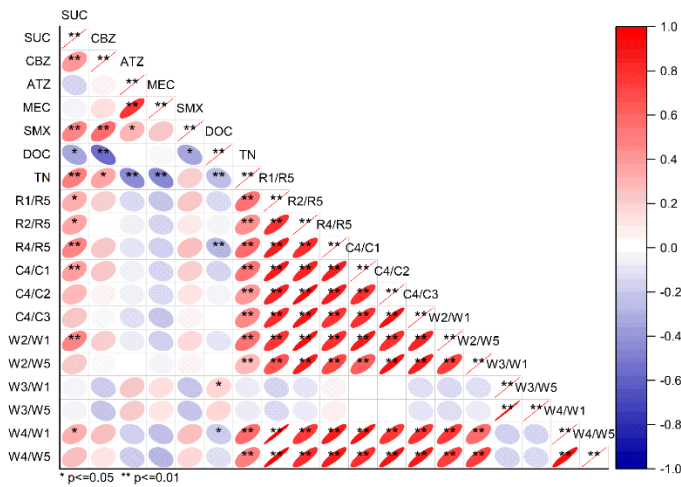


**Figure 5.5. Spearman correlations between CEC concentrations, dissolved organic carbon (DOC) contents, total nitrogen (TN) levels, and the magnitude of ratiometric fluorescence parameters for all North Branch samples.** The CECs included are sucralose (SUC), carbamazepine (CBZ), atrazine (ATZ), mecoprop (MEC), and sulfamethoxazole (SMX).

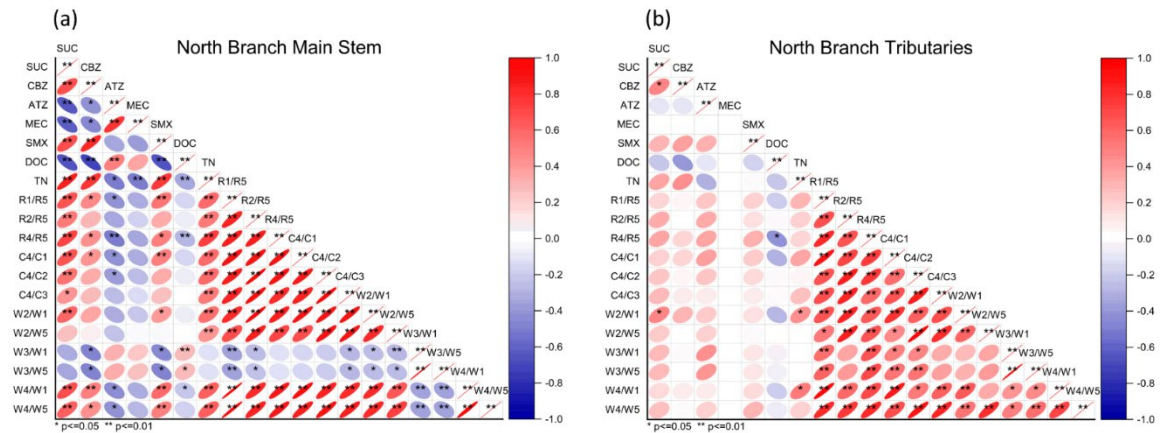


**Figure 5.6. Spearman correlations between CEC concentrations, DOC contents, TN levels, and ratiometric fluorescence parameters for North Branch samples from the (a) main stem and (b) tributaries.** The CECs were sucralose (SUC), carbamazepine (CBZ), atrazine (ATZ), mecoprop (MEC), and sulfamethoxazole (SMX).

The dataset was also subdivided according to septic density for correlation analysis (Figure 5.7). For samples collected from areas with low septic density (*i.e.*, 10-40 tanks/km<sup>2</sup>), sucralose levels and ratiometric FDOM parameters were not significantly related. Positive correlations between sucralose concentrations and fluorescence parameters were observed for samples from areas with medium (*i.e.*, 41-80 tanks/km<sup>2</sup>) and high (*i.e.*, > 80 tanks/km<sup>2</sup>) septic density. The highest Spearman coefficients were recorded for sucralose with R2/R5, R4/R5, C4/C1, and W2/W1 in samples from areas with high septic density; similar findings were attained for R4/R5, W2/W1, and C4/C1 in areas with medium septic density. These outcomes suggest that W2/W1 and C4/C1 are effective indicators of septic wastewater, but W2/W1 exhibited higher sensitivity than C4/C1 and may, therefore, be more useful.

Promising relationships between sucralose and the R2/R5, R4/R5, C4/C1, and W2/W1 parameters were further explored by Pearson correlation, which assesses the linearity of the relationship between two variables (Figure 5.8). For samples from areas with high or medium septic density, sucralose concentrations were best related to the R4/R5 ( $R^2 = 0.35 - 0.47$ ) and W2/W1 ( $R^2 = 0.39 - 0.55$ ) parameters. Figure 5.8 also shows the insignificant relationships between these parameters for samples from areas with low septic density ( $R^2 \leq 0.02$ ). Based on these outcomes, a septic density of 40 tanks/km<sup>2</sup> may serve as a threshold for the presence of wastewater indicators in adjacent streams.

The samples from areas with medium septic density also exhibited significant Spearman correlations between carbamazepine and FDOM parameters (Figure 5.7b). No significant

Pearson correlations were identified between carbamazepine and the fluorescence parameters for this subset of samples, but Pearson correlations are sensitive to outliers. NB-28 (6060 m) had a carbamazepine concentration over 40× higher than any other site and, therefore, exerted considerable leverage over the Pearson analysis. When the data from NB-28 were excluded, seven significant Pearson correlations were identified between carbamazepine and the fluorescence parameters. The highest Pearson coefficients were recorded between carbamazepine concentrations and the C4/C1, W4/W1, R1/R5, and W2/W1 parameters (Figure 5.9a). These results reinforced the promise of the W2/W1 and C4/C1 fluorescence parameters as indicators of septic wastewater in streams.

While no significant correlations were observed between carbamazepine levels and fluorescence parameters in areas with high septic density, both Spearman and Person relationships were identified for sulfamethoxazole. Figure 5.9b shows the direct relationship between the C4/C2, W2/W5, and W4/W5 ratiometric parameters and sulfamethoxazole concentrations; however, the outliers may have inflated the Pearson correlations. Without NB-101 (8020 m), for which the sulfamethoxazole concentration was almost 2× higher than in other samples, the  $R^2$  values for relationships between sulfamethoxazole and C4/C2, W2/W5, and W4/W5 decreased to less than 0.15. Given this result and the very low concentrations of sulfamethoxazole (*i.e.*, < 20 ng/L), these results were not used to inform the preferred fluorescence indicators.

The correlations involving W3/W1 and W3/W5 were notable due to the negative correlations with most of the other variables for samples from the main stem and areas

with low or medium septic density (*i.e.*, Figure 5.6 and Figure 5.7). These outcomes were driven by the low magnitude of the W3/W1 and W3/W5 parameters in the North Branch; recall, 35% of samples had W3/W1 and W3/W5 values equal to zero. For these reasons, these two parameters were excluded from further investigation.

Z-scores represent the number of standard deviations a particular measurement is away from the mean value calculated for the full data set<sup>181</sup>. To better determine which sites were enriched with the ratiometric parameters relative to other sites in the North Branch, z-scores were calculated for three EEM regional ratios (*i.e.*, R1/R5, R2/R5, R4/R5), three North Branch EEM-PARAFAC parameters (*i.e.*, C4/C1, C4/C2, C4/C3), and four ratiometric parameters from the EEM-PARAFAC model for wastewater (*i.e.*, W2/W1, W2/W5, W4/W1, W4/W5). The results are presented in Figure 5.10. The z-score trends align with septic density. There was a slight delay between the higher z-score values for the indicators and the start of the high septic density area. This was probably due to transport pathways from septic systems to the stream most likely being angled slightly downstream or there being preferential discharge pathways farther downstream.

At least 50% of the indicators exhibited z-scores greater than +1 at nine sites, and the R2/R5, C4/C2, and W2/W1 indicators were all enriched at these sites. Only one site, the NB-26 tributary in an area with medium septic density (6200 m) had a z-score greater than +1 for every indicator, suggesting the presence of septic wastewater at this site. Four sites (4000-4700 m) had z-scores less than -1 for every indicator, and at least 50% of the indicators had z-scores less than -1 at ten sites. The W2/W5 and C4/C3 ratiometric parameters were the most inconsistent with other indicators, in agreement with the



previously reported disconnect between high W2/W5 and C4/C3 values at a site with low sucralose concentration.

At four sites, namely NB-02, NB-51, NB-59, and NB-65, the z-scores for the suite of indicators led to conflicting conclusions. For example, NB-02 was considered to be an impacted site based on high z-scores for C4/C3, W2/W1, and W2/W5, but the R1/R5, W4/W1, and W4/W5 parameters had low z-scores. Caffeine, paraxanthine, carbamazepine, atrazine, and mecoprop were all detected at NB-02, suggesting the presence of septic wastewater and, thereby, lowering confidence in R1/R5, W4/W1, and W4/W5 as potential indicators. At NB-51, the z-score for C4/C1 was low, but W2/W5 had a high z-score. While sucralose, carbamazepine, and sulfamethoxazole were detected at NB-51, the corresponding concentrations were below the average for the North Branch. Given the previously noted inconsistency in W2/W5, this main stem site was likely impacted by upstream sources and not nearby discharges. The NB-59 tributary demonstrated a higher overall fluorescence compared to other sites. C4/C2, C4/C3, W2/W5, and W4/W5 had high z-scores at this site, while low z-scores were recorded for R4/R5, C4/C1, and W4/W1. Sucralose and atrazine were detected at NB-59, but both CECs were present at below-average concentrations. The results further reduced confidence in the W2/W5 and W4/W5 parameters and raised questions about the application of C4/C2 and C4/C3 as indicators.

Based on the above analyses, R2/R5 and W2/W1 were identified as the most reliable and consistent FDOM-based indicators of septic wastewater. While not as consistent, R4/R5 and C4/C1 also showed promise. These four parameters were closely related. All four

parameters showed strong correlations with sucralose and followed similar spatial profiles along the North Branch (Figure 5.4a). The greater magnitude and variability of W2/W1 over the other three parameters provided more sensitivity as a wastewater indicator. All four indicators had z-scores above +1 for four sites, and three of the four indicators had z-scores above +1 for an additional eight sites. R4/R5 was the least consistent with the other indicators. At five sites R4/R5 had a z-score less than +1 while the other three indicators had z-scores above +1 and at another five sites, R4/R5 was the only one of the four indicators with a z-score above +1. That included NB-65 where R2/R5 and W2/W1 both had z-scores less than -1 and R4/R5 had a z-score of 1.5. This inconsistency excluded R4/R5 from further consideration.

While W2/W1, R2/R5, and C4/C1 were in good agreement with each other concerning the identification of impacted sites, the other indicators provided conflicting conclusions for select sites. For example, the W2/W1, R2/R5, and C4/C1 values were low at NB-69, but five other indicators had z-scores greater than +1. NB-69 (tributary) was collected from an area with low septic density. Despite obvious fluorescence in Regions 1 and 2 of the EEM, the sucralose, atrazine, and azithromycin CECs were detected at low relative concentrations. These outcomes indicate that W2/W1, R2/R5, and C4/C1 were able to prevent false positives in areas with low septic density (*i.e.*, < 40 tanks/km<sup>2</sup>) compared to the other fluorescence parameters; furthermore, these findings suggest that geospatial tools could be used to identify areas with medium or high septic density for more targeted spatiotemporal analyses of wastewater indicators.

In a high septic density area, the R2/R5 and W2/W1 parameters were the only indicators with z-scores greater than +1 at NB-92 (main stem). C4/C1 had a z-score of 0.92 at NB-92. Sucralose, sulfamethoxazole, and octocrylene were present at above-average concentrations at this site, which was located just upstream of a tributary. At NB-92, the octocrylene concentration was 58.5 ng/L, but the tributary (NB-91) and downstream (NB-90) sites exhibited octocrylene levels below LOD and LOQ, respectively. These data indicate that the CEC source was located nearer to NB-92 and did not derive from the tributary. In fact, the z-scores for R2/R5 and W2/W1 were even higher at NB-93 (upstream of NB-92), reinforcing the relative location of septic wastewater introduction to the North Branch.

A few sites with high CEC concentrations were not identified by the R2/R5, W2/W1, and C4/C1 parameters. For example, the sample from NB-50 contained 607 ng/L sucralose, but the z-scores for R2/R5, W2/W1, and C4/C1 were less than +1. Just 150 m downstream at NB-48, eight CECs were detected, including a spike in octocrylene concentration to 45.8 ng/L. The other CECs did not exhibit increased concentrations compared to upstream sites, indicating an unknown source of octocrylene. All three radiometric indicators had z-scores less than +1 for this site, suggesting that none of these indicators picked up on the input which caused an increase in octocrylene. In addition, 880 ng/L of carbamazepine was measured at NB-28, but neither the R2/R5 nor W2/W1 parameters identified this site as being impacted by septic wastewater. Interestingly, the magnitude of the C4/C1 parameter did indicate the potential presence of wastewater at

NB-28 with a z-score of 1.2. Overall, we propose that the R2/R5, W2/W1, and C4/C1 ratiometric parameters be used in tandem to identify sites impacted by septic wastewater.

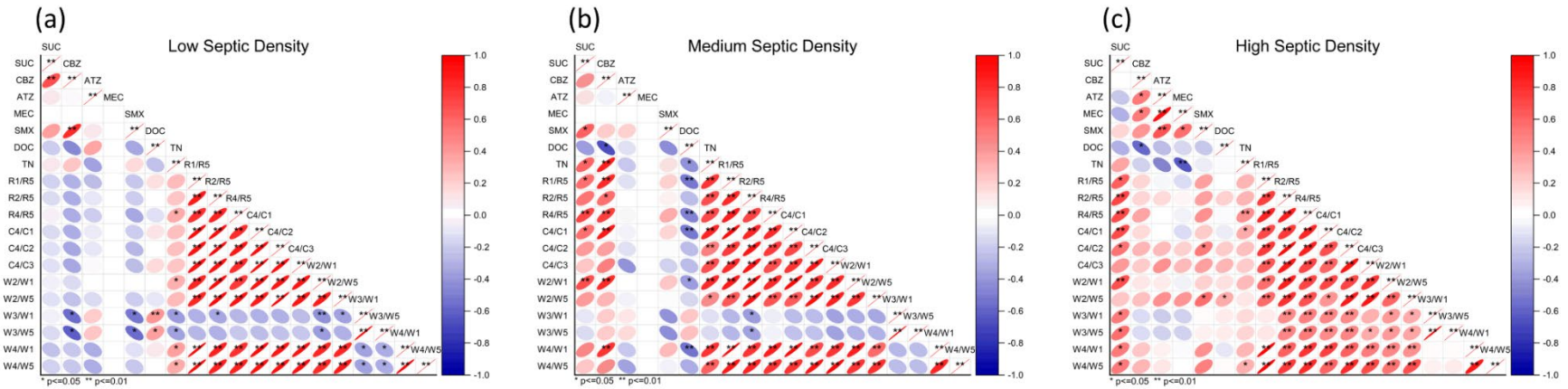


**Figure 5.7. Spearman correlations between CEC concentrations, DOC contents, TN levels, and ratiometric fluorescence parameters for North Branch samples in areas with (a) low (10-40 systems/km<sup>2</sup>), (b) medium (41-80 systems/km<sup>2</sup>), and (c) high (81-173 systems/km<sup>2</sup>) septic density. The CECs were sucralose (SUC), carbamazepine (CBZ), atrazine (ATZ), mecoprop (MEC), and sulfamethoxazole (SMX).**

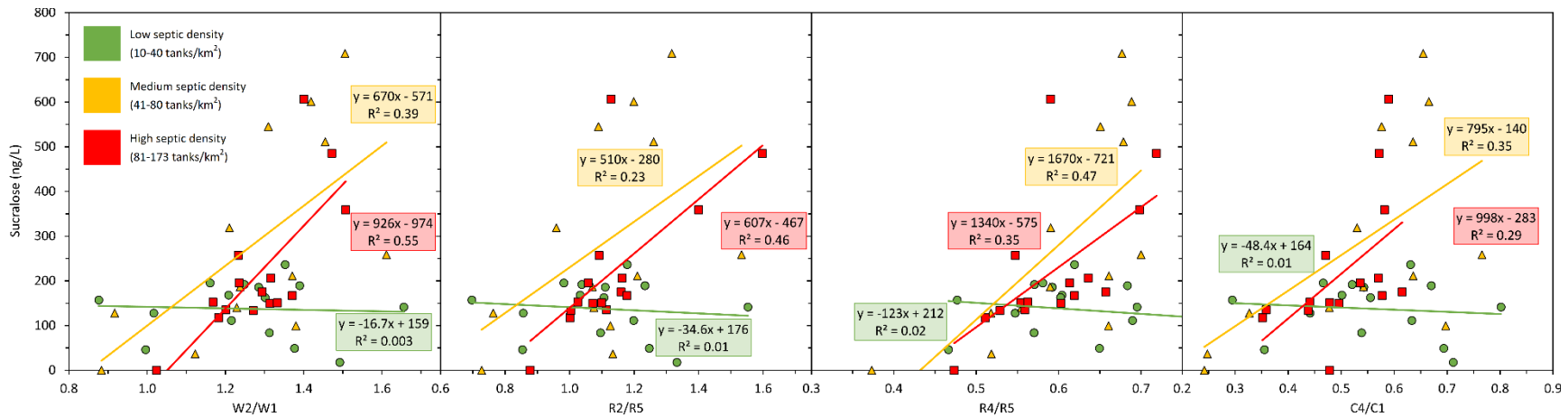


**Figure 5.8. Correlations between sucralose concentration and the W2/W1, R2/R5, R4/R5, and C4/C1 fluorescence indicators for samples collected from areas with low, medium, and high septic density.**

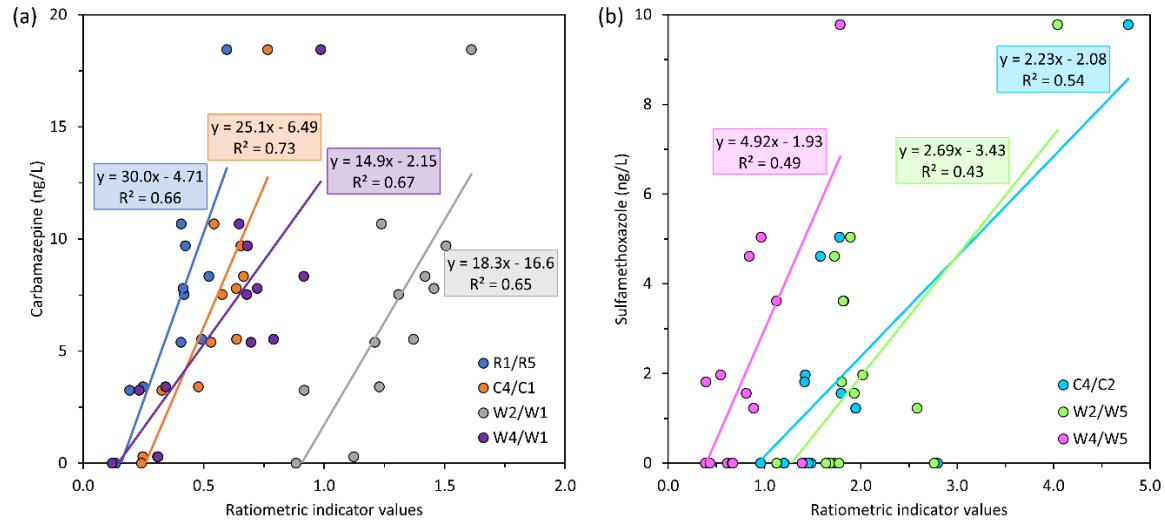


**Figure 5.9. Pearson correlations between (a) sulfamethoxazole and C4/C2, W2/W5, and W4/W5 in areas with high septic density and (b) carbamazepine and R1/R5, C4/C1, W2/W1, and W4/W1 in areas with medium septic density.**

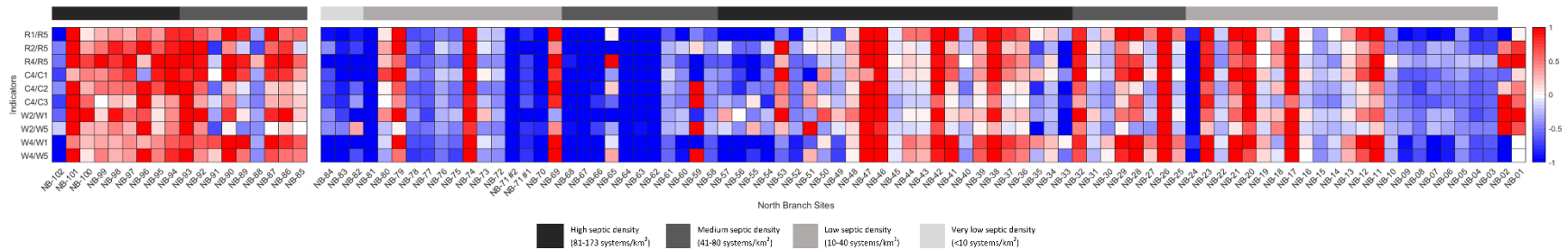


**Figure 5.10. Distribution of z-scores for the ratiometric fluorescence indicators (top to bottom: R1/R5, R2/R5, R4/R5, C4/C1, C4/C2, C4/C3, W2/W1, W2/W5, W4/W1, and W4/W5) at each site from the headwaters to the confluence with the Jones Falls (left to right). The grayscale bar at the top of the figure shows the septic density along the stream. The stream runs dry between NB-85 and NB-84, so the sites downstream of NB-85 are not connected to the upstream sites.**

## 5.5 Conclusions related to septic wastewater indicators in the North Branch

Three conservative CECs (*i.e.*, sucralose, carbamazepine, sulfamethoxazole) and one degradable CEC (*i.e.*, caffeine) were identified as potential septic effluent indicators from the septic wastewater characterization and previous literature. Nine ratiometric FDOM parameters were considered as potential indicators based on the septic wastewater characterization. Three additional FDOM indicators were identified from the North Branch EEM-PARAFAC model. Of the 12 ratiometric parameters, eight were degradable and four were conservative. Figure 5.11 summarizes the identification and selection of the most suitable indicators. Of the potential CEC indicators, caffeine and sulfamethoxazole were removed from consideration because of low detection frequency and the lack of strong and significant correlations with FDOM parameters, respectively. Both sucralose and carbamazepine showed promise with strong correlations with multiple FDOM parameters and high detection frequencies. Ultimately, sucralose generally had higher concentrations and more variability, as well as strong correlations with septic density; for that reason, sucralose was considered the most promising CEC-based indicator of septic effluent.

Of the 12 potential ratiometric FDOM indicators, two (*i.e.*, W3/W1, W3/W5) were eliminated due to low magnitude (sensitivity), and another four (*i.e.*, C4/C2, C4/C3, W2/W5, W4/W5) were removed from consideration due to a lack of significant correlations with CECs and inconsistent z-scores. Based on both the Spearman and Pearson correlation analysis, three EEM regional ratios (*i.e.*, R1/R5, R2/R5, R4/R5) and three EEM-PARAFAC component ratios (*i.e.*, C4/C1, W2/W1, W4/W1) showed promise

as septic effluent indicators. From the z-score analysis, R1/R5 and W4/W1 failed to correctly identify sites that were impacted by septic effluent based on CEC concentrations and detections. R4/R5 exhibited inconsistent z-scores with the three most promising indicators. Based on this analysis, R2/R5, W2/W1, and C4/C1 were considered to be the most promising FDOM indicators for identifying sites impacted by septic effluent. In particular, W2/W1 was characterized as a stable and conservative indicator, because of its significant positive correlations with sucralose and carbamazepine in areas with medium and high septic density; furthermore, W2/W1 exhibited greater sensitivity than R2/R5 and C4/C1. Due to the economic advantages of FDOM measurement compared to CEC analysis, this indicator may be a useful tool for evaluating the impacts of septic systems on water quality in other areas. In particular, FDOM can be used for more expansive initial monitoring campaigns to identify potentially impacted areas that can then be confirmed with CEC or other indicator measurements. The incorporation of multiple tracers, such as FDOM and CECs, leads to a higher likelihood of correctly identifying septic wastewater-impacted sites.



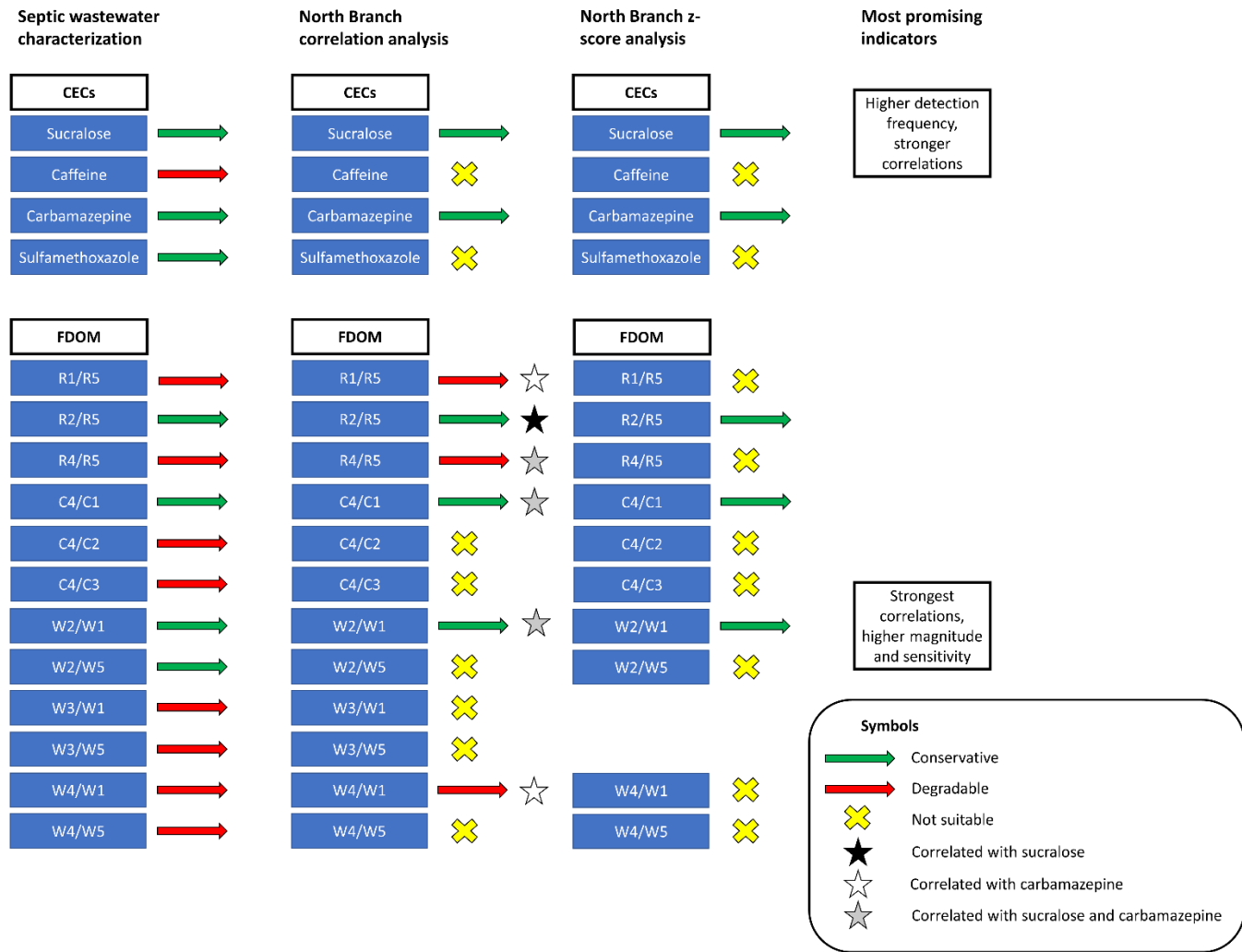


Figure 5.11. Summary of the potential CEC and FDOM indicators and recommendations from each analysis step.

## **Chapter 6: Septic wastewater transport pathways to surface water**

### 6.1 Thermal infrared (TIR) survey of preferential groundwater flows

The TIR survey was conducted along a 5.1-km reach of the North Branch to determine if preferential groundwater flows exhibited high levels of CECs and FDOM parameters identified as indicators of septic wastewater. Subsurface transport through shallow groundwater was expected to be the main pathway for septic wastewater to reach the stream. Twenty groundwater seeps were identified with the TIR camera, and another six seeps were selected based on visual observations. The temperature difference between the groundwater seeps and surface water ranged from 3 to 10 °C. Colder groundwater flows indicated shorter residence times or more direct discharges through bank sediments which prevented the groundwater from equilibrating to the surface temperature before discharging into the stream. In contrast, seeps with lower temperature differences involved longer residence times or more diffuse discharges of groundwater at the bank. Such phenomena were not identified by the TIR camera due to the similar temperatures of the groundwater and surface water. Importantly, those inputs were also expected to have lower CEC and FDOM levels due to the longer retention time and corresponding extent of natural attenuation. The approximate temperature difference between the surface water and each seep is listed in Table A.2. Sites with temperature differences greater than 6 °C between the seep and surface water were designated as "cold" preferential groundwater flows. Of the 26 sites, 14 were assigned this designation, and most of those locations were within 1400 m of each other in an area with high septic density. Six sites were designated as "cool" if the temperature difference between the

seep and the surface water was less than 6 °C. Recall, TIR data were not collected at the other six sites.

#### *6.1.1 CEC concentrations measured in areas of preferential groundwater discharge*

Fourteen CECs were detected in samples collected from preferential groundwater seeps. Carbamazepine (96%), atrazine (92%), and sucralose (88%) exhibited the highest detection frequencies, similar to outcomes from the North Branch sampling campaign (*i.e.*, 89% – 100% detection frequency). The detection frequency for sulfamethoxazole (42%) was lower than for the North Branch campaign (69%); similarly, azithromycin and mecoprop were not detected in samples from the groundwater seeps even though these compounds were regularly detected in stream water from the North Branch. While caffeine was detected more frequently in the groundwater seep samples (38%) compared to the stream samples (9%), the caffeine concentrations were all below the limit of quantitation (LOQ, 0.73 ng/L). Paraxanthine was not detected in the groundwater seeps, potentially due to the higher LOQ (1.74 ng/L). Unlike samples from the North Branch campaign, clarithromycin was frequently detected in groundwater seeps (54%). Four other antibiotics, namely nadifloxacin, roxithromycin, erythromycin, and tylosin, and two UV filters, homosalate and octisalate, that were not present in the North Branch samples were found in the groundwater seep samples. In addition, ibuprofen was detected in one sample (GW-13). The aggregate results suggested that the seeps played a role in transporting septic wastewater into the stream.

Figure 6.1 shows box plots of sucralose and carbamazepine concentrations from seeps in high versus low/medium septic density areas. Sucralose concentrations were significantly higher in seeps from high septic density areas relative to low/medium septic density areas ( $p < 0.01$ ) and in "cold" seeps relative to "cool" and "no TIR" seeps combined ( $p = 0.01$ ). No significant differences were observed for carbamazepine. In Figure 6.2, the CEC concentrations measured in groundwater seeps were co-plotted with CEC levels measured in the main stem and tributaries during the North Branch sampling campaign. The sucralose (Figure 6.2a) and carbamazepine (Figure 6.2b) concentrations were generally higher in colder seeps relative to adjacent cooler seeps. For example, the greatest temperature difference was observed for GW-18 which also had a high sucralose concentration (328 ng/L). Seeps and tributaries with high sucralose concentrations were found in a similar high septic density area (4000 – 5500 m). Tributaries had small drainage areas and therefore the CEC concentrations found in tributaries represented only a few septic systems or other sources. This was presumably also true of seeps with each seep representative of a few specific septic systems based on the preferential groundwater flow paths and septic drainfield locations. Previous studies have confirmed that preferential groundwater discharges identified by TIR were consistent over long periods<sup>182</sup>; therefore, the preferential groundwater discharges observed in September (TIR study) likely contributed to CEC levels measured in the main stem North Branch sampling campaign (June-July). The sucralose concentrations exceeded 200 ng/L at GW-15, GW-17, GW-18, GW-19, and GW-22, which were all located at 4370 – 4500 m. Given the consistency of seeps over time, these preferential groundwater discharges were likely flowing over the summer and may have contributed to the 50 ng/L increase in sucralose

levels in the main stem at 4220 – 4640 m. Likewise, the high carbamazepine concentrations measured at GW-24 (19.1 ng/L) and GW-23 (29.2 ng/L), which were located at 4300 m, suggested that preferential groundwater discharges were at least partially responsible for the 64% increase in carbamazepine concentrations at 4220 – 4460 m in the main stem over the summer.

Different trends were observed for atrazine and mecoprop, which (when detected) were present at lower concentrations in the groundwater seeps compared to the main stem but at similar levels to nearby tributaries (Figure 6.2c). This outcome may imply that herbicides enter the North Branch through another transport pathway, but the seasonal nature of herbicide application could also explain these findings. Given their primary application to grasses, herbicide transport to streams likely stemmed from stormwater or irrigation runoff. A previous study reported that the highest mecoprop concentrations in streams coincided with mecoprop application to lawns in early summer<sup>72</sup>; similar conclusions were reached for atrazine<sup>183</sup>. Because the groundwater seep samples were collected during a dry period in late September, the lower herbicide concentrations were reasonable.

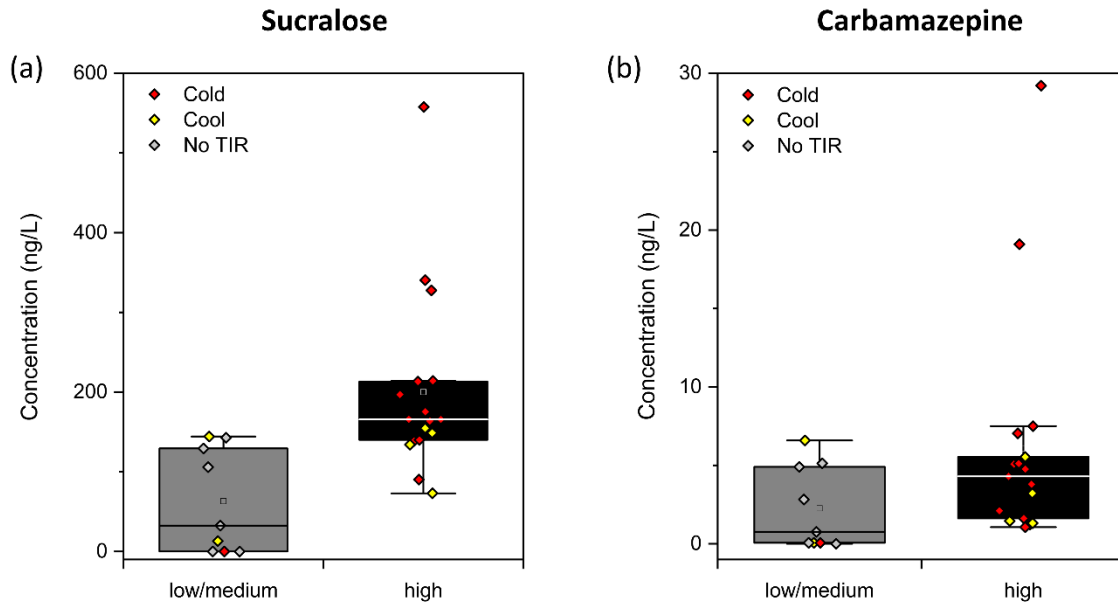


**Figure 6.1. Box plots comparing (a) sucralose and (b) carbamazepine concentrations in seeps from low/medium and high septic density areas.**

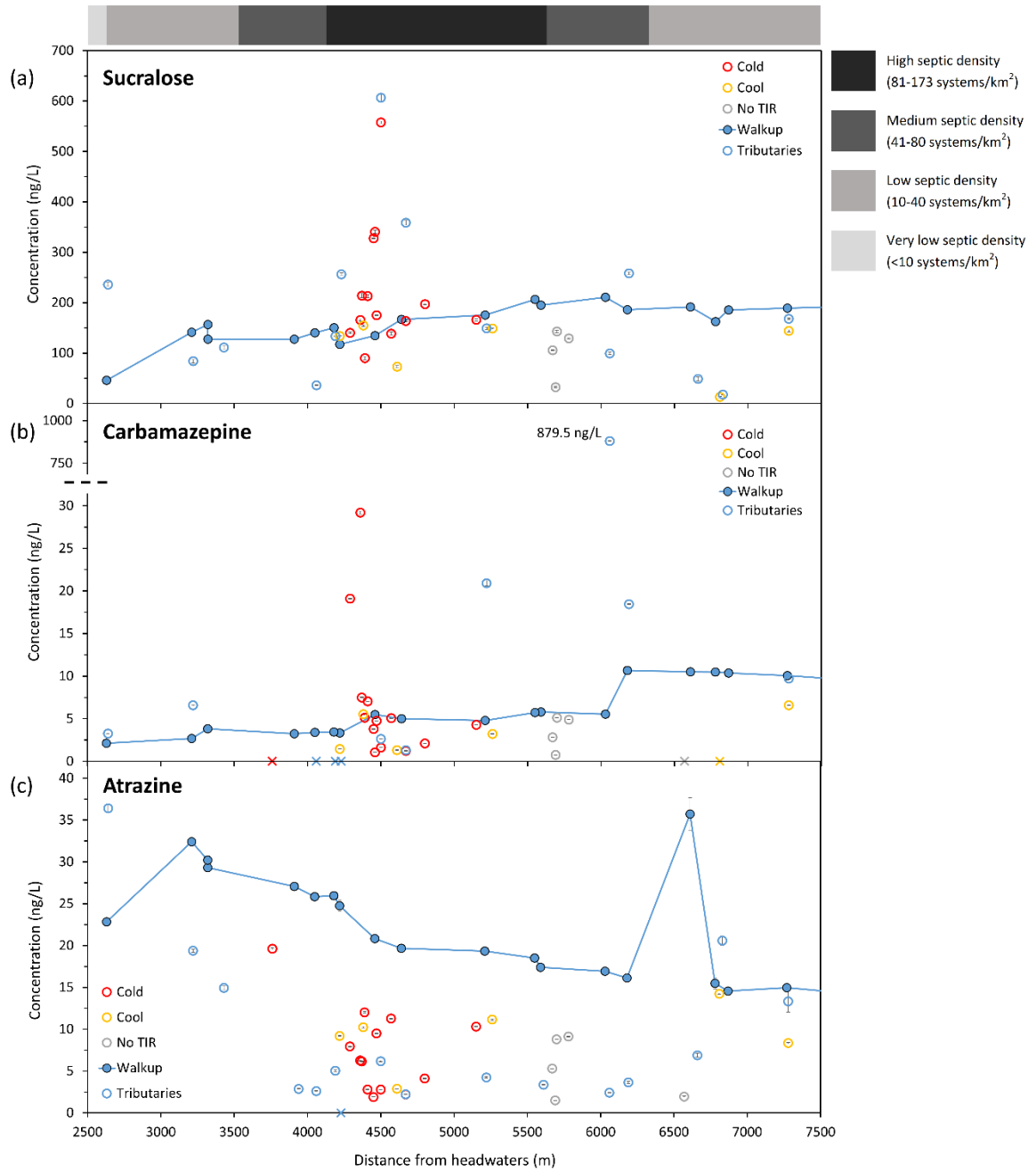


**Figure 6.2. Concentrations of (a) sucralose, (b) carbamazepine, and (c) atrazine in groundwater seep samples collected in September plotted with concentrations measured in the main stem and tributaries during the North Branch sampling campaign in June – July.** The x-axis increases with downstream distance. Concentrations below LOQ are plotted as "x" symbols. Error bars show standard deviation. The grayscale bar at the top of the figure shows the septic density along the stream.

### *6.1.2 FDOM composition in samples from the TIR survey*

The composition of FDOM in samples collected from groundwater seeps was highly variable. Most samples exhibited some fluorescence in Regions 1, 2, and 4, which suggests wastewater impacts, but 85% of the groundwater seep samples had lower total fluorescence than every sample from the North Branch sampling campaign. The total fluorescence in samples from the cold seeps at GW-17, GW-19, GW-23, and GW-26 was only 3 – 15% that of the North Branch sample with the lowest fluorescence.

Figure 6.3a compares the TIR, FDOM, and CEC data from GW-17 to GW-18, which were located in an area with high septic density but on opposite sides of the stream. Large temperature differences ( $\sim 10$  °C) between the seep and surface water were identified at each site. Low fluorescence was recorded at GW-17, which was only located  $\sim 10$  m downstream from GW-18, and FDOM-based wastewater indicators were not apparent. Interestingly, the sample from GW-18 demonstrated the highest R2/R5 (3.53) and W2/W1 (3.07) parameters of any sample collected in the North Branch. The two samples contained similar sucralose (328 – 341 ng/L), carbamazepine (1.06 – 3.80 ng/L), and sulfamethoxazole (2.16 – 2.39 ng/L) contents, but octisalate (124 ng/L) and atrazine (1.91 ng/L) were only present at GW-18. The high ratiometric FDOM indicator values and the high octisalate concentration point to the bank with the GW-18 seep being more impacted by septic systems than the opposite bank where GW-17 was located.

About 50 m upstream from GW-17, the groundwater seeps at GW-19 and GW-20 were situated  $\sim 20$  m away from each other on the same side of the stream. The temperature differences between the seeps and surface water at these two sites were similar, but the sample from GW-19 exhibited minimal fluorescence (Figure 6.3b). Even though GW-19



contained low FDOM contents, the sucralose and carbamazepine concentrations were 240% and 140% higher, respectively. Interestingly, tylosin, a veterinary antibiotic often used on cats and dogs, was also detected at GW-19. On the other hand, the atrazine concentration was 4.3× higher and more antibiotics were detected, and at higher concentrations, at GW-20. Despite the close proximity, the seeps exhibited different CEC and FDOM profiles, suggesting the need for additional studies to investigate differences in subsurface transport for septic-derived FDOM versus CECs.

GW-26 was the only "cold" seep located in a medium septic density area upstream of the other seeps. In Figure 6.3c, the TIR, FDOM, and CEC data from GW-26 were compared with GW-23, which was the nearest downstream "cold" seep with similar fluorescence intensity; note, GW-23 was in an area with high septic density. Both sites exhibited seeps that were ~8 °C colder than the surface water. While the FDOM concentrations were low at both sites, more CECs were detected, and at higher concentrations, at GW-23. The only CEC present at a higher concentration at GW-26 was atrazine (19.6 ng/L). These results reinforce the hypothesis that cold seeps introduce septic wastewater-derived CECs to the stream in areas with high septic density but not lower septic density. The implications of this campaign for FDOM transport were less clear. Some seeps (*e.g.*, GW-18) were enriched with septic wastewater-like FDOM, but others were not. To better understand the co-transport phenomena of CECs and FDOM in the subsurface, groundwater samples would need to be collected for CEC and FDOM analysis at regular intervals from a septic drainfield to nearby surface water. Future work is needed to more directly connect the transport of CECs and FDOM from septic systems, through shallow groundwater, and into streams; in addition, the shallow groundwater flow patterns in the

study area should be assessed to determine whether the spatial distribution of upgradient septic drainfields coincide with preferential groundwater flow paths.

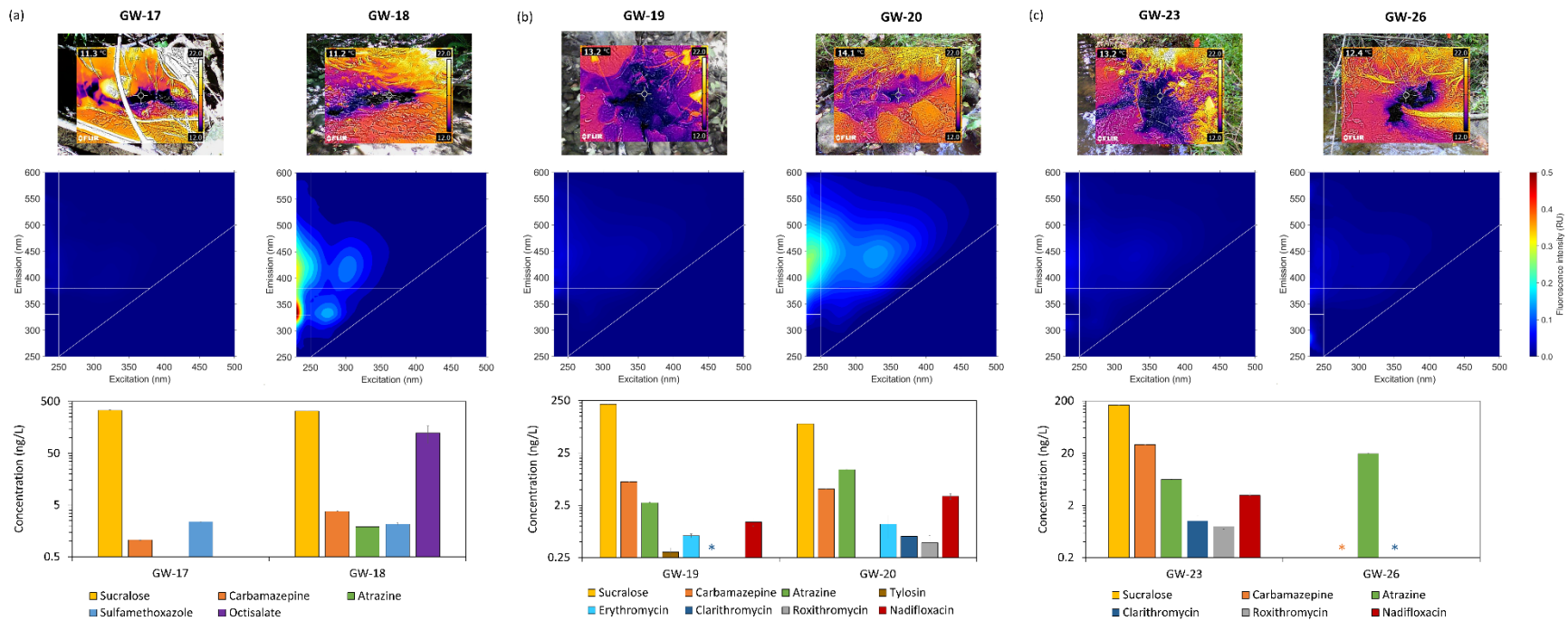


**Figure 6.3. Comparison of TIR images, EEMs, and CEC concentrations for (a) GW-17 and GW-18, (b) GW-19 and GW-20, and (c) GW-23 and GW-26. Concentrations below LOQ are plotted as "\*" symbols.**

## 6.2 Case study: storm mobilization of CECs and septic wastewater-derived FDOM into streams

While groundwater transport was assumed to be the primary pathway for septic wastewater to reach streams during low flow conditions, storm events may activate additional pathways, such as aboveground runoff or subsurface flushing. Intense storm events can also cause the groundwater table to rise, reducing the residence time for septic effluent in the drainfield and causing more CECs and wastewater-like FDOM to reach nearby surface waters. To gain insights into these transport pathways, samples were collected at NB-89 throughout a single storm event on November 11, 2022. Initially, the discharge in the stream likely stemmed from baseflow groundwater contributions followed by the flushing of local groundwater and any constituents that had been attenuated in the groundwater. Eventually, the discharge changes based on cumulative upstream contributions, which were storm dependent and require a more detailed study of subsurface flow paths and their spatial relationships with septic drainfields; such aspects were outside of the scope of this particular study.

### *6.2.1 CEC concentrations during the storm event*

Thirteen composite samples were collected during a 5.5-h period spanning from before the rain started through the rising limb of the hydrograph; 11 different CECs were detected in those samples. Figure 6.4 shows the concentration profiles for seven CECs, namely sucralose, caffeine, paraxanthine, carbamazepine, sulfamethoxazole, azithromycin, and atrazine, along with stream discharge during the storm event. The

other detected CECs included the oxybenzone, octocrylene, and octisalate UV filters and the progesterone hormone, but these compounds were only detected in 8 – 30% of the samples and only octocrylene was detected above its LOQ. Sucralose was significantly but not well correlated to discharge ( $R^2 = 0.33$ ,  $p = 0.04$ ). Previous studies of septic-impacted streams have also reported positive relationships between discharge and artificial sweeteners<sup>22,30</sup>. In this case, the sucralose concentrations were relatively consistent at 399 – 539 ng/L from 8:30 am until the peak discharge just before 1:00 pm, when sucralose concentrations quickly increased to 1170 ng/L and then decreased to 804 ng/L, presumably due to the first flush phenomenon. The first flush phenomenon is the rapid mobilization of contaminants that have accumulated in nearby sources during antecedent dry days<sup>184</sup>. If the source is limited, then the concentrations will spike before declining due to dilution. Caffeine levels were also significantly positively correlated with discharge ( $R^2 = 0.82$ ,  $p < 0.01$ ), but the concentrations steadily increased with the hydrograph. Mendoza *et al.* reported similar findings for caffeine in a California creek impacted by sewer exfiltration and overflows<sup>65</sup>. In that study, caffeine levels followed the first flush phenomenon, with concentrations increasing with the rising limb of the hydrograph, peaking just before the peak discharge, and then decreasing with discharge<sup>65</sup>. Unlike the final sucralose concentration, caffeine levels increased after the peak discharge. Previous studies measured much higher caffeine concentrations relative to sucralose during storm events in streams impacted by raw wastewater<sup>185</sup>. That trend was not observed here, presumably due to the partially treated nature of septic effluent and the rapid biodegradation of caffeine. Paraxanthine, which is a caffeine degradation product,

was initially below LOD. As the storm progressed, paraxanthine was detected and followed a similar concentration profile as caffeine.

The range of measured concentrations for the other CECs in Figure 6.4 was quite small, with maximum differences of less than 4 ng/L during the storm. The concentration profile for carbamazepine generally exhibited a steady decrease from 8:15 am until the first flush phenomenon around 11:30 am; however, carbamazepine was not significantly correlated with discharge. Sulfamethoxazole levels were correlated to discharge ( $R^2 = 0.85$ ,  $p < 0.01$ ) and followed a similar pattern as sucralose concentrations, including evidence of first flush transport. Azithromycin was not detected before the storm; interestingly, this antibiotic was detected near the middle of the rising limb of the hydrograph around 12:30 pm, but azithromycin concentrations decreased as the discharge peaked. No conclusions were proposed due to the low magnitude of azithromycin concentrations. Finally, atrazine was negatively correlated to discharge ( $R^2 = -0.88$ ,  $p < 0.01$ ), which suggests dilution effects and reinforces the aforementioned conclusions that atrazine stems from a different source than the other CECs and proposed FDOM-based indicators.

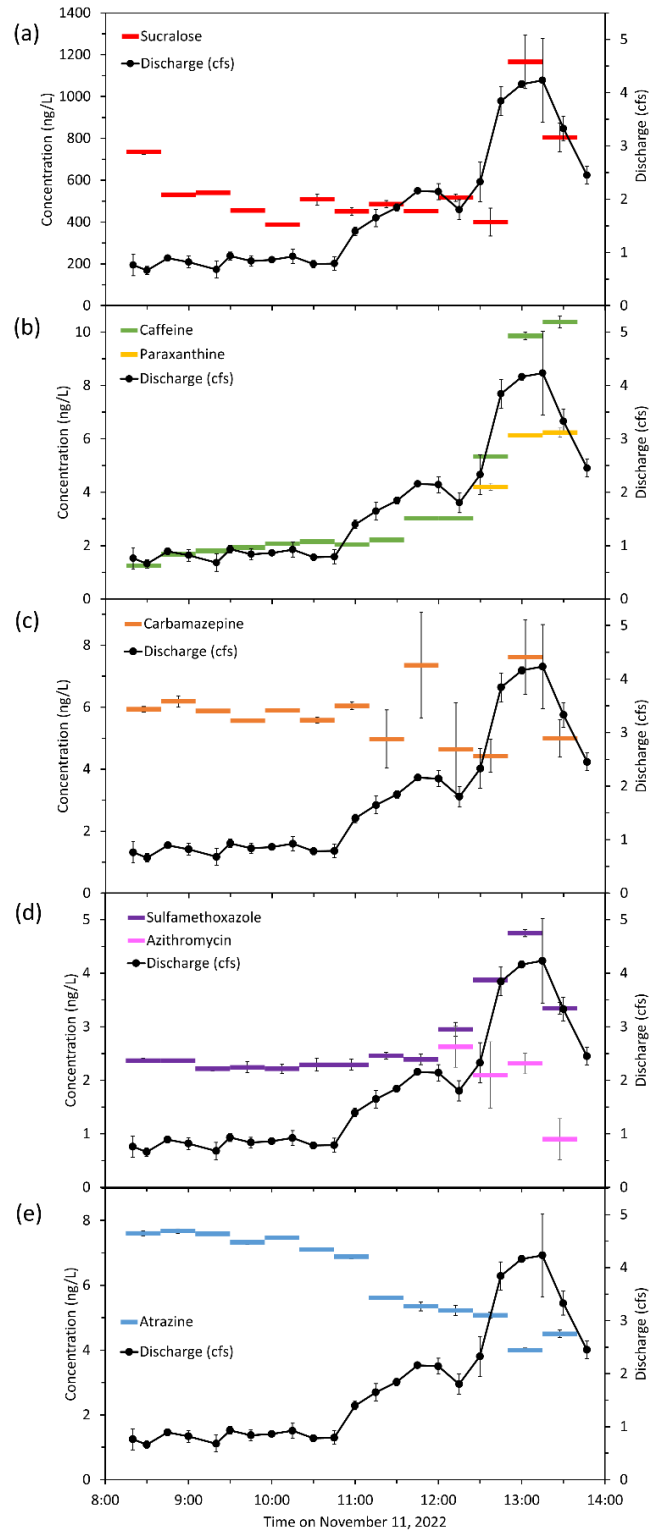


**Figure 6.4. Concentration profiles of (a) sucralose, (b) caffeine and paraxanthine, (c) carbamazepine, (d) sulfamethoxazole and azithromycin, and (e) atrazine during a single storm event. Error bars are standard deviation ( $n = 3$ ).**

### 6.2.1 Composition of storm-mobilized FDOM

We postulated that septic wastewater-like FDOM would be mobilized through similar pathways as the CECs that exhibited first flush phenomena. Figure 6.5 shows the magnitude of the regional EEM volumes and EEM-PARAFAC components during the campaign. All regional volumes and component  $F_{\max}$  values gradually increased from 8:15 am to 12:30 pm. When the discharge started to increase at 10:55 am, the R2, C4, W2, and W4 parameters spiked; similar phenomena were observed for R1, R2, R4, C4, W3, and W4 at 12:35 pm when the discharge rapidly increased before the peak of the storm. For the next 25 min, all regional volumes and components rapidly increased before peaking in a similar manner as caffeine and paraxanthine. In fact, the regional volumes and components were all well correlated with caffeine ( $R^2 \geq 0.96$ ,  $p < 0.01$ ) and discharge ( $R^2 \geq 0.78$ ,  $p < 0.01$ ). The protein-like regions and components increased 150 – 260% above their baseflow levels, while the humic-like regions and components only increased 100 – 170%. These findings aligned with previous work by Mendoza *et al.*, who reported that tryptophan- and humic-like fluorescence intensities increased with the rising limb of the hydrograph and peaked with maximum discharge for a municipal wastewater-impacted creek in California <sup>65</sup>.

Figure 6.6 reports the profiles of the most promising ratiometric indicators of septic wastewater from Chapter 5 during the storm event. Compared to the regional volumes and components, the ratiometric EEM and EEM-PARAFAC parameters were not as well correlated to caffeine concentrations or discharge. In contrast, Mendoza *et al.* observed that the ratio of tryptophan-like to humic-like fluorescence closely followed the hydrograph and better corresponded to contaminant mass flux compared to regional



fluorescence intensities<sup>65</sup>. In the current study, both W2/W1 and C4/C1 were significantly correlated with caffeine ( $R^2 = 0.67$ ,  $p < 0.01$  for both), but significant relationships were not determined for R2/R5. The ratiometric parameters accounted for changes in total fluorescence as discharge increased and provide information about changes in FDOM composition. The three ratiometric parameters captured the first flush of wastewater-like FDOM at 10:55 am, when discharge started to increase, suggesting an input of septic wastewater at that time (Figure 6.6). This input was also documented by the increased fluorescence in Regions 2 and 4 in the 10:55 am sample compared to the samples collected at 10:50 and 11:00 am (Figure 6.7). Similar spikes were not observed for the CEC concentrations at this time, but that outcome may have been affected by the collection of 25-min composite samples, which could mask higher concentrations in one of the five subsamples. A step change was also observed in all three ratiometric parameters around 12:30 pm. While this increase was not as large as the 10:55 am spike, it suggests a second flush of septic wastewater as the discharge increases rapidly towards peak discharge. This 12:30 step change aligns well with the initial rise in septic-derived CEC concentrations. The findings of this case study highlight the need for future investigations focused on the mechanistic transport phenomena that lead to the introduction of CECs and septic wastewater-derived FDOM to streams during baseflow and wet weather conditions.

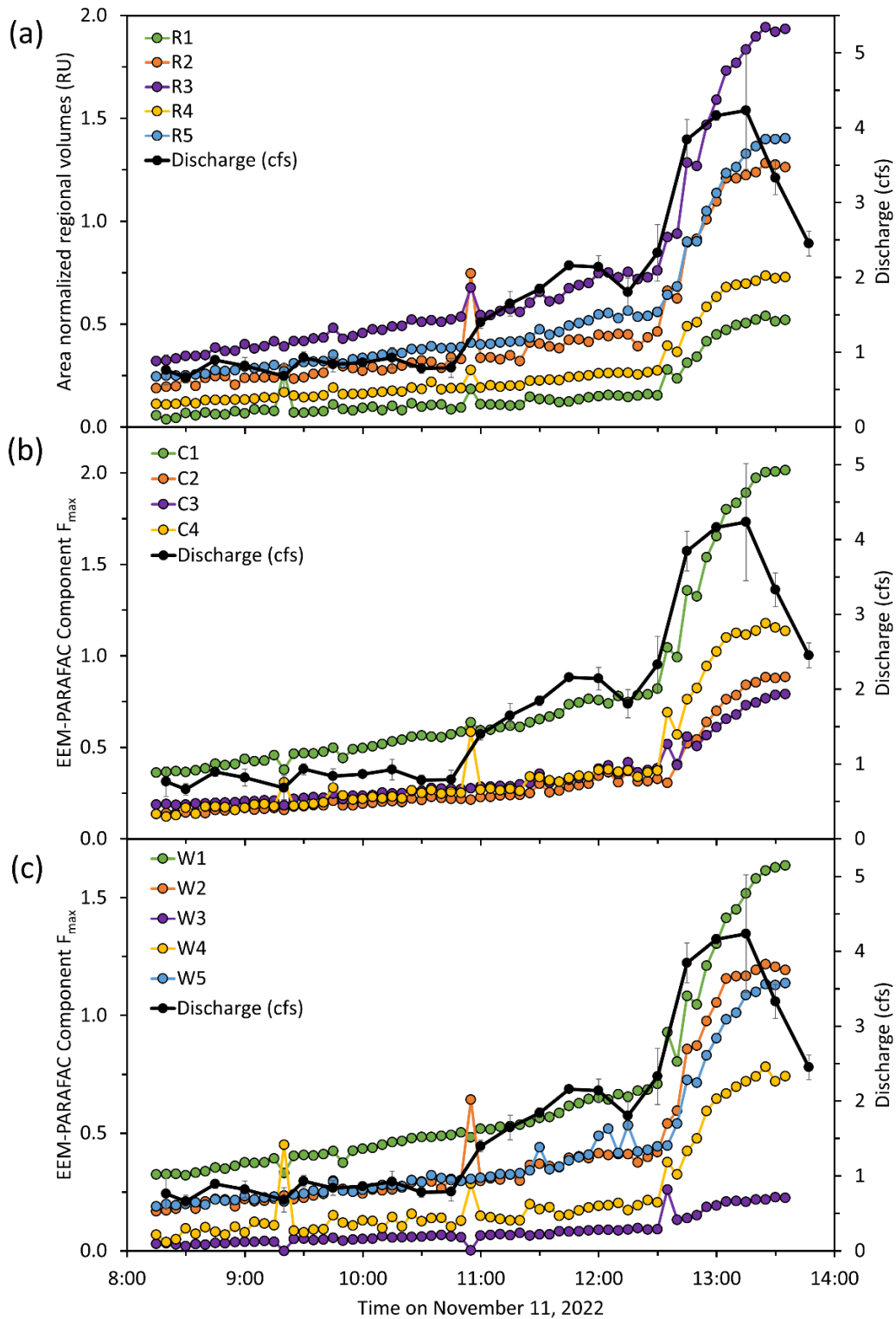


**Figure 6.5. Profiles of (a) EEM regional volumes, (b)  $F_{\max}$  values for North Branch EEM-PARAFAC components, and (c)  $F_{\max}$  values for global wastewater EEM-PARAFAC components during the November 11, 2022 storm event. Error bars are standard deviation with  $n = 3$ .**

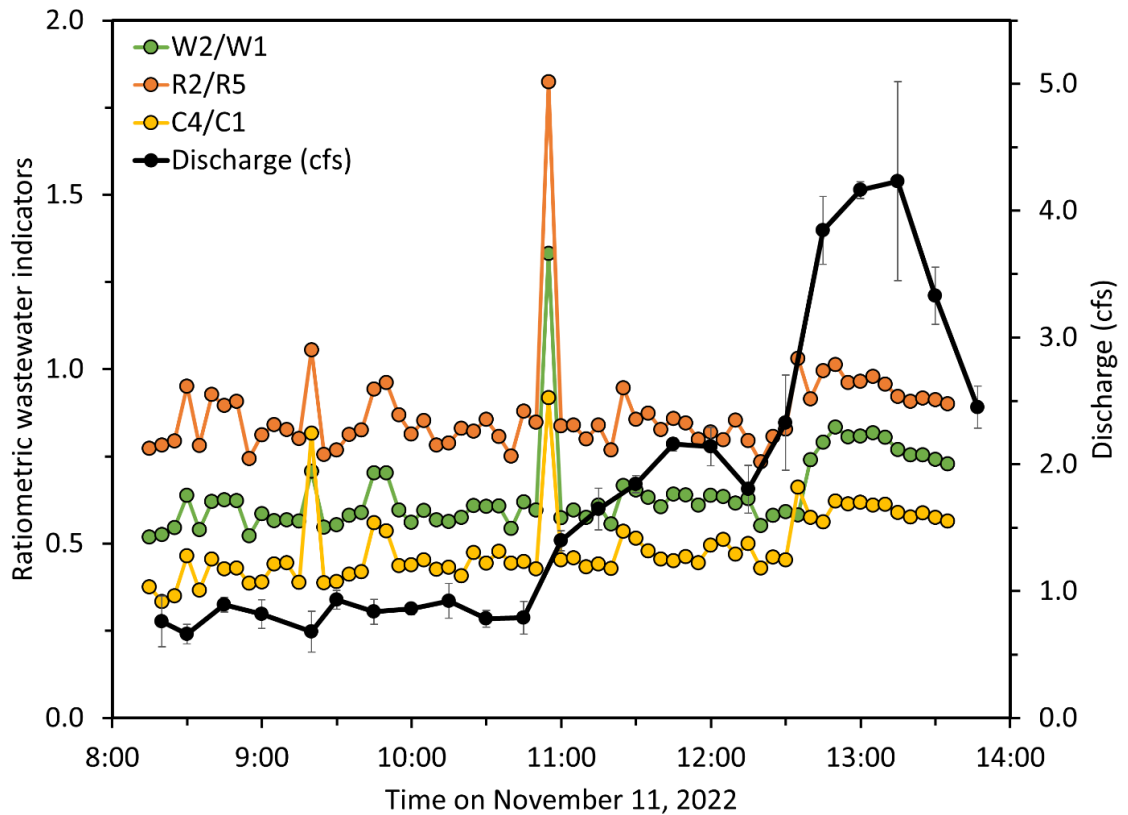


**Figure 6.6.** The profiles of the ratiometric FDOM parameters identified as indicators of septic wastewater during the November 11, 2022 storm event. Error bars are standard deviation with  $n = 3$ .

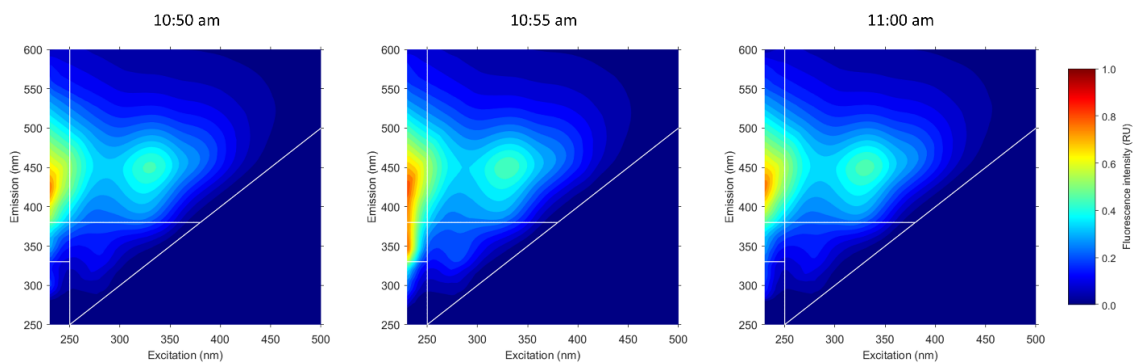


**Figure 6.7.** EEMs from samples collected before, during, and after the discharge began to increase at 10:55 am.

## Chapter 7: Conclusion

### 7.1 Summary

This thesis reported contaminants of emerging concern (CECs) in septic and municipal wastewater and stream samples from areas with varying septic density, novel ratiometric fluorescence parameters to quickly identify areas impacted by septic effluent that were developed from septic wastewater fluorescent dissolved organic matter (FDOM) analysis and multiple excitation emission matrix (EEM) with parallel factor analysis (PARAFAC) models, and case studies of septic effluent transport to surface water via preferential groundwater flows and storm event mobilization. These outcomes help improve our understanding of the septic effluent impacts on nearby surface water quality and provide useful tools for future monitoring campaigns and studies of septic-impacted areas.

Chapter 4 summarized septic wastewater characterization using CEC concentrations and FDOM analysis. High concentrations of CECs, including common wastewater indicators like sucralose (up to 71,000 ng/L) and caffeine (420,000 ng/L), reinforce the utility of CECs as indicators in nearby surface water. High concentrations of antibiotics and hormones elevated ecotoxicity concerns in areas with high septic system density. Degradable (*e.g.*, caffeine) and stable (*e.g.*, sucralose) CECs were proposed as indicators of partially- and fully-treated septic effluent, respectively. Similarly, the change in FDOM parameters in the aerobic treatment process of the advanced septic tank was used to classify proposed FDOM parameters as indicators of partially- or fully-treated septic effluent. Ultimately, three EEM regional ratios and six EEM-PARAFAC component ratios were proposed as potential septic effluent indicators based on the septic effluent characterization. Of those parameters, six were proposed as indicators of partially treated

septic effluent, while the other three were proposed as fully-treated septic effluent indicators.

These indicators were then investigated in stream samples collected from areas with variable septic density in Chapter 5. Three additional EEM-PARAFAC component ratios were proposed based on a model built generated from EEMs measured in the North Branch stream samples. Three conservative CECS, namely sucralose, carbamazepine, and sulfamethoxazole, were frequently detected in the North Branch. Sucralose and carbamazepine concentrations showed positive and significant correlations with several ratiometric FDOM parameters in samples collected from high and medium septic density areas. Based on the strong correlations with sucralose concentrations and high z-scores matching high CEC detections and concentrations, R2/R5, W2/W1, and C4/C1 were identified as the most promising septic effluent indicators.

Chapter 6 explored septic effluent transport processes via two case studies. A thermal infrared (TIR) survey successfully identified preferential groundwater seeps along the main stem of the North Branch. Several seeps contained high CEC concentrations, and antibiotics and UV filters that were not present in the main stem samples were detected in seeps, presumably due to dilution in the stream. Sucralose concentrations were higher in colder seeps, which are categorized as having shorter residence times in the bank sediments, and seeps from areas with high septic density. Overall, CEC detections and concentrations from seeps suggest that preferential groundwater flows play a role in transporting septic effluent-derived CECs to surface water. The conclusions for septic-derived FDOM were less clear, because most seeps displayed lower total fluorescence than stream samples. The divergence of CEC and FDOM profiles for seeps suggest the

need for additional studies. Chapter 6 also investigated mobilization of septic effluent during a single storm event. Most septic-derived CECs exhibited a first flush phenomenon, with a spike in concentrations corresponding to the peak discharge. Caffeine and sulfamethoxazole were well correlated with discharge. Similarly, all EEM regions and EEM-PARAFAC components were well correlated with discharge and caffeine. In contrast, the ratiometric FDOM parameters account for changes in composition, not magnitude, and were, therefore, not as well correlated with discharge. The most promising ratiometric parameters did exhibit a significant spike at the beginning of the rising limb of the hydrograph. A second spike in ratiometric FDOM parameters corresponded to the beginning of the largest discharge peak and increases in septic wastewater-derived CECs. These findings suggest the need for further investigation of the septic wastewater transport pathways.

## 7.2 Future opportunities

This work provides useful and actionable information but also points to additional knowledge gaps that can be filled by future studies. We suggest the following studies as possible future research opportunities.

*Temporal variation in septic-derived CECs and FDOM to nearby surface water.* This thesis observed temporal variations in septic FDOM fluorescence intensities with higher fluorescence generally in colder months. Using ratiometric parameters should account for these temporal variations, but a more comprehensive and longer-term study of a septic effluent-impacted stream is necessary to verify this assumption. Ideally, a future study

would collect at least monthly baseflow samples from a site that is known to be impacted by septic effluent to investigate temporal variations in septic impacts. This will help clarify the utility of FDOM parameters as indicators of septic effluent and septic effluent-derived CECs.

*Subsurface transport of septic effluent during baseflow and wet weather events.* Both the groundwater seeps that were identified using a thermal infrared survey and the single storm event case study showed variation between septic-derived FDOM and CEC transport. During baseflow, groundwater transport is expected to be the primary transport pathway for septic effluent to reach surface water. While some groundwater seeps had significant CEC detections and high concentrations, only one showed a significant wastewater-like FDOM signature. This points to the need for a future study to investigate the groundwater transport process for both FDOM and CECs from septic effluent from the septic drainfield to the stream. Additionally, the single storm event case study showed elevated CEC concentrations and a significant first flush phenomenon for ratiometric FDOM parameters. Variations through additional storm events are necessary to verify these findings.

## Appendix A

**Table A.1. North Branch walkup site names and coordinates.**

Site name	Sample type	Latitude	Longitude
NB-01	Both	39.41295	-76.70624
NB-02	Both	39.41217	-76.70947
NB-03	Both	39.41235	-76.70936
NB-04	EEM	39.41312	-76.71023
NB-05	EEM	39.41391	-76.71037
NB-06	EEM	39.41487	-76.71047
NB-07	EEM	39.41561	-76.71066
NB-08	EEM	39.41636	-76.71060
NB-09	EEM	39.41721	-76.71027
NB-10	Both	39.41737	-76.71039
NB-11	Both	39.41737	-76.71023
NB-12	EEM	39.41750	-76.70949
NB-13	EEM	39.41817	-76.70891
NB-14	EEM	39.41890	-76.70898
NB-15	EEM	39.41953	-76.70940
NB-16	Both	39.41982	-76.70961
NB-17	Both	39.42013	-76.70979
NB-18	EEM	39.42026	-76.70965
NB-19	Both	39.42051	-76.70995
NB-20	EEM	39.42118	-76.70975
NB-21	Both	39.42154	-76.70990
NB-22	Both	39.42191	-76.71016
NB-23	EEM	39.42262	-76.71056
NB-24	EEM	39.42350	-76.71128
NB-25	EEM	39.42443	-76.71168
NB-26	Both	39.42518	-76.71250
NB-27	Both	39.42506	-76.71275
NB-28	Both	39.42571	-76.71389
NB-29	Both	39.42599	-76.71384
NB-30	EEM	39.42659	-76.71411
NB-31	EEM	39.42752	-76.71482
NB-32	EEM	39.42831	-76.71647
NB-33	Both	39.42847	-76.71684
NB-34	Both	39.42864	-76.71682
NB-35	EEM	39.42893	-76.71687
NB-36	Both	39.42886	-76.71706
NB-37	EEM	39.42960	-76.71745
NB-38	EEM	39.43003	-76.71857
NB-39	EEM	39.43070	-76.71881
NB-40	Both	39.43115	-76.71909



<b>Site name</b>	<b>Sample type</b>	<b>Latitude</b>	<b>Longitude</b>
NB-41	Both	39.43101	-76.71942
NB-42	EEM	39.43075	-76.72051
NB-43	EEM	39.43151	-76.72168
NB-44	EEM	39.43188	-76.72231
NB-45	EEM	39.43249	-76.72317
NB-46	EEM	39.43297	-76.72379
NB-47	Both	39.43349	-76.72400
NB-48	Both	39.43364	-76.72369
NB-49	EEM	39.43434	-76.72372
NB-50	Both	39.43481	-76.72398
NB-51	Both	39.43477	-76.72440
NB-52	EEM	39.43456	-76.72522
NB-53	EEM	39.43419	-76.72590
NB-54	Both	39.43379	-76.72675
NB-55	Both	39.43385	-76.72683
NB-56	Both	39.43388	-76.72717
NB-57	Both	39.43399	-76.72729
NB-58	EEM	39.43469	-76.72798
NB-59	Both	39.43483	-76.72803
NB-60	Both	39.43490	-76.72801
NB-61	EEM	39.43530	-76.72884
NB-62	Both	39.43536	-76.72921
NB-63	Both	39.43565	-76.72896
NB-64	EEM	39.43634	-76.72933
NB-65	EEM	39.43618	-76.73011
NB-66	EEM	39.43597	-76.73059
NB-67	EEM	39.43596	-76.73063
NB-68	EEM	39.43618	-76.73179
NB-69	Both	39.43653	-76.73323
NB-70	EEM	39.43643	-76.73327
NB-71	Both	39.43646	-76.73440
NB-72	EEM	39.43672	-76.73531
NB-73	Both	39.43682	-76.73545
NB-74	Both	39.43677	-76.73555
NB-75	EEM	39.43728	-76.73668
NB-76	EEM	39.43747	-76.73751
NB-77	EEM	39.43756	-76.73835
NB-78	EEM	39.43717	-76.73924
NB-79	EEM	39.43655	-76.74032
NB-80	Both	39.43607	-76.74100
NB-81	Both	39.43621	-76.74102
NB-82	EEM	39.43682	-76.74177
NB-83	EEM	39.43882	-76.74425

<b>Site name</b>	<b>Sample type</b>	<b>Latitude</b>	<b>Longitude</b>
NB-84	EEM	39.43936	-76.74522
NB-85	Both	39.44830	-76.74960
NB-86	Both	39.44858	-76.74966
NB-87	EEM	39.44900	-76.74959
NB-88	EEM	39.44949	-76.74959
NB-89	EEM	39.45005	-76.74965
NB-90	Both	39.45060	-76.74956
NB-91	Both	39.45091	-76.74967
NB-92	Both	39.45076	-76.74992
NB-93	EEM	39.45127	-76.75058
NB-94	EEM	39.45150	-76.75115
NB-95	EEM	39.45179	-76.75166
NB-96	EEM	39.45214	-76.75204
NB-97	EEM	39.45250	-76.75252
NB-98	EEM	39.45298	-76.75299
NB-99	EEM	39.45343	-76.75387
NB-100	EEM	39.45419	-76.75473
NB-101	Both	39.45427	-76.75484
NB-102	Both	39.45431	-76.75470

**Table A.2. TIR groundwater seep survey site names, coordinates, and temperature differences between the seeps and the surface water.**

Site name	Sample type	Latitude	Longitude	Delta T (°C)
GW-01	Both	39.41728	-76.71025	3.8
GW-02	Both	39.42030	-76.70977	4.3
GW-03	Both	39.42222	-76.71038	n.a. <sup>a</sup>
GW-04	Both	39.42633	-76.71406	n.a. <sup>a</sup>
GW-05	Both	39.42771	-76.71524	n.a. <sup>a</sup>
GW-06	Both	39.42791	-76.71615	n.a. <sup>a</sup>
GW-07	Both	39.42794	-76.71616	n.a. <sup>a</sup>
GW-08	Both	39.42807	-76.71640	n.a. <sup>a</sup>
GW-09	Both	39.43090	-76.71889	4.2
GW-10	Both	39.43084	-76.71999	8.2
GW-11	Both	39.43241	-76.72317	6.2
GW-12	Both	39.43338	-76.72393	6.2
GW-13	Both	39.43381	-76.72361	3.2
GW-14	Both	39.43419	-76.72363	7.2
GW-15	Both	39.43486	-76.72397	6.2
GW-16	Both	39.43483	-76.72434	8.7
GW-17	Both	39.43479	-76.72445	9.7
GW-18	Both	39.43474	-76.72450	9.7
GW-19	Both	39.43458	-76.72495	7.7
GW-20	Both	39.43456	-76.72514	6.7
GW-21	Both	39.43454	-76.72535	4.7
GW-22	Both	39.43453	-76.72539	6.2
GW-23	Both	39.43453	-76.72544	7.7
GW-24	Both	39.43422	-76.72619	7.7
GW-25	Both	39.43385	-76.72682	3.7
GW-26	Both	39.43621	-76.72994	8.7

a: Seeps not confirmed with the TIR camera

## Appendix B

**Table B.1. CEC concentrations (ng/L) in samples collected from conventional Septic B.** Concentrations are reported as mean  $\pm$  standard deviation.

CECs	June	July	October	December
<b>Food additives</b>				
Sucralose	12,500 $\pm$ 186	11,300 $\pm$ 228	70,900 $\pm$ 3,710	32,500 $\pm$ 1,800
<b>Stimulants</b>				
Caffeine	7,630 $\pm$ 39	11,700 $\pm$ 91	12,800 $\pm$ 361	44,000 $\pm$ 453
Paraxanthine	n.a. <sup>a</sup>	12,300 $\pm$ 72	10,500 $\pm$ 91	49,400 $\pm$ 1,330
<b>Pharmaceuticals</b>				
Ibuprofen	n.a. <sup>a</sup>	1,990 $\pm$ 22	2,940 $\pm$ 28	836 $\pm$ 20
<b>Herbicides</b>				
Atrazine	n.a. <sup>a</sup>	< 4.6	< 3.6	2.4 $\pm$ < 0.1
<b>Antibiotics</b>				
Ofloxacin	n.d. <sup>b</sup>	16.7 $\pm$ 1.5	n.d. <sup>b</sup>	n.d. <sup>b</sup>
Sulfadiazine	n.d. <sup>b</sup>	54.7 $\pm$ 11.7	n.d. <sup>b</sup>	n.d. <sup>b</sup>
<b>UV filters</b>				
Homosalate	600 $\pm$ 44	166 $\pm$ 33	n.d. <sup>b</sup>	n.d. <sup>b</sup>
Octinoxate	< 9.1	82.7 $\pm$ 1.9	1,040 $\pm$ 54	158 $\pm$ 3
Octocrylene	123 $\pm$ 17	412 $\pm$ 8	n.d. <sup>b</sup>	363 $\pm$ 39
Oxybenzone	188 $\pm$ 4	< 28.4	n.d. <sup>b</sup>	89.6 $\pm$ 2.6
Sulisobenzone	462 $\pm$ 126	529 $\pm$ 32	351 $\pm$ 19	n.d. <sup>b</sup>
<b>Hormones</b>				
17 $\beta$ -estradiol	n.d. <sup>b</sup>	n.d. <sup>b</sup>	2040 $\pm$ 55	n.d. <sup>b</sup>
17 $\alpha$ -ethinylestradiol	n.d. <sup>b</sup>	6,840 $\pm$ 173	1200 $\pm$ 86	n.d. <sup>b</sup>
Androsterone	4,500 $\pm$ 18	n.d. <sup>b</sup>	4,830 $\pm$ 135	6,660 $\pm$ 26
Progesterone	n.d. <sup>b</sup>	n.d. <sup>b</sup>	167 $\pm$ 4	n.d. <sup>b</sup>

a: not measured

b: not detected

**Table B.2. CEC concentrations (ng/L) in samples collected from conventional Septic C.** Concentrations are reported as mean  $\pm$  standard deviation.

CECs	June	July	October	December
<b>Food additives</b>				
Sucralose	49,500 $\pm$ 1,130	12,600 $\pm$ 256	48,200 $\pm$ 559	7,910 $\pm$ 675
<b>Stimulants</b>				
Caffeine	10,400 $\pm$ 42	8,740 $\pm$ 43	41,800 $\pm$ 971	4,720 $\pm$ 92
Paraxanthine	n.a. <sup>a</sup>	4,050 $\pm$ 35	23,100 $\pm$ 514	15,100 $\pm$ 525
<b>Pharmaceuticals</b>				
Diclofenac	3.4 $\pm$ 0.1	9.7 $\pm$ 0.6	n.d. <sup>b</sup>	n.d. <sup>b</sup>
Ibuprofen	n.a. <sup>a</sup>	1,450 $\pm$ 32	1,640 $\pm$ 55	568 $\pm$ 13
<b>Herbicides</b>				
Atrazine	n.a. <sup>a</sup>	70.8 $\pm$ 0.5	67.9 $\pm$ 5.0	57.0 $\pm$ 1.3
Mecoprop	n.a. <sup>a</sup>	69.4 $\pm$ 4.5	n.d. <sup>b</sup>	n.d. <sup>b</sup>
<b>Antibiotics</b>				
Azithromycin	n.d. <sup>b</sup>	47.5 $\pm$ 5.1	n.d. <sup>b</sup>	60.6 $\pm$ 6.1
Clarithromycin	n.d. <sup>b</sup>	n.d. <sup>b</sup>	n.d. <sup>b</sup>	< 2.4
Erythromycin	n.d. <sup>b</sup>	n.d. <sup>b</sup>	3.9 $\pm$ 0.3	n.d. <sup>b</sup>
<b>UV filters</b>				
Ensulizole	n.d. <sup>b</sup>	n.d. <sup>b</sup>	767 $\pm$ 38	n.d. <sup>b</sup>
Homosalate	666 $\pm$ 210	n.d. <sup>b</sup>	n.d. <sup>b</sup>	n.d. <sup>b</sup>
Octinoxate	n.d. <sup>b</sup>	n.d. <sup>b</sup>	468 $\pm$ 51	n.d. <sup>b</sup>
Octocrylene	44.1 $\pm$ 20.4	70.1 $\pm$ 11.1	n.d. <sup>b</sup>	146 $\pm$ 8
Sulisobenzone	n.d. <sup>b</sup>	n.d. <sup>b</sup>	344 $\pm$ 15	n.d. <sup>b</sup>
<b>Hormones</b>				
Androsterone	8,540 $\pm$ 880	5,940 $\pm$ 87	2,070 $\pm$ 75	3,400 $\pm$ 54
Estrone	n.d. <sup>b</sup>	n.d. <sup>b</sup>	1,090 $\pm$ 160	109 $\pm$ 13

a: not measured

b: not detected

**Table B.3. CEC concentrations (ng/L) in samples collected from conventional Septic D.** Concentrations are reported as mean  $\pm$  standard deviation.

CECs	June	July	October	December
<b>Food additives</b>				
Sucralose	13,700 $\pm$ 106	11,300 $\pm$ 199	52,300 $\pm$ 1,500	12,300 $\pm$ 952
<b>Stimulants</b>				
Caffeine	17,500 $\pm$ 80	420,000 $\pm$ 28,600	13,600 $\pm$ 297	102,000 $\pm$ 5,830
Paraxanthine	n.a. <sup>a</sup>	5,500 $\pm$ 27	20,500 $\pm$ 1,890	17,900 $\pm$ 824
<b>Pharmaceuticals</b>				
Carbamazepine	61.7 $\pm$ 0.3	69.0 $\pm$ 0.7	47.9 $\pm$ 0.9	112 $\pm$ 1
Diclofenac	1.4 $\pm$ 0.2	n.d. <sup>b</sup>	n.d. <sup>b</sup>	n.d. <sup>b</sup>
Ibuprofen	n.a. <sup>a</sup>	7,730 $\pm$ 92	52,400 $\pm$ 2,400	56,200 $\pm$ 1,920
<b>Herbicides</b>				
Atrazine	n.a. <sup>a</sup>	152 $\pm$ 3	118 $\pm$ 6	156 $\pm$ 2
<b>Antibiotics</b>				
Azithromycin	n.d. <sup>b</sup>	11.9 $\pm$ 0.8	n.d. <sup>b</sup>	2,610 $\pm$ 108
Sulfamethoxazole	n.d. <sup>b</sup>	n.d. <sup>b</sup>	28.2 $\pm$ 0.9	n.d. <sup>b</sup>
<b>UV filters</b>				
Avobenzone	n.d. <sup>b</sup>	140 $\pm$ 20	n.d. <sup>b</sup>	n.d. <sup>b</sup>
Homosalate	2,460 $\pm$ 882	163 $\pm$ 25	n.d. <sup>b</sup>	484 $\pm$ 50
Octinoxate	51.9 $\pm$ 3.0	n.d. <sup>b</sup>	758 $\pm$ 157	n.d. <sup>b</sup>
Octocrylene	2,280 $\pm$ 313	432 $\pm$ 41	n.d. <sup>b</sup>	852 $\pm$ 59
Oxybenzone	108 $\pm$ 20	n.d. <sup>b</sup>	762 $\pm$ 54	n.d. <sup>b</sup>
Sulisobenzone	1,260 $\pm$ 128	1,220 $\pm$ 31	736 $\pm$ 16	n.d. <sup>b</sup>
<b>Hormones</b>				
Androsterone	1,600 $\pm$ 69	793 $\pm$ 60	4,320 $\pm$ 46	2,360 $\pm$ 22
Estrone	144 $\pm$ 9	290 $\pm$ 8	391 $\pm$ 30	1,270 $\pm$ 11
Progesterone	42.1 $\pm$ 2.3	n.d. <sup>b</sup>	29.2 $\pm$ 0.8	n.d. <sup>b</sup>

a: not measured

b: not detected

**Table B.4. CEC concentrations (ng/L) in municipal wastewater samples.** Concentrations are reported as mean  $\pm$  standard deviation.

CECs	June	July	October	December
<b>Food additives</b>				
Sucralose	17,700 $\pm$ 121	32,400 $\pm$ 732	42,700 $\pm$ 821	29,100 $\pm$ 4,020
<b>Stimulants</b>				
Caffeine	36,800 $\pm$ 283	68,700 $\pm$ 1,830	54,400 $\pm$ 2,030	53,000 $\pm$ 323
Paraxanthine	n.a. <sup>a</sup>	17,000 $\pm$ 412	30,200 $\pm$ 1,020	19,100 $\pm$ 238
<b>Pharmaceuticals</b>				
Carbamazepine	140 $\pm$ 1	187 $\pm$ 1	187 $\pm$ 15	297 $\pm$ 1
Diclofenac	209 $\pm$ 2	421 $\pm$ 6	377 $\pm$ 3	191 $\pm$ 3
Ibuprofen	n.a. <sup>a</sup>	10,600 $\pm$ 616	29,100 $\pm$ 123	14,300 $\pm$ 318
<b>Herbicides</b>				
Atrazine	n.a. <sup>a</sup>	117 $\pm$ 2	72.2 $\pm$ 1.7	88.7 $\pm$ 0.6
<b>Antibiotics</b>				
Azithromycin	217 $\pm$ 9	560 $\pm$ 20	n.d. <sup>b</sup>	767 $\pm$ 26
Ciprofloxacin	n.d. <sup>b</sup>	428 $\pm$ 3	1,120 $\pm$ 14	n.d. <sup>b</sup>
Clarithromycin	87.2 $\pm$ 35.6	38.3 $\pm$ 1.2	61.2 $\pm$ 3.8	126 $\pm$ 6
Erythromycin	n.d. <sup>b</sup>	n.d. <sup>b</sup>	n.d. <sup>b</sup>	47.7 $\pm$ 3.0
Ofloxacin	137 $\pm$ 4	197 $\pm$ 6	253 $\pm$ 5	n.d. <sup>b</sup>
Sulfacetamide	46.9 $\pm$ 2.9	19.5 $\pm$ 1.6	696 $\pm$ 24	316 $\pm$ 12
Sulfamethoxazole	152 $\pm$ 7	1,080 $\pm$ 12	1,360 $\pm$ 54	820 $\pm$ 9
Sulfapyridine	144 $\pm$ 1	289 $\pm$ 9	889 $\pm$ 70	686 $\pm$ 9
Tylosin	n.d. <sup>b</sup>	n.d. <sup>b</sup>	n.d. <sup>b</sup>	19.0 $\pm$ 2.1
<b>UV filters</b>				
Avobenzone	n.d. <sup>b</sup>	879 $\pm$ 53	40.5 $\pm$ 4.0	53.3 $\pm$ 3.5
Ensulizole	n.d. <sup>b</sup>	n.d. <sup>b</sup>	19,400 $\pm$ 1,370	n.d. <sup>b</sup>
Homosalate	983 $\pm$ 244	4,290 $\pm$ 224	1,063 $\pm$ 63	404 $\pm$ 64
Octinoxate	87.6 $\pm$ 1.8	676 $\pm$ 24	285 $\pm$ 3	169 $\pm$ 2
Octisalate	n.d. <sup>b</sup>	1,030 $\pm$ 81	331 $\pm$ 39	< 186.8

<b>CECs</b>	<b>June</b>	<b>July</b>	<b>October</b>	<b>December</b>
Octocrylene	750 ± 13	3,250 ± 186	1,620 ± 131	619 ± 37
Oxybenzone	328 ± 5	1,070 ± 54	449 ± 13	257 ± 3
Sulisobenzone	n.d. <sup>b</sup>	325 ± 29	n.d. <sup>b</sup>	n.d. <sup>b</sup>
<b>Hormones</b>				
17 $\alpha$ -ethinylestradiol	n.d. <sup>b</sup>	1,360 ± 78	n.d. <sup>b</sup>	n.d. <sup>b</sup>
Androsterone	1,580 ± 12	2,250 ± 56	3,000 ± 105	2,510 ± 81
Estrone	n.d. <sup>b</sup>	n.d. <sup>b</sup>	< 22.9	n.d. <sup>b</sup>
Estriol	n.d. <sup>b</sup>	205 ± 19	462 ± 10	n.d. <sup>b</sup>

a: not measured

b: not detected



**Table B.5. CEC concentrations in the liquid (ng/L) and solid (ng/g) phases of septic sludge.** Concentrations are reported as mean  $\pm$  standard deviation.

CECs	July		October		December	
	Liquid	Solid	Liquid	Solid	Liquid	Solid
<b>Food additives</b>						
Sucralose	139,000 $\pm$ 1,990	52,700 $\pm$ 2,460	79,900 $\pm$ 2,220	276,000 $\pm$ 12,300	139,000 $\pm$ 5,770	n.d. <sup>a</sup>
<b>Stimulants</b>						
Caffeine	21,700 $\pm$ 84	n.d. <sup>a</sup>	212,000 $\pm$ 14,200	n.d. <sup>a</sup>	31,500 $\pm$ 764	n.d. <sup>a</sup>
Paraxanthine	29,000 $\pm$ 65	n.d. <sup>a</sup>	19,300 $\pm$ 407	n.d. <sup>a</sup>	24,600 $\pm$ 763	n.d. <sup>a</sup>
<b>Pharmaceuticals</b>						
Carbamazepine	10.0 $\pm$ 0.2	92.0 $\pm$ 9.8	n.d. <sup>a</sup>	128 $\pm$ 15	130 $\pm$ 1	n.d. <sup>a</sup>
Diclofenac	47.7 $\pm$ 1.0	269 $\pm$ 45	200 $\pm$ 6	1,920 $\pm$ 525	75.9 $\pm$ 2.6	n.d. <sup>a</sup>
Ibuprofen	22,100 $\pm$ 90	47,900 $\pm$ 2,810	4,890 $\pm$ 87	n.d. <sup>a</sup>	30,800 $\pm$ 354	54,200 $\pm$ 2,290
<b>Herbicides</b>						
Atrazine	13.1 $\pm$ 0.1	n.d. <sup>a</sup>	89.0 $\pm$ 2.8	669 $\pm$ 117	6.9 $\pm$ 1.0	69.5 $\pm$ 3.0
<b>Antibiotics</b>						
Azithromycin	99.1 $\pm$ 1.4	16,600 $\pm$ 2,860	4,010 $\pm$ 821	256,000 $\pm$ 7,850	118 $\pm$ 21	34,700 $\pm$ 3,310
Clarithromycin	< 3.5	345 $\pm$ 40	44.0 $\pm$ 3.2	1,982 $\pm$ 509	524 $\pm$ 20	40,100 $\pm$ 3,960
Erythromycin	359 $\pm$ 32	4,470 $\pm$ 109	34.5 $\pm$ 1.3	5,792 $\pm$ 428	20.7 $\pm$ 0.9	1,137 $\pm$ 104
Sulfadiazine	219 $\pm$ 32	< 2,500	n.d. <sup>a</sup>	n.d. <sup>a</sup>	n.d. <sup>a</sup>	n.d. <sup>a</sup>
Sulfamethoxazole	757 $\pm$ 4	880 $\pm$ 112	222 $\pm$ 6	n.d. <sup>a</sup>	n.d. <sup>a</sup>	n.d. <sup>a</sup>
Sulfapyridine	92.6 $\pm$ 4.1	n.d. <sup>a</sup>	1,050 $\pm$ 19	18,700 $\pm$ 1,390	n.d. <sup>a</sup>	n.d. <sup>a</sup>
Sulfathiazole	n.d. <sup>a</sup>	8,640 $\pm$ 294	n.d. <sup>a</sup>	n.d. <sup>a</sup>	n.d. <sup>a</sup>	n.d. <sup>a</sup>
<b>UV filters</b>						
Avobenzone	892 $\pm$ 138	n.d. <sup>a</sup>	10,300 $\pm$ 324	n.d. <sup>a</sup>	657 $\pm$ 58	113,000 $\pm$ 15,000
Homosalate	1,900 $\pm$ 206	119,000 $\pm$ 18,800	n.d. <sup>a</sup>	168,000 $\pm$ 17,300	2,600 $\pm$ 46	201,000 $\pm$ 67,100
Octinoxate	n.d. <sup>a</sup>	28,100 $\pm$ 2,480	742 $\pm$ 39	152,000 $\pm$ 113,000	< 76.8	41,300 $\pm$ 9,790
Octisalate	n.d. <sup>a</sup>	n.d. <sup>a</sup>	4,190 $\pm$ 790	118,000 $\pm$ 110,000	1,230 $\pm$ 73	n.d. <sup>a</sup>
Octocrylene	5,740 $\pm$ 301	308,000 $\pm$ 28,900	25,500 $\pm$ 5,470	3,470,000 $\pm$ 348,000	5,010 $\pm$ 176	615,000 $\pm$ 23,900

CECs	July		October		December	
	Liquid	Solid	Liquid	Solid	Liquid	Solid
Oxybenzone	n.d. <sup>a</sup>	35,500 ± 4,310	384 ± 7	82,800 ± 13,700	< 26.6	42,600 ± 6,840
Sulisobenzone	352 ± 15	n.d. <sup>a</sup>	625 ± 132	n.d. <sup>a</sup>	n.d. <sup>a</sup>	n.d. <sup>a</sup>
<b>Hormones</b>						
Androsterone	4,960 ± 493	366,000 ± 10,800	13,900 ± 174	749,000 ± 30,300	3,150 ± 24	261,000 ± 484
Estrone	n.d. <sup>a</sup>	15,900 ± 925	408 ± 14	n.d. <sup>a</sup>	208 ± 17	61,100 ± 4,670
Estriol	n.d. <sup>a</sup>	n.d. <sup>a</sup>	465 ± 13	n.d. <sup>a</sup>	n.d. <sup>a</sup>	n.d. <sup>a</sup>
Equilin	n.d. <sup>a</sup>	76,900 ± 3,820	n.d. <sup>a</sup>	n.d. <sup>a</sup>	n.d. <sup>a</sup>	n.d. <sup>a</sup>
Progesterone	n.d. <sup>a</sup>	33,800 ± 5,210	n.d. <sup>a</sup>	n.d. <sup>a</sup>	n.d. <sup>a</sup>	26,000 ± 147

a: not detected

**Table B.6. Dates, times, and air temperature for collection of samples from the conventional septic systems.**

<b>Month</b>	<b>Date</b>	<b>Time</b>	<b>Air temperature (°C)</b>
June	Wednesday, June 22, 2022	5:31 pm	24
July	Sunday, July 24, 2022	12:31 pm	36
October	Friday, October 14, 2022	5:18 pm	17
December	Sunday, December 4, 2022	12:32 pm	8

**Table B.7. CEC concentrations (ng/L) at the inlet and outlet of the advanced septic system.** Concentrations are reported as mean  $\pm$  standard deviation.

CECs	June		July		October		December	
	Inlet	Outlet	Inlet	Outlet	Inlet	Outlet	Inlet	Outlet
<b>Food additives</b>								
Sucralose	4,060 $\pm$ 101	4,730 $\pm$ 66	1,610 $\pm$ 44	2,320 $\pm$ 98	37,700 $\pm$ 2,210	18,600 $\pm$ 439	n.d. <sup>a</sup>	5,370 $\pm$ 432
<b>Stimulants</b>								
Caffeine	18,600 $\pm$ 134	1,520 $\pm$ 17	7,250 $\pm$ 78	460 $\pm$ 6	10,800 $\pm$ 191	470 $\pm$ 4	8,390 $\pm$ 143	1,090 $\pm$ 13
Paraxanthine	n.a. <sup>b</sup>	n.a. <sup>b</sup>	12,600 $\pm$ 84	477 $\pm$ 6	10,600 $\pm$ 128	766 $\pm$ 6	12,300 $\pm$ 308	619 $\pm$ 1
<b>Pharmaceuticals</b>								
Carbamazepine	n.d. <sup>a</sup>	n.d. <sup>a</sup>	n.d. <sup>a</sup>	< 3.5	n.d. <sup>a</sup>	n.d. <sup>a</sup>	49.5 $\pm$ 0.2	n.d. <sup>a</sup>
Diclofenac	5.5 $\pm$ 0.4	8.4 $\pm$ 0.3	< 4.5	< 4.5	n.d. <sup>a</sup>	n.d. <sup>a</sup>	n.d. <sup>a</sup>	n.d. <sup>a</sup>
Ibuprofen	n.a. <sup>b</sup>	n.a. <sup>b</sup>	17,800 $\pm$ 108	n.d. <sup>a</sup>	23,800 $\pm$ 292	958 $\pm$ 19	12,600 $\pm$ 171	665 $\pm$ 8
<b>Herbicides</b>								
Atrazine	n.a. <sup>b</sup>	n.a. <sup>b</sup>	n.d. <sup>a</sup>	< 4.6	< 3.6	< 3.6	< 1.2	n.d. <sup>a</sup>
<b>Antibiotics</b>								
Azithromycin	n.d. <sup>a</sup>	n.d. <sup>a</sup>	9.6 $\pm$ 1.6	18.9 $\pm$ 0.2	n.d. <sup>a</sup>	n.d. <sup>a</sup>	n.d. <sup>a</sup>	n.d. <sup>a</sup>
Erythromycin	n.d. <sup>a</sup>	n.d. <sup>a</sup>	n.d. <sup>a</sup>	n.d. <sup>a</sup>	n.d. <sup>a</sup>	n.d. <sup>a</sup>	< 2.9	n.d. <sup>a</sup>
<b>UV filters</b>								
Homosalate	n.d. <sup>a</sup>	n.d. <sup>a</sup>	260 $\pm$ 79	n.d. <sup>a</sup>	562 $\pm$ 47	199 $\pm$ 31	106 $\pm$ 44	n.d. <sup>a</sup>
Octinoxate	239 $\pm$ 2	n.d. <sup>a</sup>	51.4 $\pm$ 8.2	n.d. <sup>a</sup>	< 35.2	n.d. <sup>a</sup>	n.d. <sup>a</sup>	n.d. <sup>a</sup>
Octocrylene	64.9 $\pm$ 35.5	n.d. <sup>a</sup>	450 $\pm$ 57	n.d. <sup>a</sup>	150 $\pm$ 4	n.d. <sup>a</sup>	83.9 $\pm$ 2.1	n.d. <sup>a</sup>
Oxybenzone	7.0 $\pm$ 1.0	43.1 $\pm$ 2.0	57.4 $\pm$ 4.7	n.d. <sup>a</sup>	n.d. <sup>a</sup>	n.d. <sup>a</sup>	n.d. <sup>a</sup>	n.d. <sup>a</sup>
Sulisobenzone	n.d. <sup>a</sup>	n.d. <sup>a</sup>	31.8 $\pm$ 2.1	126 $\pm$ 3	n.d. <sup>a</sup>	n.d. <sup>a</sup>	306 $\pm$ 11	138 $\pm$ 10
<b>Hormones</b>								
17 $\alpha$ -ethinylestradiol	n.d. <sup>a</sup>	n.d. <sup>a</sup>	n.d. <sup>a</sup>	n.d. <sup>a</sup>	307 $\pm$ 8	n.d. <sup>a</sup>	n.d. <sup>a</sup>	n.d. <sup>a</sup>
Androsterone	2,320 $\pm$ 126	n.d. <sup>a</sup>	3,220 $\pm$ 35	n.d. <sup>a</sup>	953 $\pm$ 52	n.d. <sup>a</sup>	985 $\pm$ 33	n.d. <sup>a</sup>
Estrone	n.d. <sup>a</sup>	n.d. <sup>a</sup>	n.d. <sup>a</sup>	n.d. <sup>a</sup>	< 22.9	n.d. <sup>a</sup>	n.d. <sup>a</sup>	n.d. <sup>a</sup>
Progesterone	n.d. <sup>a</sup>	n.d. <sup>a</sup>	n.d. <sup>a</sup>	n.d. <sup>a</sup>	31.5 $\pm$ 1.4	n.d. <sup>a</sup>	n.d. <sup>a</sup>	n.d. <sup>a</sup>

a: not detected

b: not measured

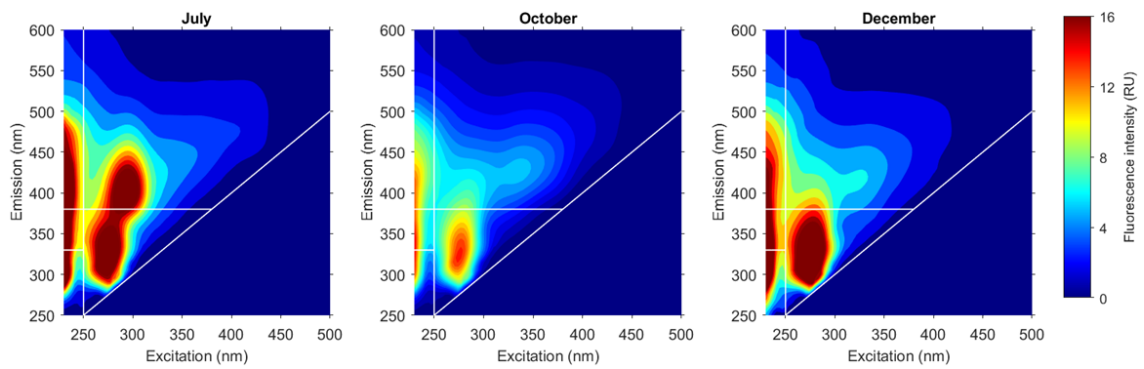


**Figure B.1. EEMs from three unique septic sludge samples collected directly from a septic pumping truck.**

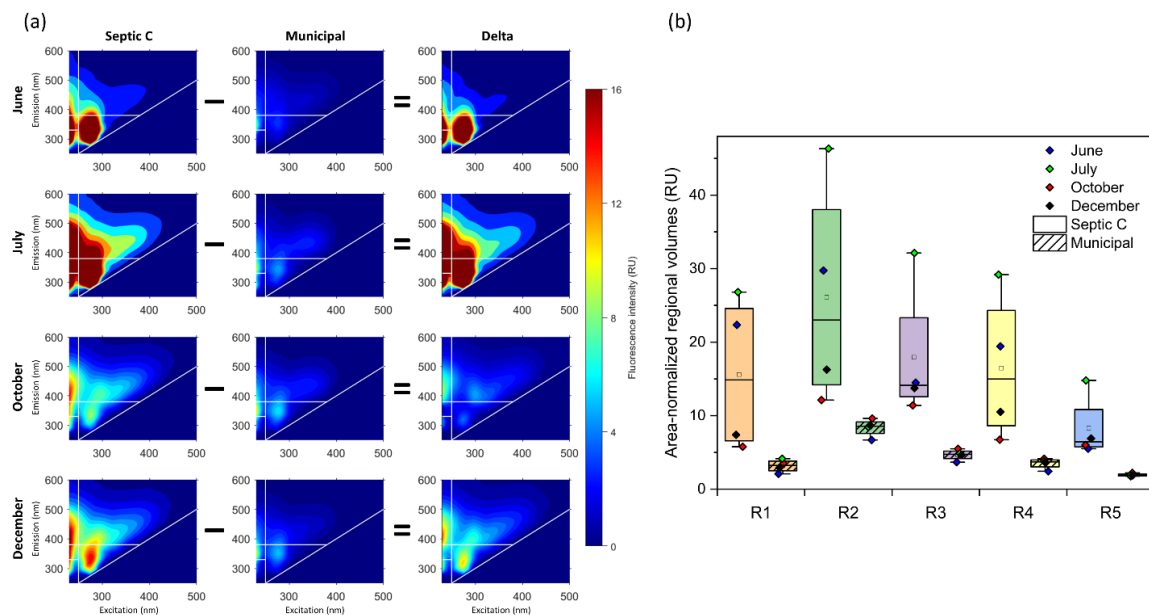


**Figure B.2. FDOM in Septic C and municipal wastewater expressed as (a) differential EEMs and (b) box plots. In (a), the fluorescence in the "Delta" plots indicate regions with higher fluorescence in Septic C wastewater compared to municipal wastewater.**

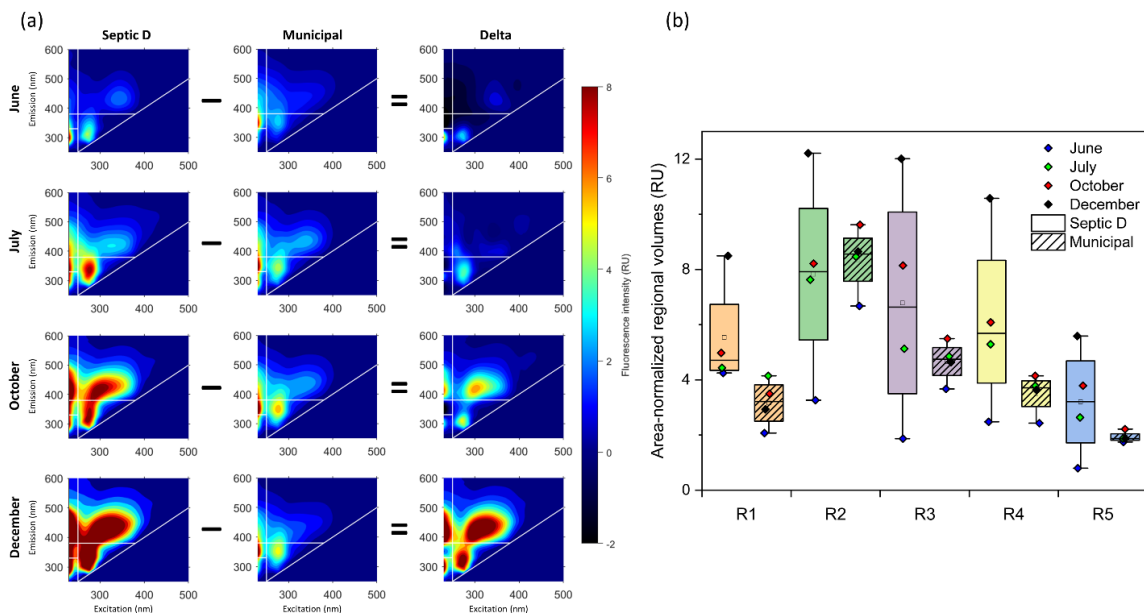


**Figure B.3. FDOM in Septic D and municipal wastewater expressed as (a) differential EEMs and (b) box plots. In (a), the fluorescence in the "Delta" plots indicate regions with higher fluorescence in Septic D wastewater compared to municipal wastewater.**

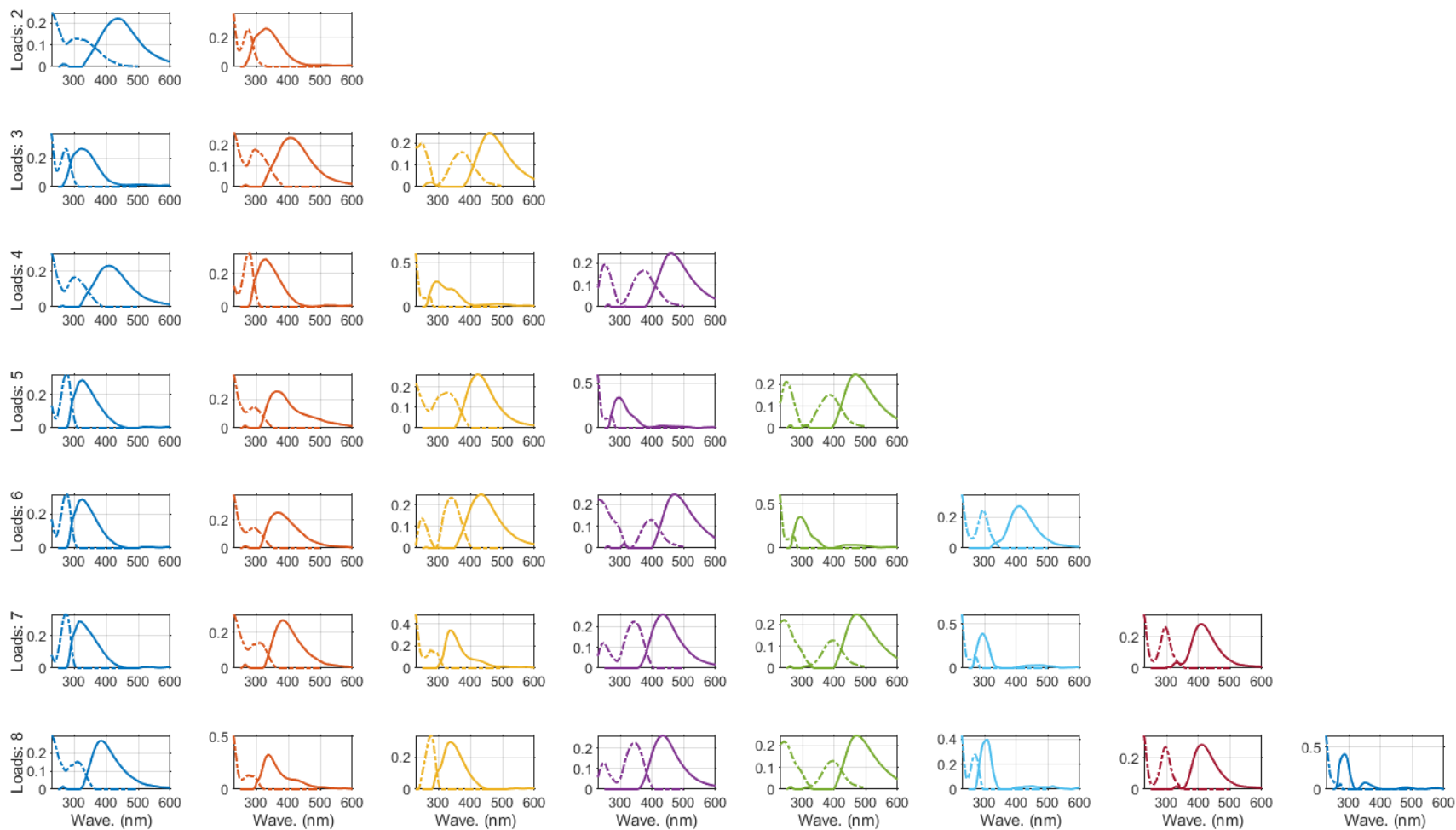


**Figure B.4. Spectral loadings for preliminary EEM-PARAFAC models with 2–8 components for FDOM in septic wastewater.** The dashed curves are excitation loadings, and the solid curves are emission loadings. Only models with 2, 3, and 4 components were validated by split-half analysis.



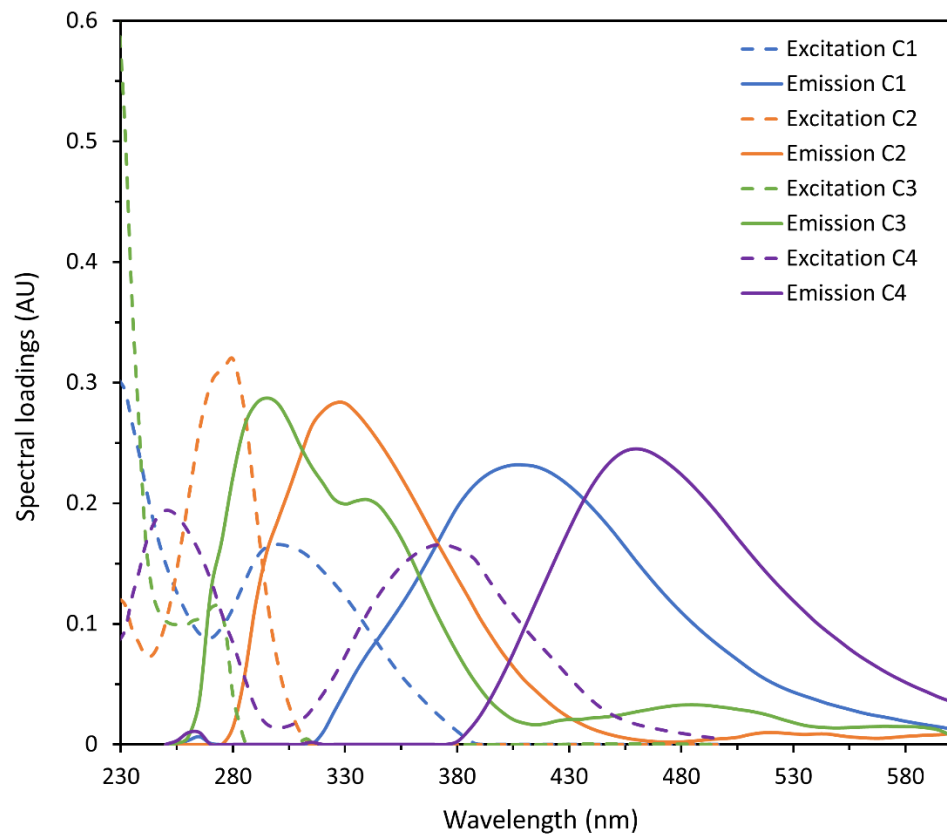


**Figure B.5. Spectral loadings for the validated four-component EEM-PARAFAC model for FDOM in septic wastewater.**

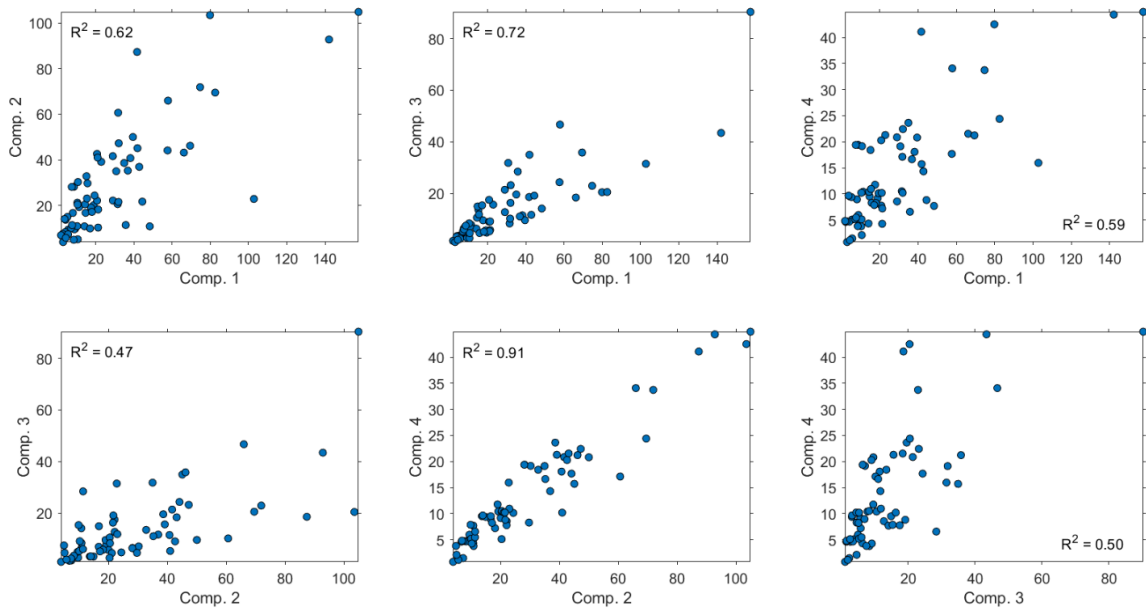


**Figure B.6. Correlations between the component scores for the four-component EEM-PARAFAC model for septic wastewater before data normalization. The strongest correlation was observed between C4 and C2.**

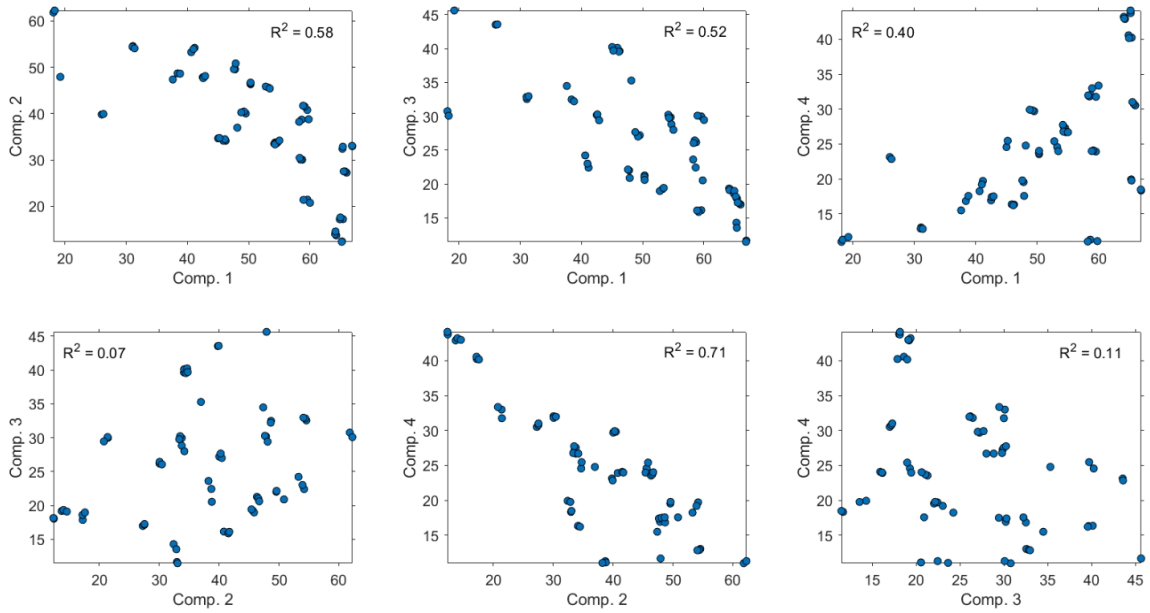


**Figure B.7. Correlations between the component scores for the four-component EEM-PARAFAC model for septic wastewater after data normalization. No strong correlations were observed.**

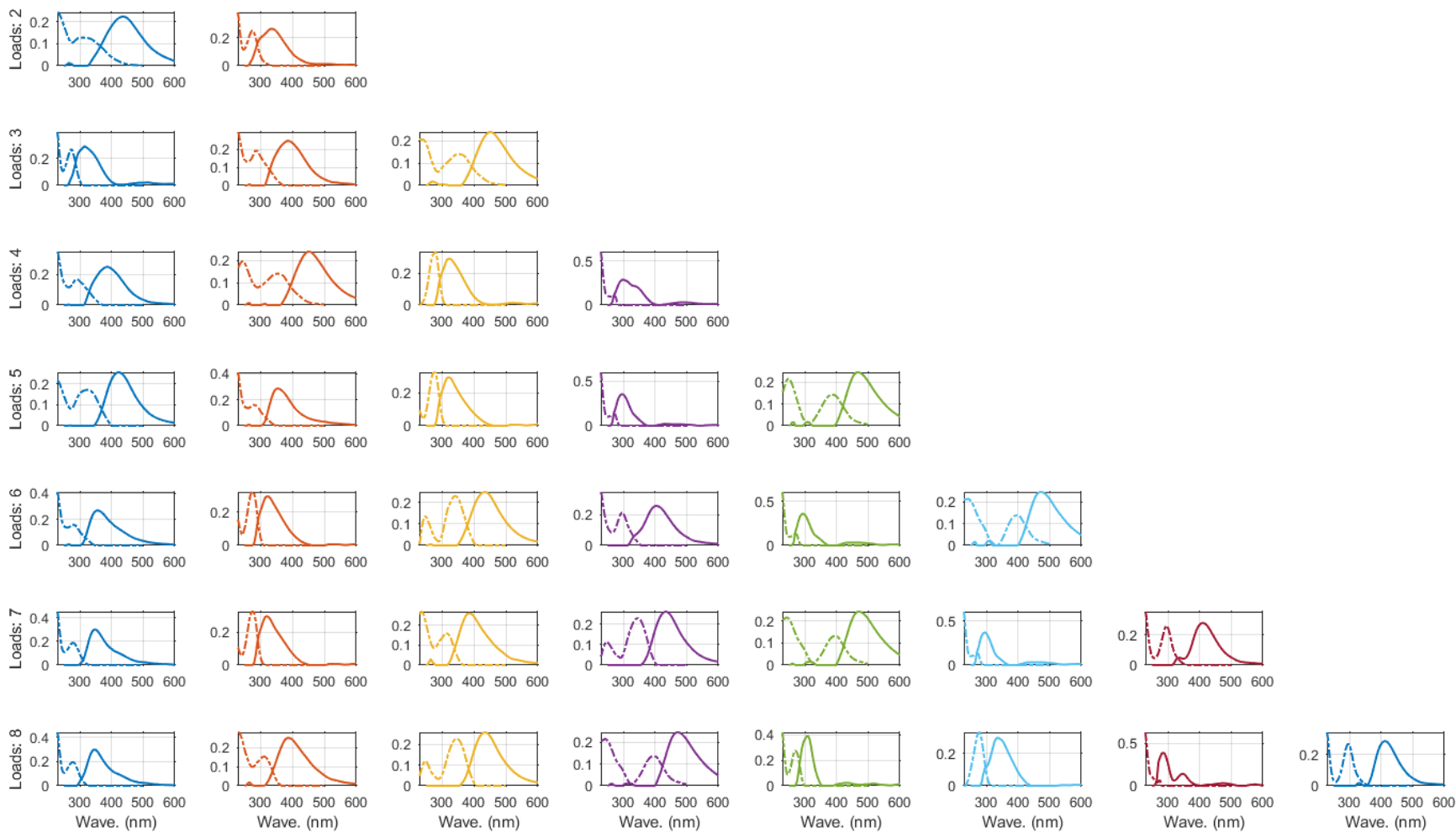


**Figure B.8. Spectral loadings for preliminary EEM-PARAFAC models with 2–8 components for FDOM in septic and municipal wastewater.** The dashed curves are excitation loadings, and the solid curves are emission loadings. Only models with 2, 5, 6, and 7 components were validated by split-half analysis.

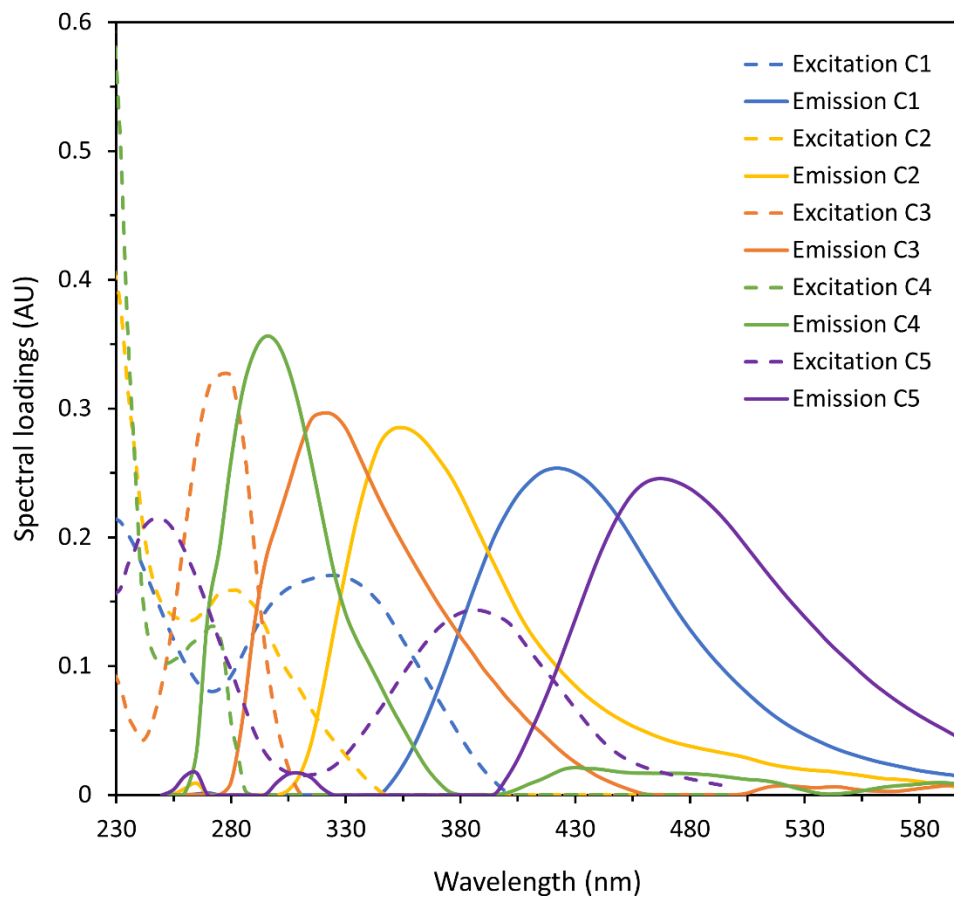


**Figure B.9. Spectral loadings for the validated five-component EEM-PARAFAC model for FDOM in septic and municipal wastewater.**

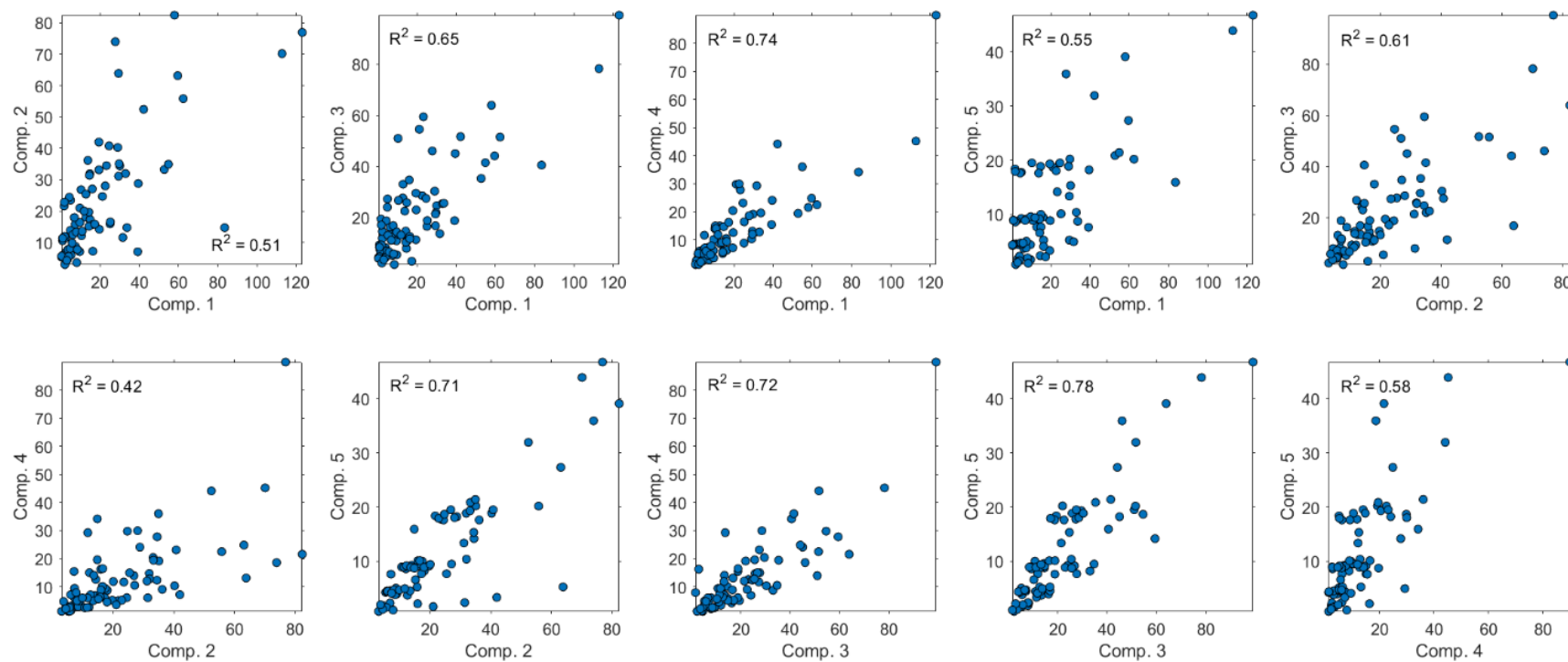


**Figure B.10. Correlations between the component scores for the five-component EEM-PARAFAC global wastewater model before data normalization.** No strong correlations were observed.

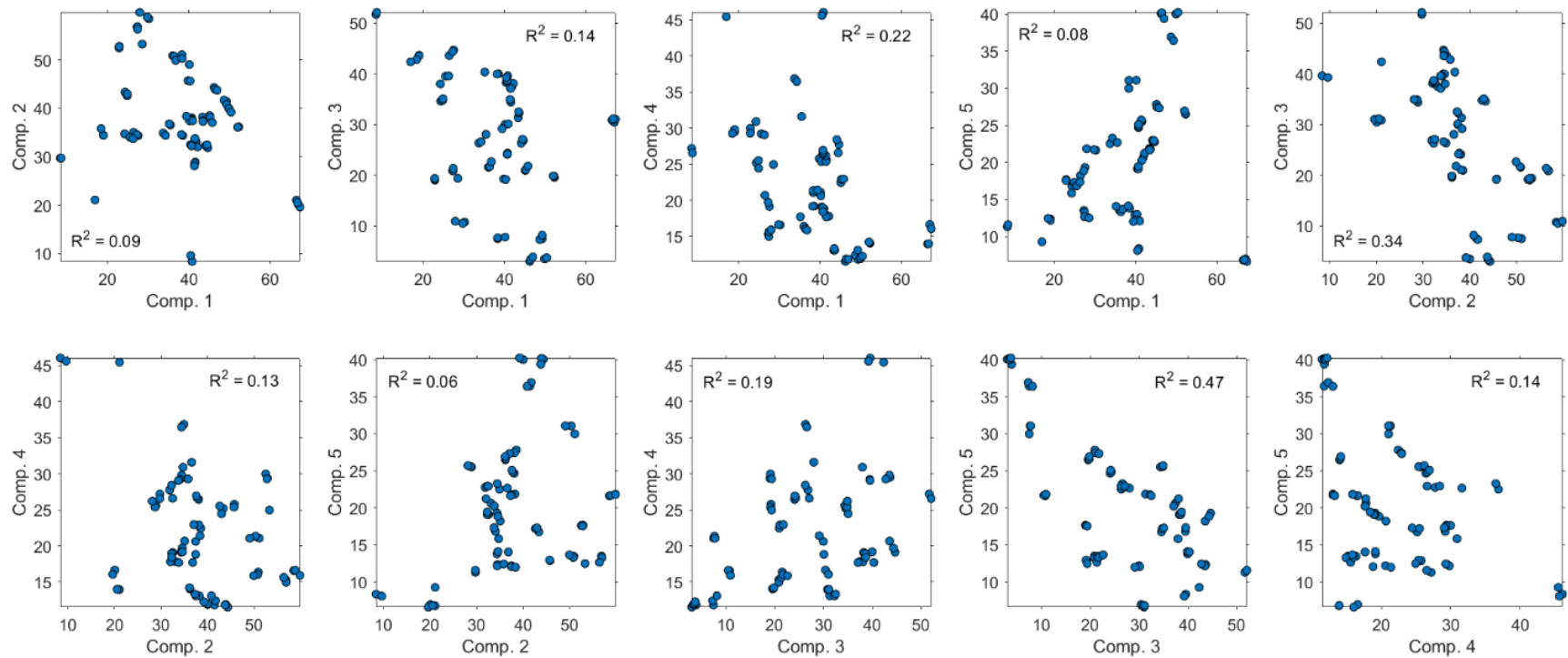


**Figure B.11. Correlations between the component scores for the five-component EEM-PARAFAC global wastewater model after data normalization. No strong correlations were observed.**

## Appendix C

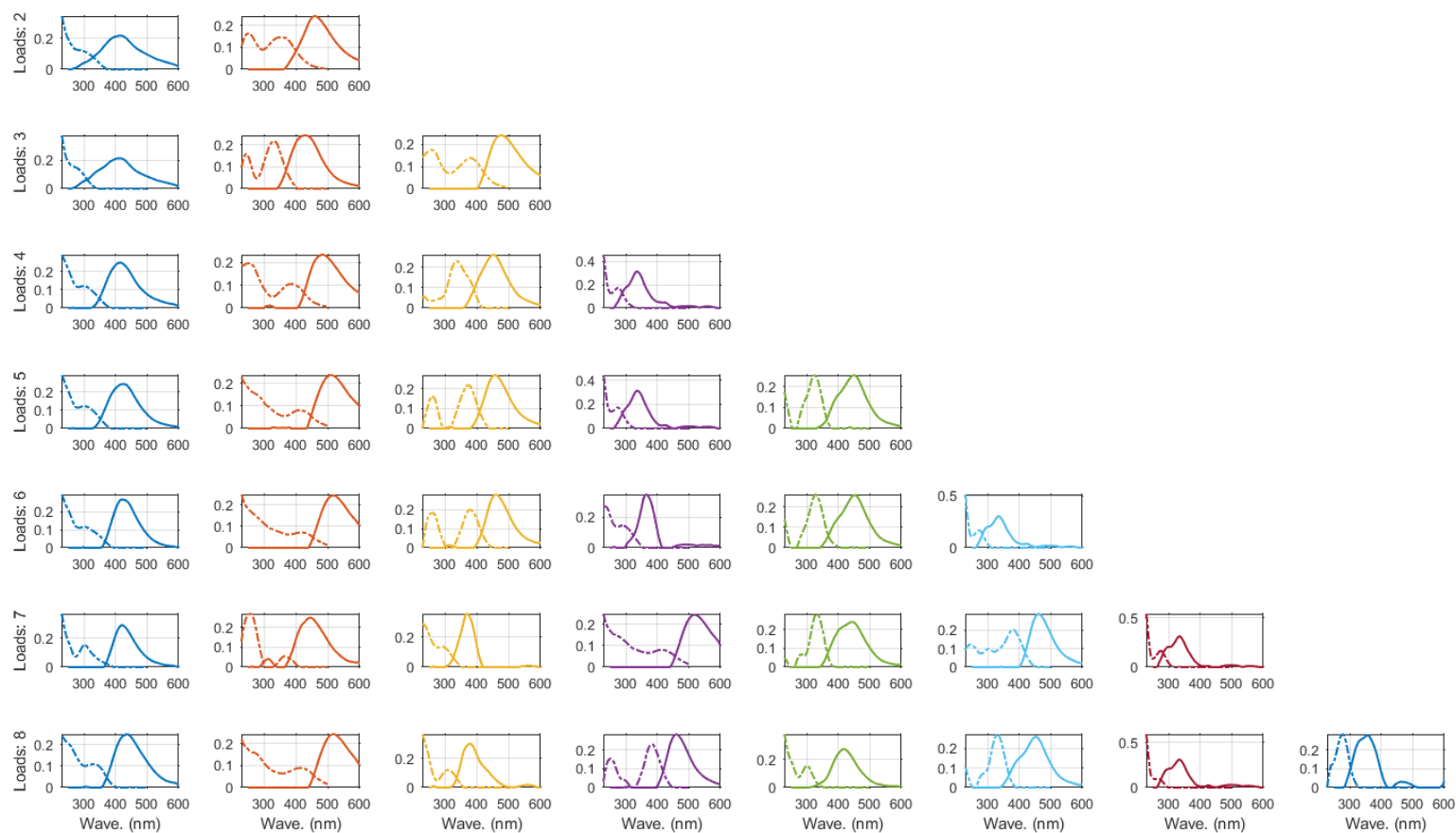


**Figure C.1. Spectral loadings for preliminary EEM-PARAFAC models with 2–8 components for FDOM in North Branch stream samples.** The dashed curves are excitation loadings, and the solid curves are emission loadings. Only models with 2, 3, 4, and 5 components were validated using split-half analysis.



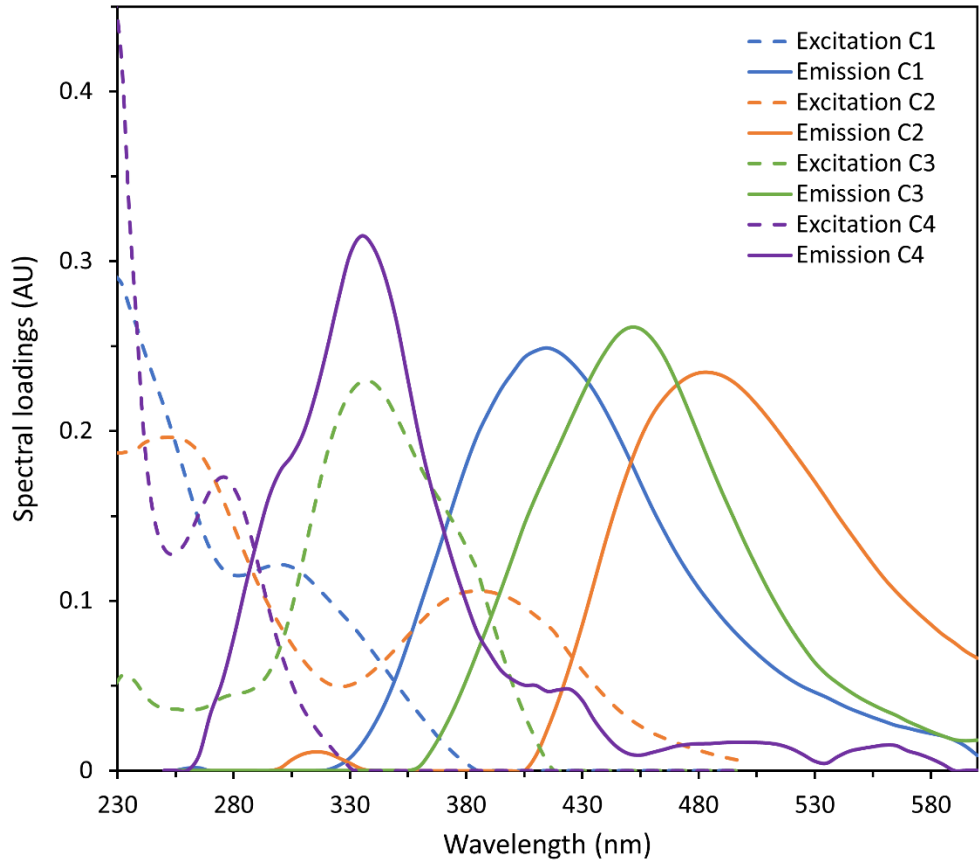


**Figure C.2. Spectral loadings for the validated four-component EEM-PARAFAC model for FDOM in the North Branch.**

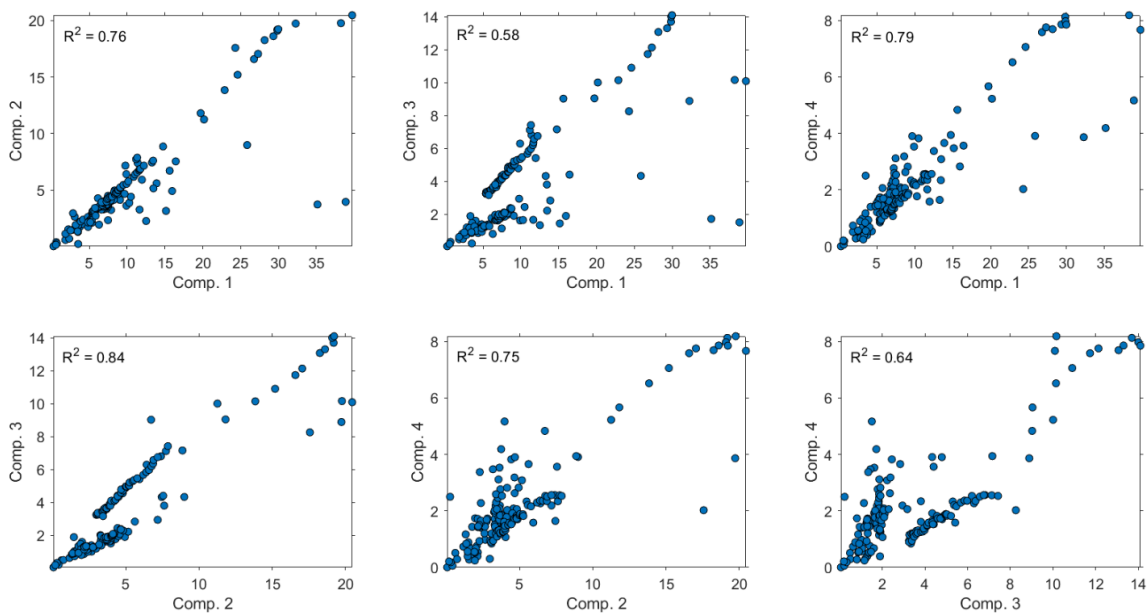


**Figure C.3. Correlations between the component scores for the four-component EEM-PARAFAC model for North Branch stream samples before data normalization. The strongest correlation was observed between C3 and C2.**

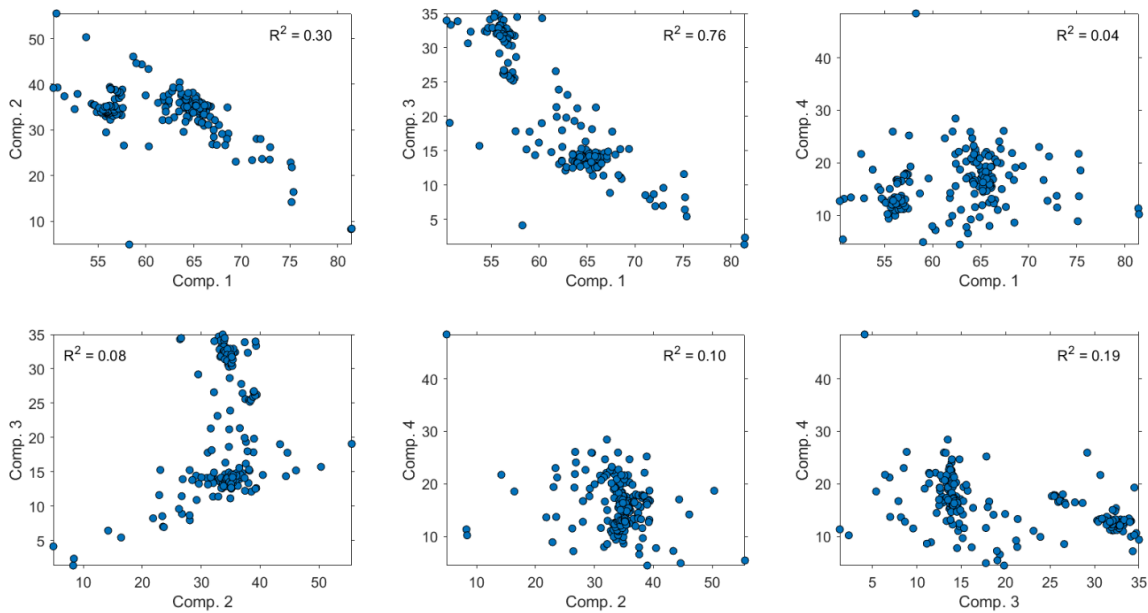


**Figure C.4. Correlations between the component scores for the four-component EEM-PARAFAC model for North Branch stream samples after data normalization. No strong correlations were observed.**

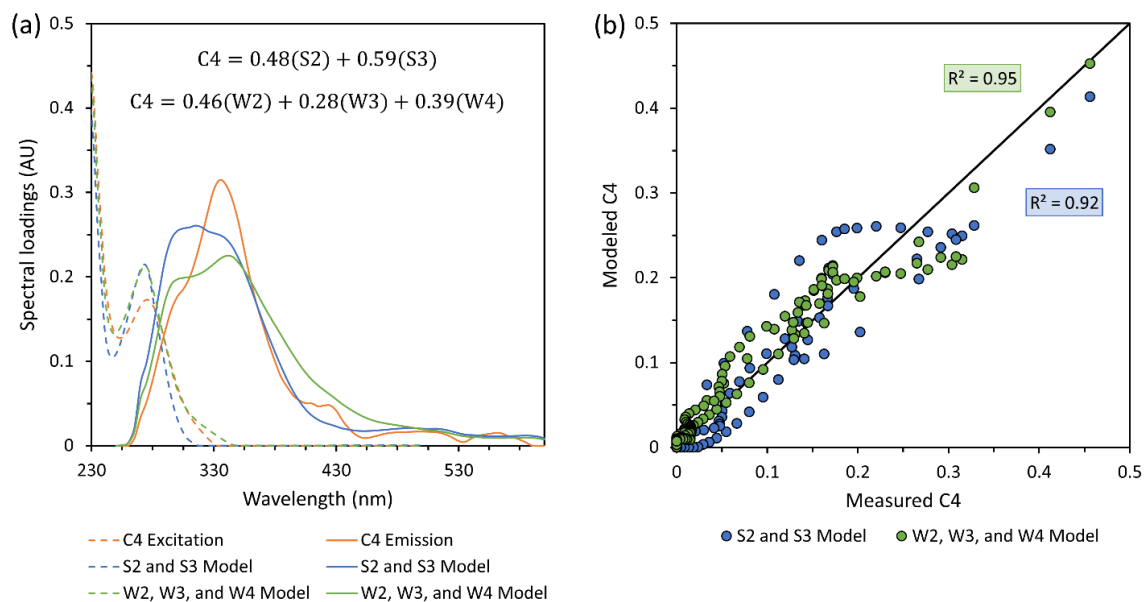


**Figure C.5. (a) Multi-linear regressions of C4 from the North Branch EEM-PARAFAC model using components from the septic wastewater and global wastewater EEM-PARAFAC models and (b) 1:1 plot of measured versus modeled C4 values demonstrating the accuracy of the models.**

## References

- (1) Harrison, M.; Stanwyck, E.; Beckingham, B.; Starry, O.; Hanlon, B.; Newcomer, J. Smart Growth and the Septic Tank: Wastewater Treatment and Growth Management in the Baltimore Region. *Land Use Policy* **2012**, *29* (3), 483–492. <https://doi.org/10.1016/j.landusepol.2011.08.007>.
- (2) Shields, C. A.; Band, L.; Law, N.; Groffman, P.; Kaushal, S.; Savvas, K.; Fisher, G.; Belt, K. Streamflow Distribution of Non-Point Source Nitrogen Export from Urban-rural Catchments in the Chesapeake Bay Watershed. **2008**. <https://doi.org/10.1029/2007WR006360>.
- (3) Diamond, J. M.; Latimer II, H. A.; Munkittrick, K. R.; Thornton, K. W.; Bartell, S. M.; Kidd, K. A. Prioritizing Contaminants of Emerging Concern for Ecological Screening Assessments. *Environ. Toxicol. Chem.* **2011**, *30* (11), 2385–2394. <https://doi.org/10.1002/etc.667>.
- (4) Godfrey, E.; Woessner, W. W.; Benotti, M. J. Pharmaceuticals in On-Site Sewage Effluent and Ground Water, Western Montana. *Groundwater* **2007**, *45* (3), 263–271. <https://doi.org/10.1111/j.1745-6584.2006.00288.x>.
- (5) Matamoros, V.; Arias, C.; Brix, H.; Bayona, J. M. Preliminary Screening of Small-Scale Domestic Wastewater Treatment Systems for Removal of Pharmaceutical and Personal Care Products. *Water Res.* **2009**, *43* (1), 55–62. <https://doi.org/10.1016/j.watres.2008.10.005>.
- (6) Swartz, C. H.; Reddy, S.; Benotti, M. J.; Yin, H.; Barber, L. B.; Brownawell, B. J.; Rudel, R. A. Steroid Estrogens, Nonylphenol Ethoxylate Metabolites, and Other Wastewater Contaminants in Groundwater Affected by a Residential Septic System on Cape Cod, MA. *Environ. Sci. Technol.* **2006**, *40* (16), 4894–4902. <https://doi.org/10.1021/es052595+>.
- (7) Batista-Andrade, J. A.; Diaz, E.; Iglesias Vega, D.; Hain, E.; Rose, M. R.; Blaney, L. Spatiotemporal Analysis of Fluorescent Dissolved Organic Matter to Identify the Impacts of Failing Sewer Infrastructure in Urban Streams. *Water Res.* **2023**, *229*, 119521. <https://doi.org/10.1016/j.watres.2022.119521>.
- (8) He, K.; Hain, E.; Timm, A.; Tarnowski, M.; Blaney, L. Occurrence of Antibiotics, Estrogenic Hormones, and UV-Filters in Water, Sediment, and Oyster Tissue from the Chesapeake Bay. *Sci. Total Environ.* **2019**, *650*, 3101–3109. <https://doi.org/10.1016/j.scitotenv.2018.10.021>.
- (9) Apeti, D. A.; Wirth, E. F.; Leight, A. (Andrew); Mason, A. L.; Pisarski, E. An Assessment of Contaminants of Emerging Concern in Chesapeake Bay, MD and Charleston Harbor, SC. **2018**. <https://doi.org/10.25923/P4NC-7M71>.
- (10) Hudson, N.; Baker, A.; Reynolds, D. Fluorescence Analysis of Dissolved Organic Matter in Natural, Waste and Polluted Waters—a Review. *River Res. Appl.* **2007**, *23* (6), 631–649. <https://doi.org/10.1002/rra.1005>.
- (11) Barbosa, M. O.; Ribeiro, A. R.; Ratola, N.; Hain, E.; Homem, V.; Pereira, M. F. R.; Blaney, L.; Silva, A. M. T. Spatial and Seasonal Occurrence of Micropollutants in Four Portuguese Rivers and a Case Study for Fluorescence Excitation-Emission Matrices. *Sci. Total Environ.* **2018**, *644*, 1128–1140. <https://doi.org/10.1016/j.scitotenv.2018.06.355>.
- (12) Chen, H.; Liao, Z.; Gu, X.; Xie, J.; Li, H. Anthropogenic Influences of Paved Runoff and Sanitary Sewage on the DOM Quality of Wet Weather Overflows: An

- EEM-PARAFAC Assessment. *Environ. Sci. Technol.* **2016**, *51*.  
<https://doi.org/10.1021/acs.est.6b03727>.
- (13) Kamenetz, K. *Upper Jones Falls Small Watershed Action Plan: Final Report*; Baltimore County Department of Environmental Protection and Sustainability, 2015.
  - (14) Reay, W. Septic Tank Impacts on Ground Water Quality and Nearshore Sediment Nutrient Flux. *Ground Water* **2004**, *42*, 1079–1089. <https://doi.org/10.1111/j.1745-6584.2004.tb02645.x>.
  - (15) US EPA, R. 03. *Chesapeake Bay Total Maximum Daily Load (TMDL)*.  
<https://www.epa.gov/chesapeake-bay-tmdl> (accessed 2022-04-24).
  - (16) US EPA, O. *Septic Systems Overview*. <https://www.epa.gov/septic/septic-systems-overview> (accessed 2022-04-23).
  - (17) Withers, P. J.; Jordan, P.; May, L.; Jarvie, H. P.; Deal, N. E. Do Septic Tank Systems Pose a Hidden Threat to Water Quality? *Front. Ecol. Environ.* **2014**, *12* (2), 123–130. <https://doi.org/10.1890/130131>.
  - (18) Mallin, M. A.; McIver, M. R. Pollutant Impacts to Cape Hatteras National Seashore from Urban Runoff and Septic Leachate. *Mar. Pollut. Bull.* **2012**, *64* (7), 1356–1366. <https://doi.org/10.1016/j.marpolbul.2012.04.025>.
  - (19) Beal, C.; Gardner, E.; Menzies, N. Process, Performance, and Pollution Potential: A Review of Septic Tank-Soil Absorption Systems. *Aust. J. Soil Res.* **2005**, *43*.  
<https://doi.org/10.1071/SR05018>.
  - (20) Robertson, W. D.; Van Stempvoort, D. R.; Schiff, S. L. Review of Phosphorus Attenuation in Groundwater Plumes from 24 Septic Systems. *Sci. Total Environ.* **2019**, *692*, 640–652. <https://doi.org/10.1016/j.scitotenv.2019.07.198>.
  - (21) Schaidler, L. A.; Ackerman, J. M.; Rudel, R. A. Septic Systems as Sources of Organic Wastewater Compounds in Domestic Drinking Water Wells in a Shallow Sand and Gravel Aquifer. *Sci. Total Environ.* **2016**, *547*, 470–481.  
<https://doi.org/10.1016/j.scitotenv.2015.12.081>.
  - (22) Tamang, A.; Roy, J. W.; Boreux, M. P.; Robinson, C. E. Variation in Septic System Effluent Inputs to Tributaries in Multiple Subwatersheds and Approaches to Distinguish Contributing Pathways and Areas. *Sci. Total Environ.* **2022**, *807* (Pt 3), 151054. <https://doi.org/10.1016/j.scitotenv.2021.151054>.
  - (23) Spiese, C.; Berry, J.; Boulanger, B. What Caffeine Tells Us about Nutrient Source Apportionment in Rural Watershed Tile Drainage. **2014**, 1718–1726.  
<https://doi.org/10.1061/9780784413548.170>.
  - (24) Oldfield, L.; Rakhimbekova, S.; Roy, J. W.; Robinson, C. E. Estimation of Phosphorus Loads from Septic Systems to Tributaries in the Canadian Lake Erie Basin. *J. Gt. Lakes Res.* **2020**, *46* (6), 1559–1569.  
<https://doi.org/10.1016/j.jglr.2020.08.021>.
  - (25) Arnold, W. A.; Longnecker, K.; Kroeger, K. D.; Kujawinski, E. B. Molecular Signature of Organic Nitrogen in Septic-Impacted Groundwater. *Environ. Sci. Process. Impacts* **2014**, *16* (10), 2400–2407. <https://doi.org/10.1039/C4EM00289J>.
  - (26) Palmer-Felgate, E. J.; Mortimer, R. J. G.; Krom, M. D.; Jarvie, H. P. *Impact of Point-Source Pollution on Phosphorus and Nitrogen Cycling in Stream-Bed Sediments*. ACS Publications. <https://doi.org/10.1021/es902706r>.
  - (27) Katz, B. G.; Eberts, S. M.; Kauffman, L. J. Using Cl/Br Ratios and Other Indicators to Assess Potential Impacts on Groundwater Quality from Septic Systems:

- A Review and Examples from Principal Aquifers in the United States. *J. Hydrol.* **2011**, *397* (3), 151–166. <https://doi.org/10.1016/j.jhydrol.2010.11.017>.
- (28) Iverson, G.; Humphrey, C. P.; O'Driscoll, M. A.; Sanderford, C.; Jernigan, J.; Serozi, B. Nutrient Exports from Watersheds with Varying Septic System Densities in the North Carolina Piedmont. *J. Environ. Manage.* **2018**, *211*, 206–217. <https://doi.org/10.1016/j.jenvman.2018.01.063>.
- (29) Sowah, R. A.; Habteselassie, M. Y.; Radcliffe, D. E.; Bauske, E.; Risse, M. Isolating the Impact of Septic Systems on Fecal Pollution in Streams of Suburban Watersheds in Georgia, United States. *Water Res.* **2017**, *108*, 330–338. <https://doi.org/10.1016/j.watres.2016.11.007>.
- (30) Oldfield, L. E.; Roy, J. W.; Robinson, C. E. Investigating the Use of the Artificial Sweetener Acesulfame to Evaluate Septic System Inputs and Their Nutrient Loads to Streams at the Watershed Scale. *J. Hydrol.* **2020**, *587*, 124918. <https://doi.org/10.1016/j.jhydrol.2020.124918>.
- (31) Spoelstra, J.; Schiff, S. L.; Brown, S. J. Septic Systems Contribute Artificial Sweeteners to Streams through Groundwater. *J. Hydrol. X* **2020**, *7*, 100050. <https://doi.org/10.1016/j.hydroa.2020.100050>.
- (32) Withers, P. J. A.; Jarvie, H. P.; Stoate, C. Quantifying the Impact of Septic Tank Systems on Eutrophication Risk in Rural Headwaters. *Environ. Int.* **2011**, *37* (3), 644–653. <https://doi.org/10.1016/j.envint.2011.01.002>.
- (33) Withers, P.; May, L.; Jarvie, H.; Jordan, P.; Doody, D.; Foy, B.; Bechmann, M.; Cookesly, D.; Dils, R. M.; N, D. Nutrient Emissions to Water from Septic Tank Systems in Rural Catchments: Uncertainties and Implications for Policy. *Environ. Sci. Policy* **2012**, *24*. <https://doi.org/10.1016/j.envsci.2012.07.023>.
- (34) Ramage, S.; Camacho-Muñoz, M.; Petrie, B. Enantioselective LC-MS/MS for Anthropogenic Markers of Septic Tank Discharge. *Chemosphere* **2018**, *219*. <https://doi.org/10.1016/j.chemosphere.2018.12.007>.
- (35) Subedi, B.; Codru, N.; Dziejwski, D. M.; Wilson, L. R.; Xue, J.; Yun, S.; Braun-Howland, E.; Minihane, C.; Kannan, K. A Pilot Study on the Assessment of Trace Organic Contaminants Including Pharmaceuticals and Personal Care Products from On-Site Wastewater Treatment Systems along Skaneateles Lake in New York State, USA. *Water Res.* **2015**, *72*, 28–39. <https://doi.org/10.1016/j.watres.2014.10.049>.
- (36) Yang, Y.-Y.; Toor, G. S.; Wilson, P. C.; Williams, C. F. Micropollutants in Groundwater from Septic Systems: Transformations, Transport Mechanisms, and Human Health Risk Assessment. *Water Res.* **2017**, *123*, 258–267. <https://doi.org/10.1016/j.watres.2017.06.054>.
- (37) Graves, A. K.; Hagedorn, C.; Teetor, A.; Mahal, M.; Booth, A. M.; Reneau, R. B. Antibiotic Resistance Profiles to Determine Sources of Fecal Contamination in a Rural Virginia Watershed. *J. Environ. Qual.* **2002**, *31* (4), 1300–1308. <https://doi.org/10.2134/jeq2002.1300>.
- (38) Robertson, W. D.; Van Stempvoort, D. R.; Solomon, D. K.; Homewood, J.; Brown, S. J.; Spoelstra, J.; Schiff, S. L. Persistence of Artificial Sweeteners in a 15-Year-Old Septic System Plume. *J. Hydrol.* **2013**, *477*, 43–54. <https://doi.org/10.1016/j.jhydrol.2012.10.048>.
- (39) Richards, S.; Withers, P. J. A.; Paterson, E.; McRoberts, C. W.; Stutter, M. Potential Tracers for Tracking Septic Tank Effluent Discharges in Watercourses.

- Environ. Pollut. Barking Essex 1987* **2017**, 228, 245–255.  
<https://doi.org/10.1016/j.envpol.2017.05.044>.
- (40) James, C. A.; Miller-Schulze, J. P.; Ultican, S.; Gipe, A. D.; Baker, J. E. Evaluating Contaminants of Emerging Concern as Tracers of Wastewater from Septic Systems. *Water Res.* **2016**, *101*, 241–251.  
<https://doi.org/10.1016/j.watres.2016.05.046>.
- (41) Oppenheimer, J.; Eaton, A.; Badruzzaman, M.; Haghani, A. W.; Jacangelo, J. G. Occurrence and Suitability of Sucralose as an Indicator Compound of Wastewater Loading to Surface Waters in Urbanized Regions. *Water Res.* **2011**, *45* (13), 4019–4027. <https://doi.org/10.1016/j.watres.2011.05.014>.
- (42) Oppenheimer, J. A.; Badruzzaman, M.; Jacangelo, J. G. Differentiating Sources of Anthropogenic Loading to Impaired Water Bodies Utilizing Ratios of Sucralose and Other Microconstituents. *Water Res.* **2012**, *46* (18), 5904–5916.  
<https://doi.org/10.1016/j.watres.2012.07.060>.
- (43) Snider, D. M.; Roy, J. W.; Robertson, W. D.; Garda, D. I.; Spoelstra, J. Concentrations of Artificial Sweeteners and Their Ratios with Nutrients in Septic System Wastewater. *Groundw. Monit. Remediat.* **2017**, *37* (3), 94–102.  
<https://doi.org/10.1111/gwmr.12229>.
- (44) Spoelstra, J.; Senger, N. D.; Schiff, S. L. Artificial Sweeteners Reveal Septic System Effluent in Rural Groundwater. *J. Environ. Qual.* **2017**, *46* (6), 1434–1443.  
<https://doi.org/10.2134/jeq2017.06.0233>.
- (45) Daneshvar, A.; Aboulfadl, K.; Viglino, L.; Broséus, R.; Sauvé, S.; Madoux-Humery, A.-S.; Weyhenmeyer, G. A.; Prévost, M. Evaluating Pharmaceuticals and Caffeine as Indicators of Fecal Contamination in Drinking Water Sources of the Greater Montreal Region. *Chemosphere* **2012**, *88* (1), 131–139.  
<https://doi.org/10.1016/j.chemosphere.2012.03.016>.
- (46) Van Stempvoort, D. R.; Roy, J. W.; Grabuski, J.; Brown, S. J.; Bickerton, G.; Sverko, E. An Artificial Sweetener and Pharmaceutical Compounds as Co-Tracers of Urban Wastewater in Groundwater. *Sci. Total Environ.* **2013**, *461–462*, 348–359.  
<https://doi.org/10.1016/j.scitotenv.2013.05.001>.
- (47) Liu, S.; He, Z.; Tang, Z.; Liu, L.; Hou, J.; Li, T.; Zhang, Y.; Shi, Q.; Giesy, J. P.; Wu, F. Linking the Molecular Composition of Autochthonous Dissolved Organic Matter to Source Identification for Freshwater Lake Ecosystems by Combination of Optical Spectroscopy and FT-ICR-MS Analysis. *Sci. Total Environ.* **2020**, *703*, 134764. <https://doi.org/10.1016/j.scitotenv.2019.134764>.
- (48) Chen, W.; Westerhoff, P.; Leenheer, J. A.; Booksh, K. Fluorescence Excitation–Emission Matrix Regional Integration to Quantify Spectra for Dissolved Organic Matter. *Environ. Sci. Technol.* **2003**, *37* (24), 5701–5710.  
<https://doi.org/10.1021/es034354c>.
- (49) Murphy, K. R.; Stedmon, C. A.; Graeber, D.; Bro, R. Fluorescence Spectroscopy and Multi-Way Techniques. PARAFAC. *Anal. Methods* **2013**, *5* (23), 6557.  
<https://doi.org/10.1039/c3ay41160e>.
- (50) Guo, W.; Xu, J.; Wang, J.; Wen, Y.; Zhuo, J.; Yan, Y. Characterization of Dissolved Organic Matter in Urban Sewage Using Excitation Emission Matrix Fluorescence Spectroscopy and Parallel Factor Analysis. *J. Environ. Sci. China* **2010**, *22* (11), 1728–1734. [https://doi.org/10.1016/s1001-0742\(09\)60312-0](https://doi.org/10.1016/s1001-0742(09)60312-0).



- (51) Lapworth, D. J.; Goody, D. C.; Butcher, A. S.; Morris, B. L. Tracing Groundwater Flow and Sources of Organic Carbon in Sandstone Aquifers Using Fluorescence Properties of Dissolved Organic Matter (DOM). *Appl. Geochem.* **2008**, *23* (12), 3384–3390. <https://doi.org/10.1016/j.apgeochem.2008.07.011>.
- (52) Murphy, K. R.; Stedmon, C. A.; Waite, T. D.; Ruiz, G. M. Distinguishing between Terrestrial and Autochthonous Organic Matter Sources in Marine Environments Using Fluorescence Spectroscopy. *Mar. Chem.* **2008**, *108* (1), 40–58. <https://doi.org/10.1016/j.marchem.2007.10.003>.
- (53) Goncalves-Araujo, R.; Granskog, M. A.; Bracher, A.; Azetsu-Scott, K.; Dodd, P. A.; Stedmon, C. A. Using Fluorescent Dissolved Organic Matter to Trace and Distinguish the Origin of Arctic Surface Waters. *Sci. Rep.* **2016**, *6*, 33978. <https://doi.org/10.1038/srep33978>.
- (54) Yang, L.; Cheng, Q.; Zhuang, W.-E.; Wang, H.; Chen, W. Seasonal Changes in the Chemical Composition and Reactivity of Dissolved Organic Matter at the Land-Ocean Interface of a Subtropical River. *Environ. Sci. Pollut. Res. Int.* **2019**, *26* (24), 24595–24608. <https://doi.org/10.1007/s11356-019-05700-2>.
- (55) Holbrook, R. D.; Yen, J. H.; Grizzard, T. J. Characterizing Natural Organic Material from the Occoquan Watershed (Northern Virginia, US) Using Fluorescence Spectroscopy and PARAFAC. *Sci. Total Environ.* **2006**, *361* (1), 249–266. <https://doi.org/10.1016/j.scitotenv.2005.11.020>.
- (56) Retelletti Brogi, S.; Jung, J. Y.; Ha, S.-Y.; Hur, J. Seasonal Differences in Dissolved Organic Matter Properties and Sources in an Arctic Fjord: Implications for Future Conditions. *Sci. Total Environ.* **2019**, *694*, 133740. <https://doi.org/10.1016/j.scitotenv.2019.133740>.
- (57) Dubber, D.; Knappe, J.; Gill, L. W. Characterisation of Organic Matter and Its Transformation Processes in On-Site Wastewater Effluent Percolating through Soil Using Fluorescence Spectroscopic Methods and Parallel Factor Analysis (PARAFAC). *Water* **2021**, *13* (19), 2627. <https://doi.org/10.3390/w13192627>.
- (58) Richards, S.; Paterson, E.; Withers, P. J. A.; Stutter, M. Septic Tank Discharges as Multi-Pollutant Hotspots in Catchments. *Sci. Total Environ.* **2016**, *542* (Pt A), 854–863. <https://doi.org/10.1016/j.scitotenv.2015.10.160>.
- (59) Baker, A. Fluorescence Excitation-Emission Matrix Characterization of Some Sewage-Impacted Rivers. *Environ. Sci. Technol.* **2001**, *35* (5), 948–953. <https://doi.org/10.1021/es000177t>.
- (60) Yang, X.; Chen, F.; Meng, F.; Xie, Y.; Chen, H.; Young, K.; Luo, W.; Ye, T.; Fu, W. Occurrence and Fate of PPCPs and Correlations with Water Quality Parameters in Urban Riverine Waters of the Pearl River Delta, South China. *Environ. Sci. Pollut. Res. Int.* **2013**, *20* (8), 5864–5875. <https://doi.org/10.1007/s11356-013-1641-x>.
- (61) Sgroi, M.; Roccaro, P.; Korshin, G. V.; Vagliasindi, F. G. A. Monitoring the Behavior of Emerging Contaminants in Wastewater-Impacted Rivers Based on the Use of Fluorescence Excitation Emission Matrixes (EEM). *Environ. Sci. Technol.* **2017**, *51* (8), 4306–4316. <https://doi.org/10.1021/acs.est.6b05785>.
- (62) Baker, A.; Inverarity, R. Protein-like Fluorescence Intensity as a Possible Tool for Determining River Water Quality. *Hydrol. Process.* **2004**, *18* (15), 2927–2945. <https://doi.org/10.1002/hyp.5597>.

- (63) Sorensen, J. P. R.; Lapworth, D. J.; Marchant, B. P.; Nkhuwa, D. C. W.; Pedley, S.; Stuart, M. E.; Bell, R. A.; Chirwa, M.; Kabika, J.; Liemisa, M.; Chibesa, M. In-Situ Tryptophan-like Fluorescence: A Real-Time Indicator of Faecal Contamination in Drinking Water Supplies. *Water Res.* **2015**, *81*, 38–46. <https://doi.org/10.1016/j.watres.2015.05.035>.
- (64) Baker, A.; Cumberland, S. A.; Bradley, C.; Buckley, C.; Bridgeman, J. To What Extent Can Portable Fluorescence Spectroscopy Be Used in the Real-Time Assessment of Microbial Water Quality? *Sci. Total Environ.* **2015**, *532*, 14–19. <https://doi.org/10.1016/j.scitotenv.2015.05.114>.
- (65) Mendoza, L. M.; Mladenov, N.; Kinoshita, A. M.; Pinongcos, F.; Verbyla, M. E.; Gersberg, R. Fluorescence-Based Monitoring of Anthropogenic Pollutant Inputs to an Urban Stream in Southern California, USA. *Sci. Total Environ.* **2020**, *718*, 137206. <https://doi.org/10.1016/j.scitotenv.2020.137206>.
- (66) Jarvie, H. P.; Neal, C.; Withers, P. J. A. Sewage-Effluent Phosphorus: A Greater Risk to River Eutrophication than Agricultural Phosphorus? *Sci. Total Environ.* **2006**, *360* (1), 246–253. <https://doi.org/10.1016/j.scitotenv.2005.08.038>.
- (67) Shah, V. G.; Dunstan, R. H.; Geary, P. M.; Coombes, P.; Roberts, T. K.; Rothkirch, T. Comparisons of Water Quality Parameters from Diverse Catchments during Dry Periods and Following Rain Events. *Water Res.* **2007**, *41* (16), 3655–3666. <https://doi.org/10.1016/j.watres.2007.02.052>.
- (68) Bhaskar, A. S.; Welty, C.; Maxwell, R. M.; Miller, A. J. Untangling the Effects of Urban Development on Subsurface Storage in Baltimore. *Water Resour. Res.* **2015**, *51* (2), 1158–1181. <https://doi.org/10.1002/2014WR016039>.
- (69) Bhaskar, A. S.; Jantz, C.; Welty, C.; Drzyzga, S. A.; Miller, A. J. Coupling of the Water Cycle with Patterns of Urban Growth in the Baltimore Metropolitan Region, United States. *JAWRA J. Am. Water Resour. Assoc.* **2016**, *52* (6), 1509–1523. <https://doi.org/10.1111/1752-1688.12479>.
- (70) Bhaskar, A. S.; Welty, C. Water Balances along an Urban-to-Rural Gradient of Metropolitan Baltimore, 2001–2009. *Environ. Eng. Geosci.* **2012**, *18* (1), 37–50. <https://doi.org/10.2113/gseegeosci.18.1.37>.
- (71) Janssen, E. M. L.; Marron, E.; McNeill, K. Aquatic Photochemical Kinetics of Benzotriazole and Structurally Related Compounds. *Environ. Sci. Process. Impacts* **2015**, *17* (5), 939–946. <https://doi.org/10.1039/C5EM00045A>.
- (72) Fairbairn, D. J.; Karpuzcu, M. E.; Arnold, W. A.; Barber, B. L.; Kaufenberg, E. F.; Koskinen, W. C.; Novak, P. J.; Rice, P. J.; Swackhamer, D. L. Sources and Transport of Contaminants of Emerging Concern: A Two-Year Study of Occurrence and Spatiotemporal Variation in a Mixed Land Use Watershed. *Sci. Total Environ.* **2016**, *551–552*, 605–613. <https://doi.org/10.1016/j.scitotenv.2016.02.056>.
- (73) Dickenson, E. R. V.; Snyder, S. A.; Sedlak, D. L.; Drewes, J. E. Indicator Compounds for Assessment of Wastewater Effluent Contributions to Flow and Water Quality. *Water Res.* **2011**, *45* (3), 1199–1212. <https://doi.org/10.1016/j.watres.2010.11.012>.
- (74) Gonsior, M.; Powers, L. C.; Williams, E.; Place, A.; Chen, F.; Ruf, A.; Hertkorn, N.; Schmitt-Kopplin, P. The Chemodiversity of Algal Dissolved Organic Matter from Lysed *Microcystis Aeruginosa* Cells and Its Ability to Form Disinfection By-

- Products during Chlorination. *Water Res.* **2019**, *155*, 300–309.  
<https://doi.org/10.1016/j.watres.2019.02.030>.
- (75) Derrien, M.; Yang, L.; Hur, J. Lipid Biomarkers and Spectroscopic Indices for Identifying Organic Matter Sources in Aquatic Environments: A Review. *Water Res.* **2017**, *112*, 58–71. <https://doi.org/10.1016/j.watres.2017.01.023>.
- (76) Coble, P. G. Marine Optical Biogeochemistry: The Chemistry of Ocean Color. *Chem. Rev.* **2007**, *107* (2), 402–418. <https://doi.org/10.1021/cr050350+>.
- (77) Lu, K.; Gao, H.; Yu, H.; Liu, D.; Zhu, N.; Wan, K. Insight into Variations of DOM Fractions in Different Latitudinal Rural Black-Odor Waterbodies of Eastern China Using Fluorescence Spectroscopy Coupled with Structure Equation Model. *Sci. Total Environ.* **2022**, *816*, 151531.  
<https://doi.org/10.1016/j.scitotenv.2021.151531>.
- (78) Rodríguez-Vidal, F. J.; García-Valverde, M.; Ortega-Azabache, B.; González-Martínez, Á.; Bellido-Fernández, A. Characterization of Urban and Industrial Wastewaters Using Excitation-Emission Matrix (EEM) Fluorescence: Searching for Specific Fingerprints. *J. Environ. Manage.* **2020**, *263*, 110396.  
<https://doi.org/10.1016/j.jenvman.2020.110396>.
- (79) Murphy, K. R.; Stedmon, C. A.; Wenig, P.; Bro, R. OpenFluor– an Online Spectral Library of Auto-Fluorescence by Organic Compounds in the Environment. *Anal. Methods* **2014**, *6* (3), 658–661. <https://doi.org/10.1039/C3AY41935E>.
- (80) He, K.; Timm, A.; Blaney, L. Simultaneous Determination of UV-Filters and Estrogens in Aquatic Invertebrates by Modified Quick, Easy, Cheap, Effective, Rugged, and Safe Extraction and Liquid Chromatography Tandem Mass Spectrometry. *J. Chromatogr. A* **2017**, *1509*, 91–101.  
<https://doi.org/10.1016/j.chroma.2017.06.039>.
- (81) Mitchelmore, C. L.; He, K.; Gonsior, M.; Hain, E.; Heyes, A.; Clark, C.; Younger, R.; Schmitt-Kopplin, P.; Feerick, A.; Conway, A.; Blaney, L. Occurrence and Distribution of UV-Filters and Other Anthropogenic Contaminants in Coastal Surface Water, Sediment, and Coral Tissue from Hawaii. *Sci. Total Environ.* **2019**, *670*, 398–410. <https://doi.org/10.1016/j.scitotenv.2019.03.034>.
- (82) Yang, Y.-Y.; Toor, G. S.; Wilson, P. C.; Williams, C. F. Septic Systems as Hot-Spots of Pollutants in the Environment: Fate and Mass Balance of Micropollutants in Septic Drainfields. *Sci. Total Environ.* **2016**, *566–567*, 1535–1544.  
<https://doi.org/10.1016/j.scitotenv.2016.06.043>.
- (83) Robertson, W. D.; Van Stempvoort, D. R.; Spoelstra, J.; Brown, S. J.; Schiff, S. L. Degradation of Sucralose in Groundwater and Implications for Age Dating Contaminated Groundwater. *Water Res.* **2016**, *88*, 653–660.  
<https://doi.org/10.1016/j.watres.2015.10.051>.
- (84) Wilcox, J. D.; Bahr, J. M.; Hedman, C. J.; Hemming, J. D. C.; Barman, M. A. E.; Bradbury, K. R. Removal of Organic Wastewater Contaminants in Septic Systems Using Advanced Treatment Technologies. *J. Environ. Qual.* **2009**, *38* (1), 149–156.  
<https://doi.org/10.2134/jeq2007.0365>.
- (85) Tang-Liu, D. D.; Williams, R. L.; Riegelman, S. Disposition of Caffeine and Its Metabolites in Man. *J. Pharmacol. Exp. Ther.* **1983**, *224* (1), 180–185.
- (86) Teerlink, J.; Hering, A. S.; Higgins, C. P.; Drewes, J. E. Variability of Trace Organic Chemical Concentrations in Raw Wastewater at Three Distinct Sewershed

- Scales. *Water Res.* **2012**, *46* (10), 3261–3271.  
<https://doi.org/10.1016/j.watres.2012.03.018>.
- (87) Wang, M.; Lv, J.; Deng, H.; Liu, Q.; Liang, S. Occurrence and Removal of Triazine Herbicides during Wastewater Treatment Processes and Their Environmental Impact on Aquatic Life. *Int. J. Environ. Res. Public Health* **2022**, *19* (8), 4557. <https://doi.org/10.3390/ijerph19084557>.
- (88) Gerecke, A. C.; Schärer, M.; Singer, H. P.; Müller, S. R.; Schwarzenbach, R. P.; Sägesser, M.; Ochsenbein, U.; Popow, G. Sources of Pesticides in Surface Waters in Switzerland: Pesticide Load through Waste Water Treatment Plants—Current Situation and Reduction Potential. *Chemosphere* **2002**, *48* (3), 307–315.  
[https://doi.org/10.1016/S0045-6535\(02\)00080-2](https://doi.org/10.1016/S0045-6535(02)00080-2).
- (89) US EPA, O. *Atrazine*. <https://www.epa.gov/ingredients-used-pesticide-products/atrazine> (accessed 2023-02-19).
- (90) *Atrazine | Public Health Statement | ATSDR*.  
<https://wwwn.cdc.gov/TSP/PHS/PHS.aspx?phsid=336&toxid=59> (accessed 2023-02-19).
- (91) Langford, K. H.; Reid, M. J.; Fjeld, E.; Øxnevad, S.; Thomas, K. V. Environmental Occurrence and Risk of Organic UV Filters and Stabilizers in Multiple Matrices in Norway. *Environ. Int.* **2015**, *80*, 1–7.  
<https://doi.org/10.1016/j.envint.2015.03.012>.
- (92) Balmer, M. E.; Buser, H.-R.; Müller, M. D.; Poiger, T. Occurrence of Some Organic UV Filters in Wastewater, in Surface Waters, and in Fish from Swiss Lakes. *Environ. Sci. Technol.* **2005**, *39* (4), 953–962. <https://doi.org/10.1021/es040055r>.
- (93) Conn, K. E.; Siegrist, R. L.; Barber, L. B.; Meyer, M. T. Fate of Trace Organic Compounds during Vadose Zone Soil Treatment in an Onsite Wastewater System. *Environ. Toxicol. Chem.* **2010**, *29* (2), 285–293. <https://doi.org/10.1002/etc.40>.
- (94) McKinley, J. W.; Siegrist, R. L. Accumulation of Organic Matter Components in Soil under Conditions Imposed by Wastewater Infiltration. *Soil Sci. Soc. Am. J.* **2010**, *74* (5), 1690–1700. <https://doi.org/10.2136/sssaj2009.0395>.
- (95) Teerlink, J.; Martínez-Hernández, V.; Higgins, C. P.; Drewes, J. E. Removal of Trace Organic Chemicals in Onsite Wastewater Soil Treatment Units: A Laboratory Experiment. *Water Res.* **2012**, *46* (16), 5174–5184.  
<https://doi.org/10.1016/j.watres.2012.06.024>.
- (96) Hinkle, S. R.; Weick, R. J.; Johnson, J. M.; Cahill, J. D.; Smith, S. G.; Rich, B. J. Organic Wastewater Compounds, Pharmaceuticals, and Coliphage in Ground Water Receiving Discharge from Onsite Wastewater Treatment Systems near La Pine, Oregon: Occurrence and Implications for Transport. *US Geol. Surv. Sci. Investig. Rep.* 2005-5055 98 p.
- (97) Schaidler, L. A.; Rodgers, K. M.; Rudel, R. A. Review of Organic Wastewater Compound Concentrations and Removal in Onsite Wastewater Treatment Systems. *Environ. Sci. Technol.* **2017**, *51* (13), 7304–7317.  
<https://doi.org/10.1021/acs.est.6b04778>.
- (98) *U.S. Outpatient Antibiotic Prescribing, 2010 | NEJM*.  
<https://www.nejm.org/doi/full/10.1056/NEJMc1212055> (accessed 2023-02-21).

- (99) Andreozzi, R.; Raffaele, M.; Nicklas, P. Pharmaceuticals in STP Effluents and Their Solar Photodegradation in Aquatic Environment. *Chemosphere* **2003**, *50* (10), 1319–1330. [https://doi.org/10.1016/S0045-6535\(02\)00769-5](https://doi.org/10.1016/S0045-6535(02)00769-5).
- (100) Scheurer, M.; Brauch, H.-J.; Lange, F. T. Analysis and Occurrence of Seven Artificial Sweeteners in German Waste Water and Surface Water and in Soil Aquifer Treatment (SAT). *Anal. Bioanal. Chem.* **2009**, *394* (6), 1585–1594. <https://doi.org/10.1007/s00216-009-2881-y>.
- (101) Subedi, B.; Kannan, K. Fate of Artificial Sweeteners in Wastewater Treatment Plants in New York State, U.S.A. *Environ. Sci. Technol.* **2014**, *48* (23), 13668–13674. <https://doi.org/10.1021/es504769c>.
- (102) Patterson, R. A. Temporal Variability of Septic Tank Effluent. **2003**.
- (103) Van Stempvoort, D. R.; Robertson, W. D.; Brown, S. J. Artificial Sweeteners in a Large Septic Plume. *Groundw. Monit. Remediat.* **2011**, *31* (4), 95–102. <https://doi.org/10.1111/j.1745-6592.2011.01353.x>.
- (104) Hwang, J. H.; Oleszkiewicz, J. A. Effect of Cold-Temperature Shock on Nitrification. *Water Environ. Res. Res. Publ. Water Environ. Fed.* **2007**, *79* (9), 964–968. <https://doi.org/10.2175/106143007x176022>.
- (105) Sgroi, M.; Roccaro, P.; Korshin, G. V.; Greco, V.; Sciuto, S.; Anumol, T.; Snyder, S. A.; Vagliasindi, F. G. A. Use of Fluorescence EEM to Monitor the Removal of Emerging Contaminants in Full Scale Wastewater Treatment Plants. *J. Hazard. Mater.* **2017**, *323*, 367–376. <https://doi.org/10.1016/j.jhazmat.2016.05.035>.
- (106) Wells, M. J. M.; Hooper, J.; Mullins, G. A.; Bell, K. Y. Development of a Fluorescence EEM-PARAFAC Model for Potable Water Reuse Monitoring: Implications for Inter-Component Protein–Fulvic–Humic Interactions. *Sci. Total Environ.* **2022**, *820*, 153070. <https://doi.org/10.1016/j.scitotenv.2022.153070>.
- (107) Li, W.-T.; Chen, S.-Y.; Xu, Z.-X.; Li, Y.; Shuang, C.-D.; Li, A.-M. Characterization of Dissolved Organic Matter in Municipal Wastewater Using Fluorescence PARAFAC Analysis and Chromatography Multi-Excitation/Emission Scan: A Comparative Study. *Environ. Sci. Technol.* **2014**, *48* (5), 2603–2609. <https://doi.org/10.1021/es404624q>.
- (108) Guo, X.; Yu, H.; Yan, Z.; Gao, H.; Zhang, Y. Tracking Variations of Fluorescent Dissolved Organic Matter during Wastewater Treatment by Accumulative Fluorescence Emission Spectroscopy Combined with Principal Component, Second Derivative and Canonical Correlation Analyses. *Chemosphere* **2018**, *194*, 463–470. <https://doi.org/10.1016/j.chemosphere.2017.12.023>.
- (109) Gao, Z.; Guéguen, C. Size Distribution of Absorbing and Fluorescing DOM in Beaufort Sea, Canada Basin. *Deep Sea Res. Part Oceanogr. Res. Pap.* **2017**, *121*, 30–37. <https://doi.org/10.1016/j.dsr.2016.12.014>.
- (110) Gao, Z.; Guéguen, C. Distribution of Thiol, Humic Substances and Colored Dissolved Organic Matter during the 2015 Canadian Arctic GEOTRACES Cruises. *Mar. Chem.* **2018**, *203*, 1–9. <https://doi.org/10.1016/j.marchem.2018.04.001>.
- (111) Chen, M.; Kim, J.-H.; Nam, S.-I.; Niessen, F.; Hong, W.-L.; Kang, M.-H.; Hur, J. Production of Fluorescent Dissolved Organic Matter in Arctic Ocean Sediments. *Sci. Rep.* **2016**, *6* (1), 39213. <https://doi.org/10.1038/srep39213>.
- (112) Sheng, Y.; Yan, C.; Nie, M.; Ju, M.; Ding, M.; Huang, X.; Chen, J. The Partitioning Behavior of PAHs between Settled Dust and Its Extracted Water Phase:

- Coefficients and Effects of the Fluorescent Organic Matter. *Ecotoxicol. Environ. Saf.* **2021**, *223*, 112573. <https://doi.org/10.1016/j.ecoenv.2021.112573>.
- (113) Pitta, E.; Zeri, C. The Impact of Combining Data Sets of Fluorescence Excitation - Emission Matrices of Dissolved Organic Matter from Various Aquatic Sources on the Information Retrieved by PARAFAC Modeling. *Spectrochim. Acta. A. Mol. Biomol. Spectrosc.* **2021**, *258*, 119800. <https://doi.org/10.1016/j.saa.2021.119800>.
- (114) Schafer, T.; Powers, L.; Gonsior, M.; Reddy, K. R.; Osborne, T. Z. Contrasting Responses of DOM Leachates to Photodegradation Observed in Plant Species Collected along an Estuarine Salinity Gradient. *Biogeochemistry* **2021**, *152* (2), 291–307. <https://doi.org/10.1007/s10533-021-00756-0>.
- (115) Chen, M.; Jung, J.; Lee, Y. K.; Hur, J. Surface Accumulation of Low Molecular Weight Dissolved Organic Matter in Surface Waters and Horizontal Off-Shelf Spreading of Nutrients and Humic-like Fluorescence in the Chukchi Sea of the Arctic Ocean. *Sci. Total Environ.* **2018**, *639*, 624–632. <https://doi.org/10.1016/j.scitotenv.2018.05.205>.
- (116) Dainard, P. G.; Guéguen, C. Distribution of PARAFAC Modeled CDOM Components in the North Pacific Ocean, Bering, Chukchi and Beaufort Seas. *Mar. Chem.* **2013**, *157*, 216–223. <https://doi.org/10.1016/j.marchem.2013.10.007>.
- (117) Wünsch, U. J.; Geuer, J. K.; Lechtenfeld, O. J.; Koch, B. P.; Murphy, K. R.; Stedmon, C. A. Quantifying the Impact of Solid-Phase Extraction on Chromophoric Dissolved Organic Matter Composition. *Mar. Chem.* **2018**, *207*, 33–41. <https://doi.org/10.1016/j.marchem.2018.08.010>.
- (118) Vines, M.; Terry, L. G. Evaluation of the Biodegradability of Fluorescent Dissolved Organic Matter via Biological Filtration. *AWWA Water Sci.* **2020**, *2* (5), e1201. <https://doi.org/10.1002/aws2.1201>.
- (119) Yamashita, Y.; Scinto, L. J.; Maie, N.; Jaffé, R. Dissolved Organic Matter Characteristics Across a Subtropical Wetland's Landscape: Application of Optical Properties in the Assessment of Environmental Dynamics. *Ecosystems* **2010**, *13* (7), 1006–1019. <https://doi.org/10.1007/s10021-010-9370-1>.
- (120) Graeber, D.; Tenzin, Y.; Stutter, M.; Weigelhofer, G.; Shatwell, T.; von Tümpling, W.; Tittel, J.; Wachholz, A.; Borchardt, D. Bioavailable DOC: Reactive Nutrient Ratios Control Heterotrophic Nutrient Assimilation—An Experimental Proof of the Macronutrient-Access Hypothesis. *Biogeochemistry* **2021**, *155* (1), 1–20. <https://doi.org/10.1007/s10533-021-00809-4>.
- (121) Ryan, K. A.; Palacios, L. C.; Encina, F.; Graeber, D.; Osorio, S.; Stubbins, A.; Woelfl, S.; Nimptsch, J. Assessing Inputs of Aquaculture-Derived Nutrients to Streams Using Dissolved Organic Matter Fluorescence. *Sci. Total Environ.* **2022**, *807*, 150785. <https://doi.org/10.1016/j.scitotenv.2021.150785>.
- (122) Harjung, A.; Ejarque, E.; Battin, T.; Butturini, A.; Sabater, F.; Stadler, M.; Schelker, J. Experimental Evidence Reveals Impact of Drought Periods on Dissolved Organic Matter Quality and Ecosystem Metabolism in Subalpine Streams. *Limnol. Oceanogr.* **2019**, *64* (1), 46–60. <https://doi.org/10.1002/lno.11018>.
- (123) Guéguen, C.; Cuss, C. W.; Cassels, C. J.; Carmack, E. C. Absorption and Fluorescence of Dissolved Organic Matter in the Waters of the Canadian Arctic Archipelago, Baffin Bay, and the Labrador Sea. *J. Geophys. Res. Oceans* **2014**, *119* (3), 2034–2047. <https://doi.org/10.1002/2013JC009173>.

- (124) Cohen, E.; Levy, G. J.; Borisover, M. Fluorescent Components of Organic Matter in Wastewater: Efficacy and Selectivity of the Water Treatment. *Water Res.* **2014**, *55*, 323–334. <https://doi.org/10.1016/j.watres.2014.02.040>.
- (125) Stedmon, C. A.; Markager, S. Tracing the Production and Degradation of Autochthonous Fractions of Dissolved Organic Matter by Fluorescence Analysis. *Limnol. Oceanogr.* **2005**, *50* (5), 1415–1426. <https://doi.org/10.4319/lo.2005.50.5.1415>.
- (126) Wang, H.; Wang, Y.; Zhuang, W.-E.; Chen, W.; Shi, W.; Zhu, Z.; Yang, L. Effects of Fish Culture on Particulate Organic Matter in a Reservoir-Type River as Revealed by Absorption Spectroscopy and Fluorescence EEM-PARAFAC. *Chemosphere* **2020**, *239*, 124734. <https://doi.org/10.1016/j.chemosphere.2019.124734>.
- (127) Yamashita, Y.; Cory, R. M.; Nishioka, J.; Kuma, K.; Tanoue, E.; Jaffé, R. Fluorescence Characteristics of Dissolved Organic Matter in the Deep Waters of the Okhotsk Sea and the Northwestern North Pacific Ocean. *Deep Sea Res. Part II Top. Stud. Oceanogr.* **2010**, *57* (16), 1478–1485. <https://doi.org/10.1016/j.dsr2.2010.02.016>.
- (128) Dall'Osto, M.; Vaqué, D.; Sotomayor-Garcia, A.; Cabrera-Brufau, M.; Estrada, M.; Buchaca, T.; Soler, M.; Nunes, S.; Zeppenfeld, S.; van Pinxteren, M.; Herrmann, H.; Wex, H.; Rinaldi, M.; Paglione, M.; Beddows, D. C. S.; Harrison, R. M.; Berdalet, E. Sea Ice Microbiota in the Antarctic Peninsula Modulates Cloud-Relevant Sea Spray Aerosol Production. *Front. Mar. Sci.* **2022**, *9*.
- (129) Retelletti Brogi, S.; Cossarini, G.; Bachi, G.; Balestra, C.; Camatti, E.; Casotti, R.; Checcucci, G.; Colella, S.; Evangelista, V.; Falcini, F.; Francocci, F.; Giorgino, T.; Margiotta, F.; Ribera d'Alcalà, M.; Sprovieri, M.; Vestri, S.; Santinelli, C. Evidence of Covid-19 Lockdown Effects on Riverine Dissolved Organic Matter Dynamics Provides a Proof-of-Concept for Needed Regulations of Anthropogenic Emissions. *Sci. Total Environ.* **2022**, *812*, 152412. <https://doi.org/10.1016/j.scitotenv.2021.152412>.
- (130) D'Andrilli, J.; McConnell, J. R. Polar Ice Core Organic Matter Signatures Reveal Past Atmospheric Carbon Composition and Spatial Trends across Ancient and Modern Timescales. *J. Glaciol.* **2021**, *67* (266), 1028–1042. <https://doi.org/10.1017/jog.2021.51>.
- (131) Kida, M.; Kojima, T.; Tanabe, Y.; Hayashi, K.; Kudoh, S.; Maie, N.; Fujitake, N. Origin, Distributions, and Environmental Significance of Ubiquitous Humic-like Fluorophores in Antarctic Lakes and Streams. *Water Res.* **2019**, *163*, 114901. <https://doi.org/10.1016/j.watres.2019.114901>.
- (132) Lozada, M.; Diéguez, M. C.; García, P. E.; Bigatti, G.; Livore, J. P.; Giarratano, E.; Gil, M. N.; Dionisi, H. M. Undaria Pinnatifida Exudates Trigger Shifts in Seawater Chemistry and Microbial Communities from Atlantic Patagonian Coasts. *Biol. Invasions* **2021**, *23* (6), 1781–1801. <https://doi.org/10.1007/s10530-021-02471-1>.
- (133) Shakil, S.; Tank, S. E.; Kokelj, S. V.; Vonk, J. E.; Zolkos, S. Particulate Dominance of Organic Carbon Mobilization from Thaw Slumps on the Peel Plateau, NT: Quantification and Implications for Stream Systems and Permafrost Carbon

- Release. *Environ. Res. Lett.* **2020**, *15* (11), 114019. <https://doi.org/10.1088/1748-9326/abac36>.
- (134) Bernal, S.; Lupon, A.; Catalán, N.; Castelar, S.; Martí, E. Decoupling of Dissolved Organic Matter Patterns between Stream and Riparian Groundwater in a Headwater Forested Catchment. *Hydrol. Earth Syst. Sci.* **2018**, *22* (3), 1897–1910. <https://doi.org/10.5194/hess-22-1897-2018>.
- (135) Murphy, K. R.; Hambly, A.; Singh, S.; Henderson, R. K.; Baker, A.; Stuetz, R.; Khan, S. J. Organic Matter Fluorescence in Municipal Water Recycling Schemes: Toward a Unified PARAFAC Model. *Environ. Sci. Technol.* **2011**, *45* (7), 2909–2916. <https://doi.org/10.1021/es103015e>.
- (136) Bittar, T. B.; Berger, S. A.; Birsa, L. M.; Walters, T. L.; Thompson, M. E.; Spencer, R. G. M.; Mann, E. L.; Stubbins, A.; Frischer, M. E.; Brandes, J. A. Seasonal Dynamics of Dissolved, Particulate and Microbial Components of a Tidal Saltmarsh-Dominated Estuary under Contrasting Levels of Freshwater Discharge. *Estuar. Coast. Shelf Sci.* **2016**, *182*, 72–85. <https://doi.org/10.1016/j.ecss.2016.08.046>.
- (137) Ren, W.; Wu, X.; Ge, X.; Lin, G.; Zhou, M.; Long, Z.; Yu, X.; Tian, W. Characteristics of Dissolved Organic Matter in Lakes with Different Eutrophic Levels in Southeastern Hubei Province, China. *J. Oceanol. Limnol.* **2021**, *39* (4), 1256–1276. <https://doi.org/10.1007/s00343-020-0102-x>.
- (138) Garcia, R. D.; Reissig, M.; Queimaliños, C. P.; Garcia, P. E.; Dieguez, M. C. Climate-Driven Terrestrial Inputs in Ultraoligotrophic Mountain Streams of Andean Patagonia Revealed through Chromophoric and Fluorescent Dissolved Organic Matter. *Sci. Total Environ.* **2015**, *521–522*, 280–292. <https://doi.org/10.1016/j.scitotenv.2015.03.102>.
- (139) Yamashita, Y.; Kloeppel, B. D.; Knoepp, J.; Zausen, G. L.; Jaffé, R. Effects of Watershed History on Dissolved Organic Matter Characteristics in Headwater Streams. *Ecosystems* **2011**, *14* (7), 1110–1122. <https://doi.org/10.1007/s10021-011-9469-z>.
- (140) Walker, S. A.; Amon, R. M. W.; Stedmon, C. A. Variations in High-Latitude Riverine Fluorescent Dissolved Organic Matter: A Comparison of Large Arctic Rivers. *J. Geophys. Res. Biogeosciences* **2013**, *118* (4), 1689–1702. <https://doi.org/10.1002/2013JG002320>.
- (141) Zhuang, W.-E.; Chen, W.; Yang, L. Effects of Photodegradation on the Optical Indices of Chromophoric Dissolved Organic Matter from Typical Sources. *Int. J. Environ. Res. Public Health* **2022**, *19* (21), 14268. <https://doi.org/10.3390/ijerph192114268>.
- (142) Wünsch, U. J.; Murphy, K. R.; Stedmon, C. A. The One-Sample PARAFAC Approach Reveals Molecular Size Distributions of Fluorescent Components in Dissolved Organic Matter. *Environ. Sci. Technol.* **2017**, *51* (20), 11900–11908. <https://doi.org/10.1021/acs.est.7b03260>.
- (143) Weigelhofer, G.; Jirón, T. S.; Yeh, T.-C.; Steniczka, G.; Pucher, M. Dissolved Organic Matter Quality and Biofilm Composition Affect Microbial Organic Matter Uptake in Stream Flumes. *Water* **2020**, *12* (11), 3246. <https://doi.org/10.3390/w12113246>.



- (144) Stedmon, C. A.; Sereďyńska-Sobecka, B.; Boe-Hansen, R.; Le Tallec, N.; Waul, C. K.; Arvin, E. A Potential Approach for Monitoring Drinking Water Quality from Groundwater Systems Using Organic Matter Fluorescence as an Early Warning for Contamination Events. *Water Res.* **2011**, *45* (18), 6030–6038. <https://doi.org/10.1016/j.watres.2011.08.066>.
- (145) Borisover, M.; Laor, Y.; Saadi, I.; Lado, M.; Bukhanovsky, N. Tracing Organic Footprints from Industrial Effluent Discharge in Recalcitrant Riverine Chromophoric Dissolved Organic Matter. *Water, Air, Soil Pollut.* **2011**, *222* (1), 255–269. <https://doi.org/10.1007/s11270-011-0821-x>.
- (146) Queimaliños, C.; Reissig, M.; Pérez, G. L.; Soto Cárdenas, C.; Gereá, M.; García, P. E.; García, D.; Diéguez, M. C. Linking Landscape Heterogeneity with Lake Dissolved Organic Matter Properties Assessed through Absorbance and Fluorescence Spectroscopy: Spatial and Seasonal Patterns in Temperate Lakes of Southern Andes (Patagonia, Argentina). *Sci. Total Environ.* **2019**, *686*, 223–235. <https://doi.org/10.1016/j.scitotenv.2019.05.396>.
- (147) Graeber, D.; Gelbrecht, J.; Pusch, M. T.; Anlanger, C.; von Schiller, D. Agriculture Has Changed the Amount and Composition of Dissolved Organic Matter in Central European Headwater Streams. *Sci. Total Environ.* **2012**, *438*, 435–446. <https://doi.org/10.1016/j.scitotenv.2012.08.087>.
- (148) Dainard, P. G.; Guéguen, C.; Yamamoto-Kawai, M.; Williams, W. J.; Hutchings, J. K. Interannual Variability in the Absorption and Fluorescence Characteristics of Dissolved Organic Matter in the Canada Basin Polar Mixed Waters. *J. Geophys. Res. Oceans* **2019**, *124* (7), 5258–5269. <https://doi.org/10.1029/2018JC014896>.
- (149) Cory, R. M.; McKnight, D. M. Fluorescence Spectroscopy Reveals Ubiquitous Presence of Oxidized and Reduced Quinones in Dissolved Organic Matter. *Environ. Sci. Technol.* **2005**, *39* (21), 8142–8149. <https://doi.org/10.1021/es0506962>.
- (150) Dainard, P. G.; Guéguen, C.; McDonald, N.; Williams, W. J. Photobleaching of Fluorescent Dissolved Organic Matter in Beaufort Sea and North Atlantic Subtropical Gyre. *Mar. Chem.* **2015**, *177*, 630–637. <https://doi.org/10.1016/j.marchem.2015.10.004>.
- (151) Gonçalves-Araujo, R.; Stedmon, C. A.; Heim, B.; Dubinenkov, I.; Kraberg, A.; Moiseev, D.; Bracher, A. From Fresh to Marine Waters: Characterization and Fate of Dissolved Organic Matter in the Lena River Delta Region, Siberia. *Front. Mar. Sci.* **2015**, *2*.
- (152) Jutaporn, P.; Armstrong, M. D.; Coronell, O. Assessment of C-DBP and N-DBP Formation Potential and Its Reduction by MIEX® DOC and MIEX® GOLD Resins Using Fluorescence Spectroscopy and Parallel Factor Analysis. *Water Res.* **2020**, *172*, 115460. <https://doi.org/10.1016/j.watres.2019.115460>.
- (153) Romero, C. M.; Engel, R. E.; D’Andrilli, J.; Chen, C.; Zabinski, C.; Miller, P. R.; Wallander, R. Bulk Optical Characterization of Dissolved Organic Matter from Semiarid Wheat-Based Cropping Systems. *Geoderma* **2017**, *306*, 40–49. <https://doi.org/10.1016/j.geoderma.2017.06.029>.
- (154) Osburn, C. L.; Handsel, L. T.; Mikan, M. P.; Paerl, H. W.; Montgomery, M. T. Fluorescence Tracking of Dissolved and Particulate Organic Matter Quality in a River-Dominated Estuary. *Environ. Sci. Technol.* **2012**, *46* (16), 8628–8636. <https://doi.org/10.1021/es3007723>.

- (155) Yamashita, Y.; Boyer, J. N.; Jaffé, R. Evaluating the Distribution of Terrestrial Dissolved Organic Matter in a Complex Coastal Ecosystem Using Fluorescence Spectroscopy. *Cont. Shelf Res.* **2013**, *66*, 136–144. <https://doi.org/10.1016/j.csr.2013.06.010>.
- (156) Cawley, K. M.; Ding, Y.; Fourqurean, J.; Jaffé, R.; Cawley, K. M.; Ding, Y.; Fourqurean, J.; Jaffé, R. Characterising the Sources and Fate of Dissolved Organic Matter in Shark Bay, Australia: A Preliminary Study Using Optical Properties and Stable Carbon Isotopes. *Mar. Freshw. Res.* **2012**, *63* (11), 1098–1107. <https://doi.org/10.1071/MF12028>.
- (157) Yamashita, Y.; Kojima, D.; Yoshida, N.; Shibata, H. Relationships between Dissolved Black Carbon and Dissolved Organic Matter in Streams. *Chemosphere* **2021**, *271*, 129824. <https://doi.org/10.1016/j.chemosphere.2021.129824>.
- (158) Shutova, Y.; Baker, A.; Bridgeman, J.; Henderson, R. K. Spectroscopic Characterisation of Dissolved Organic Matter Changes in Drinking Water Treatment: From PARAFAC Analysis to Online Monitoring Wavelengths. *Water Res.* **2014**, *54*, 159–169. <https://doi.org/10.1016/j.watres.2014.01.053>.
- (159) Peleato, N. M.; McKie, M.; Taylor-Edmonds, L.; Andrews, S. A.; Legge, R. L.; Andrews, R. C. Fluorescence Spectroscopy for Monitoring Reduction of Natural Organic Matter and Halogenated Furanone Precursors by Biofiltration. *Chemosphere* **2016**, *153*, 155–161. <https://doi.org/10.1016/j.chemosphere.2016.03.018>.
- (160) Zhuang, W.-E.; Chen, W.; Cheng, Q.; Yang, L. Assessing the Priming Effect of Dissolved Organic Matter from Typical Sources Using Fluorescence EEMs-PARAFAC. *Chemosphere* **2021**, *264*, 128600. <https://doi.org/10.1016/j.chemosphere.2020.128600>.
- (161) Smith, M. A.; Kominoski, J. S.; Gaiser, E. E.; Price, R. M.; Troxler, T. G. Stormwater Runoff and Tidal Flooding Transform Dissolved Organic Matter Composition and Increase Bioavailability in Urban Coastal Ecosystems. *J. Geophys. Res. Biogeosciences* **2021**, *126* (7), e2020JG006146. <https://doi.org/10.1029/2020JG006146>.
- (162) Murphy, K. R.; Ruiz, G. M.; Dunsmuir, W. T. M.; Waite, T. D. Optimized Parameters for Fluorescence-Based Verification of Ballast Water Exchange by Ships. *Environ. Sci. Technol.* **2006**, *40* (7), 2357–2362. <https://doi.org/10.1021/es0519381>.
- (163) Chen, B.; Huang, W.; Ma, S.; Feng, M.; Liu, C.; Gu, X.; Chen, K. Characterization of Chromophoric Dissolved Organic Matter in the Littoral Zones of Eutrophic Lakes Taihu and Hongze during the Algal Bloom Season. *Water* **2018**, *10* (7), 861. <https://doi.org/10.3390/w10070861>.
- (164) Lambert, T.; Bouillon, S.; Darchambeau, F.; Massicotte, P.; Borges, A. V. Shift in the Chemical Composition of Dissolved Organic Matter in the Congo River Network. *Biogeosciences* **2016**, *13* (18), 5405–5420. <https://doi.org/10.5194/bg-13-5405-2016>.
- (165) Wang, S.; Wasswa, J.; Feldman, A. C.; Kabenge, I.; Kiggundu, N.; Zeng, T. Suspect Screening to Support Source Identification and Risk Assessment of Organic Micropollutants in the Aquatic Environment of a Sub-Saharan African Urban Center. *Water Res.* **2022**, *220*, 118706. <https://doi.org/10.1016/j.watres.2022.118706>.
- (166) Lapierre, J.-F.; del Giorgio, P. A. Partial Coupling and Differential Regulation of Biologically and Photochemically Labile Dissolved Organic Carbon across Boreal

- Aquatic Networks. *Biogeosciences* **2014**, *11* (20), 5969–5985.  
<https://doi.org/10.5194/bg-11-5969-2014>.
- (167) Hong, H.; Wu, S.; Wang, Q.; Dai, M.; Qian, L.; Zhu, H.; Li, J.; Zhang, J.; Liu, J.; Li, J.; Lu, H.; Yan, C. Fluorescent Dissolved Organic Matter Facilitates the Phytoavailability of Copper in the Coastal Wetlands Influenced by Artificial Topography. *Sci. Total Environ.* **2021**, *790*, 147855.  
<https://doi.org/10.1016/j.scitotenv.2021.147855>.
- (168) Søndergaard, M.; Stedmon, C. A.; Borch, N. H. Fate of Terrigenous Dissolved Organic Matter (DOM) in Estuaries: Aggregation and Bioavailability. *Ophelia* **2003**, *57* (3), 161–176. <https://doi.org/10.1080/00785236.2003.10409512>.
- (169) Wünsch, U. J.; Murphy, K. A Simple Method to Isolate Fluorescence Spectra from Small Dissolved Organic Matter Datasets. *Water Res.* **2021**, *190*, 116730.  
<https://doi.org/10.1016/j.watres.2020.116730>.
- (170) Yamashita, Y.; Maie, N.; Briceño, H.; Jaffé, R. Optical Characterization of Dissolved Organic Matter in Tropical Rivers of the Guayana Shield, Venezuela. *J. Geophys. Res. Biogeosciences* **2010**, *115* (G1).  
<https://doi.org/10.1029/2009JG000987>.
- (171) Kothawala, D. N.; Stedmon, C. A.; Müller, R. A.; Weyhenmeyer, G. A.; Köhler, S. J.; Tranvik, L. J. Controls of Dissolved Organic Matter Quality: Evidence from a Large-Scale Boreal Lake Survey. *Glob. Change Biol.* **2014**, *20* (4), 1101–1114.  
<https://doi.org/10.1111/gcb.12488>.
- (172) Zhou, Y.; Martin, P.; Müller, M. Composition and Cycling of Dissolved Organic Matter from Tropical Peatlands of Coastal Sarawak, Borneo, Revealed by Fluorescence Spectroscopy and Parallel Factor Analysis. *Biogeosciences* **2019**, *16* (13), 2733–2749. <https://doi.org/10.5194/bg-16-2733-2019>.
- (173) Kida, M.; Watanabe, I.; Kinjo, K.; Kondo, M.; Yoshitake, S.; Tomotsune, M.; Iimura, Y.; Umnouysin, S.; Suchewaboripont, V.; Pongparn, S.; Ohtsuka, T.; Fujitake, N. Organic Carbon Stock and Composition in 3.5-m Core Mangrove Soils (Trat, Thailand). *Sci. Total Environ.* **2021**, *801*, 149682.  
<https://doi.org/10.1016/j.scitotenv.2021.149682>.
- (174) Kim, J.; Kim, Y.; Kang, H.-W.; Kim, S. H.; Rho, T.; Kang, D.-J. Tracing Water Mass Fractions in the Deep Western Indian Ocean Using Fluorescent Dissolved Organic Matter. *Mar. Chem.* **2020**, *218*, 103720.  
<https://doi.org/10.1016/j.marchem.2019.103720>.
- (175) Ternes, T. A. Occurrence of Drugs in German Sewage Treatment Plants and Rivers | Dedicated to Professor Dr. Klaus Haberer on the Occasion of His 70th Birthday.1. *Water Res.* **1998**, *32* (11), 3245–3260. [https://doi.org/10.1016/S0043-1354\(98\)00099-2](https://doi.org/10.1016/S0043-1354(98)00099-2).
- (176) Heberer, T.; Massmann, G.; Fanck, B.; Taute, T.; Dünnbier, U. Behaviour and Redox Sensitivity of Antimicrobial Residues during Bank Filtration. *Chemosphere* **2008**, *73* (4), 451–460. <https://doi.org/10.1016/j.chemosphere.2008.06.056>.
- (177) Beal, S. L. Ways to Fit a PK Model with Some Data below the Quantification Limit. *J. Pharmacokinet. Pharmacodyn.* **2001**, *28* (5), 481–504.  
<https://doi.org/10.1023/a:1012299115260>.

- (178) Bergstrand, M.; Karlsson, M. O. Handling Data Below the Limit of Quantification in Mixed Effect Models. *AAPS J.* **2009**, *11* (2), 371–380. <https://doi.org/10.1208/s12248-009-9112-5>.
- (179) Senn, S.; Holford, N.; Hockey, H. The Ghosts of Departed Quantities: Approaches to Dealing with Observations below the Limit of Quantitation. *Stat. Med.* **2012**, *31* (30), 4280–4295. <https://doi.org/10.1002/sim.5515>.
- (180) Keizer, R. J.; Jansen, R. S.; Rosing, H.; Thijssen, B.; Beijnen, J. H.; Schellens, J. H. M.; Huitema, A. D. R. Incorporation of Concentration Data below the Limit of Quantification in Population Pharmacokinetic Analyses. *Pharmacol. Res. Perspect.* **2015**, *3* (2), e00131. <https://doi.org/10.1002/prp2.131>.
- (181) *Finding and Using Health Statistics: Common Terms and Equations*. NIH National Library of Medicine. [https://www.nlm.nih.gov/nichsr/stats\\_tutorial/section2/mod9\\_z-score.html](https://www.nlm.nih.gov/nichsr/stats_tutorial/section2/mod9_z-score.html) (accessed 2023-03-21).
- (182) Majcher, E.; Phelan, D.; Lorah, M.; McGinty, A. Characterization of Preferential Ground-Water Seepage from a Chlorinated Hydrocarbon-Contaminated Aquifer to West Branch Canal Creek, Aberdeen Proving Ground, Maryland, 2002–04. *US Geol. Surv. Sci. Investig. Rep.* **2007**, 2006–5233.
- (183) Byer, J. D.; Struger, J.; Sverko, E.; Klawunn, P.; Todd, A. Spatial and Seasonal Variations in Atrazine and Metolachlor Surface Water Concentrations in Ontario (Canada) Using ELISA. *Chemosphere* **2011**, *82* (8), 1155–1160. <https://doi.org/10.1016/j.chemosphere.2010.12.054>.
- (184) Mamun, A. A.; Shams, S.; Nuruzzaman, Md. Review on Uncertainty of the First-Flush Phenomenon in Diffuse Pollution Control. *Appl. Water Sci.* **2020**, *10* (1), 53. <https://doi.org/10.1007/s13201-019-1127-1>.
- (185) Pinongcos, F.; Mladenov, N.; Calderon, J.; Verbyla, M. E.; Kinoshita, A. M.; Gersberg, R.; Batikian, C. M. Chemical and Microbial Markers for Discriminating Sanitary Sewer Contamination in Coastal, Urban Streams. *ACS EST Water* **2022**, *2* (10), 1747–1759. <https://doi.org/10.1021/acsestwater.2c00265>.



ProQuest Number: 30427044

INFORMATION TO ALL USERS

The quality and completeness of this reproduction is dependent on the quality and completeness of the copy made available to ProQuest.



Distributed by ProQuest LLC (2023).

Copyright of the Dissertation is held by the Author unless otherwise noted.

This work may be used in accordance with the terms of the Creative Commons license or other rights statement, as indicated in the copyright statement or in the metadata associated with this work. Unless otherwise specified in the copyright statement or the metadata, all rights are reserved by the copyright holder.

This work is protected against unauthorized copying under Title 17, United States Code and other applicable copyright laws.

Microform Edition where available © ProQuest LLC. No reproduction or digitization of the Microform Edition is authorized without permission of ProQuest LLC.

ProQuest LLC  
789 East Eisenhower Parkway  
P.O. Box 1346  
Ann Arbor, MI 48106 - 1346 USA